CAMPBELL: I would like to know if other countries have documents similar to the DOE Air Cleaning Handbook? And if they do, would it be possible to get copies?

DYMENT: We do not have an Air Cleaning Handbook. We have spent quite a lot of time looking at your Air Cleaning Handbook. We do have various other documentation, though. In particular we have a nuclear industry purchasing specification for HEPA filters, which was arrived at after a consensus over many years. And there are various other documents as I've said earlier, which taken together would form the seeds of a handbook but that process has not yet occurred.

PORCO: In China and also in Korea you will find the DOE Air Cleaning Handbook.

CAMPBELL: What I hear is that, there is no equivalent to the DOE Air Cleaning Handbook anywhere else, from what we know?

PORCO: They are currently using the DOE handbook as a reference, and as you know it is out of date and is being revised.

WEIDLER: A quick summary. I would say that what we heard in our tour of the nuclear world for this afternoon is that we have a lot of pleas for international standards, that we have a plea for redeveloping our technical expertise, at least in the United States, and that we have a lot of concern for the regulations. The one on the standards I will convey to the Board of the Nuclear Codes and Standards and I know they are interested in this subject. I want to thank this panel, we've enjoyed it.

SESSION 7

OPEN END

Tuesday July 16, 1996
Co-Chairmen: K. Duval
M.W. First

STANDARDIZED METHODS FOR IN-PLACE FILTER TESTING
M. Dykes, J.K. Fretthold, and J. Slawski

CHARCOAL FILTER TESTING
J. Lyons

INTRODUCTION

FIRST: This is the Open End session. It is intended for short presentations and presentations on projects that are in progress but the information that has been gathered so far is interesting enough to present it to this audience. The Open End is also intended for people who have serious questions about issues or equipment and who wish to ask the audience if anyone has a solution or can suggest one from basic principles. This session contains a variety of topics. We have two speakers. My Co-Chairmen on this session is Kenneth Duvall from the Department of Energy. He is with the Office of Environmental Guidance. You may recall Ken was the DOE representative at the 23rd Conference.

DUVALL: Our first speaker is Jan Fretthold. He is affiliated with the Rocky Flats Environmental Technology Safe Sites of Colorado and his discussion is going to focus on the standardized methods for in-place filter testing.

STANDARDIZED METHODS FOR IN-PLACE FILTER TESTING

M. Dykes, *Westinghouse Savannah River Co.*
J.K. Fretthold, *Safe Sites of Colorado, Rocky Flats Environmental Technology Site*
J. Slawski, *US Department of Energy*

Complex - Wide Conference on In-Place filter testing

Monday, March 25 - Friday, March 29, 1996

Westinghouse Savannah River Company, Aiken, SC

As a response to the Defense Nuclear Facilities Safety Board (DNFSB) staff's suggestion on the sharing of testing technology, a conference has been scheduled at the Savannah River Site to begin exchange of information.

Who Should Attend:

- Field in-place test personnel and their management
- Purchasing Representative familiar with blanket-type subcontracting
- Technical Representative familiar with HEPA Filter requirements and specification

Conference Participants Will Share Information For The Following Objectives:

- Work together to develop and standardize a complex-wide procurement specification for HEPA Filters
- Develop an in-place test procedure that will include all requirements that each particular site may have
- Develop a training for future test personnel
- Develop a guide for in-place tests of Non-ASME N509 Systems

As part of the conference, if available, please bring copies of the following documents:

- In-Place test method/procedures
- Purchase specification for HEPA filters for your site
- Receiving inspection procedures/description
- Storage procedure/methods
- In-Place personnel training methods
- Certification requirement for test personnel
- Form of documentation of In-Place test
- Description or photographs of testing equipment
- Test of vacuum, air movers, exhausters

- Information on aerosol generators
- Information on your site's use of different aerosol agents (e.g. EMERY,DOP,DOS)
- Information on your use of private test company (contracting out the in-place testing)
- Respirator testing...documentation of the technical basis for method used

COMPLEX-WIDE CONFERENCE ON IN-PLACE FILTER TEST

CONFERENCE MINUTES

Monday, March 25, 1996

Meeting began at 9:00 a.m. Welcome was given by Maynor Dykes, SRS.

This week's agenda was reviewed and all attendees (28) were introduced.

Purchase Requisitions

Maynor Dykes reviewed the procurement specification used by the Savanna River Site. This was a detailed review to show how current standards are used to control supplier quality. The group was told that this was the specification that will be used in the formation of BOA (Basic Ordering Agreement) to provide HEPA filters on a "as needed" basis to government owned/contractors operated (GOCO) facility throughout the Department of Energy complex. Seven GOCO facilities will participate in the BOA.

Other areas highlighted in this review were:

- All HEPA filters are Level 1 procurement and require Level B storage.
- All HEPA filters receive a visual inspection by qualified trained inspectors prior to storage.

Meeting was adjourned at 11:30 p.m. For lunch.

Jon Fretthold, Rocky Flats, reviewed his company's Procurement Specification. A lengthy discussion was raised of shelf life of a filter. This is a problem were there is no technical guidelines. Jon stated that his company used ten (10) years with a five (5) year requalification. Reasoning behind the use of 10 years explained. Other area discussed by Jon were:

- Level B storage, controlled by filter systems personal
- Filter Inspections are performed by the FTF test personal

V. Martinez, Los Alamos National Laboratory, described his company's procurement specification. Victor stated basically all of the specification and purchase requisitions included the same information. Purchase requisitions are written, then forwarded to purchasing and bids go out. At receiving, QA and visual inspection are performed. Filters are reinspected after received from Rocky Flats. Filters are stored in warehouses and installed as needed. Victor indicated that 1-2% of their filters are rejected each year at receiving. Most of these are administrative problems.

J. Kriskovich, Westinghouse Hanford, stated they were in the process of updating their specification. They are using AG-1 as a base. Jim feels that all filters should not be tested. There is a 1-3% failure rate od Hanford filters at the Rocky Flats test station. At Hanford, visual and beach tests are performed. Receiving personal do all inspections. Hanford has a 1% defective rate at receiving. Most damage is caused by shipping and forklift.

Meeting adjourned at 4:00 p.m.

Tuesday, March 26, 1996

Maynor Dykes, SRS gave opening remarks and introduced Roger Zavadoski, DNFSB.

Roger described the DNFSB and its purpose. "The board consists of 100 members. Roger is the technical staff member that deals with filtered ventilation systems. Roger discussion included the following:

- Protection of the public.
- The role of HEPA filters in D&D.
- Safety Class sys. reduced to Safety Significant - loss of margin of safety.
- The role of the Filter Test Facility; filter QPL; effects of aging, wetting, radiation.

In-Place Testing

Maynor Dykes described the SRS test program highlighting test procedures and test personnel training. He answered questions from the group concerning test frequencies of portable air movers and fixed exhaust systems.

There was a full conference discussion with each GOCO site describing their In-Place test program, procedures and training. There were many difference in training of test personnel. Some sites had no classroom training and depended on "on-the-job" training. There were several problems seen in using Union personnel as testers.

Each site discussed the instrumentation used in their test programs. All sites basically used the same type penetrometer with exception of Los Alamos. There was a long discussion on aerosols with no decision being reached on which was best DOP was being used at Rocky Flats, INEL & SRS; Emery 3004 was being used at LANL and

LLNL; Emery was used at Hanford. ASME N510 was discussed and the conference thought a rewrite was in order.

Wednesday, March 27, 1996

Instrumentation
- NIST Calibration
- Bench Test

It appeared that all sites were using the same photometer with the exception of Los Alamos was using the laser field testing.

Questions were asked concerning calibration of the photometer. Do we require NIST calibration? Do we bench test the photometer on regular intervals, how often do we calibrate to NIST requirement? Do we use a NIST transfer method on our contaminated instruments?

Oak Ridge reviewed these calibration methods stating the Instrumentation Control Division on-site performs calibration to an ATI procedure and it is good for one year. They seldom send there field instruments off-site because of the potential contamination problem. They do not perform bench tests. The FTF instruments are sent off-site for calibration. Oak Ridge uses Thompson's Calibration Laboratory for their off-site calibration.

LLNL described their calibration procedure stating their instruments are sent to ATI for NIST calibration. They have four sets of instruments and a small test station with a known aerosol source. When an instrument gives a suspect reading, it is taken through a bench test procedure.

Hanford requires annual calibration. The Instrument Tech. Group maintains their test equipment and test instrument are sent off-site for recalibration. Hanford uses PNL (Pacific Northwest Laboratory), which is at Hanford, for recalibration. Hanford performs bench testing.

Los Alamos requires annual calibration on their lasers. Sizing is performed on a quarterly basis.

SRS required annual calibration. Instruments are sent to ATI for NIST certifications. SRS maintains two NIST calibration instrument for bench test and calibration transfer on the highly contaminated instruments. When instruments are returned from calibration, the documentation is reviewed, particularly the "As Found" section. If a problem is seen in this section, retests are performed on systems where this instrument was used.
Rocky Flats has personal trained by ATI to calibrate and rebuild their instruments. This is performed on an annual basis.

SRS asked if anyone was checking the penetrometer flow. SRS had discovered a problem with flow on new instruments. All sites indicated they did perform flow checks.

The group agreed that we need to know more about calibration. They wanted to know if their instruments were calibrated to a know traceable concentration of aerosol. Maynor Dykes, SRS, agreed to investigate this problem.

There was a long discussion on penetrometer failure while in service. Hanford stated that they had problems with motors freezing. Some sites had problems in movement and handling. One site leaves instruments in the building where tests are performed to prevent damage. One site stated it was rare to have damage to an instrument from transportation by their group.

All sites have the required documentation in their record keeping.

Thursday, March 28, 1996

In-Place Test Personnel

There was a great deal of discussion on training. Training problems was seen as one of the major problems in HEPA filter testing. Some facility do not have in-house training programs. Others have full classroom training followed by on-the-job and JPM (Job Performance Measures). Testing was required at each level of training. Off-site training at Harvard or NUCON was the only requirement by some. Most sites considered off-site training as "basic" and feel that they could not provide much help in testing their systems. Most sites do not use ASME N510 criteria since they could not test their system to standards. The use of Union personnel as testers was reviewed and seen as a problem since supervision has no control over the people or who received the test assignment. The conference group thinks we should have DOE assistance in development of a training policy. Since test requirements are basically the same at all sites, there was no reason why training should not be alike. At the present time, there is no certification for in-place test personnel.

Site Training Program Qualifications:

- Oak Ridge - Has no in-house training program. Requires training from Harvard or NUCON and on-the-job training.
- Rocky Flats - Requires two-four days supervisor administered training for Union people then on-the-job training for each system.
- Livermore - Requires Harvard training with one year on-the-job.
- LANL - Requires 39 hours classroom, 9 JPMS and 2 years on-the-job.
- SRS - Requires 39 hours classroom, 9 JPMS and 2 years on-the-job. Requalification is required every two years after qualification.
- Hanford - Union tech. OJT by supervisor,Qual. cards.

Test of Air Mover, Vacuum and Portable Exhausters

No one knew of any technical specification for testing portable equipment. Most sites perform tests alike and require qualified HEPA filters.

SRS requires qualification of all portable equipment before purchase. All equipment failing qualification testing will not be purchased. The SRS Filters Test Group has final approval of all portable air movers.
At all other sites, the test personnel have no say in procurement of equipment. Problems arise in this policy because some of the equipment can not be tested or altered so that basic testing can be performed. One site had to alter a vacuum cleaner to eliminate carbon fibers getting into the test instrument.

Private Test Companies

A very short discussion. No one had experience with private companies. Problem areas include security clearances and training on special filtration systems.

Friday, March 29, 1996

Conference Review

The positive response to this conference was outstanding. Everyone agreed that the conference was a great success and should continue. The indicated it was long overdue. All agreed this was the best method to transfer technical in-place testing knowledge throughout the DOE complex. A large number stated this was a training experience where they learned how to better perform their job function as a tester or supervisor.

The group saw the need for better standards, procedures and training of test personnel. It was very evident that most sites are basically doing business alike but with different approaches. It is now known that procedures common to all sites can be written and used effectively.

Many problems were identified at this conference. The one most common to all sites was, the test groups have no authority even though their job function is required by DOE. They cannot require correction of deficiencies and are not included in designs or procurement.

Everyone agreed that DOE should provide direction and support to the test groups. It was agreed that the FTF groups should continue to function. Every site saw a cost savings (waste reduction) in their programs by requiring retest at these facilities.

During the conference, participants were asked to write some of their major concerns. Given below are these concerns:

- Lack of official DOE policy regarding testing at FTF's.
- Lack of DOE or Site specification for portable HEPA systems or filters for these systems.
- Lack of minimum training requirements for filter testing personnel; no DOE guidance.
- Referencing of ASME N510 for the testing of DOE filter systems results in auditing confusion and problems demonstrating compliance with referenced requirements.
- Lack of DOE guidance document or standard for testing of filter systems unique to DOE sites.
- Procurement of HEPA filters by personnel not knowledgeable of requirement for Nuclear Air Cleaning Components.
- Systems have old filters, >20 years. They are routinely tested and pass but the quality of media is in question. Testers have no authority to require replacement.
- Lack of DOE policy concerning shelf and service life of a HEPA filter.
- There is no formal DOE policy that requires facility managers to correct deficiencies found by the test groups.
- How will QPL be handled?
- If testing stations go away, who will perform a calibration efficiency (versus a leak test) tests.
- When will the whole filtration area stop being the unwanted step child at DOE?
- Will the conference continue? How Often? Where?
- There is a large disparity on how you meet or not meet an OSR (TSR, BIO, etc.) requirement.

The conference adjourned at 11:30 a.m.

Future Actions:

Establish a Complex wide (DOE) policy on :

Training requirements for filter test tech.
Test tech. certification
Test aerosol
In-place test procedure - mandatory / optional requirements.
Receiving inspection / QA
Filter specification (ASME / DOE)
QPL requirements for filters
Use of FILTER TEST FACILITIES
Filter service life

List of attendees:

Maynor Dykes	WSRC	Greg Helland	LANL
Ernest R. Brinkley	WSRC	J.C. "Tony" Gross	Lockhead Martin/OR
Gary Mullis	WSRC	George M. May	Lockhead Martin/OR
Dave Simpson	WSRC	David L. Monroe	Lockhead Martin/OR
Kurt Breitinger	WSRC	Gary N. Norman	ORNL
Richard Proctor	WSRC	Terry Schubert	Lockhead Martin/OR
Jim Kriskovich	WHC	Jim Slawski	DOE DP-45 (GTN)
Charles DuPré	Kaiser Hill/Rocky Flats	Jack Jacox	Jacox Associates
Brian Mokler	LANL	Micheal Brandon	RMRS/Rocky Flats
Lawrnel Harrison	INEL	Richard A. Caufield	Dyn Corp/Rocky Flats
John Comer	WHC	J.K. Fretthold	SSOC/Rocky Flats
Roger Zavadoski	DNSFB	Werner Bergman	LLNL
Bruce Bettencourt	LLNL	Victor A. Martinez	LANL
Wayne R. Krause	LLNL		

DISCUSSION

DUVALL: Some time ago at Rocky Flats it was reported that there was significant plutonium discovered in the ventilation system on the walls downstream from the HEPA filters. And I am wondering what was concluded as to how that happened and did it have any bearing on the testing of the filters after that?

FRETTHOLD: Downstream from the filters?

DUVALL: Yes, there was a significant amount of plutonium that was lining the ventilation walls and there was some concern about criticality. In fact, I think that subsequently there were liners put on the ducts.

FRETTHOLD: That was upstream from the filter system between the glove boxes and the final filter plenum entrance. And here again it was a build up that had occurred because of the different processes. The basic systems are designed to move air, not particles. The original concept was, let's stop the particles at the glove box. Unfortunately, not every glove box operation had a filter at that point. Consequently, depending on the type of material, there was a migration into the duct work. Usually there was a reasonable velocity to carry the material, but as soon as any change in direction occurs or where you had a change in velocity you would have material fall out. They went through the system with an external counting device and identified where they had roughly the material. I won't say it was accurate because of background, reflections, and everything else that they were dealing with. But from that point on they could identify the worst locations and they went in with various small vacuum cleaners, scrapers, various other things and removed material from the worst locations. I do not have the numbers handy but I believe they removed one-tenth of what they estimated was there. It was a very successful operation.

BERGMAN: I want to add a comment to yours. I have not seen a report but I have had personal communications with people who know the major sources for this buildup. Regarding the question by Ken Duvall on Pu accumulation in the ventilation ducts at Rocky Flats let me offer the following: The HEPA filters used in glove boxes would plug rapidly and restrict the air flow into the box. This caused insufficient vacuum within the box and occasionally allowed Pu to escape from the box. To prevent this from happening, some workers would punch holes in the glove box HEPA filters to allow air to pass through the plugged HEPA filters.

FRETTHOLD: This took place during the early 60's, and then it stopped. The glove box filter was used as a pre-filter but was not a filter for which credit was taken from a testing standpoint. We had a lot of production going on, so the filters would load up fairly fast. There was a butterfly valve just downstream from the filter which could be opened to a certain point to maintain a negative pressure on the glove box. What you reported was early practice. It was definitely stopped and better maintenance instituted for filter systems and glove boxes.

DERDERIAN: In defense of DOE management, I would like to say that we are beginning to move in a direction that will resolve some of these important issues. Tip Rollins' group in EM is now tasked with coming through with a comprehensive report that will address the filter testing facilities. It will address QPL testing, it will address a number of technical issues that have not been addressed before. I find myself defending management, a very awkward position to be in for an engineer.

FIRST: I was very much interested in your exposition, particularly the aspect of training and certification of personnel. My first introduction to the Committee on Nuclear Air and Gas Treatment standards was to prepare a standard for personnel who did in-place testing. I spent six or seven frustrating years revising that document, because every time I revised it, the utility industry found good reasons why it was not sufficient. We finally had a conference with industry representatives who told us all the things that they wanted to have changed. We dutifully made the changes but then they told us they would not accept the standard under any circumstance. This remains a real problem. I did get the proposed personnel standard published, not in the air cleaning conferences, but in a special conference that took place in France on the subject of high efficiency filtration. If your group ever wants a personnel standard for certification, we have a good start and you can fight with the utility industry from now on.

DUVALL: Our next speaker is from NRC. He is James Lyons, section chief of the plant systems branch. His discussion will be on charcoal filter testing.

CHARCOAL FILTER TESTING

James Lyons
US Nuclear Regulatory Commission
Washington, DC

Yesterday Dr. Kovach was saying that he could count on two fingers the number of NRC personnel who had experience in air cleaning. I will admit that I am not one of those two, this is certainly not my field of expertise. I have been involved in this for about a year. At Plant Systems Branch we are in charge of the systems aspects of all the ventilation systems. We have inherited the issue of charcoal filter testing and have been working closely with Jack Hayes, who has been involved with it for a number of years. Earlier this year a couple of plants went through this process. If you start stepping through the standard Tech Specs, and a lot of plants only reference Reg. Guide 1.52, Rev 2, what you end up doing is taking yourself there. Figure 1 is somewhat confusing. In fact, I tried to make it this way because as I go forward to talk to my management, one of the things that I want to do is convince them that this is a confusing process. When you go to Reg Guide 1.52, section C.6.a, it says perform the test according to Table 2. When you go to Table 2, it says to do your laboratory test per Test 5.B of Table 5.1 of ANSI N-509-1976. When you go there, it says an acceptable test method is RDT-M16-1T, paragraph 4.5.3, except that 80°C and 95% RH is required for the test, but the pre- and post-loading sweep is at 25°C. That leads you to a test as we all know, that is going to fail. This problem has been around for quite a while. As Ron Bellamy discussed earlier, one of the problems we have is that in the current climate at the NRC verbatim compliance with Tech. Specs. is required. It does not matter that the tests you are performing actually give you a better picture of what your charcoal can do than the test that would be required by your Tech. Specs. This is what I am trying to correct. That is my goal, or one of my goals, right now and I have a couple of other issues that I am working on, too. Basically, what I am going forward with to my management is that, because of the confusion that surrounds the requirement for testing carbon, it takes you through this torturous path, and some plants are not in verbatim compliance with their Tech. Specs. However, in most cases, the tests that people are doing, (I think in all cases, but I have not been able to go through and actually check this to make sure) are more accurate than if they did the test in accordance with their Tech. Specs. We processed emergency Tech. Specs. changes for three plants, Davis Besse, Onconee, and Summer. Summer was the first. Also, Brunswick, in order to restart, flew a test sample up to Ohio to be tested in accordance with their Tech. Specs., because they wanted to be able to start up. We are trying to get around that. There is a second issue here, as far back as '87, through work that CONAGT and INEL did for the NRC, it was determined the that there were some problems with the testing protocol of the '79 version of ASTM D 3803. We put out an informational notice that recommended that when the revision to D 3803 came out, which was the '89 revision, that people should start using that test protocol. We see that some people have gone to that test protocol, but a number have not. I see two issues that I would like to correct. One, is this verbatim compliance with Tech. Specs. and, two, is to get everybody testing to D 3803 - 1989. I am working on a paper that will tell the Commission what is going on and to see which way the wind is blowing when that floats up there. Eventually, what I want to do is put out some sort of generic communication, either a generic letter, or an administrative letter. I really think a generic letter is probably the best way to go. That would give the agency's position on this issue. As part of the generic letter process we would have to issue it for public comment. When you see the generic letter you will have an opportunity to comment on it. Your first indication of where we are going will be when the Commission paper is issued; it will probably be within the next month. As we worked on how to resolve this issue, we met with NHUG in April. They provided some good

information and were very supportive of going to the D 3803-1989 standard. It has been really good to work with a group that is proactive in trying to solve some of the problems we are having in this area. Maybe utility representatives that are here that are not part of NHUG, or not supporting their meeting, which is next week, might want to think of trying to support that group. It is a very good group. Another thing that I am working on is improved standard Tech. Specs. We are going to add a reviewer's note that will explain this issue very briefly to the Tech. Spec. reviewer at the NRC and, at the same time, will tell industry that we would like to see people go to D 3803-1989. One of the things we are looking at doing is to change the safety factor of 5-7 to determine the penetration, back down to a safety factor of about two. That may help people go to the standard. A lot of talk has been about fixing Reg. Guide 1.52 Rev 2, why we don't update it and put out Rev 3. There was a draft Rev 3 that the NRC put together a few years ago, but it did not go very far because of priorities. I do not know what is takes to get it to a higher level of priority. Maybe, as a result of this Commission paper and the actions that I am working on the effort might be able to be revived and we might be able to move forward on it. I can not guarantee anything, but I would hope to get out an updated version of the Reg. Guide, so that we do not have an agency position that is not right.

Figure 1

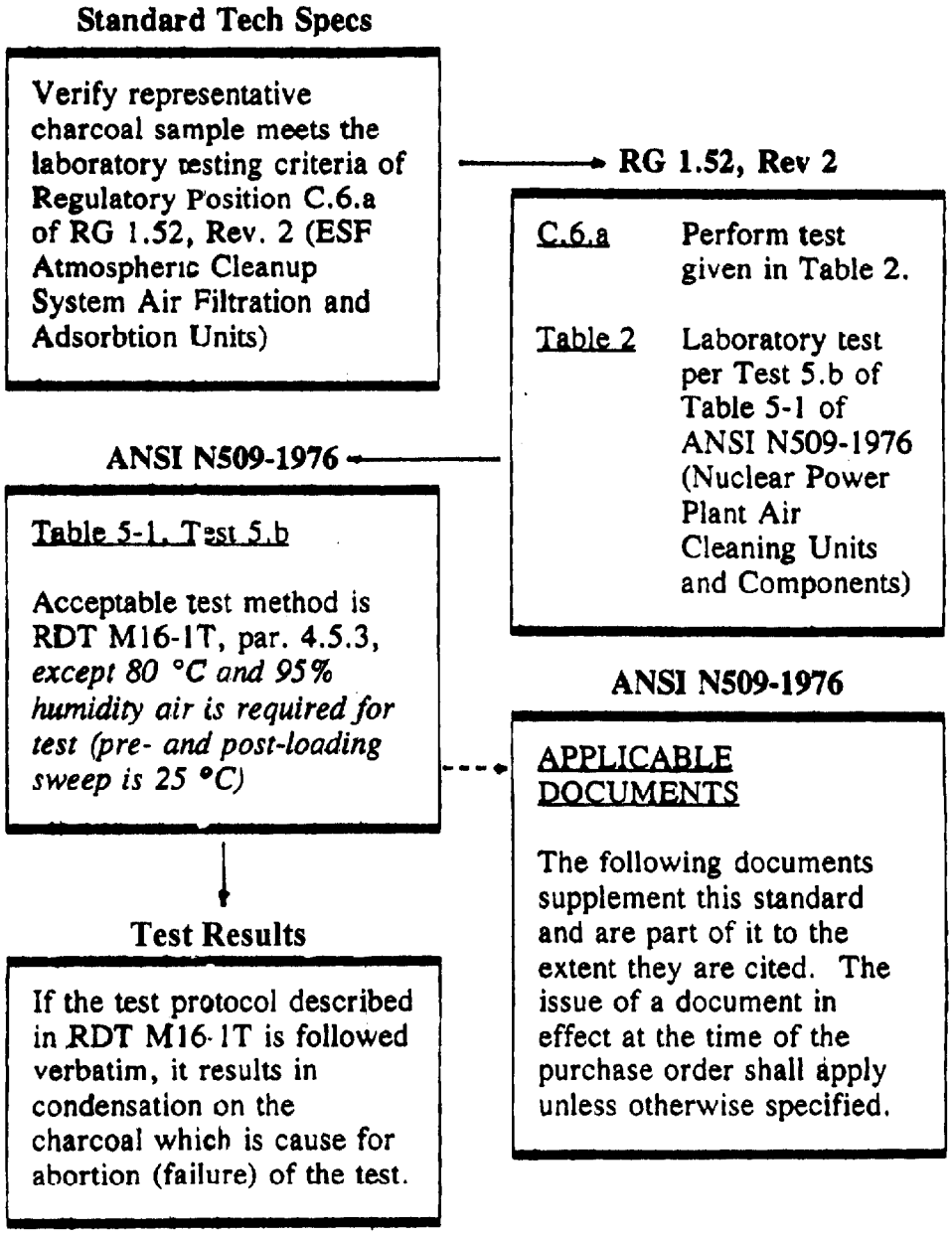

DISCUSSION

KOVACH: One of the reasons why I was upset with the hassle that we went through on charcoal testing was not the question of violating technical specifications. I expect that when you set technical specifications, people should be paying attention to them and they should be following them, I have no argument with that aspect of it. My major technical heartache related to the regulatory guide changing the standards and values for temperature and humidity, and therefore the NRC expecting that a temperature change from 80°C to 25°C, at the exact same relative humidity, would be technically feasible. Certainly you can run a test at 25°C and 95% RH but you have to have the carbon come to thermal and humidity equilibrium and maintain them throughout the test period. But I can't see why anybody who has a basic physical chemistry understanding of relative humidity and its dependence on temperature, would expect an instantaneous change from 25°C, 95% RH to 80°C ,95% RH and then back again to occur without condensing water in the bed. This is where I have a problem. Certainly you can run tests under three different conditions, but there has to be a time for change of equilibrium in between, you can't just make a turn on a switch and suddenly change from 25°C to 80°C and back to 25°C while maintaining the same relative humidity. This is a physical impossibility.

LYONS: I agree with that. In defense of the NRC we were referencing the standard.

KOVACH: But the standard does not tell you that you have to do it instantaneously.

LYONS: The words are directly out of the table in the standard.

KOVACH: I understand that, but how can you end up with the intent of the latest version of D3803 if you start interpreting the wording in your own way. Even though there is a code of federal regulation that contains an acceptable test, that does not exclude other acceptable tests that are more appropriate from a scientific standpoint than the exact wording as it reads now.

LYONS: It does not. In fact, people that have Tech. Specs., that either call for specific temperatures or cite other standards are the ones that don't get involved with D-3803. It is a problem with the wording that then becomes involved with a legal interpretation. N-509 leaves you with 80°C and 95% RH with a pre- and post- setting of 25°C. We have to fix it.

KOVACH: Another thing the industry's regulations writers have to understand is that when you cite standards that are in draft form, such as RDT M161-T, the T stands for tentative, because it is still evolving. There may be technical mistakes that have not been corrected. It is very hazardous to cite draft documents and then enforce them years later. The last issue of RDT M161-T looks very different from the original issue.

LYONS: What I have learned as I walk myself through some of these documents is that both the industry's and the staff's position on what is an appropriate test, and what conditions produce the most conservative results, have changed over the years. We have tended to flip-flop and that got us into this problem. When we issued Information Notice 87-32, the staff was trying to correct the problem. However, I do not think we were able to correct it as forcefully as we would have liked to have done and even then we would have been in the same predicament that you are pointing out. However, it would have probably worked out okay at that point.

SESSION 8

HVAC & DECOMMISSIONING

Wednesday July 17, 1996
Co-Chairmen: J.D. Paul
R. Porco

HVAC

CONTROL ROOM ENVELOPE UNFILTERED AIR INLEAKAGE TEST PROTOCOLS
P.L. Lagus and R.A. Grot

VARIABLE PATTERN CONTAMINATION CONTROL UNDER POSITIVE PRESSURE
H.M. Philippi

AEROSOL DEPOSITION IN BENDS WITH TURBULENT FLOW
A.R. McFarland, H. Gong, W.B. Wente, N.K. Anand, and A. Muyshondt

DECOMMISSIONING

ATMOSPHERIC DISCHARGES FROM NUCLEAR FACILITIES DURING DECOMMISSIONING: GERMAN EXPERIENCES AND CONCEPTS
H. Braun, R. Görtz, and L. Weil

HEATING, VENTILATING, AND AIR CONDITIONING DEACTIVATION THERMAL ANALYSIS OF PUREX PLANT
W.W. Chen and R.A. Gregonis

24th DOE/NRC NUCLEAR AIR CLEANING AND TREATMENT CONFERENCE

CONTROL ROOM ENVELOPE UNFILTERED AIR INLEAKAGE TEST PROTOCOLS

Peter L. Lagus, Ph.D., CIH
Lagus Applied Technology
San Diego, CA 92121

Richard A. Grot, Ph.D.
Lagus Applied Technology
Olney, MD 20832

ABSTRACT

In 1983, the Advisory Committee on Reactor Safeguards (ACRS) recommended that the US NRC develop a control room HVAC performance testing protocol. To date no such protocol has been forthcoming. Beginning in mid-1994, an effort was funded by NRC under a Small Business Innovation Research (SBIR) grant to develop several simplified test protocols based on the principles of tracer gas testing in order to *measure* the total unfiltered inleakage entering a CRE during emergency mode operation of the control room ventilation system. These would allow accurate assessment of unfiltered air inleakage as required in SRP 6.4.

The continuing lack of a standard protocol is unfortunate since one of the significant parameters required to calculate operator dose is the amount of unfiltered air inleakage into the control room. Often it is *assumed* that, if the Control Room Envelope (CRE) is maintained at +1/8 in. w.g. differential pressure relative to the surroundings, no significant unfiltered inleakage can occur it is further assumed that inleakage due to door openings is the only source of unfiltered air.

The specific technical objectives of the effort were:

1) to define three simple tracer gas tests that would allow accurate measurement of CRE unfiltered air inleakage,

2) to define those additional engineering parameters knowledge of which would be required for each basic type of emergency ventilation system to allow measurement of unfiltered inleakage,

3) to provide a thorough error analysis of the inleakage measurement technique(s) so that defensible bounds could be placed on any resulting data, and

4) to generate test protocols based on the above three objectives that would allow measurement of unfiltered air inleakage by responsible plant personnel.

This paper summarizes the test protocols that were developed and discusses the accuracy to be expected from each of them.

1.0 INTRODUCTION

In 1983, the Advisory Committee On Reactor Safeguards (ACRS) provided a series of recommendations to the NRC regarding control room habitability (Hayes, et al., 1984). One of the ACRS concerns was that NRC did not have a protocol for testing control room heating ventilating and air conditioning (HVAC) systems. It was recommended that the NRC develop such a protocol. Writing in the 18th DOE Nuclear Airborne Waste Management & Air Cleaning Conference, members of the ACRS observed "The NRC staff needs to expedite it's efforts to develop a protocol for testing control room HVAC and air cleaning systems. Such tests should be conducted under realistic operating conditions.....all parts of the systems including dampers, ducts, etc. should be tested simultaneously as an integral unit.....particular attention should be given to assure that sections of such systems that are under negative pressure will not bring in contaminants which later can be transferred to the control room." (Moeller and Kotra, 1984).

As of early 1995, no control room HVAC performance testing protocol has been put forward by NRC. This lack of a standard test protocol is particularly unfortunate in light of the methodology used to calculate control room staff doses (Murphy and Campe, 1974, Stage, 1995). One of the significant parameters contained within either formalism is the amount of unfiltered air inleakage into the control room.

Present practice appears to assess inleakage based on models of air flow through cracks combined with assumed pressure differences. Often it is *assumed* that if the CRE is maintained at +1/8 in. w.g. differential pressure relative to the surroundings, no significant unfiltered inleakage can occur and that inleakage due to door openings is the only source of unfiltered air. Theoretically this can be true *only* if no portion of the return leg (or legs) of the CRE emergency ventilation system lies outside the CRE.

Negative differential pressure portions of return ducting, fan shaft seals, expansion boots, control dampers, ventilation fan or filter access panels, actuator shaft seals, and miscellaneous unsealed penetrations that lie outside the CRE can contribute substantial unfiltered air inleakage. Other sources of unfiltered air inleakage include improperly seated low leakage intake dampers and leakage from HVAC supply ductwork that traverses the CRE, but provides airflow to non-CRE portions of the building.

Sometimes, unfiltered air inleakage is extrapolated from simple fan pressurization test data. Such an extrapolation is usually unwarranted since the pressure conditions that exist in a ventilation system/control room envelope under emergency operating conditions may not be the same as those generated by a fan pressurization test. ASTM Standard E779-87 (ASTM, 1992) which covers fan pressurization testing provides an explicit warning that extrapolation of fan pressurization data to actual operating conditions *is not feasible*.

It is often claimed that unfiltered air inleakage can be discerned by visual inspection coupled with a ventilation system walkdown. Sometimes this walkdown is augmented by use of smoke tracing to identify inleakage pathways. Since visual inspection is not quantitative, it can only discover obvious (open) leakage pathways and cannot deduce the magnitude of

potential inleakage due to any pathway so discovered. For inleakage sites that are hidden from view, visual inspection cannot discern their existence much less quantitatively assess the magnitude of any air inleakage into a CRE.

Smoke testing was originally developed for use in visualizing airflows in mines and has proven to be useful in following airflow patterns within a limited volume. However, it provides no *quantitative* estimate of actual unfiltered inleakage. In addition, care must be exercised in the interpretation of smoke flow patterns since the results often respond to localized airflows occurring at specific points within the CRE. Frequently, false indications of flow are caused by temperature gradients or transient atmospheric conditions that have nothing to do with actual inleakage.

In light of the above enumerated deficiencies of existing CRE inleakage testing techniques, a protocol based on the principles of tracer gas ventilation testing was felt to be appropriate. Tracer gas ventilation tests directly respond to the volumetric ventilation performance in the structure under test and hence do not possess the intrinsic drawbacks of the other methods.

The specific technical objectives of this effort were:

1. to define three simple tracer gas tests that would allow accurate measurement of control room emergency ventilation system operating characteristics, specifically unfiltered air inleakage, on a reconnaissance basis,
2. to categorize the various types of emergency ventilation systems and, having done so, to define those additional engineering parameters that may be required in addition to tracer gas data to allow interpretation of tracer gas data in terms of unfiltered inleakage,
3. to provide a thorough error analysis of the inleakage measurement technique(s) so that defensible bounds may be placed on any resulting data, and
4. to generate test protocols based on the above three objectives that would allow the performance by responsible plant personnel of a simple tracer test to measure unfiltered air inleakage.

Note that the test protocol developed in this effort would not, in general, disclose the actual location(s) of unfiltered inleakage, but only the total amount. For a reconnaissance measurement, this quantity is sufficient to decide if the unfiltered inleakage presents a problem in terms of compliance with GDC 19. To provide quantitative information as to leak location and magnitude requires more sophisticated testing than is being discussed in this paper.

2.0 TECHNICAL BACKGROUND

Tracer gases have been used to measure air infiltration and ventilation characteristics of buildings for over 30 years. Tracer gas techniques have been successfully used in other areas of ventilation engineering and industrial hygiene to provide accurate characterization of HVAC performance under actual operating conditions (Lagus and Persily, 1985, Grot and Lagus, 1991).

Within the nuclear power community, tracer gas techniques have been used since the early 1980's to measure, for instance, airflow patterns to investigate health and safety monitor locations (Hickey, et al., 1991) as well as to understand potential gaseous radioactive contaminant migration within selected buildings (Vavasseur, 1985, Lagus et al., 1988). Recently the results of a series of tracer gas measurements designed to measure total unfiltered inleakage into a nuclear power plant control room have been published (Lagus et al., 1992).

2.1 MEASURING BUILDING AIR FLOWS USING TRACER GASES

There are three principal tracer gas techniques for quantifying air flow rates within a structure; namely, the tracer dilution method, the constant injection method, and the constant concentration method. All are based on applying the conservation of mass equation to a tracer gas concentration established in a test volume. The tracer dilution method is a direct way of measuring the air flow rate extant within a test volume under ambient flow conditions by measuring the decay in tracer concentration within the volume as a function of time. The constant injection method is an indirect method, i.e., it measures the equilibrium tracer concentration within a ventilated area. This concentration can be related to the air flow rate if the tracer release rate is known. The constant concentration method is primarily a research method at this time and will not be discussed further. All three of these techniques are incorporated in the most recent revision of ASTM Standard E741-93 "Standard Test Method for Determining Air Change Rate in a Single Zone by Means of a Tracer Gas Dilution" (ASTM, 1993).

The mass balance equation and its various solutions that lead to the tests described above, have been provided in previous papers (Lagus and Persily, 1985, Grot and Lagus, 1991) and hence will not be reproduced here. These methods allow determination of either A or q. The air exchange or infiltration rate, A, is given by $A(t) = q(t)/V$ where A is in air changes per hour (h^{-1} or ACH), V is the test volume, and q(t) is the volumetric airflow rate into (or out of) the test volume. In the simplest case, the value of A represents the flowrate of "dilution air" entering the volume during the test interval. Note that this "dilution air" can be actual outside fresh air or, more generally, it can be air whose origin is not within the test volume.

2.2 TRACER GAS MEASUREMENT TECHNIQUES

Instrumental techniques used to measure tracer gas concentrations are listed in Table 2.1, along with some of the gases appropriate to each measuring instrument. All of the gases listed have been used for airflow measurements either within buildings or within individual rooms. Several characteristics of nuclear power plant CREs influence the manner in which tracer techniques are applied. First, because of the large volumes, the quantity (and therefore cost) of tracer gas required for a test becomes important. The expense depends on the cost per unit volume of tracer gas, the CRE volume, and the magnitude of the lowest tracer concentration measurable. Table 2.2 shows the range of maximum volumes that can be measured for one dollars worth of tracer gas (1994 prices). These volumes range from about 9000 Ft^3 for helium to about 5.6×10^{10} Ft^3 for SF6.

Carbon dioxide exhibits an atmospheric background of approximately 350 ppm and is also generated by both combustion sources and human metabolism. Accordingly, it is difficult to assure that a non-variable background of CO2 is maintained during a particular testing interval. In fact, detailed review and studies undertaken by the National Institute for Standards and Technology (NIST) have concluded that except for a limited set of circumstances, the use of CO2 as a ventilation tracer gas is inappropriate (Persily, 1993).

Nitrous oxide has been used as a tracer gas primarily by European researchers. However, N2O exhibits a Threshold Limit Value (TLV) of 50 ppm and hence may not be an appropriate choice for control room testing where test duration may approach eight hours. In the United States, health concerns related to the TLV of N2O have resulted in little use of N2O as a tracer.

The fact that SF6, some halocarbons and some perfluorocarbons can be measured to levels of 10 parts per trillion and below yields maximum measurable volumes in the range of 5×10^8 to 5.6×10^{10} Ft^3 per dollars worth of tracer gas. From Table 2.2 it is apparent that these gases (analyzed at the five to ten part per trillion level or even the part per billion level) are most appropriate for the large volumes encountered in Control Room Envelopes.

2.3 TRACER GAS MIXING

Because of the relatively large volume of the CRE, mixing of tracer gas is an important issue. Mixing by molecular diffusion is a slow process; however, even in naturally ventilated enclosures, there are significant convective mixing mechanisms. In mechanically ventilated environments, the air distribution system has been shown to be effective at mixing of the tracer gas (Grot and Persily, 1986). Experimentally, portable fans have been used to augment mixing of tracer at the expense of altering internal air movement patterns. The attainment of a uniform concentration can also be assisted by injecting tracer gas at several locations.

The issue of mixing of tracer gas in the CRE volume is of critical importance to the measurement and interpretation of concentration decay measurements in the determination of unfiltered inleakage. In order for the solutions to the mass conservation equation to be valid for the *entire* CRE volume it is required that the tracer be well mixed, i.e., the measured concentration anywhere in the volume is only a function of time. In practice, concentration homogeneity is taken to be +/- 10 % or better throughout the test volume (as specified in ASTM Standard E741).

A number of selected references in the published literature provide data supporting the feasibility of attaining "good mixing" of tracer within a test volume. In general, these references provide experimental tracer concentration data which show that mixing occurs fairly rapidly (within thirty minutes to, at most, one hour) in ventilated rooms or entire buildings ranging in volumes from 76 m^3 up to over of 10^5 m^3 (Alevantis and Hayward, 1990, Evans and Shaw, 1988, Shaw et al., 1993, Reardon et al., 1994).

Previous measurements by the authors in two control rooms (one a single story CRE with a volume of approximately 1700 m^3 and the other a two story CRE with a volume of approximately 4000 m^3) that were mechanically ventilated, demonstrated that it was possible to attain concentration variations of less than +/- 2% in the single story CRE and less than +/- 5% in the two story CRE, by including of a number of auxiliary mixing fans at various points with the volumes.

ASTM Standard E741 suggests that inleakage can be measured using a tracer gas technique with an error of 10% or less of the measured value. The experimental conditions considered in the examples of this study suggest that errors of half (i.e. approximately 5%) of this value are attainable.

Note that most of the instrumental techniques utilize electron capture detector gas chromatography for measurements in large volumes primarily due to tracer gas cost considerations. However, measurements have been performed in large buildings using other techniques such as infrared absorption (Potter et al., 1983, Zeurcher and Feustel, 1983) and flame ionization gas chromatography (Prior et al., 1983).

3.0 CONTROL ROOM ENVELOPE TEST METHODS

Four basic types of CRE emergency ventilation systems were considered:

1. Isolation of normal ventilation with filtered pressurization,
2. Isolation of normal ventilation with filtered recirculation,
3. Isolation of normal ventilation with filtered pressurization and recirculation,
4. Bottled Air for Pressurization.

All four basic ventilation types are amenable to a tracer gas decay test to determine unfiltered inleakage. Type 2 above can be measured by a simple tracer decay test, while types 1, 3, and 4 require both a tracer decay test and an independent measure of the pressurization flowrate.

3.1 TRACER DECAY TEST

The tracer decay test method requires only the measurement of relative tracer gas concentrations, as opposed to absolute concentrations, and the analysis required to determine A is straightforward. Equation (1) serves as a starting point for an actual test .

$$A = 1/t \ln (C_0/C) \qquad (1)$$

In practice one obtains a series of concentration versus time points and then performs regression analysis on the logarithm of concentration versus time to find the best straight line fit to the form of the equation given by equation (7). The slope of this regression yields the air exchange rate, A. Knowledge of the volume, V, allows calculation of the leakage flowrate q since

$q = A*V$.

In the case of a CRE with makeup flow, the value of q (or A) determined is the total air inleakage rate. This will consist of the unfiltered inleakage and the actual makeup flow rate. For this case an independent determination of the makeup (or pressurization) flowrate, q_{makeup}, is required. The unfiltered inleakage is then determined as follows;

$$q_{unfiltered} = q - q_{makeup} \qquad (2)$$

where q is the rate determined from the tracer concentration decay measurement (and is equal to A*V) and now represents the total "fresh air" inleakage rate into the CRE. Equation (2) can be written

$$q_{unfiltered} = A*V - q_{makeup} \qquad (3)$$

In the case of a CRE with recirculation only (no makeup) then q (or A) measures the unfiltered inleakage *directly* and q_{makeup} would be identically equal to zero.

Standard statistical arguments applied to equation (3) lead to the following estimate of the uncertainty in the determination of $q_{unfiltered}$:

$$S_{qu} = SQRT\{ (S_A)^2 + (S_V)^2 + (S_{qm})^2 \} \qquad (4)$$

where S_{qu} = Probable error in the value of $q_{unfiltered}$
S_A = Probable error in the value of A
S_V = Probable error in the value of V
S_{qm} = Probable error in the value of q_{makeup}

In Figures 1 to 5 the probable error in a given value of unfiltered inleakage for several assumed error values in measured concentration, CRE volume and inleakage rate. The assumed measurement errors attendant to each case are described below:

- CASE I Error in V = 2%, Error in q_{makeup} = 3%, Error in A = 2%
- CASE II Error in V = 3%, Error in q_{makeup} = 5%, Error in A = 5%
- CASE III Error in V = 3%, No Makeup flow, Error in A =5%
- CASE IV Error in V = 5%, Error in q_{makeup} = 10%, Error in A = 10%
- CASE V Error in V = 5%, No Makeup flow, Error in A =10%

As can be readily seen, the error in the measured value of $q_{unfiltered}$ is never very large. The error in the measured value of unfiltered inleakage is smaller for those cases having recirculation only (no makeup air). For relatively modest measurement errors in the variables needed to obtain unfiltered inleakage, the error in the resulting unfiltered inleakage

remains moderate. Note that the measurement errors in Cases I, II, and III above are considered more representative of actual practice than those in Cases IV and V.

It is possible to use equation (1) to estimate the length of time required for a given measurement error. Taking differentials of C and A and rearranging, one arrives at

$$\text{TEST TIME} = \{2*(dC/C)\}/\{(dA/A)*A\} \qquad (5)$$

where (dC/C) = Concentration measurement error
(dA/A) = Total air exchange rate measurement error

Note that the test times calculated from equation (5) use the *end* points of the measured concentration decay, i.e. the calculation assumes that only two points are used to determine the slope of the line. By performing a regression analysis on a number of concentration data points as described above, it is possible to reduce the probable error in the measured value of A or the time required to achieve a given value of probable error.

To illustrate this, a number of regression analyses were undertaken on simulated concentration decay data to calculate the probable error in the "measured" value of A as a function of elapsed time. Two series of calculations were performed for several inleakage rates (corresponding to makeup rates from 100 to 800 CFM) assuming one data point every thirty minutes and also one every fifteen minutes. An additional series of calculations was undertaken in which the inleakage rate was fixed and the number of data points sampled at each measurement time was systematically increased.

Figures 6 and 7 show probable error for various inleakage rates as a function of total test time. For a sampling interval of thirty minutes, for all cases considered, the probable error does not drop below 15% in less than six hours. Decreasing the sampling time to fifteen minutes decreases the probable error to less than fifteen percent in a four hour test. Note also that as the inleakage rate *increases*, the probable error for a given test time *decreases*. For these simulations the measurement error was assumed to be +/- 2%.

Figure 8 demonstrates the effect of increasing the number of concentration data points taken at each sampling interval. This plot illustrates calculations for A = 0.125 ACH. For higher air leakage rates, the corresponding test times to attain a given probable error will decrease. Based on this calculation it appears that sampling at eight points every half hour will ensure that the probable error will lie below 5% within four hours assuming that the uncertainty in concentration is +/- 2%.

Figure 9 provides a similar calculation assuming the concentration measurement uncertainty is +/- 5%. In this case, by taking eight concentration data points per measurement interval, the probable error in the inleakage rate will be less than 10% for test times of four hours or more.

To assure that good mixing has been achieved, a careful experimenter should obtain at least four spatially separated samples at each sampling time. Based on the above examples, a four hour test will generate an inleakage value that is precise to within +/- 10% if the individual concentration data points differ by less than +/- 5%. Higher precision is possible if the scatter in the concentration data points at each time interval is less (i.e. mixing is better).

During the actual testing, ingress and egress to the CRE should be kept to an absolute minimum. Any necessary ingress and egress should be through a single door and accomplished as rapidly as possible. No more than two door openings should be allowed during each hour of testing. At no time during a test should *two* doors to the CRE be opened simultaneously. **If two doors to the CRE are opened simultaneously, any test results should be considered invalid.**

All internal ventilation fans (such as bathroom and kitchen ventilators) in the CRE should be turned off unless they remain in operation during an emergency. These fans should be disabled in such a way as to ensure that the fans will not be accidentally energized during a test.

To assist in attainment of a well mixed volume within the CRE, one auxiliary mixing fan should be provided for each 1,000 to 2000 ft^2 of CRE floor area. Fans should be arranged throughout the CRE area to enhance air movement within the CRE. For CREs having drop ceilings, experience has shown that removal of a small fraction (5% to 10%) of the ceiling panels coupled with the placement of several of the required mixing fans above the drop ceiling will enhance air flow across the drop ceiling boundary and hence, overall air mixing within the CRE. Air samples from above the drop ceiling should be analyzed to demonstrate that good mixing has been achieved.

3.1.1 TRACER DECAY TEST PROCEDURE

Tracer gas is injected into a CRE emergency ventilation supply duct at a rate calculated to achieve a desired concentration. Experience has shown that for mechanically ventilated structures, injection of a diluted mixture of tracer gas over approximately thirty minutes enhances the mixing of gas with the test volume.

Air samples from at least four, and as many as eight, spatially diverse locations within the CRE, should be obtained at thirty minute intervals. For most conditions likely to be encountered in testing unfiltered inleakage a maximum test duration of four hours should be used. Note that it is possible to terminate a test in less than four hours if the actual regression data indicate that a 95% probable error of less than 10% (5%) has been achieved in less time.

If the CRE incorporates makeup flow in its emergency operating mode, then this makeup flowrate should be measured using a pitot tube or hot wire traverse or a tracer flow technique both *before* and *after* the tracer decay test, and the results averaged.

3.1.2 CALCULATIONS

If the CRE does not provide makeup flow in the emergency ventilation mode, the value of A calculated by regression of the tracer concentration decay data is also the *unfiltered inleakage*.

If the CRE does provide makeup flow in the emergency mode, then the values of makeup flow measured Pre and Post test are averaged:

$$q_{makeup} = (\text{Pretest Makeup Flow} + \text{Post Test Makeup Flow})/2 \qquad (6)$$

The unfiltered inleakage is then given by equation (3) rewritten here as equation (7):

$$q_{unfiltered} = A*V - q_{makeup} \qquad (7)$$

Note that regression analysis should be performed after the first three sampling intervals and should be continued for each subsequent sample interval. When then 95% probable error calculated in the regression drops below 10% (or 5%), air sampling and analysis may be discontinued. As noted above, the maximum test interval contemplated in the tracer decay test is approximately four hours.

3.2 CONSTANT FLOWRATE TEST PROCEDURE

The constant flowrate test is an alternate technique that avoids the requirement for accurate knowledge of the CRE volume. Uncertainty in the accurate knowledge of CRE volume can contribute to the uncertainty in the final measured result. Also, for CRE's that exhibit high makeup air flowrates (values of A greater than approximately 1.5, or makeup flows of 2500 CFM for a 100,000 cubic foot CRE), tracer concentration decay may occur very quickly. Also, the tracer gas analyzer may not possess a sufficiently broad measurement range to encompass data taken over a four hour interval.

Accordingly a tracer test that uses a constant flowrate injection of tracer gas into the CRE while measuring the resulting concentrations at selected locations can be used. For the following derivation the return air system is included in the CRE volume. If it is assumed that the volume is well mixed, one can apply conservation of mass to the elements of a CRE shown in Figure 10, and arrive at equation (8):

$$Q_{in} = Q_{sup} ((C_{sup}/C_r) - 1) \qquad (8)$$

where Q_{in} = Inleakage (anywhere into CRE)
Q_{sup} = Total Supply Flowrate
C_{sup} = Equilibrium Concentration in Supply duct
C_r = Equilibrium Concentration at end of return duct

In deriving equation (8) it is assumed that tracer is injected at a constant flowrate into the supply duct.

Note that this expression does not require knowledge of the control room volume. Standard statistical arguments applied to equation (8) lead to the following estimate of the uncertainty in Q_{in} :

$$S_{inleak} = SQRT\{ (S_{qsup})^2 + (S_{csup})^2 + (S_r)^2 \} \qquad (9)$$

where S_{inleak} = Probable error in the value of Q_{in}
S_{qsup} = Probable error in the value of Q_{sup}
S_{csup} = Probable error in the value of C_{sup}
S_r = Probable error in the value of C_r

Note that there are the same number of terms in equation (9) as in equation (4), but two of them are related to the gas analyzer measurement error and one to the error in flowrate measurement. These errors are intrinsically more amenable to statistical treatment than is the control room envelope volume.

Figures 11 and 12 provide a graphical illustration of the uncertainty in the measured inleakage value using this technique. Note that what is plotted is the minimum measurable inleakage as a function of total supply flowrate (Makeup flowrate plus return flowrate). Any value of inleakage greater than the minimum shown can be determined reliably by this method. The fact that there is a minimum value of inleakage measurable by this technique arises from the ability of the measurement device to discriminate between two concentrations that are close in value. This technique is complementary to that provided in Section 3.1 and is provided as a way to eliminate the uncertainty engendered by imprecise knowledge of the control room envelope volume and to allow testing in CREs possessing a high value of makeup air flowrate.

3.2.1 CONSTANT FLOW TEST PROCEDURE

Tracer gas is injected into a CRE emergency ventilation supply duct at a rate calculated to achieve a desired concentration. For this test the target tracer gas concentration should lie in the middle of the measurement range of the gas analyzer.

An approximate value of the total air change rate is calculated based on a measured or assumed value of the makeup flowrate. This value, A_A, can be used to estimate the length of time that must elapse before concentration equilibrium will occur within the CRE. If one starts with a zero initial concentration and injects at a constant rate, it can be shown that the tracer gas will reach 95% of the equilibrium concentration within the CRE volume after a time equal to $3/A_A$.

Air samples from at least four spatially diverse locations within the CRE should be obtained at thirty minute intervals. Air samples must also be taken from the supply duct as well as the beginning and end of the return duct of the control room emergency ventilation system. For most conditions likely to be encountered in testing unfiltered inleakage, a maximum test duration of four hours should be used.

The total mechanical air supply flowrate (makeup plus recirculation) into the CRE should be measured using a pitot tube or hot wire traverse or a tracer flow technique.

3.2.2 CALCULATIONS

Tracer gas concentration data are treated by forming the mean of five measurements for each of the two concentration values, C_{sup} and C_r. The CRE Supply Rate is calculated by averaging the Pre and Post Test Supply Flowrates as follows:

$$Q_{sup} = (\text{Pretest Supply Flow} + \text{Post Test Supply Flow})/2 \qquad (10)$$

The unfiltered inleakage is then given by inserting these concentration values and flowrate into equation (8) to obtain Q_{in}.

3.3 DIRECT TRACER GAS INLEAKAGE TEST

Direct measurement of leakage (leak testing) using a tracer gas (usually helium and, less frequently, sulfur hexafluoride) is a powerful technique that is used extensively in the micro-electronics and defense/aerospace industries. In this technique, an object to be tested is either filled with tracer gas and the periphery monitored for leaking tracer, or the exterior is flooded with tracer gas and the interior is sampled for the presence of tracer gas. The measurement of non-zero quantities of tracer gas in either of these situations provides unambiguous evidence for the existence of leakage. The resulting tracer gas concentration can be used to infer leakage rate for a suitably designed experiment.

It is possible to apply this same reasoning to nuclear power plant CRE's. If one imagines a ventilated test volume surrounded by tracer gas as shown in Figure 13, leakage into the volume can be determined using conservation of mass. For this case;

$$Q_{in} = (C/C_0) \times Q_{makeup} \qquad (11)$$

where Q_{in} = unfiltered inleakage rate

Q_{makeup} = makeup flowrate

C = tracer concentration in CRE

C_0 = tracer concentration outside CRE.

In practice it is possible to challenge one boundary of the CRE at a time (if necessary for experimental convenience) with a concentration of tracer gas. Any tracer measured within the CRE would provide unambiguous evidence of inleakage through that boundary. Furthermore, by measuring the challenge concentration and the makeup flowrate within the CRE it is possible to calculate an inleakage rate across this boundary using equation (11) above.

An experimental complication to this technique is the potential for exhaust reentrainment to occur. If air containing tracer gas is exhausted from the CRE, it may reenter the CRE from the outside via the makeup fan. This reentrainment would render the results of any calculation based on equation (11) meaningless.

For those CRE's that possess filtered makeup air (i.e. filtered pressurization emergency ventilation system), it is possible to use a perfluorocarbon tracer and eliminate the possibility of reentrainment into the CRE. It has been documented that perfluorocarbon vapors exhibit exceptionally long hold-up times on carbon. Perfluordimethlycyclobutane (PDCB) exhibits at least thirty minutes hold-up in a nuclear industry standard two inch bed, while perfluoromethylcyclohexane (PMCH) exhibits a hold-up that is easily six times this value (Pearson et al., 1992). These vapors also possess a high detection sensitivity (approaching that of SF6) when analyzed using the techniques of electron capture gas chromatography.

Accordingly, if one were to challenge the exterior of a CRE with a moderate concentration of PMCH, one could sample inside the CRE for up to three hours without any concern about reentrainment of tracer gas. Measurement of PMCH within the CRE would provide unambiguous evidence of inleakage. Use of equation (11) above would allow a calculation of inleakage to be made.

For CREs that are wholly located within a plant building, it may be possible to seed the HVAC system that supplies the regions surrounding the CRE directly with tracer gas. Injection of a constant, known flowrate of tracer gas into the supply systems coupled with measurement of the resulting concentration in the regions surrounding the CRE would allow use of equation (8) to infer unfiltered inleakage.

Note that it is possible to use builders plastic (Visqueen) mounted on a lightweight wooden or metal framework to create a test volume surrounding some of the boundary walls of the CRE. This could be useful if one of the boundaries was, for instance, an outside wall or a roof. Mixing of the tracer gas within this plastic tent could be easily accomplished using several oscillating fans. The structure itself would not have to last longer than a few days. Using a combination of injection into rooms adjacent to the CRE and into fabricated plastic tents that enclose adjacent regions not contained within rooms, allows tracer inleakage testing to be performed on many CREs that rely on filtered pressurization during emergency operation.

3.3.1 DIRECT INLEAKAGE TEST PROCEDURE

Tracer gas is injected into the supply that provides ventilation air to the region surrounding the CRE (or into a specially fabricated plastic tent) at a rate calculated to achieve a desired concentration. For this test the target tracer gas concentration within the region(s) surrounding the CRE should be approximately 1 ppm. Anticipated concentrations within the CRE should lie in the middle of the measurement range of a second gas analyzer.

An approximate value of the total air change rate is calculated based on a measured or assumed value of the makeup flowrate. This value, A_A, can be used to estimate the length of time that must elapse before concentration equilibrium will occur within the CRE. If one starts with a zero initial concentration and injects at a constant rate, it can be shown that the tracer gas will reach 95% of the equilibrium concentration within the CRE volume after a time equal to $3/A_A$.

Air samples from at least four spatially diverse locations within the CRE should be obtained at thirty minute intervals. Air samples must also be taken from each region surrounding the CRE as well as on the delivery side of the charcoal filter in the control room emergency ventilation system. If significant breakthrough of tracer is detected at this point, the test must be terminated. For most conditions likely to be encountered in testing unfiltered inleakage a maximum test duration of three hours should be used.

The makeup flowrate supplied to the CRE should be measured using a pitot tube or hot wire traverse or a tracer flow technique.

3.3.2 CALCULATIONS

Tracer gas concentration data are treated by forming the mean of the final CRE concentration measurements and the final surrounding region concentration measurements to provide values of C and C_0 as required in equation (11).

The CRE Makeup Rate is calculated by averaging the Pre and Post Test Makeup Flowrates as follows:

$$Q_{makeup} = (\text{Pretest Makeup Flow} + \text{Post Test Makeup Flow})/2 \qquad (12)$$

The unfiltered inleakage, Q_{in} , is then calculated from equation (11).

4.0 CONCLUSIONS AND RECOMMENDATIONS

The preceding has provided a brief introduction to the principles of tracer gas ventilation measurements. Three different methods that allow assessment of unfiltered inleakage into a nuclear power plant Control Room Envelope (CRE) using

tracer gas techniques have been described. It has been shown that unfiltered inleakage within a CRE *can* be measured in a straightforward manner to better than +/- 10% in periods of less than eight hours.

The ability to measure actual inleakage in an operating ventilation system relates directly to the entire issue of safety and habitability of operating nuclear power plants during accident conditions as specified in GDC 19. An experimental method (or methods) to measure inleakage will result in more reliable estimates of Control Room Envelope integrity, and hence operator safety, in the event of a toxic gas release or radiological accident. The ability to reliably demonstrate the safety of control room occupants under accident conditions will provide immeasurable benefits both to the federal government and to the nuclear power generating industry.

5.0 ACKNOWLEDGMENT

This work was supported in part by a US Nuclear Regulatory Commission Small Business Innovation Research (SBIR) Grant, number NRC-04-94-070.

6.0 REFERENCES

Alevantis, L.E., and S.E. Hayward, "The Feasibility of Achieving Necessary Initial Mixing when using Tracer Gas Decays for Ventilation Measurements," in *Proceedings of the Fifth International Conference on Indoor Air Quality and Climate*, Toronto Canada, 1990.

American Society for Testing and Materials, ASTM Standard E779-87 "Standard Test Method for Determining Air Leakage by Fan Pressurization," Philadelphia, 1992.

--ASTM Standard E741-93 "Standard Test Method for Determining Air Change Rate in a Single Zone by Means of a Tracer Gas Dilution," Philadelphia, 1993.

Evans, R.G., and C.Y. Shaw, "A Multiposition Tracer Gas Sampling System for Building Air Movement Studies," in *AIVC Technical Note 24*, Air Infiltration and Ventilation Centre, University of Warwick, England, 1988.

Hayes, J.J., D.R. Moeller, and W.P. Gammill, "NRC Study of Control Room Habitability," in *Proceedings of the 18th DOE/NRC Air Cleaning Conference*, August, 1984.

Grot, R.A., and P.L. Lagus, "Application of Tracer Gas Analysis to Industrial Hygiene Investigations," in *Proceedings of the 12th Air Infiltration and Ventilation Centre Conference*, Ottawa, 1991.

Grot, R.A., and A.K. Persily, "Measured Infiltration and Ventilation Rates in Eight Large Office Buildings," in *Measured Air Leakage of Buildings*, ASTM STP 904, H.R. Trechsel and P.L. Lagus, Eds., ASTM, Philadelphia, 1986.

Hickey, E.E., G.A. Stoetzel, P.C. Olsen, and S.A. McGuire, "Air Sampling in the Workplace," *NUREG-1400*, USNRC, Washington, 1991.

Lagus, P.L., and A. Persily, "A Review of Tracer Gas Techniques for Measuring Airflows in Buildings," ASHRAE Trans. Vol. 91, 1985.

Lagus, P.L., V. Kluge, P. Woods, and J. Pearson, "Tracer Gas Testing Within the PaloVerde Nuclear Generating Station," in *Proceedings of the 20th DOE/NRC Air Cleaning Conference*, Boston, 1988.

Lagus, P.L., L. DuBois, K. Fleming, and J. Brown, "Control Room Inleakage Testing Using Tracer Gases at Zion Generating Station," in *Proceedings of the 22nd DOE/NRC Air Cleaning Conference*, Denver, 1992.

Moeller, D.W. and J.P. Kotra, "Commentary on Nuclear Power Plant Control Room Habitability," in *Proceedings of the 18th DOE/NRC Air Cleaning Conference*, August, 1984.

Murphy, K.G. and K. M. Campe, "Nuclear Power Plant Control Room Ventilation System Design for Meeting GDC 19," in *Proceedings of the 13th AEC Air Cleaning Conference*, August, 1974.

Pearson, J.P., K.M. Fleming, J.R. Hunt, and P.L. Lagus, "Replacement Tracer Agents for the In-place Testing of Adsorbers in NATS," in *Proceedings of the 22nd Doe/NRC Nuclear Air Cleaning and Treatment Conference*, Denver, 1992.

Persily, A.K., "Ventilation, Carbon Dioxide and ASHRAE Standard 62-1989," *ASHRAE Journal*, September, 1993.

Persily, A.K., and L.K. Norford, "Simultaneous Measurements of Infiltration and Intake in an Office Building," *ASHRAE Trans.*, Vol. 93, Pt. 2, 1987

Potter, N., J. Dewsbury, and T. Jones, "The Measurement of Air Infiltration Rates in Large Enclosures and Buildings," in *Air Infiltration Reduction in Existing Buildings*, proceedings of the Fourth Air Infiltration Centre Conference, Elm Switzerland, 1983.

Prior, J., J. Littler, and M. Adlard, "Development of Multi-tracer Gas Technique for Observing Air Movement in Buildings," *Air Infil. Rev.*, Vol. 4, No. 3, 1983.

Reardon, J.T., C.Y. Shaw, and F. Vaculik, "Air Change Rates and Carbon Dioxide Concentrations in a High Rise Office Building," *ASHRAE Trans.*, No. 100, Pt. 2, 1994.

Shaw, C.Y., J.S. Zhang, M.N. Said, R.J. Magee, and F. Vaculik, "Effect of Air Diffuser Layout on the Ventilation Conditions of a Workstation," *ASHRAE Trans.*, No.99, Pt.2, 1993.

Stage, S.A., "Computer Codes for Control Room Habitability (HABIT), NUREG/CR6210, US NRC, Washington, 1995

Vavasseur, C., "Application of Tracer Gas Methods to the Measurement of Ventilation Parameters in Nuclear Power Plants and Various Industrial Sectors," in *1st International Symposium on Ventilation for Contaminant Control*, Toronto, Canada, 1985.

Zuercher, C.H. and H. Feustel, "Air Infiltration in High-rise Buildings," in *Air Infiltration Reduction in Existing Buildings*, proceedings of the Fourth Air Infiltration Centre Conference, Elm Switzerland, 1983.

TABLE 2.1

TRACER GASES AND MEASUREMENT DEVICES

Techniques	Gases
Thermal Conductivity Detector	H_2, He, CO_2
Electron Capture Gas Chromatograph	SF_6, Refrigerants, Perfluorocarbons
Flame Ionization Gas Chromatograph	C_2H_6
Infrared Absorption Continuous Analyzer	CO, CO_2, SF_6, N_2O, C_2H_6, CH_4

TABLE 2.2

RELATIVE GAS COSTS
TAKING DETECTABILITY INTO ACCOUNT*

Gas	Detectable Concentration (ppm)	Maximum Measurable Volume per Dollar Ft^3	m^3
He	300	9.3×10^3	2.6×10^2
CO2	350**	3.2×10^4	8.9×10^2
N2O	1	2.8×10^6	7.9×10^4
SF6	5×10^{-6} (a)	5.6×10^{10}	1.6×10^9
SF6	1 (b)	5.6×10^4	1.6×10^3
CBrF3	5×10^{-5}	5.0×10^8	1.4×10^7
PDCB (c)	10×10^{-6}	1.3×10^9	3.7×10^7

* Based on 1994 Gas Prices for Size 1A Gas Cylinders. (1 Kgm liquid for PDCB)

** Average Background Concentration in the atmosphere.

(a) Detection by Electron Capture Gas Chromatography.

(b) Detection by Continuous IR Monitor.

(c) Perfluorodimethylcyclobutane

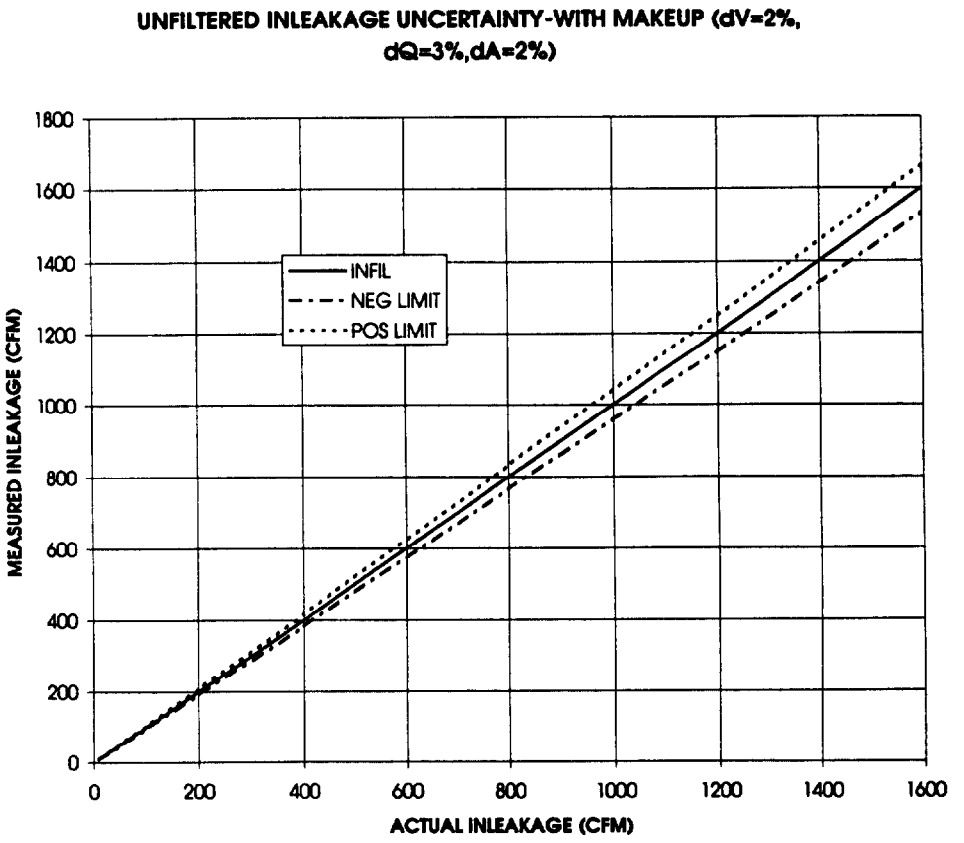

Figure 1. Unfiltered Inleakage with Makeup-Case I

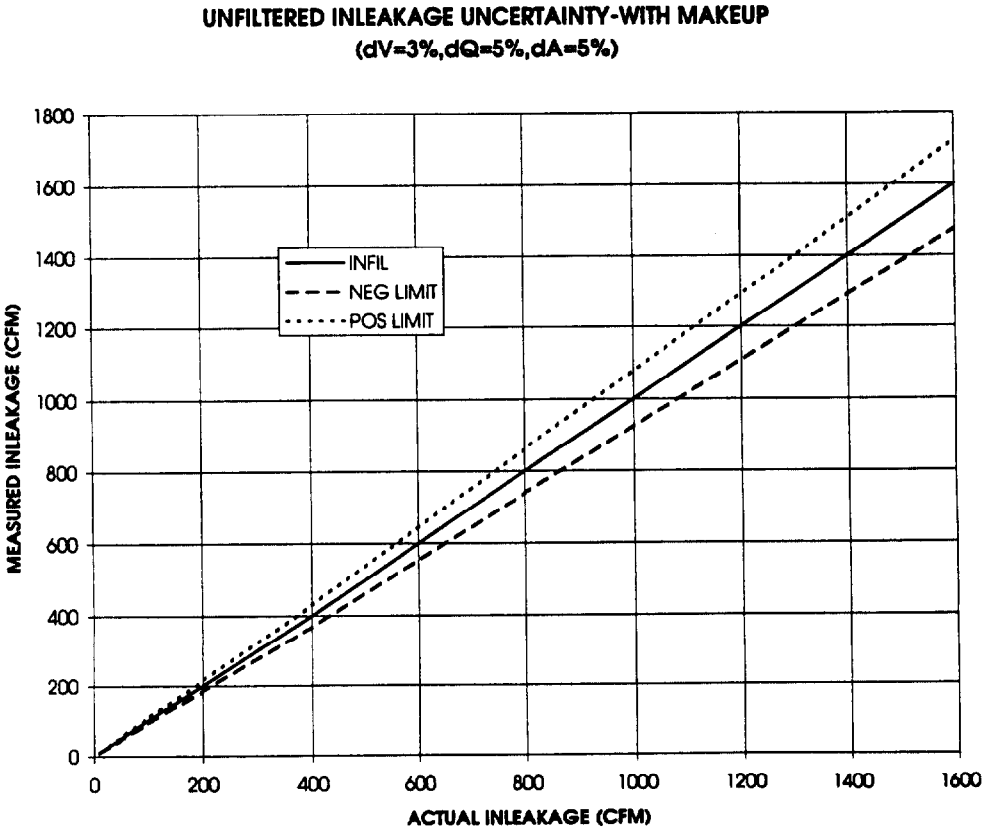

Figure 2. Unfiltered Inleakage with Makeup-Case II

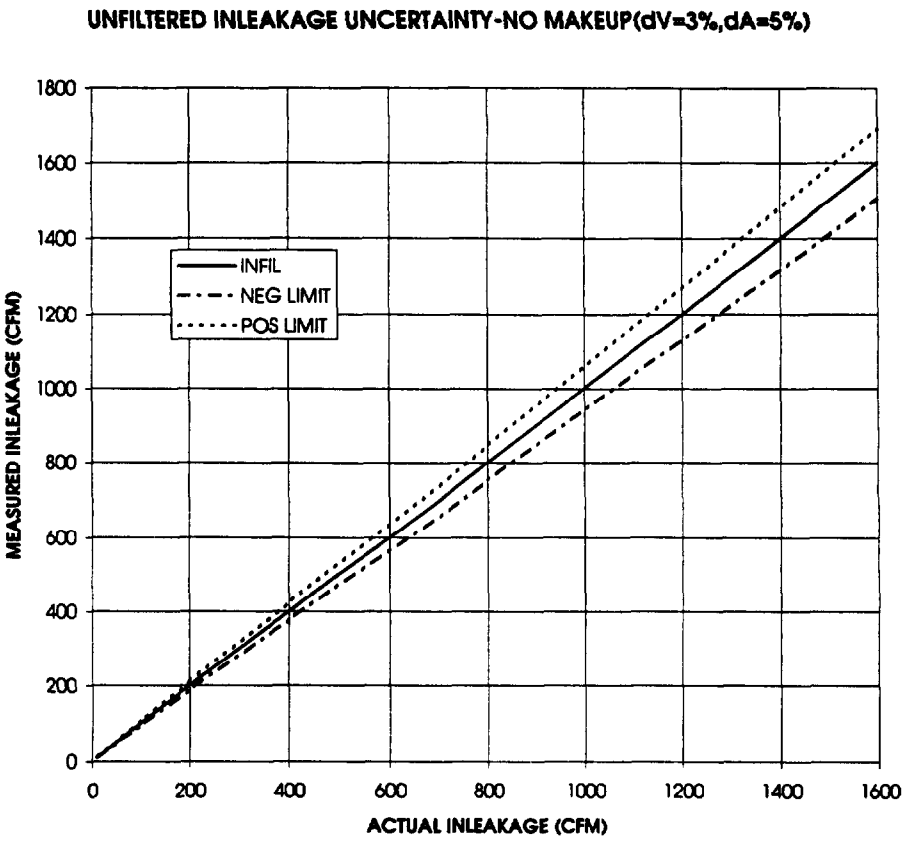

Figure 3. Unfiltered Inleakage no Makeup-Case III

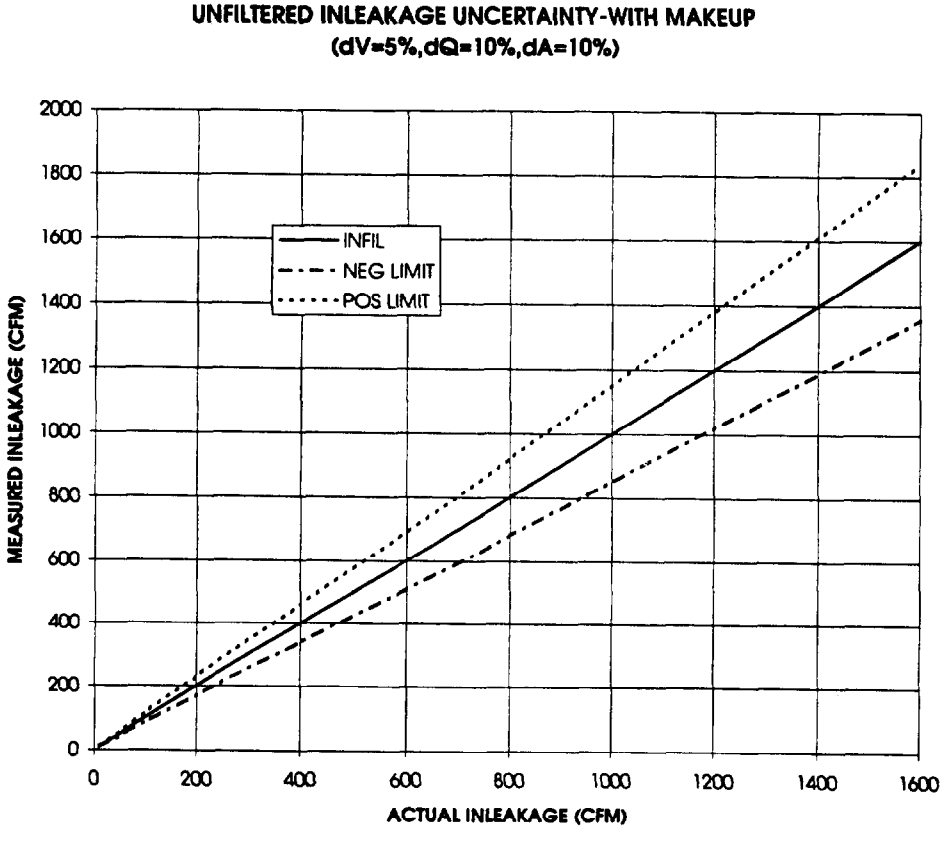

Figure 4. Unfiltered Inleakage with makeup-Case IV

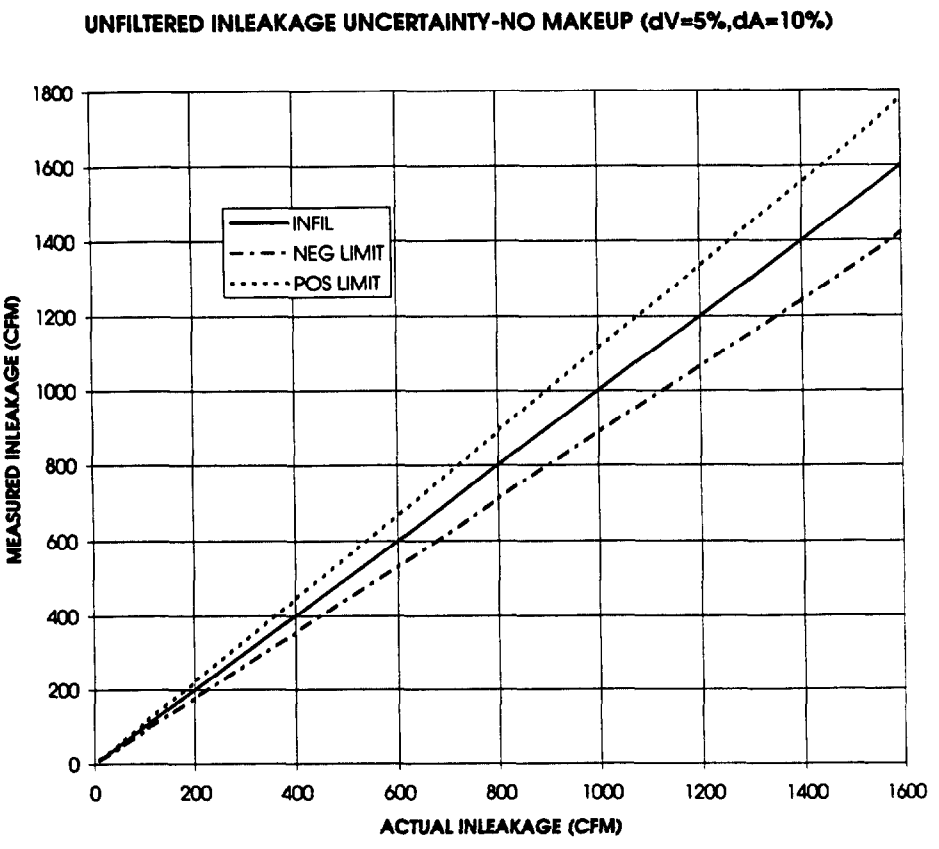

Figure 5. Unfiltered Inleakage no Makeup-Case V

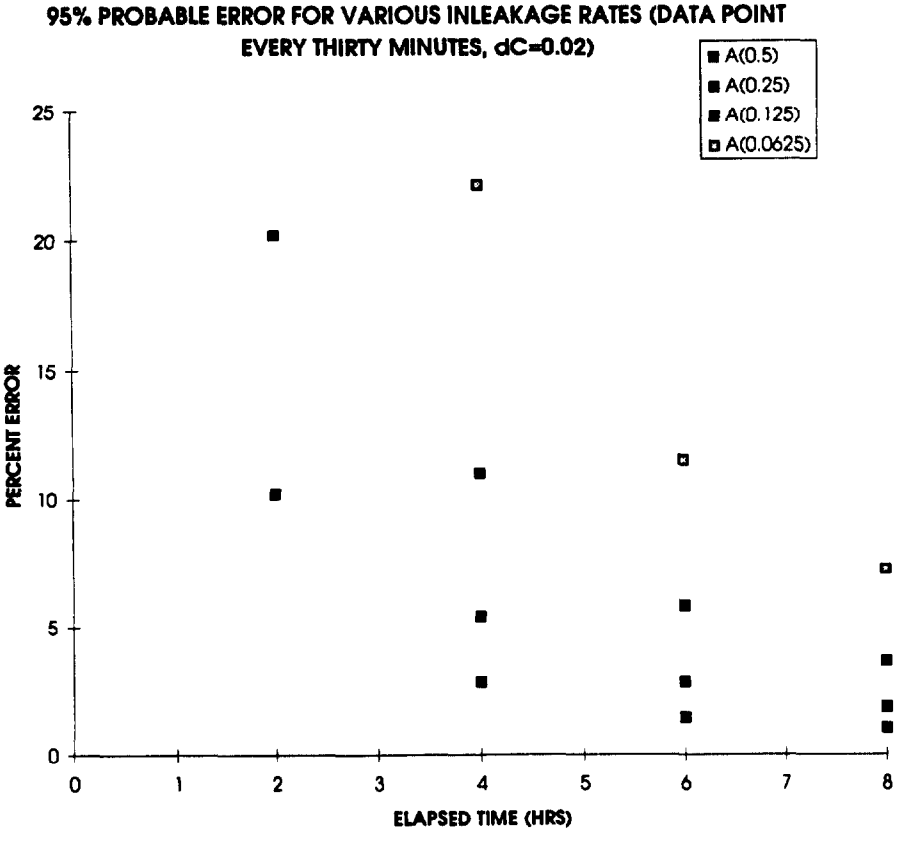

Figure 6. Probable Error-Data Point Every Thirty Minutes

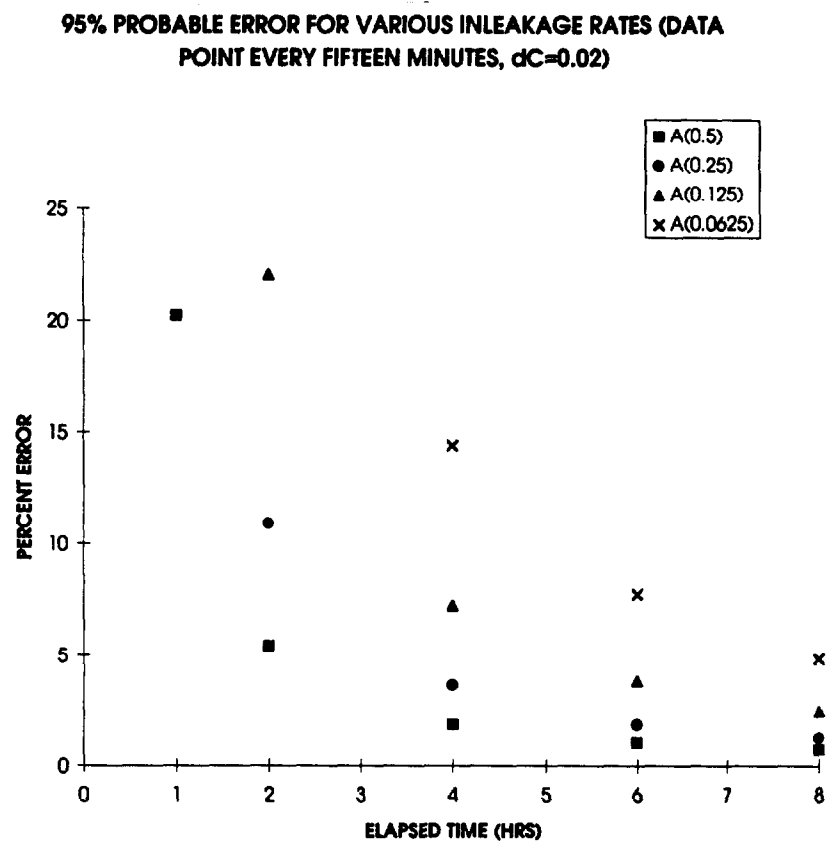

Figure 7. Probable Error-Data Point Every Fifteen Minutes

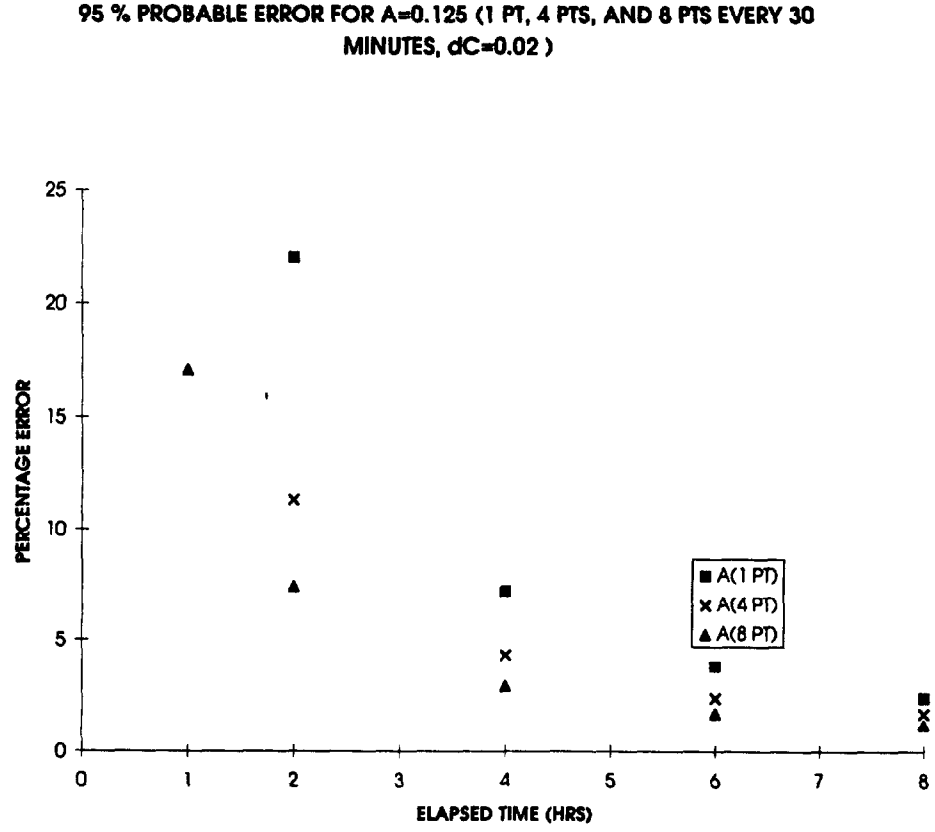

Figure 8. Probable Error-Multiple Points, dC=0.02

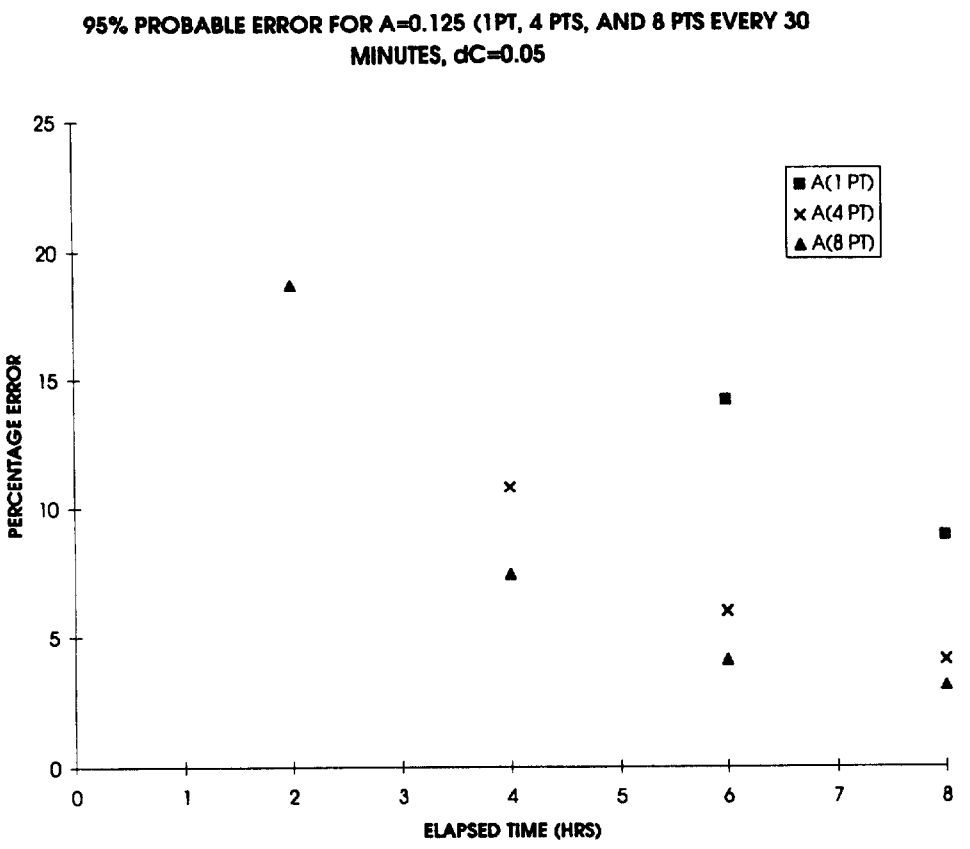

Figure 9. Probable Error- Multiple Points, dC=0.05

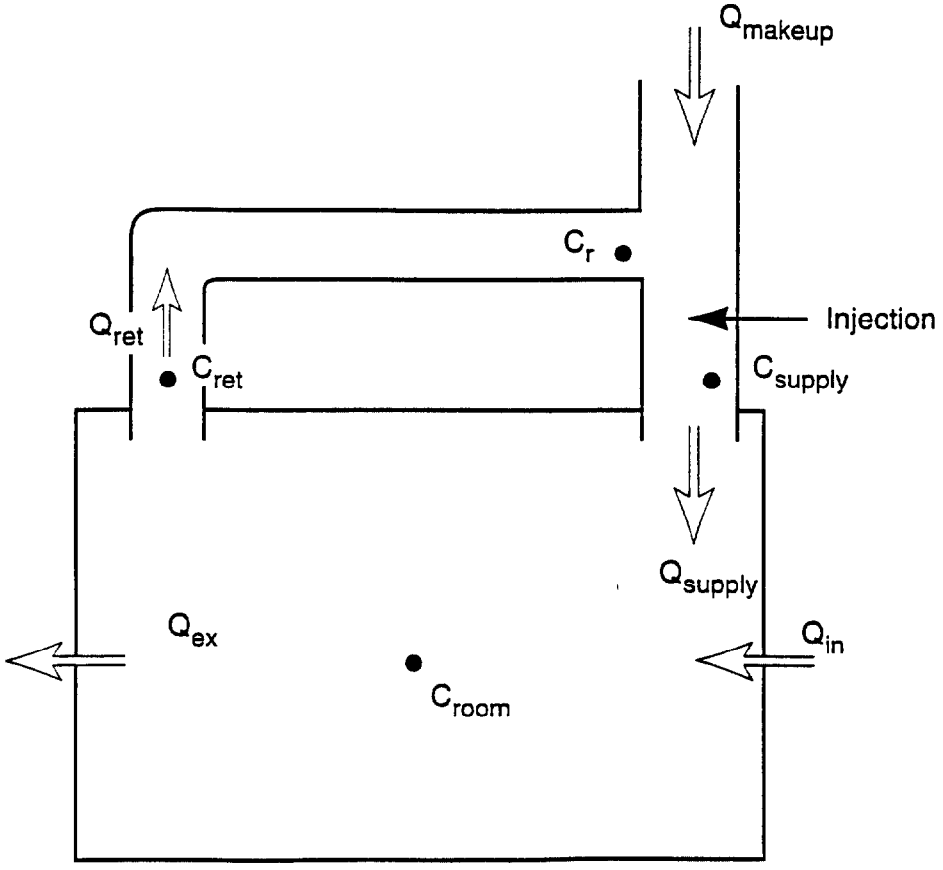

Figure 10. Control Room Envelope Test Parameters

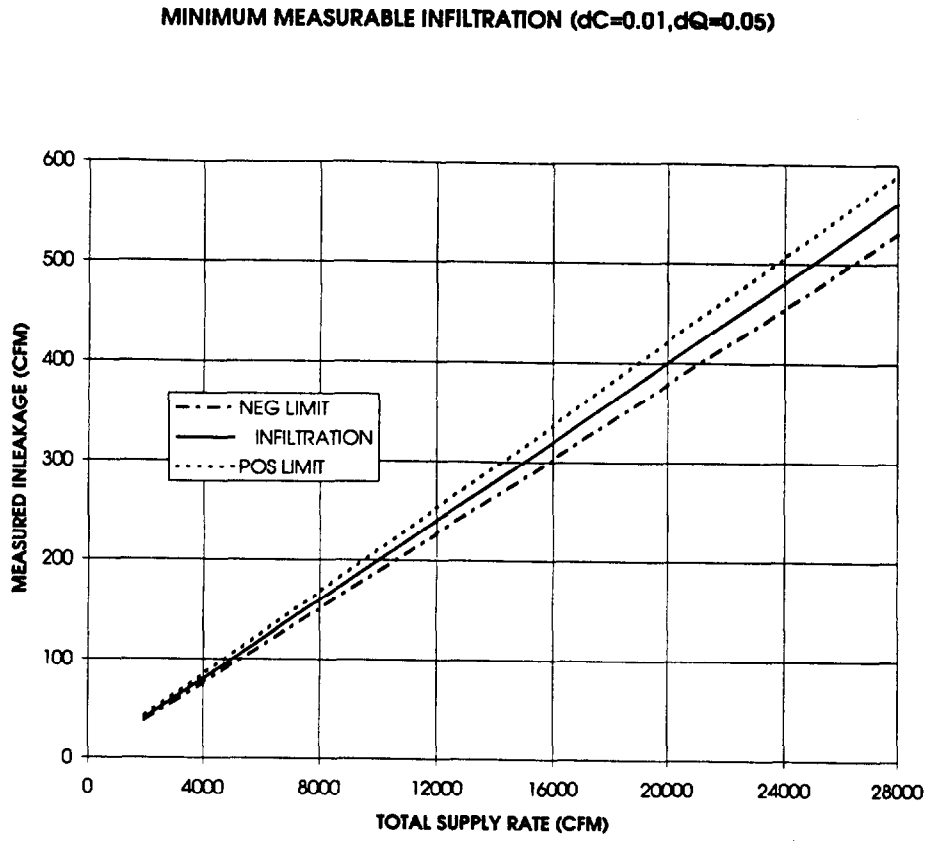

Figure 11. Minimum Measurable Inleakage, dC=0.01, dQ=0.05

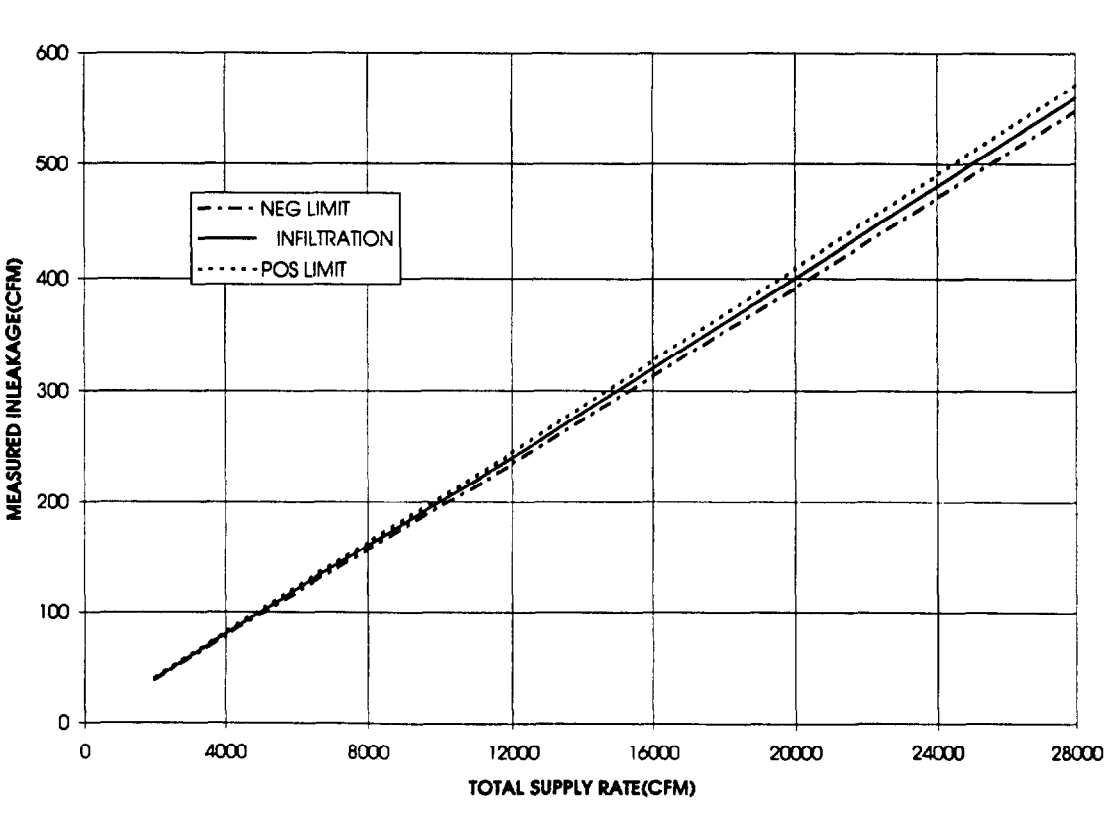

Figure 12. Minimum Measurable Inleakage, dC=0.005, dQ=0.02

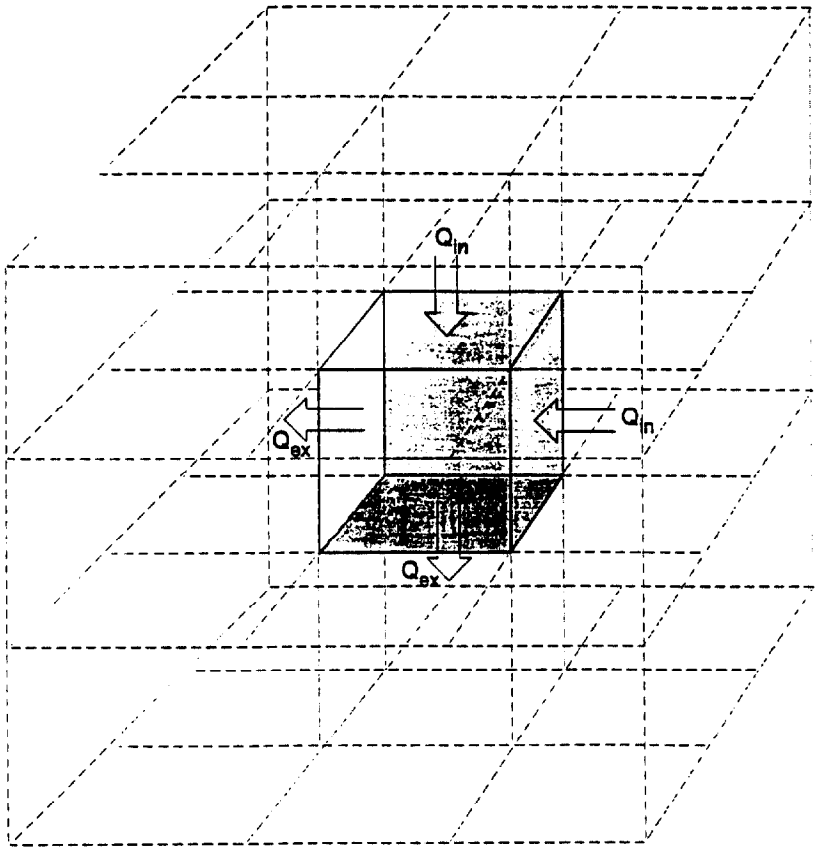

Figure 13. Control Room Envelope and Surrounding Regions

DISCUSSION

PORCO: I will exercise the chairman's prerogative and ask you a couple of very quick questions. How many control rooms has your protocol been applied to? How good was the data correlation? If you would, also mention how you achieved the good mixing that you mentioned in your paper.

LAGUS: We have done three plants, two systems in two of them and one in one of them including a control room. In terms of the uniformity test protocols, we were getting mixing of better than about 3%.

PORCO: What was your correlation between plants?

LAGUS: I do not understand what you mean by correlation between the plants.

PORCO: Was your inleakage consistent at different plants?

LAGUS: Very different from plant to plant.

PORCO: By about how much?

LAGUS: By a factor of six.

PORCO: The last part of my question was about mixing, how do you achieve good mixing of the tracer gas?

LAGUS: We achieved mixing by careful placement of the rather large twenty-four inch diameter mixing fans. We used six or eight of them in conjunction with the control room recirculation system to provide additional mixing. We would make measurements at a minimum of six or eight points at diverse locations and then run standard deviations on the numbers. In a single source control we were able to obtain mixing with relative standard deviations on the order of 3%. We did one at a two story control room where we got mixing of about 5%.

PHILIPPI: How does the control room leakage measurement protocol accommodate wind pressure changes from the outside, or pressure excursions in adjacent rooms? How do they affect the leakage of your control room?

LAGUS: On these tests we normally measure the control room envelope differential pressure between the inside and the outside, however that happens to be defined for a particular plant. Instead of accommodating, we basically measure it. What we are asking is, how does the system perform as it is being used? We have no control over the wind. What we have to do is be a) aware of the wind, b) be aware of the pressure characteristics, and then c) measure the performance of the system as it is being affected by the external variables. For instance, we try to minimize ingress and egress and things like that, but naturally occurring variables are the same variables that a plant is going to be subjected to. So, we are much more interested in finding out how it behaves under those circumstances than trying to make calculations or allowances for it. What you are going to find is that the effects of wind are certainly going to be a secondary effect, simply because, for most of the winds, you are not going to have wind pressures that are comparable to the kinds of pressures that one actually tries to generate inside a control room.

ENGELMANN: We know that there is in-leakage into ventilation systems when operating even in recirculation mode. Also, the air exchange of the room is enhoused with fans or recirculation are operating. Will you please discuss how you account for this?

LAGUS: The tracer technique incorporates all inleakage paths into the control room envelope (CRE), even those due to the CRE ventilation system, if that system or part of it is located outside the CRE boundary. Since the tracer technique allows one to measure the inleakage under actual operating conditions, if air exchange (unfiltered inleakage) is enhanced by operation of fans or recirculation, the data will reflect that. In fact we have undertaken a test in one control room in which the difference in inleakage was measured between the case of the pressurizing fan operating and not operating.

VARIABLE PATTERN CONTAMINATION CONTROL UNDER POSITIVE PRESSURE

Hardy M. Philippi
Chalk River Laboratories
Atomic Energy of Canada Limited
Chalk River, Ontario, Canada K0J 1P0

Abstract

Airborne contamination control in nuclear and biological laboratories is traditionally achieved by directing the space ventilation air at subatmospheric pressures in one fixed flow pattern. However, biological and nuclear contamination flow control in the new Biological Research Facility, to be commissioned at the Chalk River Laboratories in 1996, will have the flexibility to institute a number of contamination control patterns, all achieved at positive (above atmospheric) pressures. This flexibility feature, made possible by means of a digitally controlled ventilation system, changes the facility ventilation system from being a relatively rigid building service operated by plant personnel into a flexible building service which can be operated by the facility research personnel. This paper focuses on and describes the application of these unique contamination control features in the design of the new Biological Research Facility.

I. Introduction

Airborne contamination control in nuclear and biological laboratories is traditionally achieved by directing the space ventilation air at subatmospheric pressures in one fixed flow pattern. However, in the new Biological Research Facility (BRF) to be commissioned at the Chalk River Laboratories in 1996, the ventilation system will have the flexibility to effect a number of contamination control patterns at positive (above atmospheric) pressures. This pattern flexibility feature, made possible by means of a digitally controlled ventilation system, provides the researcher with the ability to design contamination control patterns which serve the unique requirements of each research program and to accommodate abnormal ventilation system conditions. The ventilation system is therefore no longer a relatively rigid building service operated by plant personnel, but it can become the direct responsibility of the research personnel who are intimately aware of animal welfare and the research program requirements. The requirement to pressurize the facility arises from the fact that the animal housing rooms, laboratories which may temporarily house animals and the animal care support rooms must be pressurized with High-Efficiency Particulate Air (HEPA) filter ventilation air in order to minimize the intrusion of air-borne contamination (viruses and bacteria) from the outside.

This paper focuses on and describes this unique contamination control approach as it is applied in the BRF. (Ref. Figure 1 Main Floor Plan & Figure 2 Upper Floor Plan). The BRF classification, hazards, special requirements and a brief ventilation system description are given to provide a facility overview and an appreciation of its contamination control issues.

II. Facility Usage, Hazards, Classification & Requirements

The new BRF will be used to conduct animal-based biological research work on rodents using carcinogens, radiation and radioisotopes. The research is primarily to study the carcinogenic effects of ionizing radiation separately and in combination with other materials and the facility is intended to support these studies at the molecular, cellular and whole-animal levels.

Hazardous materials used in the research laboratories are limited to small quantities of:

- carcinogenic tumor initiators (DMBA and MNNG) and promoters (TPA and Mezerein);
- Radioisotopes (Tritiated water, tritiated organic compounds, C-14 amino acid or other C-14 compounds); and
- uranium oxide (dust).

The external beam radiation facilities utilizes Co-60 and Sr-90. [1]

The facility is classified as CRL Category 2, that is, one where the potential for a significant hazard is limited to the facility and its operators. [2]

The BRF specification included the following requirements to provide

- animal housing and care to meet and exceed current Canadian Council on Animal Care standards [3];
- a research environment consistent with quality-assured research programs;
- effective, predictable and flexible contamination control means under both normal * and abnormal ** operating conditions;
- a safe, licensable laboratory; and
- ALARA working conditions for the facility operating and research staff.

III. Ventilation System Description

Ventilation System:

The supply side of the ventilation system consists of two parallel roof-mounted draw-through air-handling and air-conditioning units, each rated at 50% of the total building ventilation air supply rate. Each unit has means to prefilter, heat, cool/dehumidify, reheat, supply and final filter the building fresh air supply to meet the building space air change and environmental conditioning requirements. Supply air terminal reheat is provided to meet the specific temperature requirements of each room and laboratory. The ventilation exhaust side consists of the following six main exhaust systems:

E-1/2/3 General Building Exhaust ***
E-4/5/6 Fumehood and BSC Exhaust ***
E-7/8/9 Carcinogen Area Exhaust ***
E-10 Janitor and Washroom Exhaust,
E-12/13 Scavenger and Solvent Storage Exhaust and
E-14/15 Cage Washer Exhaust

---

* Normal operating conditions are day-to-day operations when all electrical power demands are met from the local electrical power utility, all ventilation system equipment is functioning or available and all ventilation and contamination control requirements are achieved.

** Abnormal operating conditions are when the facility is on limited standby diesel-generated electrical power or when vital ventilation equipment is not available because of failure or maintenance outage.

*** Any two fans can achieve full system exhaust rate.

Due to severe budget limitations this project could not support the provision of 100% standby boilers, diesel generated electrical power and ventilation system redundancy. Alternative design features, described in Section VII, were therefore provided to ensure continuous normal operating condition ventilation rates to all rooms housing animals under both maintenance outage and power-failure abnormal condition scenarios.

Ventilation System Control:

Ventilation system supply and exhaust flow control is by Direct Digital Control (DDC). The DDC system to operator interface is by means of a central computer unit (CCU), which is basically a personal computer complete with a keyboard , screen and various in/output devices. The CCU directs and monitors a number of remote processing units, which in turn regulate the terminal equipment controllers.

The system is programmed to automatically regulate the ventilation system variable volume ventilation (VAV) boxes, equipment start/stop and damper or valve open/shut functions to one specific contamination control pattern until it is manually or automatically told to change to another pattern. Each pattern is a memorized number of ventilation system VAV box-flow-rate set points together with preset start-stop functions for several lesser ventilation systems. Pattern changes are initiated automatically when an abnormal condition is detected or manually to suit a different research program requirement. The system continually monitors specific system conditions and will automatically change to a suitable abnormal conditions pattern.

The facility operator can automatically or manually monitor and record facility environmental conditions, select preprogrammed operational scenarios or manually adjust individual system parameters and receive system annunciation and failure alarms. The remote processing units will stand alone and provide local system control even though they are disconnected from the CCU.

IV. Ventilation System Balancing

Balancing the BRF ventilation system supply and exhaust flow rates is vital to understanding, developing and documenting the various ventilation air flow patterns required to meet the normal and abnormal facility operations requirements. A basic spread sheet was prepared to account for and balance the supply, exhaust and in/out leakage for each of 68 spaces in the facility. Spaces varied in size from a 37 m-(120') long irradiation room to a 1 m-(3.3') deep janitor's closet under normal conditions. This basic normal operations ventilation system balance pattern is the starting point for the development alternative normal and abnormal operations patterns. All patterns have to be checked against the capabilities of the fan systems and the 110 space supply and exhaust VAV boxes. It should be noted that the accuracy and control range of VAV boxes is ± 24 L/s (50 cfm) of their set point down to about 20% of their rated flow. A number of VAV boxes serving nonanimal related spaces may be shut off under abnormal conditions. Figure 3 is a typical balancing spread sheet for rooms Y144, Y146 and Y148. Note that all the exhaust, transfer, out-leakage, supply and in-leakage rates are rigorously accounted for. It is through this form of accounting that any room rate changes being considered for a new pattern can be assessed for their impact on the whole building ventilation system capability.

V. Facility Contamination Control Features:

A broad range of contamination control features that affect all aspects of facility operations, covering all contamination routes into, within and out of the facility were incorporated into the BRF design. All rooms are color-coded denoting the space usage, contamination potential and appropriate material and personnel traffic limitations. Special consideration was taken in the design of ventilation, mechanical and electrical services for each color-coded area so that their peculiar requirements were met.

The main features are:

Facility Personnel and Material Traffic Contamination Control:

The BRF is connected to an adjacent Biology Laboratory Building by a second floor bridge. Entry is electronically controlled and research personnel entering the facility shower and change into appropriate clothing on the second floor level before proceeding to the main floor.

Shipping and receiving entrances, at the main floor level, are equipped with fumigation, sterilization and storage facilities to control the entry and exit of contaminated materials.

Facility Contamination Arising from Maintenance Operations:

The facility building upper level plan (Figure 2) shows that an area almost as large as the entire building plan is provided for mechanical and electrical services. A considerable effort has gone into separating service equipment and piping from the animal and laboratory spaces. The location of ventilation equipment, ducting, dampers, piping, valves, power supplies, electrical panels, controls and instrumentation outside of the animal and laboratory spaces minimizes the probability that maintenance personnel will have to enter them.

Airborne Contamination Entry from Outside:

The number of window and door penetrations in the facility exterior building wall have been kept to a minimum and, by keeping the building at above atmospheric pressure with an over-supply of HEPA-filtered and temperature/humidity-conditioned air, out-leakage at the building perimeter minimizes the entry of airborne contaminants from outside the building.

Airborne Contamination Movement Within the Building:

The uncontrolled movement of facility ventilation air is minimized by placing great emphasis on sealing all wall, ceiling and floor penetrations. The controlled movement of facility ventilation air is effected by regulating the relative rates of room supply and exhaust. This regulation of room ventilation air supply and exhaust rates is used to produce directional air flow patterns and air change rates customized for the specific research program requirements. For example, in Figure 4 the animal holding rooms, Y144 and Y148, are over-supplied to leak ventilation air into the adjacent ante room, Y146, which in turn leaks it to an adjacent corridor.

Airborne Contamination Movement When a Door Between Adjacent Rooms is Opened:

There is a relatively small contingent of personnel (3 to 5 people) in charge of the facility. Entry into the facility by other research, operating and maintenance personnel is very restricted. Facility operating personnel are trained to work to formal procedures and are aware of the special requirements of the animal based research facility. Room-to-room traffic is kept to a minimum: thus doors between adjacent spaces are closed most of the time and only opened for very short periods throughout a typical work day for very specific purposes. It is recognized that the rate of flow through an open door is too small to prevent upstream contamination movement. However, adjacent spaces such as the ante rooms, serve as air-locks that minimize/restrict the spread/flow of contamination to areas that are beyond the immediate attention of the trained personnel entering or leaving the area.

Work Station Airborne Contamination Control:

Work stations such as Class II B2 Bio-safety cabinets (BSC) and fume hoods, located inside the above atmospheric pressure rooms and laboratories, serve to control the spread of contamination from the stations by maintaining inflow velocities consistent with proper cabinet and fume-hood operation practices.

Animal Cage Airborne Contamination Control:

Recent developments in small animal cages rack designs, Figure 5, have included a means of connecting each rack of cages directly to the building HVAC system, thereby isolating each animal cage from the ones adjacent to it and providing each cage with a known ventilation supply and exhaust rate. As this development becomes the norm for up-to-date animal care, this facility will be able to accommodate the change from room supply and exhaust ventilation to a combination of room and direct cage rack ventilation. An additional complexity is introduced here in that the number of racks in each animal holding room is a variable that must be accommodated by the room ventilation supply and exhaust control system. The BRF animal housing room and laboratory ventilation systems have the ability to divert room ventilation air to and from one to six cage racks in each housing room.

VI. Normal Operations Contamination Control Pattern Variations

Typical Pattern With Direct Room Ventilation

The Figure 4 Normal Operations #1a Pattern Diagrammatic Flow Sheet shows Rooms Y144, Y146 and Y148 with direct room ventilation. The excess supply air is shown as out-leakage and is added to the exhaust total to create a supply and exhaust balance in the room. The out-leakage of course becomes part of the supply balance in the adjacent Y146 room. Any number of Normal Operations ventilation patterns can be devised to suit current research programs. For example, Room Y144 could be balanced to leak inwards from Room Y146.

Typical Pattern with Direct Cage Ventilation

Figure 6 shows the Normal Operations #1b Pattern Diagrammatic Flow Sheet for Animal Housing Room Y144 when it is equipped with six directly ventilated cage racks rated at 28 L/s (60 cfm) supply and exhaust. The total animal housing room rack exhaust and supply rates of 170 L/s (360 cfm) are diverted from the direct room supply and exhaust ventilation rates. The room ventilation air change rate is however not allowed to drop below a prescribed value. A number of contamination control patterns with direct cage ventilation for from one to six cage racks to suit current research programs will be required for each room equipped with ventilated cage rack supply and exhaust services.

VII. Abnormal Operations Contamination Control Pattern Variations

The ability to provide flexible ventilation/contamination control patterns provides a method of dealing with abnormal power and equipment outage conditions. Figure 7 shows the Abnormal Conditions Pattern #2 diagrammatic arrangement for Animal Housing Rooms, Y144. Y146 and Y148, where the fume-hood exhaust rate in Room Y146 is reduced to conserve supply air for the animal related spaces. The DDC-controlled ventilation system is thereby able to provide normal contamination control patterns in animal-related rooms, and rooms that can tolerate ventilation changes are either shut down or their rates are significantly reduced during the abnormal condition.

VIII. Conclusion

Variable contamination control pattern capability provides facility operations flexibility that meets current and future animal welfare and research program environmental requirements. It takes facility ventilation systems from being a relatively rigid building service operated by plant operating personnel and gives facility research personnel the responsibility for and means to provide quality-assured animal, personnel and program environments.

IX. References

1	NSN-ESRSD-140	AECL, CRL Environmental Safety & Regulatory Services, Safety Analysis Report of the Biological Research Facility (BRF)
2	SRC-R-1	AECL Safety Review Committee Requirements for Review and Approval of New Facilities
3	CCAC	Canadian Council on Animal Care Guideline

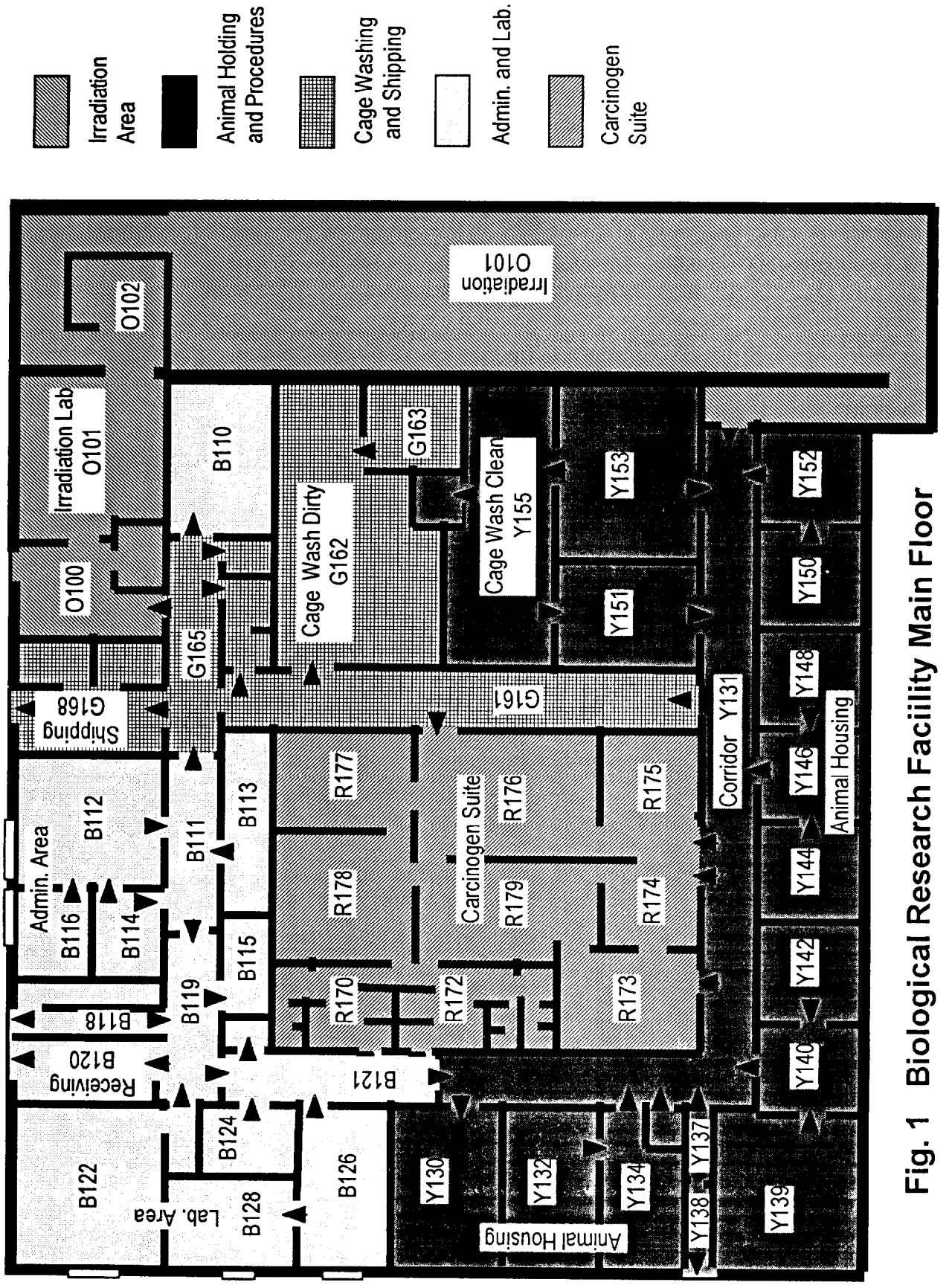

Fig. 1 Biological Research Facility Main Floor

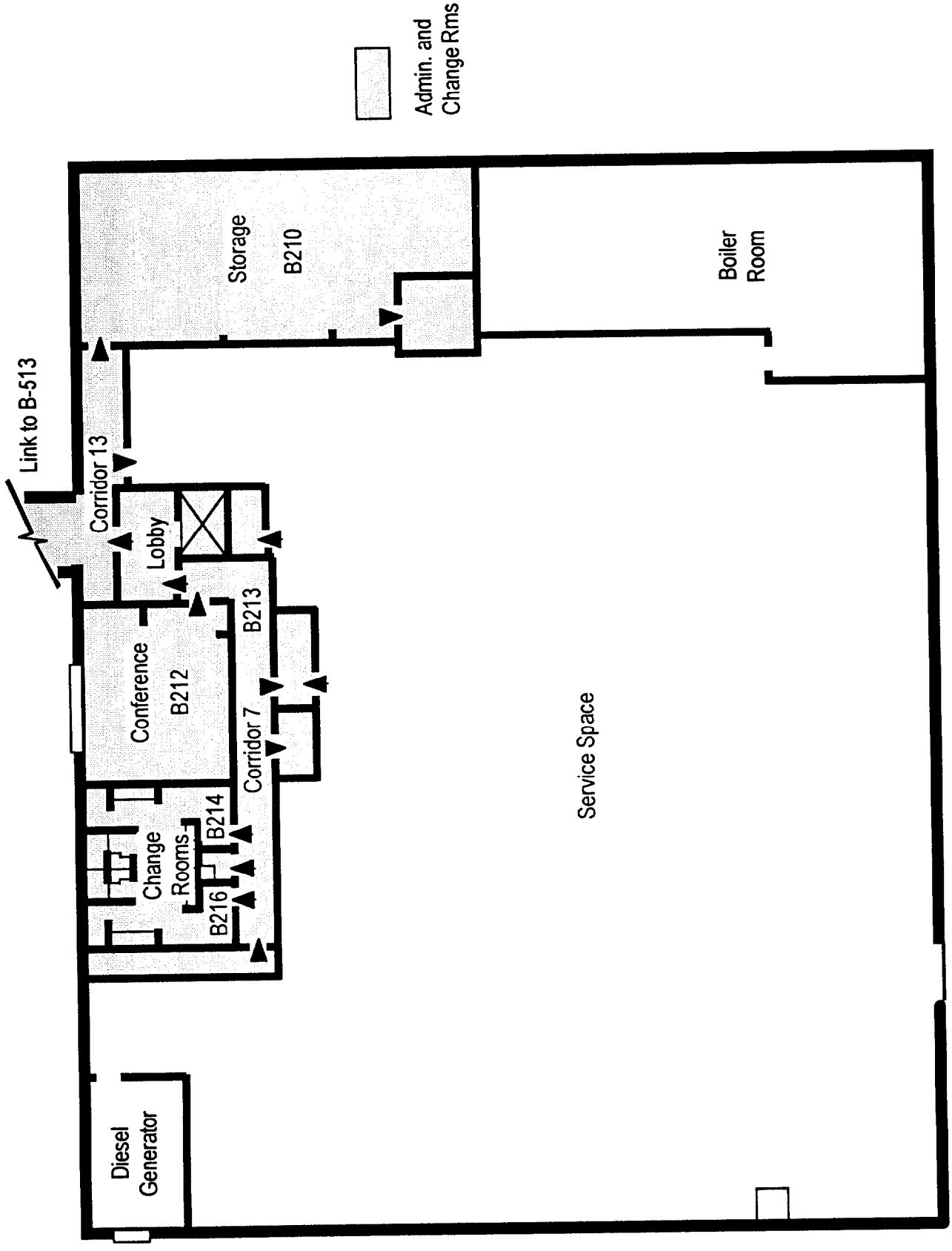

Fig. 2 Biological Research Facility Upper Floor

Rm Y144 Housing AB		Exhaust Fan System (litres / sec.)									OUTFLOW (litres / sec.)			INFLOW (litres / sec.)			
		VAV #	E-123	E-456	E-789	E-10	E-1213	E-14	E-15	Transf	Exh.	Transf	Exfilt.	VAV #	Supply	Transf	Infilt.
Length (m)	Room	Y144EB1	198											Y144SB1	245		
4.0	Doors																
Width (m)	146												47				
4.0	sealed145																
Height (m)	Transfer																
2.6	Rack	Y144EB2	0											Y144SB2	0		
Vol. (m3)	Fume:																
41.6	Fume Hood																
Room	BSc																
Chg./Hr	Canopy																
21.2	Room Totals		198	0	0	0	0	0	0	0	198	0	47		245	0	0

Rm Y146 AnteRoom AB		Exhaust Fan System (litres / sec.)									OUTFLOW (litres / sec.)			INFLOW (litres / sec.)			
		VAV #	E-123	E-456	E-789	E-10	E-1213	E-14	E-15	Transf	Exh.	Transf	Exfilt.	VAV #	Supply	Transf	Infilt.
Length (m)	Room													Y146SB1	496		
4.0	Doors																
Width (m)	147												47				
3.6	146 148																94
Height (m)	Transfer																
2.6	Rack	Y146EB2	0											Y146SB2	0		
Vol. (m3)	Fume:																
37.4	Fume Hood	Y146EB1		543													
Room	BSc																
Chg./Hr	Canopy																
56.7	Room Totals		0	543	0	0	0	0	0	0	543	0	47		496	0	94

Rm Y148 Housing AD		Exhaust Fan System (litres / sec.)									OUTFLOW (litres / sec.)			INFLOW (litres / sec.)			
		VAV #	E-123	E-456	E-789	E-10	E-1213	E-14	E-15	Transf	Exh.	Transf	Exfilt.	VAV #	Supply	Transf	Infilt.
Length (m)	Room	Y148EB1	198											Y148SB1	245		
4.0	Doors																
Width (m)	148												47				
4.0	sealed149																
Height (m)	Transfer																
2.6	Rack	Y148EB2	0											Y148SB2	0		
Vol. (m3)	Fume:																
41.6	Fume Hood																
Room	BSc																
Chg./Hr	Canopy																
21.2	Room Totals		198	0	0	0	0	0	0	0	198	0	47		245	0	0

FIG. 3 BRF - Normal Contamination Control Pattern #1a (No Ventilated Racks)

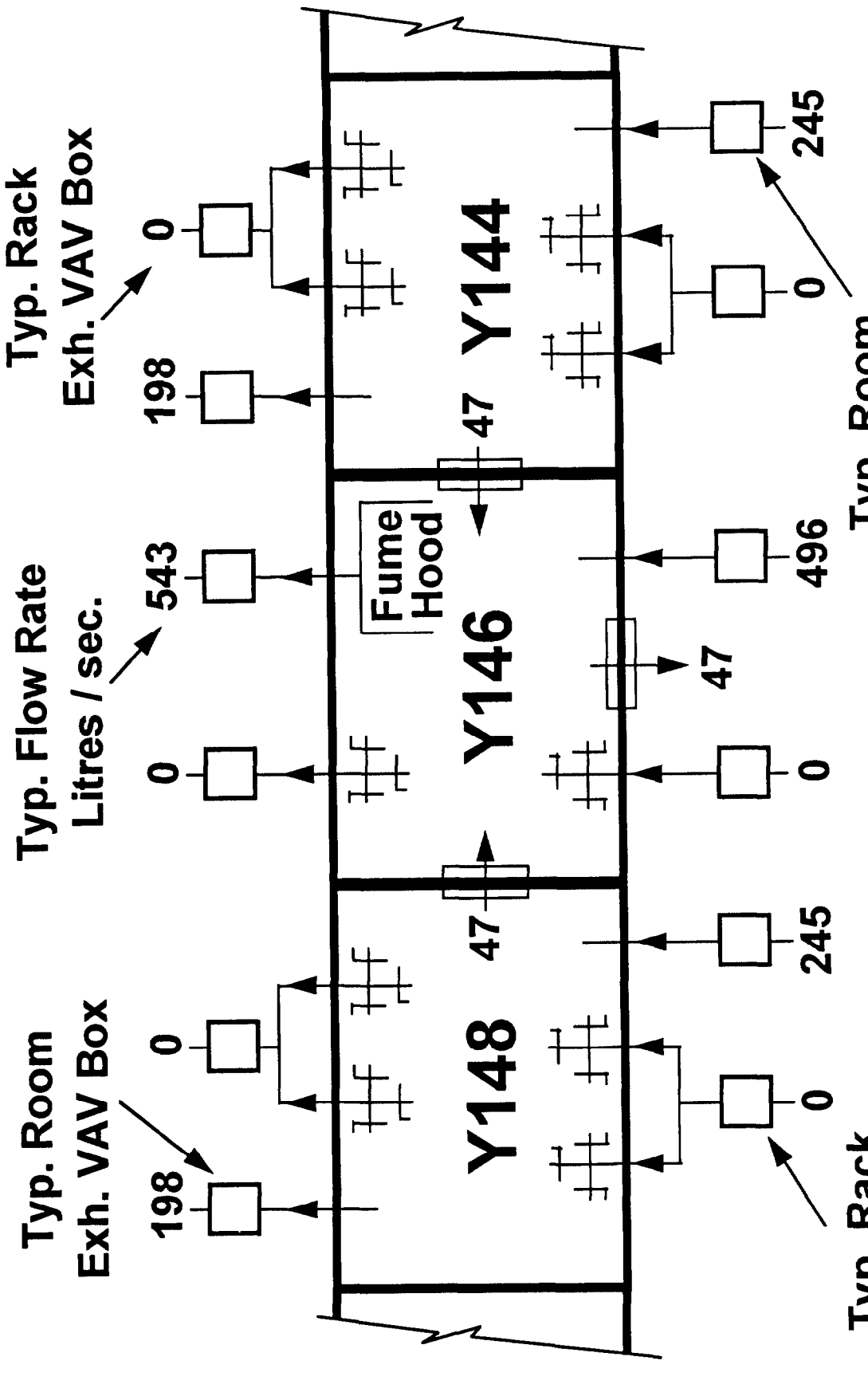

FIG. 4 Bioological Research FacilityNormal Conditions
Pattern #1a Rooms. Y144, Y146 and Y148 Flow Sheet Diag.

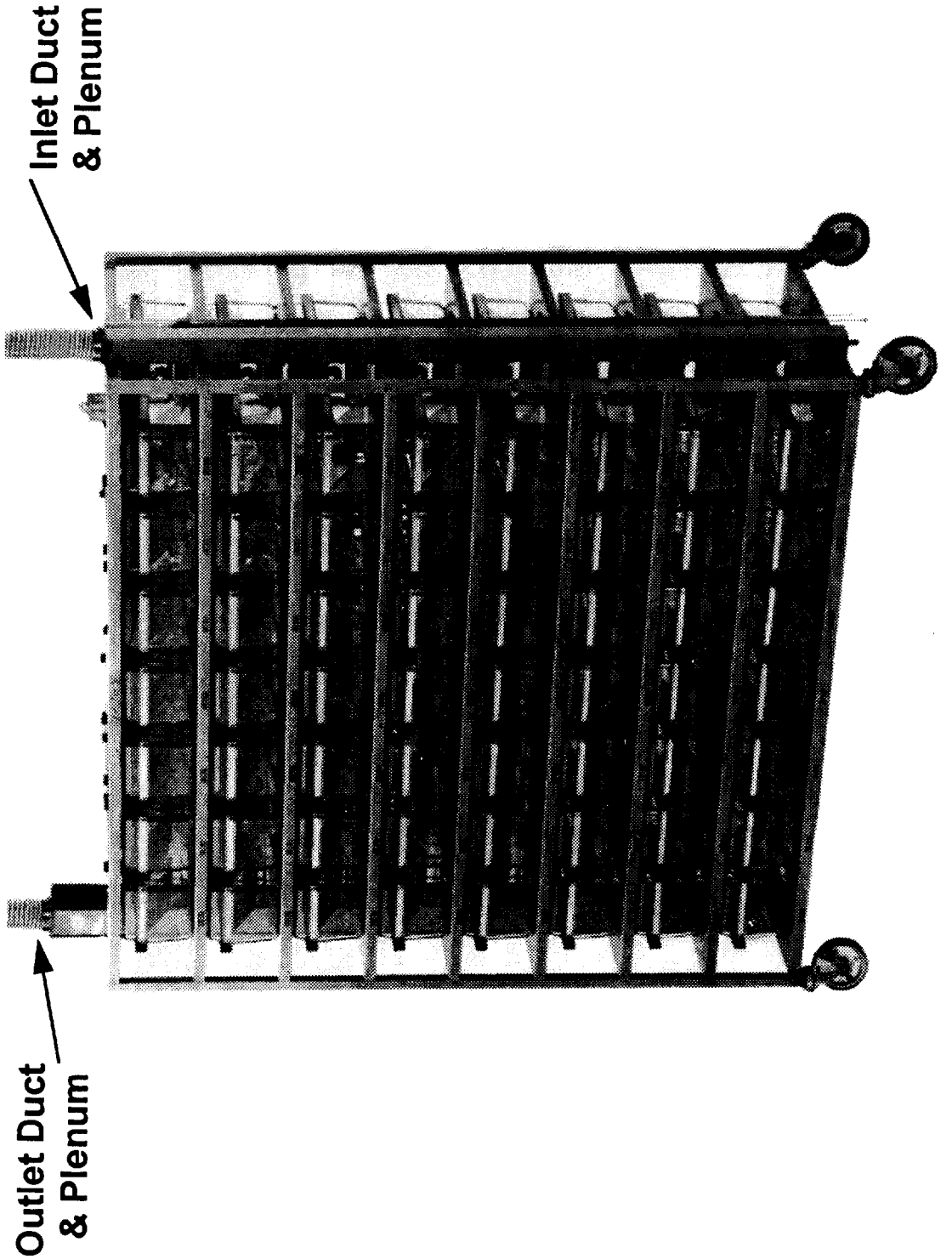

FIG. 5 Biological Research Facility Directly Ventilated Animal Cage Rack

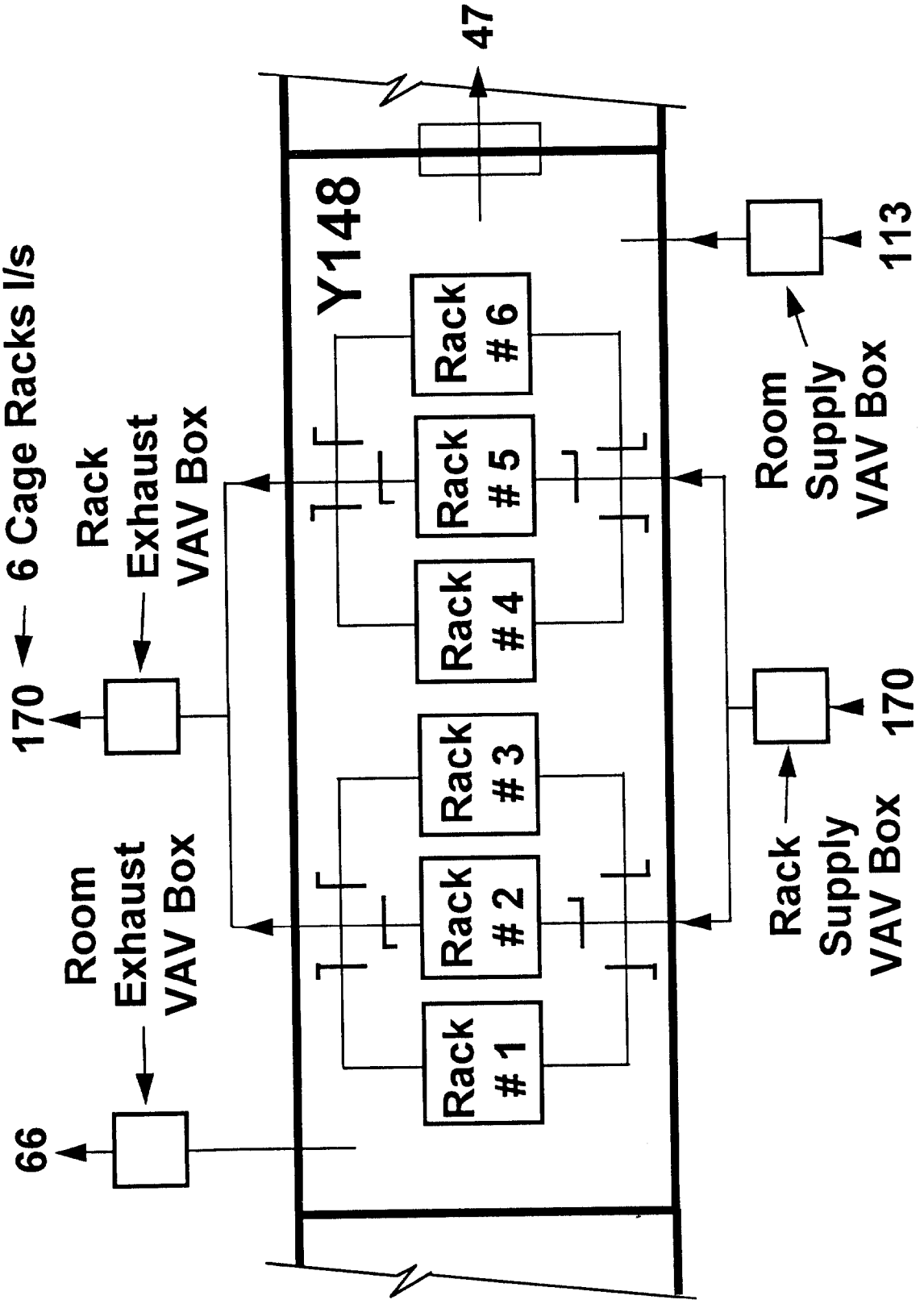

FIG. 6 Biological Research Facility Normal Conditions Pattern #1B Room. Y144 Flow Sheet Diag.

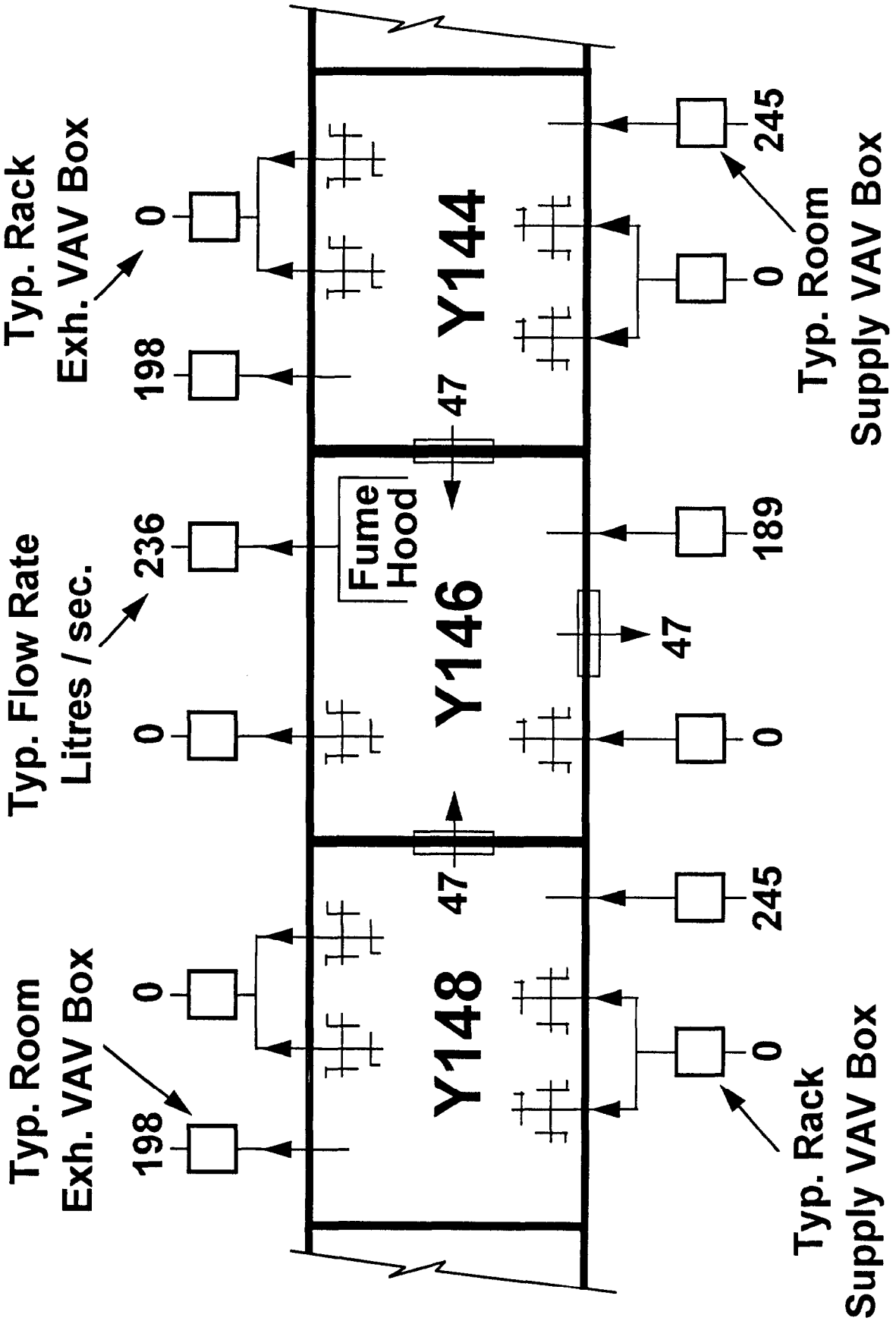

FIG. 7 Biological Research Facility Abnormal Conditions Pattern #2 Room. Y144 Flow Sheet Diag.

AEROSOL DEPOSITION IN BENDS WITH TURBULENT FLOW[1]

A.R. McFARLAND[2,*], H. GONG*, A. MUYSHONDT[†], W.B. WENTE*, and N.K. ANAND*
*Department of Mechanical Engineering
Texas A&M University
College Station, TX 77843
[†]Department of Mechanical Engineering
University of Arkansas
Fayettesville, AK 72701

Abstract

The losses of aerosol particles in bends were determined numerically for a broad range of design and operational conditions. Experimental data were used to check the validity of the numerical model, where the latter employs a commercially available computational fluid dynamics code for characterizing the fluid flow field and Lagrangian particle tracking technique for characterizing aerosol losses. Physical experiments have been conducted to examine the effect of curvature ratio and distortion of the cross section of bends. If it curvature ratio ($\delta = R/a$) is greater than about 4, it has little effect on deposition, which is in contrast with the recommendation given in ANSI N13.1-1969 for a minimum curvature ratio of 10. Also, experimental results show that if the tube cross section is flattened by 25% or less, the flattening also has little effect on deposition. Results of numerical tests have been used to develop a correlation of aerosol penetration through a bend as a function of Stokes number (Stk), curvature ratio (δ) and the bend angle (θ).

I. Introduction

Aerosol losses in bends can be significant. For example, the wall loss of 10 μm aerodynamic diameter aerosol particles in a 25.4 mm (1-inch) diameter 90° bend at a flow rate of 57 L/min (2-cfm) is calculated to be 9.5% by the DEPOSITION code (Anand et al., 1993). The code predicts the same losses would occur in 95 m of vertical tubing of the same size at the same flow rate. A typical system that continuously extracts a sample from a stack or duct will have at least one bend, which is generally needed to change the flow direction of the sampled stream from parallel to the duct axis to perpendicular to the axis. For batch sampling applications, such as US Environmental Protection Agency (EPA) Methods 5 and 17 (US EPA, 1995a and 1995b), the losses of aerosol particles in a transport system are of little consequence because the inside walls are washed at the completion of a

[1] Funding for this study provided by the U.S. NRC under Grant NRC-04-94-099 and by the Amarillo National Resource Center for Plutonium (ANRCP). ANRCP funding was awarded through the University of Texas under Contract UTA95-0278. Dr. Stephen A. McGuire is the Project Officer for the NRC Grant, and Dr. Howard Liljestrand if the Principal Investigator for the ANRCP Grant.

[2] Corresponding author. E-mail address: ARM9136@acs.tamu.edu

batch test to recover inadvertently deposited aerosol sample. In contrast, for continuous emission sampling (CES), the system must operate for extended time periods and may be required to provide samples for near-real time data on aerosol concentration in the stack or duct (continuous emission monitoring, CEM). Any losses on the internal walls of a sampling system degrade the quality of emission or concentration data. For sampling potentially significant nuclear sources, EPA requires that methodology for CES must follow the protocol of the American National Standards Institute N13.1-1969 (ANSI, 1969), which stipulates that an evaluation shall be made of aerosol losses in a sampling system. However, EPA also permits US Department of Energy facilities (DOE) to use Alternate Reference Methodologies (EPA, 1994). The Alternate Reference Methodologies require that at least 50% of 10 μm aerodynamic diameter (AD) aerosol particles must penetrate through a transport system from the free stream in a stack or duct to the collector or analyzer. Use of the DEPOSITION software for determining compliance with this requirement is part of the Alternate Reference Methodologies.

The DEPOSITION software includes submodels for predicting losses in probes, straight transport lines, bends, and expansion and contraction fittings. For the bends, the software currently uses the model of Cheng and Wang (1981) for laminar flow and the model of Pui et al. (1987) for turbulent flow. Because most flows in sample transport systems are turbulent, the model of Cheng and Wang is not generally applicable. The model of Pui et al. only takes into account the effect of the Stokes number, and as it shall be shown herein, the curvature ratio and bend angle also affect deposition in turbulent flow. In this study, we established a numerical base for penetration of elbows and used that data base to develop a correlation model to predict particle penetration. Such a model could be used in the DEPOSITION software.

In the numerical modeling effort, we have assumed that geometrical extent of the a bend encompasses only the region where the centerline of the bend is curved, Figure 1a. On the other hand, tests with physical models involved geometries where the extent of the bends reached the same two points in space, Figure 1b. The reason for using different geometries is that the purpose of the numerical work is to establish a data base for the correlation model. When a user employs the correlation model, deposition in any straight tubing attached to the bend will be analyzed separately from the bend itself. But, when we seek to compare the effects of curvature ratio on deposition, it is necessary to add straight tubing onto bends with small values of δ to provide a common basis of comparison, so that a bend with a short curvature ratio will not have an apparent advantage over a curve with a large curvature ratio as a result of the smaller distance that the flow travels in the bend.

Flow Considerations.

Flow through straight tubes is generally characterized by the Reynolds number, with the flow being considered laminar when the Reynolds number, $Re = \rho U d_t/\mu$, is less than about 2300, turbulent when the flow is greater than about 3000 and transitional between those values. Here: ρ = fluid density; U = average (spatial) fluid velocity; d_t = tube diameter; and, μ = fluid viscosity. On the other hand, flow through bends of circular tubing depends upon both the Reynolds number and the curvature of the bend and can be characterized the Dean number, De, which is:

$$De = \frac{Re}{\delta^{1/2}} \qquad (1)$$

where: $\delta = R/a$; R = radius of curvature of the bend; and $a = d_t/2$ = tube internal radius. The parameter δ is the curvature ratio of the bend. Flow is considered laminar for $De \leq 370$, which

corresponds to a Reynolds number of 1170 for a curvature ratio of 10; however, the secondary flow in a bend causes the overall flow to be more stable. The critical Reynolds number can be as large as 7800 for a curvature ratio of 7 (Soh and Berger, 1984).

In general, flow through a bend is developing, so aerosol particle deposition should vary with length along the bend. For this reason, angle of the bend was treated as a variable in this investigation.

Particle deposition.

Landahl and Herrmann (1949) proposed a model for deposition of aerosol particles in a bend, where the deposition depended only on Stokes number (*Stk*). The Stokes number is defined as:

$$Stk = \frac{C\rho_p D_p^2 U}{9\mu d_t} \tag{2}$$

where: C = Cunningham's slip correction (Fuchs, 1964); ρ_p = particle density; D_p = particle diameter; and, μ = dynamic viscosity of air. Davis (1964) used aerosol particles to visualize the secondary flow patterns due to laminar flow in pipes with a bend angles ranging from 30° to 180°; however, no data on the particle loss in the pipe were gathered. Cheng and Wang (1975) developed a model for the impaction efficiency of aerosol particles in 90° bends. Their model was based on an analytical laminar flow solution and the correlation they developed gave penetration as a function of the Stokes number, curvature ratio, and bend angle. Crane and Evans (1977) performed numerical calculations to predict the behavior of aerosol particles in laminar flow in 90° bends. They examined curvature ratios ranging from 4 to 20 and their results showed reasonable agreement with those of Cheng and Wang (1975). Chen and Wang (1981) re-examined the deposition of particles in pipe bends. They concluded that in the laminar flow regime, the aerosol particle deposition was mainly a function of Stokes number and flow Reynolds number for curvature ratios between 4 and 20. Pui et al. (1987) experimentally evaluated the deposition of aerosol particles in a 90° bends for Reynolds numbers of 100, 1000, 6000, and 10,000; and curvature ratios of 5.7 and 7. They suggested the penetration does not depend on either curvature ratio or Reynolds number and offered the following correlation for predicting the aerosol particle penetration in 90° elbows:

$$P = 10^{-0.963\,Stk} \tag{3}$$

where: P is the aerosol particle penetration. Tsai and Pui (1990) used a three-dimensional numerical procedure to examine the aerosol particle deposition for laminar flow in a pipe with a 90° bend. They found significant variation in the deposition efficiency as a function of curvature ratio. They also noticed an influence of the inflow velocity profile on the deposition efficiency. Their results using a parabolic inlet velocity profile agree well with the results of Cheng and Wang (1981).

Goals of the Present Study

There have been significant recent developments in numerical predictions of three dimensional flow fields and in particle tracking. For example, FLUENT, which is a commercially-available finite volume code (Fluent, Inc., Lebanon, NH) accommodates prediction of three dimensional turbulent flow fields using advanced turbulence models. Abuzeid et al. (1991) developed a numerical scheme for particle tracking in turbulent flows. Gong et al. (1993) used the Abuzeid approach to model aerosol sampling by a shrouded probe in an axi-symmetric (two-dimensional) turbulent flow field. Good agreement was

obtained with experimental data. In the present study, that model was extended to particle tracking in three-dimensional flows, and it was used in combination with a three-dimensional flow field to predict particle losses in bends. At the present time, the only model for predicting aerosol particle penetration in turbulent flow through bends is the empirical correlation of Pui et al. (1987). A goal of this study was to evaluate the effects of bend angle, curvature ratio, Reynolds number and Stokes number, and to develop a correlation that would taken into account the necessary parameters. Also, we sought to determine experimentally the effects of curvature ratio and flattening of the cross section of a bend, and to generalize those results as design criteria.

II. Methodology

Physical experiments.

The bends were fabricated by milling the correct curvature ratio into a split block of wax, then adding tube stubs to either end of the bend. Care was taken that the transitions between the bends and the tube stubs were smooth. For all bends, tube diameter was 16 mm and the distance from the entrance plane of the bend to the centerline of the exit tube was 151 mm. The layout was setup so a bend with a value of $\delta = 20$ would require no additional straight sections; whereas, for all other bends, with smaller values of δ, straight tube stubs were added. To investigate the effect of flattening of the bend cross section, we fabricated six identical 90° bends from 16 mm diameter tubing that had curvature ratios of 10. At the 45° location, the bends were pinched to reduce the diameter in the radial direction.

The apparatus used in testing bends is shown in Figure 2. Monodisperse aerosols were generated with a vibrating orifice aerosol generator (Berglund and Liu, 1973) from a solution of a non-volatile oil (oleic acid) and an analytical tracer (sodium fluorescein) dissolved in a volatile solvent (isopropyl alcohol). A particle size of 10 μm aerodynamic diameter (AD) was used for all tests. The monodisperse aerosol was drawn into a mixing chamber plenum with a blower. A clean-up filter, which was placed in front of the blower, collected the excess aerosol.

An upstream aerosol sample was collected by replacing the bend with a sampling filter. The bend was then inserted into the flow system and an aerosol sampling filter was used to collect a downstream sample. Analytical tracer was eluted from the filters and quantified. The penetration, P, was determined from:

$$P = \frac{c_e}{c_i} \tag{4}$$

where: c_e = aerosol concentration at the exit section of the elbow; and, c_i = aerosol concentration at the inlet section. The flow rate through the system was measured with a calibrated rotameter and corrected for the actual pressure level in the system. Four replicate experiments were conducted for each set of experimental conditions.

Numerical Calculations.

Flow fields were setup through use of FLUENT. Because the flow in bends can be turbulent, with swirl, the traditional engineering κ-ϵ turbulent closure model is not adequate. Instead, a more accurate model, the Reynolds stress model (RSM), was used to describe the turbulent behavior of the flow. In the RSM, each Reynolds stress component, the turbulence dissipation rate and the velocity components

are calculated. An example of the flow field in a bend is shown in Figure 3, where the velocity vectors are illustrated for a location that is two tube diameters downstream of the bend exit plane.

Particle trajectories in bends were calculated by solving the particle equations of motion as affected by the gravitational force, particle inertial force and fluid drag. In the equation for particle motion, the instantaneous fluid velocity is needed, which consists of mean and turbulent components. The mean velocity is available from the flow field computation, and the fluctuating component is generated from Gaussian random sampling of Reynolds stresses. The duration of interaction between particle and turbulence eddy is determined by the eddy lifetime, which, in turn is determined by the turbulent kinetic energy and the dissipation rate. The penetration of aerosol through a bend is calculated by tracking a large number of simultaneously released particles and determining which are deposited on the walls and which penetrate the bend.

A series of numerical experiments were conducted to establish a grid independent solution. Based on these studies, a grid size of $103\times21\times25$ was used. A similar set of numerical experiments was use to establish the time steps for particle tracking. A time step of 10^{-5} s was selected, which ensures at a particle travels at least 5 steps within a turbulence eddy.

Computations were carried out for bends with curvature ratios of 2, 4, and 10; and for bend angles of 45°, 90° and 180° at a Reynolds number of 8210. The effect of varying the Reynolds number was investigated by maintaining the Stokes number constant and varying the Reynolds number over the range of 3200 to 19,800.

III. Results

Validation of the Numerical Model. Initially, we attempted to use a particle tracking model that is imbedded in the FLUENT software; however, the agreement with experiment was not satisfactory. As a consequence we developed the three dimensional extension to the model of Gong et al. (1993). A comparison of the numerical predictions with experimental results is given in Table 1. Results are shown for different bend angles, curvature ratios and mean flow velocities. For a given set of conditions, the relative difference between the experimental value and th numerical predicition is 5%. The numerical value is higher, and the standard error of the estimate is 4%. for example, if the numerically predicted penetration is 50%, the experimental value will be about 52.5%, with an error of ±2%.

Effect of Turbulence on Particle Deposition

A flow field was setup for a 45° bend with a curvature ratio of 10, and for a Reynolds number of 8210. The penetration of particles of 5, 10 and 15 μm AD was then determined with and without the turbulence model for particle tracking. The results, which are shown in Table 2, illustrate the need for including the effects of turbulence on particle motion. For example, at a particle size of 10 μm AD, the predicted penetration is 80% without including turbulence and 62% with turbulence. Neglecting the efect of turbulence on particle motion would cause unacceptable errors in the analyses.

Effect of Reynolds Number on Aerosol Penetration

Numerical predictions were made of the effect of flow Reynolds number on aerosol penetration through a 90° bend that has a curvature ratio of 10. In the calculational procedure, the Stokes number was held constant and the Reynolds number varied from 3200 to 19,800. The results, which are shown in Figure 4, suggest that the effect of Reynolds number is sufficiently small such that it can be

neglected. Over the range of Reynolds numbers tested, at a Stokes number of 0.67, the penetration ranges from 22% to 27%; and, at a Stokes number of 0.074, the penetration varies from 87.5 to 89.5%.

Experimental Results Showing the Effect of Curvature Ratio on Penetration

With reference to Figure 5, results are shown on the effect of curvature ratio on penetration for a range of Stokes numbers. The Stokes number was varied by changing the flow rate through a bend. Bends were designed as illustrated in Figure 1b to allow direct comparisons on the effect of curvature ratio, i.e., tube stubs were added to bends with short radii of curvature. The results show that increasing the curvature ratio improves the aerosol penetration. For example, at a Stokes number of 0.3, a bend with a curvature ratio of unity has a penetration of 32%, a bend with $\delta = 2$ has $P = 42\%$, and if $\delta = 4$, $P = 50\%$. However as δ is increased from 4 to 20, the penetration only changes from 50% to 58%. Also, there is very little difference in penetration between bends with curvature ratios of 4 and 10. These results suggest that a bend with a curvature ratio of 4 should be satisfactory for aerosol transport. The curvature ratio of 10 recommended in ANSI N13.1-1969 is probably too conservative.

Experimental Study of the Effect of Flattening of the Bend Cross Section

Test conducted on pinched bends provided the results shown in Figure 6 . The degree of flattening is the amount by which a diameter was reduced, divided by the original tube diameter. The bends used in these tests had initial diameters of 16 mm with curvature ratios of 10. The data show that the penetration decreases with flattening; however, if the flattening is less than about 25%, the effect is quite small. For example, at a Stokes number of 0.3, the penetration decreases from 52% to 45% as the degree of flattening is increased from 0% to 25%. On the other hand, as the flattening is increased from 25% to 50%, the penetration decreases from 45% to 16%. These data suggest that if a bend is somewhat flattened (less than 25%) during the fabrication process, the aerosol penetration characteristics would not be significantly impacted.

Numerical Modeling of Aerosol Penetration

Computational results were generated for a range of Stokes numbers ($0.07 \leq Stk \leq 1.2$); for bend angles of 45°, 90° and 180°; and for curvature ratios of 2, 4 and 10. The results are presented in Figures 7a, 7b, and 7c in the form of penetration as a function of Stokes number for constant values of the curvature ratio. With reference to Figure 7a, which is for a bend angle of 45°, it appears that curvature ratio has a pronounced effect on penetration; however, that is illusionary because of the smaller path length through which the aerosol must flow in the smaller curvature ratio bends. The experimental data shown in Figure 5 present a more appropriate view of the effect of curvature ratio, where those data are based on all bends starting and ending at the same points in space.

The data shown in Figures 7a, 7b and 7c have been used to generate a correlation of aerosol penetration as a function of Stokes number, curvature ratio and bend angle. We chose a functional form for the correlation that would have the appropriate limiting conditions over the range of the correlation of $P \to 0$ for large Stokes number, and $P \to 1$ for small Stokes number. The functional form that we selected is:

$$\ln P = \frac{c_1 + c_2 \ln Stk + c_3 \ln^2 Stk + c_4 \theta}{1 + c_5 \ln Stk + c_6 \ln^2 Stk + c_7 \theta} \qquad (5)$$

where each c_i is a function of the curvature ratio, δ. A three-dimensional surface fitting program (TableCurve 3D, Jandel Scientific, San Rafael, CA) was used to generate least squares fits of the data for each curvature ratio. The results are shown in Figures 8a, 8b and 8c for curvature ratios of 2, 4 and 10, respectively. Values of the coefficients as functions of the curvature ratio were then obtained by using a two dimensional curve fitting program that was based on use of least squares (TableCurve 2D, Jandel Scientific). The results are:

$$c_1 = 6.77 - 12.8\exp(-\delta)$$
$$c_2 = -9.18 + 62.4\exp(-\delta)$$
$$c_3 = 11.3 - 66.3\exp(-\delta)$$
$$c_4 = -0.00393 + \frac{0.0277}{\delta}$$
$$c_5 = -2.23 + \frac{8.49}{\delta^2}$$
$$c_6 = 2.39 - 13.94\exp(-\delta)$$
$$c_7 = 0.0055 - 0.0609\exp(-\delta)$$

A comparison of predictions from the correlation model (Equation 5) with those from Pui et al. model (Equation 3) is shown in Figure 9. Good agreement is obtained between the two models for the case of $\delta = 10$; however, the model of Pui et al. under predicts the correlation model for the case of $\delta = 2$.

The need for inclusion of bend angle into the correlation model can be demonstrated by reference to Figure 10, where computational results are shown for the average deposition of aerosol per radian of bend angle, as a function of Stokes number. The developing nature of the flow causes the aerosol loss/radian to be less in a 45° bend than in a 90° bend for most Stokes numbers, although at a Stokes number of 1.2, the deposition/radian for a 45° bend is somewhat larger than in a 90° bend. For Stokes numbers less than 0.3, the aerosol particle loss/radian is about the same in either a 90° bend or a 180° bend; however, for larger Stokes numbers, the aerosol losses/radian can be considerably less in a 180° bend than in a 90° bend. This suggests that in most cases, the penetration of aerosol through a 180° bend cannot be treated as the product of the penetration of two 90° bends in series, nor can the penetration through a 45° bend be treated as the square root of the penetration through a 90° bend. Rather, the bend angle needs to be considered as a variable.

IV. Summary and Conclusions

This study employed a combination of numerical and experimental techniques to characterize aerosol penetration through bends. Agreement was achieved between numerical and physical experiments when the numerical approach was based on use of a specially developed three dimensional particle tracking technique. It was also demonstrated that turbulence needs to be included in a particle tracking model.

The effect of Reynolds number upon particle deposition was examined numerically through calculations made with the Stokes number and curvature ratio held constant. Based on experimental evidence, Pui et al. (1987) stated that there is no Reynolds number effect. Although the numerical results show some dependency of penetration upon flow Reynolds number, the effect does not seem to be sufficiently significant to warrant its inclusion in any correlation model. For Stokes numbers of 0.07 to 0.7 and a

curvature ratio of 10, the aerosol penetration does not change by more than 5% when the Reynolds number is varied from 3200 to 19,800.

Physical experiments were conducted to investigate the effect of curvature ratio on aerosol penetration. The bends were constructed such that each bend had the same initial and final spatial co-ordinates, regardless of the curvature ratio. There is a continuum of change of penetration with bend angle, where the aerosol penetration increases with the curvature ratio. However, the change is much greater for curvature ratios less than 4 than it is for the larger curvature ratios. ANSI N13.1-1969 recommends that the curvature ratio should be at least 10, but the results of this study suggest that the value could be four.

When bends are fabricated from straight tubing, there is a tendency for the tubing to flatten. The flattening can be minimized by filling a tube with oil prior to bendin it, and maintaining the oil at a high pressure during the bending operation. Because that approach is expensive as compared with simpler techniques (that can cause flattening) we experimentally evaluated the effect of flattening upon aerosol penetration. Ninety degree bends were pinched at the 45° location and tested for aerosol penetration. The degree of flattening of the bends was from 0% to 50%, where the degree of flattening is the ratio of the change in diameter (caused by the pinching) divided by the initial diameter. If the degree of flattening is less than about 25%, it does not have a substantial impact on aerosol penetration.

Numerical experiments were carried out to characterize the penetration of aerosols through bends. The geometrical extent of the bends covered only the region of tubing where the radius of curvature is non-zero. Calculations were conducted for a range of Stokes numbers, curvature ratios and bend angles. Results were used to generate a correlation model that designers and users of aerosol transport systems can employ to predict aerosol penetration. The correlation is valid for $0.07 \le Stk \le 1.2$; $45° \le \theta \le 180°$; and $2 \le \delta \le 10$. Of immediate interest to us is the use of such a model in DEPOSITION software. A comparison of the correlation model with the empirical model of Pui et al. shows good agreement for $\delta = 10$; however, the model of Pui et al. under predicts the present correlation for $\delta = 2$. Also, the model of Pui et al. is limited to 90° bends..

References

American National Standards Institute, ANSI. (1969). Guide to sampling airborne radioactive materials in nuclear facilities. ANSI N13.1-1969. New York: American National Standards Institute.

Abuzeid, S.; Busnaina, A.A.; Amadi, G. (1991). Wall deposition of aerosol particles in a turbulent channel flow. *J. Aerosol Sc.* 22:43-62.

ANAND, N.K., A.R. McFarland. (1993). *DEPOSITION: Software to calculate particle penetration through aerosol transport lines.* NUREG/GR-006. Washington D.C.: Division of Regulatory Applications, U.S. Nuclear Regulatory Commission. (1993).

Berglund, R.N.; Liu, B.Y.H. (1973). Generation of monodisperse aerosol standards. *Env. Sc.. Technol.* 7:147-153.

Cheng, Y.S.; Wang, C.S. (1975). Inertial deposition of particles in a bend. *J. Aerosol Sc..* 6:139-145.

Cheng, Y.S.; Wang, C.S. (1981). Motion of particles in bends of circular pipes. *Atmos. Env.* 15:301-306.

Crane, R.I.; Evans, R.L. (1977). Inertial deposition of particles in a bent pipe. *J. Aerosol Sci.* 8:161-170.

Davis, R.E. (1964). The visual examination of gas flow round pipe bends using a new aerosol technique. *Int. J. Air Wat. Pollut.* 8:177-184.

Fuchs, N.A. (1964). *The Mechanics of Aerosols.* New York: The Macmillan Company.

Gong, H.; Anand, N.K.; McFarland, A.R. (1993). Numerical prediction of the performance of a shrouded probe sampling in turbulent flow. *Aerosol Sci. and Technol.* 19:294-304

Langdahl, H.D.; Herrmann, R.G. (1949). Sampling of liquid aerosols by wires, cylinders and slides, and the efficiency of impaction of the droplets. *J. Colloid Sci.* 4:103-136.

Pui, D.Y.H.; Romay-Novas, F.; Liu, B.Y.H. (1987). Experimental study of particle deposition in bends of circular cross section. *Aerosol Sci. Technol.* 7:301-315.

Soh, W.Y.; Berger, S.A. (1984). Laminar entrance effects in a curved pipe. *J. Fluid. Mech.* 148:109-135.

Tsai, C.J.; Pui, D.Y.H. (1990). Numerical study of particle deposition ion bends of a circular cross-section - Laminar flow regime. *Aerosol Sci. Technol.* 12:813-831.

U.S. Environmental Protection Agency. (1994). Letter from Mary D. Nichols, Assistant Administrator for Air and Radiation, U.S. Environmental Protection Agency, Washington, DC to Raymond F. Pelletier, Director, Office of Environmental Guidance, U.S. Department of Energy, Washington, DC.

U.S. Environmental Protection Agency. (1995a). Determination of particulate emissions from stationary sources. 40CFR60, Appendix A, Method 5. *Code of Federal Regulations.* Washington, DC: U.S. Government Printing Office.

U.S. Environmental Protection Agency. (1995b). Determination of particulate emissions from stationary sources (in stack filtration method. 40CFR60, Appendix A, Method 17. *Code of Federal Regulations.* Washington, DC: U.S. Government Printing Office.

Table 1. A comparison of experimental data and numerical predictions of aerosol penetration through bends. Additional length was added to the inlet and outlet sections of the numerical configurations so the geometries would be similar for both numerical and experimental testing.

Elbow Angle	Curvature Ratio, $\delta = R_t/a$	Velocity, m/s	Numerically Predicted Penetration	Experimentally Observed Penetration[1]
45°	10	7.7	62.7%	61.8±2.1%%
90°	10	7.7	51.0%	58.3±1.7%
180°	10	7.7	27.7%	28.5±0.9%
90°	2	7.7	42.9%	39.8±1.1%
90°	4	7.7	47.2%	54.1±0.6%
90°	10	18.6	12.2%	12.1±0.3%

[1]The value following the ± sign is one standard deviation.

Table 2. A comparison of numerically predicted aerosol penetration through a 45° bend with and without the turbulence in the particle tracking model. The curvature ratio is 10 and the flow Reynolds number is 8210. Inlet and outlet tube sections were added to the geometrical configuration to make it similar to that shown in Figure 1b rather than Figure 1a.

Particle Diameter, μm AD	Penetration without Turbulence in the Particle Tracker	Penetration with Turbulence in the Particle Tracker
5	97%	82%
10	80%	62%
15	46%	35%

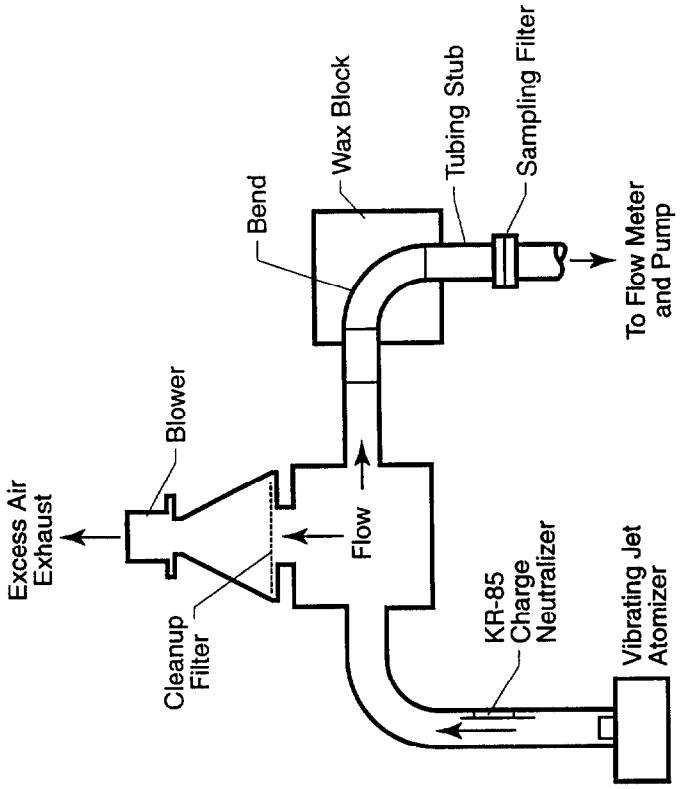

Figure 2. Experimental apparatus used in testing aerosol losses in bends.

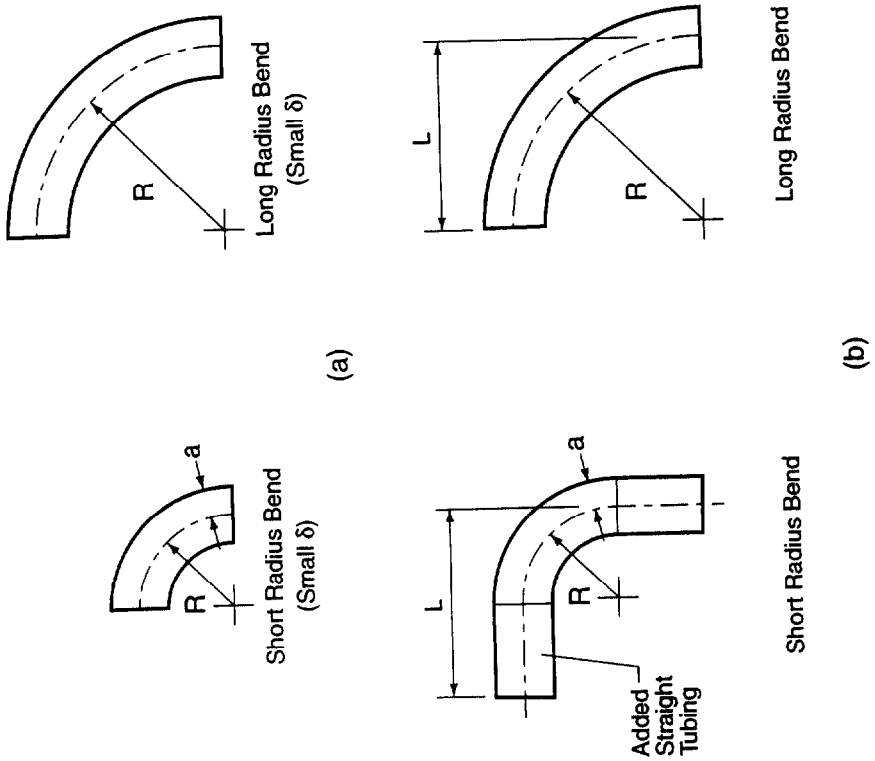

Figure 1. Geometries of bends used in a) numerical modeling, and b) physical testing.

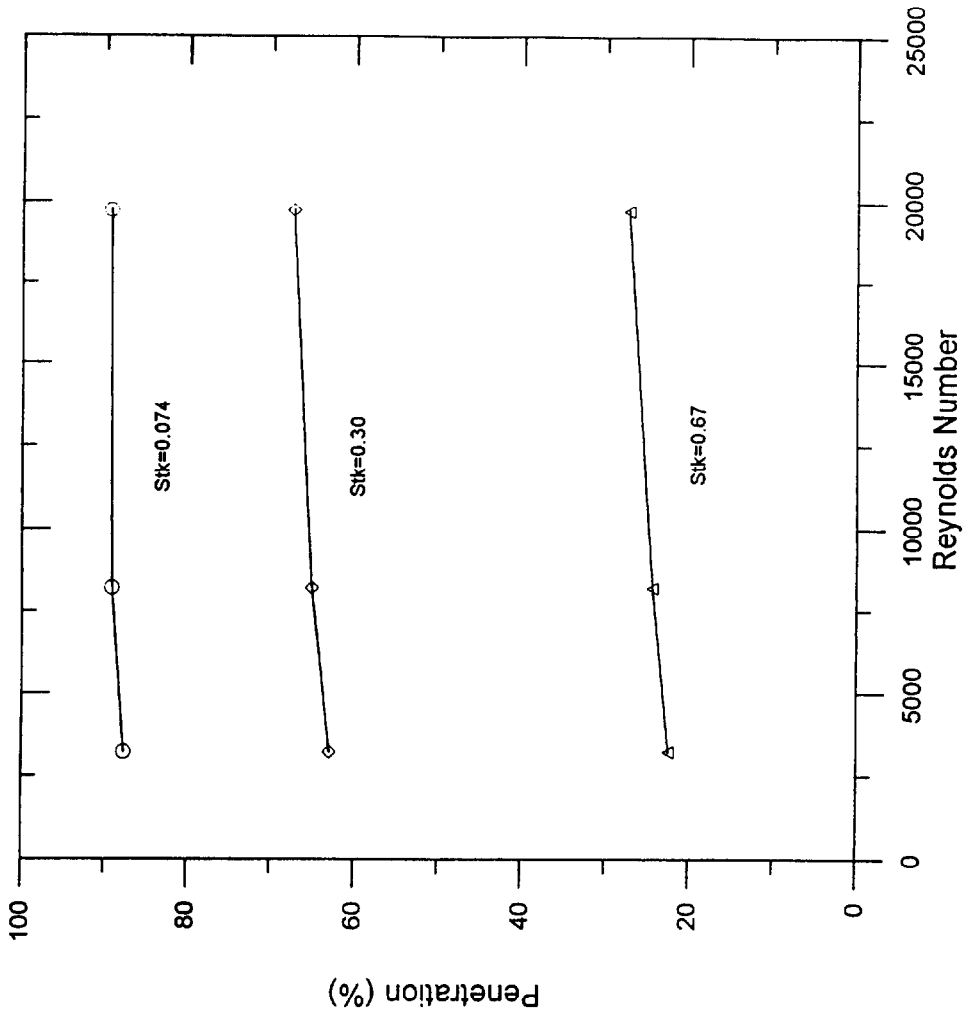

Figure 4. Numerical prediction of the effect of flow Reynolds number on aerosol penetration through a 90° bend with a curvature ratio of 10.

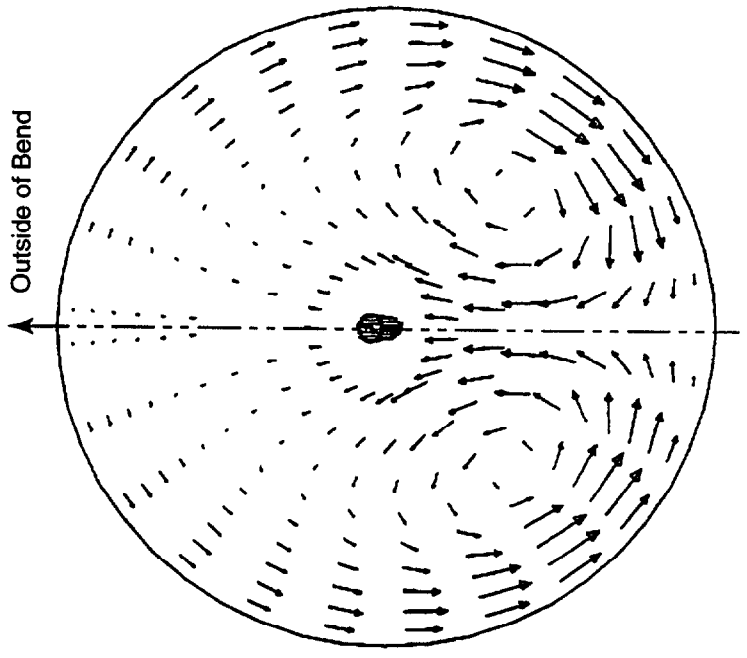

Figure 3. Secondary flow field at a distance of two diameters downstream from the exit plane of a 90° bend. The tube size is 16 mm, the Reynolds number is 8210, and the curvature ratio is 10.

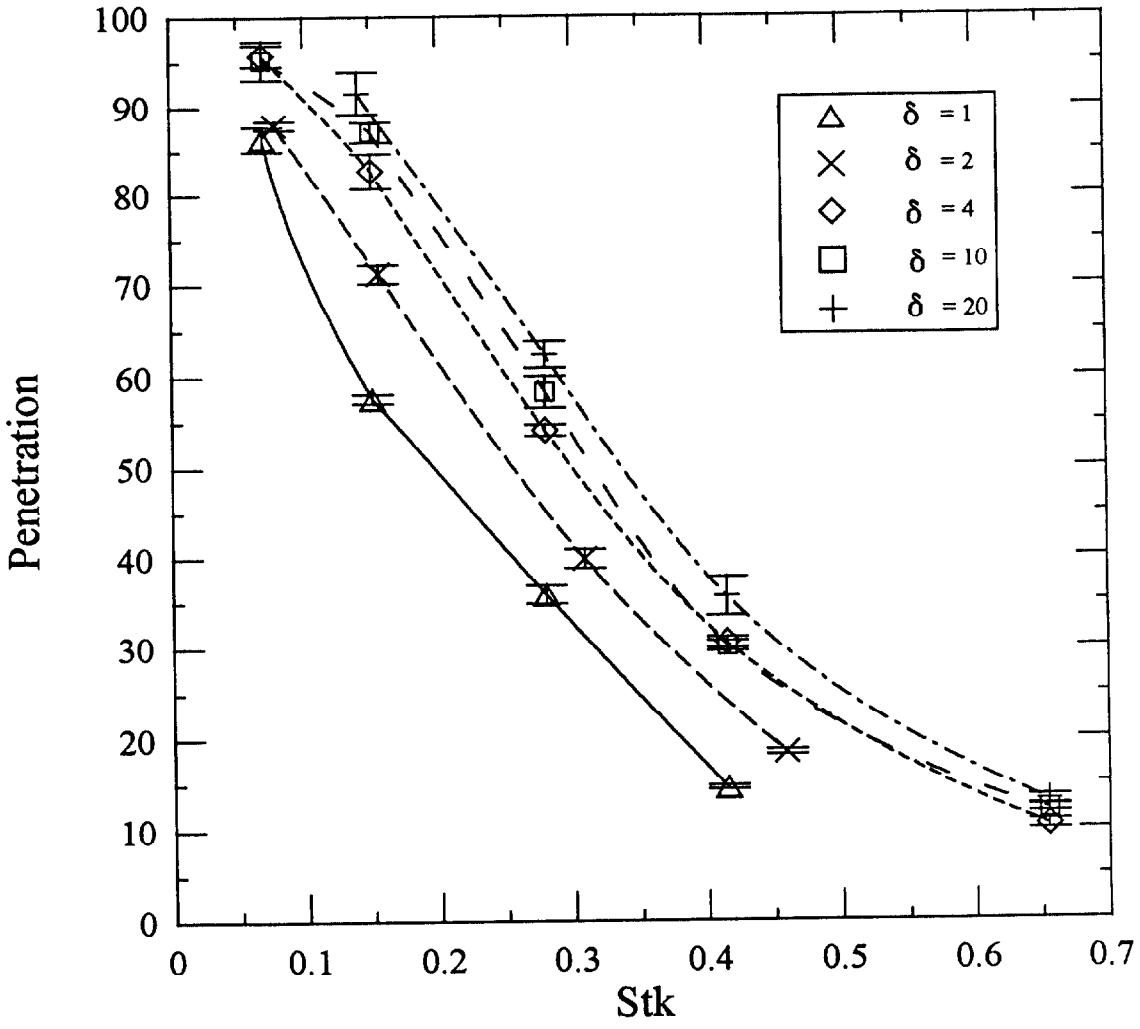

Figure 5. Experimental results showing the effect of curvature ratio on aerosol penetration through bends. The bends were designed as illustrated in Figure 1b, i.e., tube stubs were added to the bends with short radii of curvature.

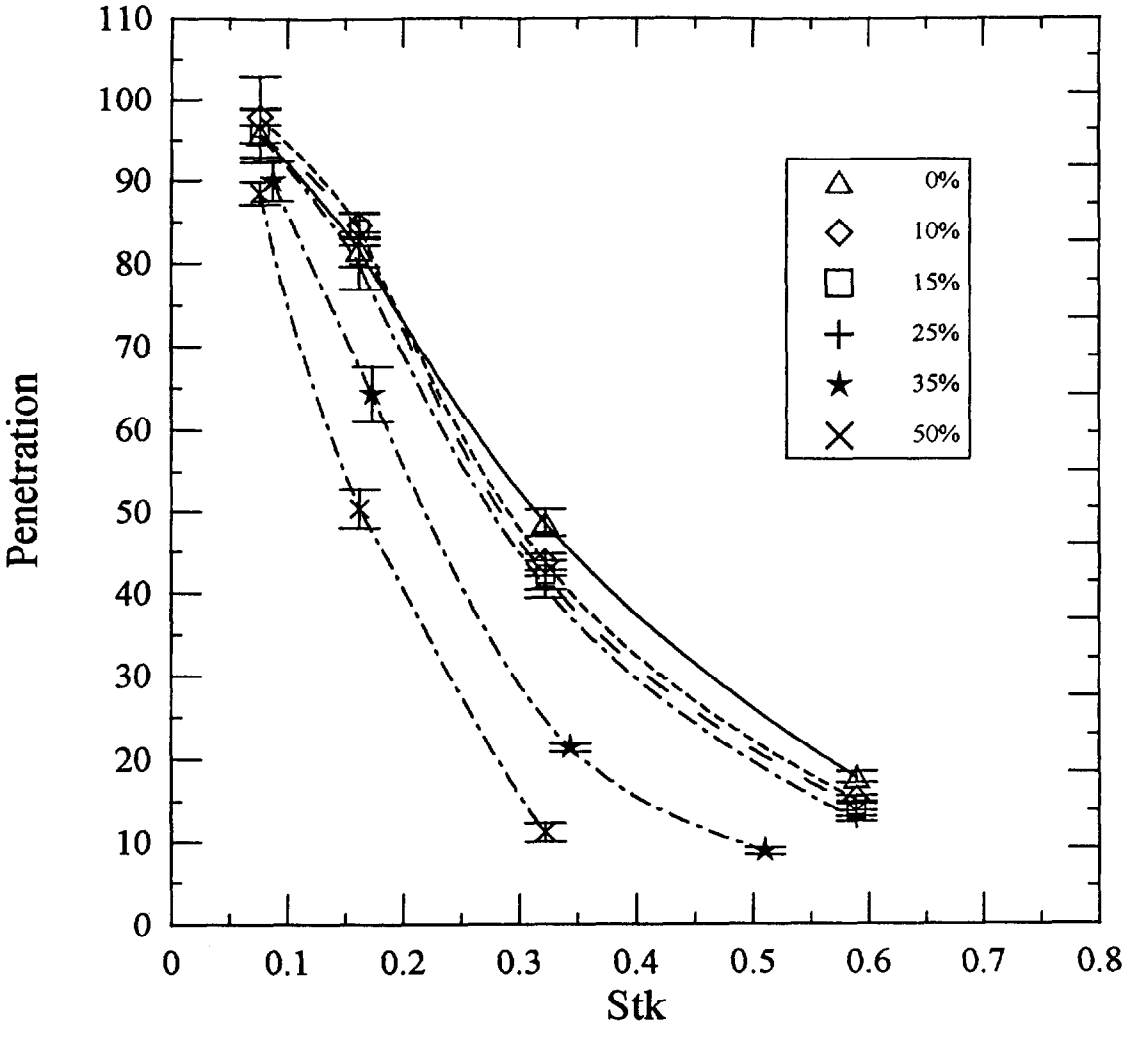

Figure 6. The effect of flattening the cross section of a bend. A 90° bend was pinched at the 45° location. The degree of flattening is the amount by which the tube diameter was reduced divided by the initial diameter. Data are for a tube that was initially 16 mm diameter with a curvature ratio of 10. Particle size used in the testing was 10 μm AD.

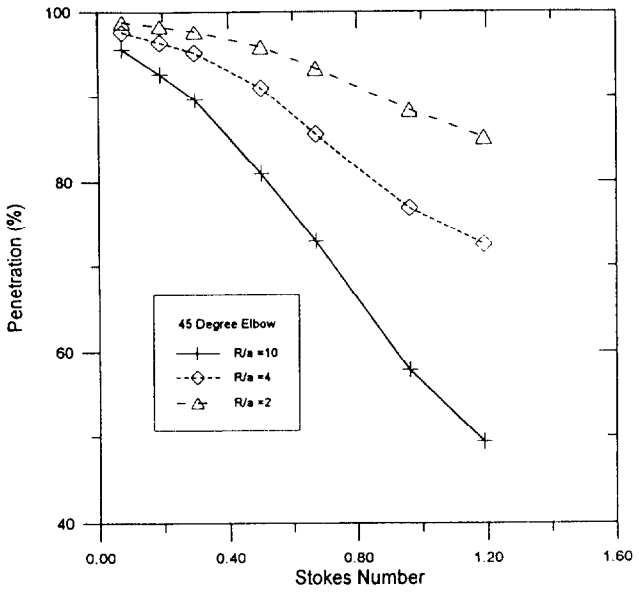

a)

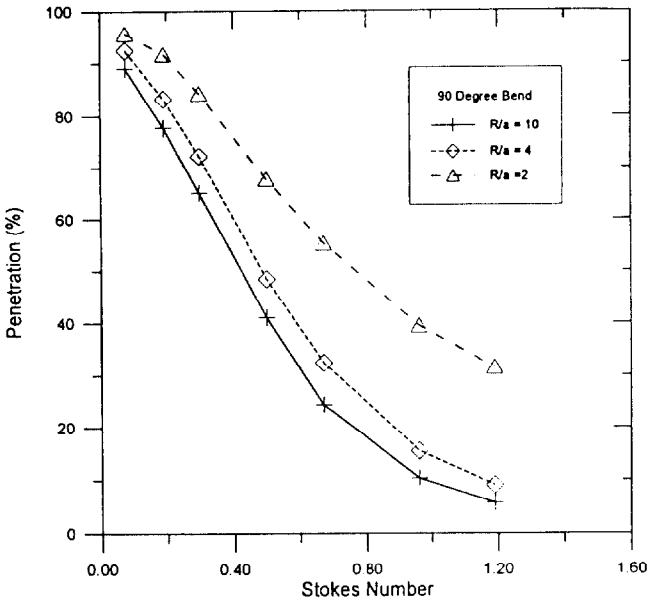

b)

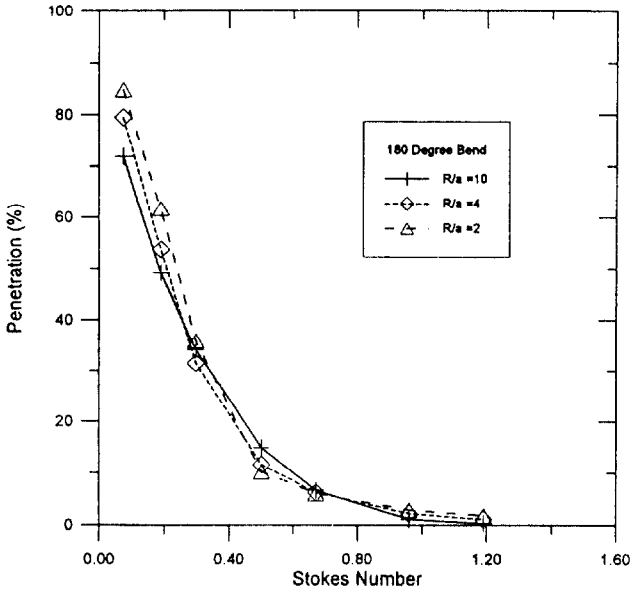

c)

Figure 7. Numerical results that show penetration as a function of Stokes number for constant values of curvature ratio and *Re* = 8210. a) Bend angle of 45° b) Bend angle of 90°. c) Bend angle of 180°.

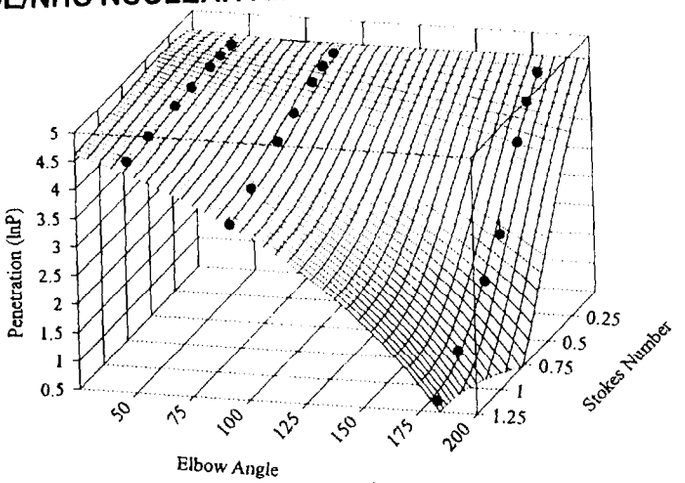

a)

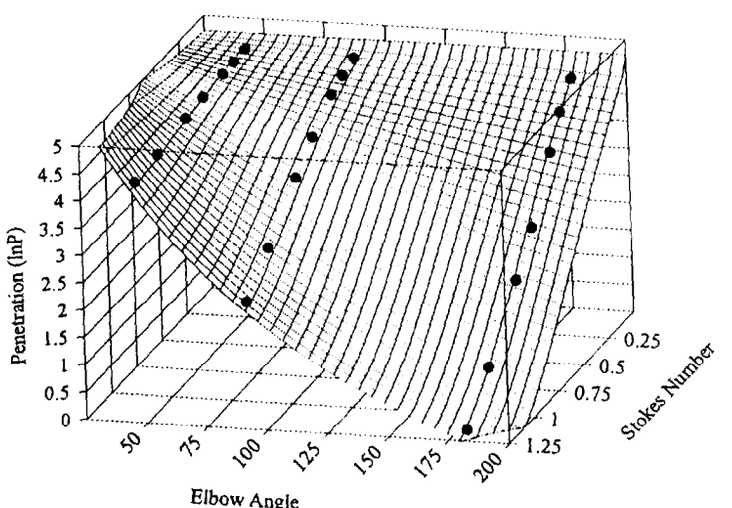

b)

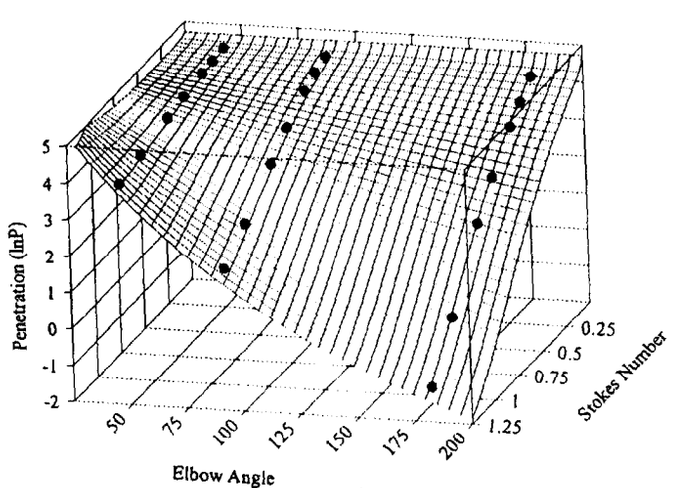

c)

Figure 8. Surface fitting of penetration as a function of Stokes number and bend angle, for constant values of curvature ratio. a) $\delta = 2$, b) $\delta = 4$, and c) $\delta = 10$.

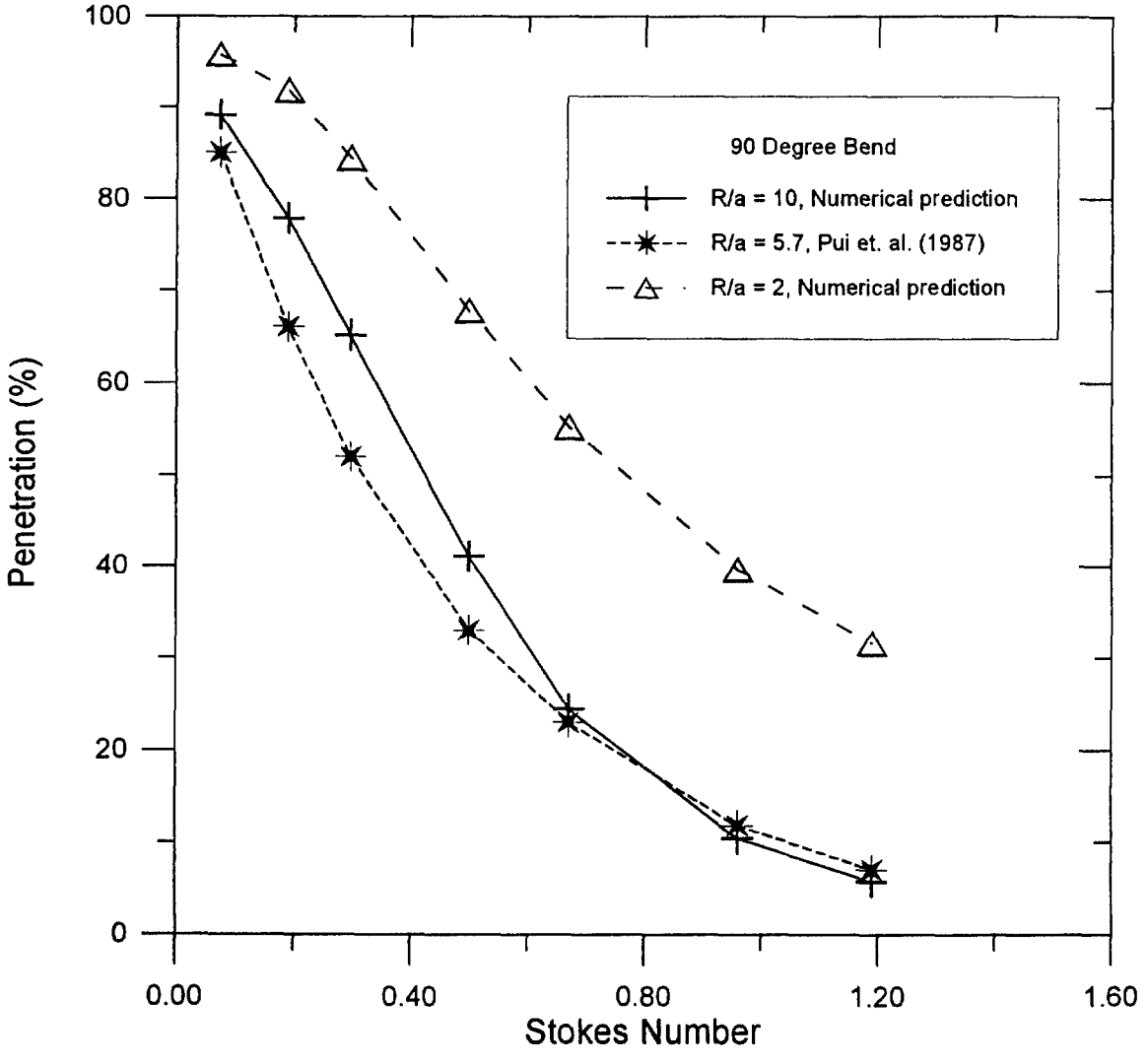

Figure 9. A comparison of the predictions of the correlation model (Equation 5) and the model of Pui et al. (1987).

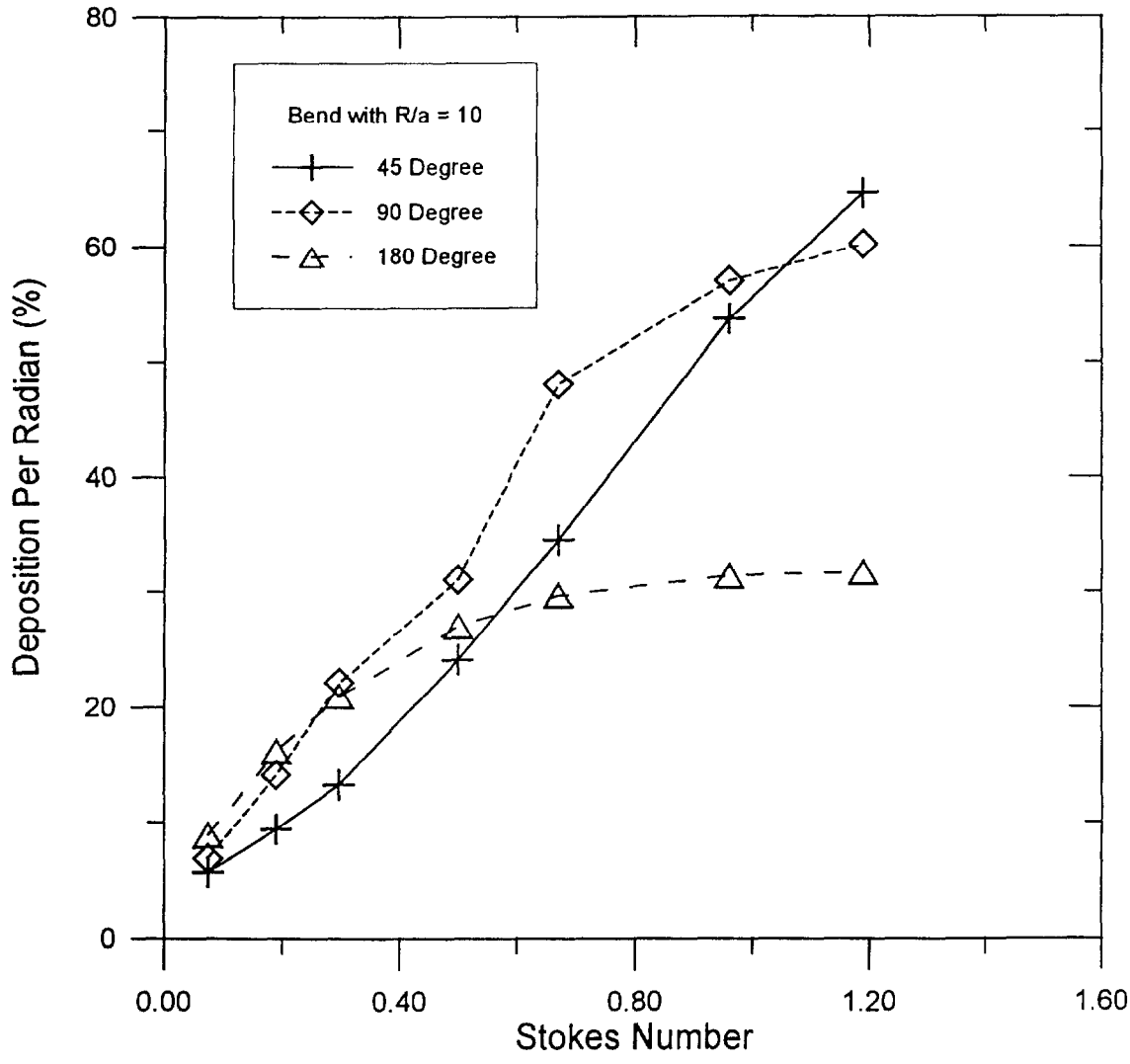

Figure 10. Effect of bend angle on deposition rate. The deposition per radian is the total aerosol lost to the internal wall of a bend divided by the bend angle.

DISCUSSION

FLEMING: How do you account for the effects of your filter sampling on your flow patterns in the downstream portion of the tube? How does that affect your flow patterns through the tube, and how do you sort that out?

MCFARLAND: What we do is assume that the sample transport line ends where the filter starts. Therefore, we make our predictions up to and including any sort of a transition, for example, an expansion or a contraction right ahead of the filter. However, the transport of aerosol from the free stream excludes the filter itself.

ADAMS: As most filter lines are lined and heated, would that have an effect on any of the data collection?

MCFARLAND: If a sample transport line was heated, I assume it is to prevent condensation of reactive gases or of water. In the code that we developed, the DEPOSITION code, we have built into it a sampling temperature and sample line pressure. The sample line pressure does not have a great impact on particle sampling transmission through a line. On the other hand, the temperature can have an effect. The temperature will influence the viscosity, which in turn will influence the particle DEPOSITION. But that is built into the deposition code, or at least into codes numbered 3.1 or higher. I am going to add that we have developed a Windows version of the DEPOSITION code. Those of you who have used the DEPOSITION code have a version which is DOS-only. The code in Windows-form is currently being reviewed by the sponsors of the work. I assume that we should be ready to release it within a couple months. If there is anyone that is interested in a copy, at no charge, leave a card with me and I will send you a free copy at the time that we do the release.

ENGELMANN: If you used the Reynolds number at the pinched bend, would you then find the deposition to be dependent upon Reynolds number? Have you any data on deposition downstream of the pinched bend? One might think it to be greater than deposition in straight tubes without bends.

MCFARLAND: In answer to the first question, we have not examined the effect of Reynolds number on a pinched bend. The data that we have on pinched bends is experimental, whereas our data on the effect of Reynolds numbers on un-pinched bends is numerical. With respect to the second question, the losses in a pinched bend are the sum of those in the pinched region and the regions of circular cross section in the bend. No experiments were conducted to directly compare losses downstream of pinched bends with the losses downstream of un-pinched bends; however, the data in Figure 4 show there are similar overall losses in bends that are pinched $\leq$ 25%, which suggests there may not be much difference between the losses downstream of pinched and un-pinched bends. Your comment on the losses in bends being greater than losses in straight tubes is well taken. Often the losses in bends are a couple of orders of magnitude greater than the losses in an equal length of straight vertical tubing.

ATMOSPHERIC DISCHARGES FROM NUCLEAR FACILITIES DURING DECOMMISSIONING: GERMAN EXPERIENCES AND CONCEPTS

H. Braun, R. Görtz, L. Weil
Federal Office for Radiation Protection, Germany

Abstract

In Germany, a substantial amount of experience is available with planning, licensing and realization of decommissioning projects. In total, a number of 18 nuclear power plants including prototype facilities as well as 6 research reactors and 3 fuel cycle facilities have been shut down finally and are at different stages of decommissioning. Only recently the final „green field" stage of the Niederaichbach Nuclear Power Plant total dismantlement project has been achieved.

From the regulatory point of view, a survey of the decommissioning experience in Germany is presented highlighting the aspects of production and retention of airborne radioactivity. Nuclear air cleaning technology, discharge limits prescribed in licences and actual discharges are presented. As compared to operation, the composition of the discharged radioactivity is different as well as the off-gas discharge rate. In practically all cases, there is no significant amount of short-lived radionuclides. The discussion further includes lessons learned, for example inadvertant discharges of radionuclides expected not to be in the plants inventory. It is demonstrated that, as for operation of nuclear power plants, the limits prescribed in the Ordinance on Radiological Protection can be met using existing air cleaning technology. Optmization of protection results in public exposures substantially below the limits.

In the frame of the regulatory investigation programme a study has been conducted to assess the airborne radioactivity created during certain decommissioning activities like decontamination, segmentation and handling of contaminated or activated parts. The essential results of this study are presented, which are supposed to support planning for decommissioning. for LWRs, Co-60 and Cs-137 are expected to be the dominant radionuclides in airborne discharges.

I. Introduction

During the operational phase of nuclear installations radioactive substances are discharged to the environment in liquid and airborne form. These discharges are subject to licensing and to surveillance and control.

When operation is terminated the transition to decommissioning takes place. This implies in general that plant states are essentially modified, media no longer required are removed and new systems for decommissioning purposes installed. Along with the technical changes, regulatory conditions change. In many cases, a new license is required. As the dominant mechanisms of discharge are different from operation as well, discharge limits or more general criteria for discharges prescribed in the license for decommissioning are in most cases different from those valid for operation.

In this paper, information is provided on German experiences and insights with the assessment, control and regulation of airborne discharges from nuclear installations in the phase of decommissioning. The discussion comprises an overview on plants being shut down permanently, the mechanisms leading to airborne radioactivity inside the plant, technology of discharge control, discharge limits, actual discharges and further regulatory aspects.

II. Nuclear Power Plants in Germany

II.I Overview

The situation concerning the use of nuclear power in the Federal Republic of Germany (early 1995) is as follows [1]:

19 nuclear power plants with a capacity of 21,824 MWe gross (20,735 MWe net) are in operation,

1 nuclear power plant unit with 1,302 MWe (gross capacity) is shut down for an undefined period, following court order,

1 nuclear power plant unit with 806 MWe gross was out of operation in 1993 and 1994 for hot repair works and adaptations,

15 nuclear power plant units with 3,330 MWe (gross) in total are finally shut down, i.e. decommissioning has been started, applied for or planned,

for

6 nuclear power plant units, the construction and assembly works have been stopped or the application for construction and operation has been revoked.

II.II Plants finally shut-down in Germany

The decommissioning of the first nuclear power plant of the Federal Republic of Germany, **Versuchsatomkraftwerk Kahl (VAK Experimental Reactor)** was decided in 1985. The decommissioning concept provides the total dismantling of the plant. The first two decommissioning licences for decommissioning allow the dismantling of internal and external systems of the controlled area, the handling with contaminated tools and equipment and with low activity secondary radioactive waste. Furthermore, procedures and equipment for the dismounting, disassembling, and packaging of contaminated and activated parts of the facility were tested. On 25th September 1993, the third licence for decommissioning according to section 7 of the Atomic Energy Act (Atomgesetz, AtG) was issued. Action against this third licence was dismissed by the Higher Administrative Court of the State of Bavaria on 17th August 1994, which means that the disassembling of the reactor pressure vessel and the biological shield as well as the clearance for reuse or disposal, of non-hazardous substances which have been authorized as non-radioactive waste has been approved. It is planned to finish decommissioning, including site restoration, by the year 2000.

For the **Mehrzweckforschungsreaktor (MZFR Research Reactor)**, which was finally shut down in 1984, it was decided in 1989, after comparison of various decommissioning options, to perform the immediate and complete dismantling of the installation. The dismantling of the MZFR takes place stepwise, each step requiring a licence according to Atomic Energy Act. On the basis of the five issued decommissioning licences for MZFR, the decontamination of the heat removal system and the moderator system, the dismantling of equipment, such as equipment of the turbine building, electric installations, reactor auxiliary and supporting systems, water treatment system as well as the dismantling of the cooling tower was performed or initiated. The dismantling including restoration of the site should be finished by the year 2001 after altogether 6 partial steps. On 15th April 1994, the fourth, on 30th May 1994, the fifth partial licence for the decommissioning of the MZFR were issued, approving further dismantling works.

Rheinsberg Nuclear Power Plant (KKR) with a gross capacity of 70 MWe (reactor WWER) was finally shut down in 1990. Application for decommissing of the plant was made on 30th March 1992. The first licence for decommissioning was granted on 28th April 1995. Demolition work has been started.

Total dismantling is planned for **Gundremmingen Nuclear Power Plant Unit A (KRB-A)** which was shut down in 1977. Dismantling is taking place in several project phases which are based on the corresponding atomic energy law licences. Phase I, in which lowly contaminated components and the steam- and feedwater circuits in the turbine building were dismounted, was finished in 1989. In phase II, the disassembling of highlier contaminated reactor coolant contacted components and systems from the reactor building was performed. In phase III, the last dismantling step, the disassembling of the reactor pressure vessel and its equipment including the reactor shield, will be provided. Based on the licence for phase III issued on 12th August 1992, the disassembly of the reactor equipment was partly achieved in 1994 (e. g. 2 steam dryer units).

The **Jülich Atomversuchskraftwerk (AVR-Reactor, an experimental high temperature gas-cooled reactor with pebble bed)**, shut down in 1988, shall be transferred to safe enclosure after disassembly of equipment parts such as turbine, generator, condenser and condensate treatment system. The competent regulatory authority has approved the decommissioning concept and the safe enclosure in 1991. In the period from April to June 1992, the available 5,704 unused fresh fuel spheres balls were removed from the AVR-facility. The licence for decommissioning, unloading of the reactor core, dismantling and disassembling of equipment and safe enclosure of the AVR was issued on 9th March 1994.

The unloading of the spherical fuel elements out of the reactor into the central interim storage facility in the Jülich Research Centre was started.

The **Lingen Nuclear Power Plant (KWL)** was decommissioned in 1977 after 9 years of operation. Based on the licence of 21st November 1985, the facility was transferred to safe enclosure, which began in 1988. The safe enclosure involves the reactor building and the auxiliary building including the connecting building. All controlled areas situated outside this area were decontaminated, cancelled, and partly dismounted. The safe enclosure is monitored from the adjacent Emsland Nuclear Power Plant. After about 25 years of safe enclosure operation, it is planned to start the complete dismantling of the plant.

The **Heißdampfreaktor Großwelzheim (HDR, a nuclear superheated BWR)** finally shut down in 1971, was used after shut down for non-nuclear investigations and R&D on behavior of nuclear installations in the case of severe accidents. Decommissioning of the reactor was approved on 16th February 1983. The above-mentioned test programme was finished in 1991. Complete dismantling of the facility is planned until 1998. A second licence for decommissioning was granted on 29th December 1994 which also covers the disassembling of the reactor pressure vessel and parts of the primary circuit.

The **Niederaichbach Nuclear Power Plant (KKN, a heavy water moderated, gas cooled pressure tube reactor)**, which was decommissioned in 1974, is the first NPP in the Federal Republic of Germany being completely dismantled. The NPP was permanently shut down and transferred into safe enclosure in 1983, dismantling began in 1987. The dismantling of inactive and contaminated parts of the facility, except from activated areas near the core, was finished in 1990. The dismantling of the activated parts was finished at the end of 1993. Evidence taking measurements performed in the facility for clearance of the buildings were completed. The Ministry of State for Regional Development and Environmental Aspects of the State of Bavaria dismissed the KKN plant from the application of the Atomic Energy Act on 17th August 1994 and reported that the plant is released for conventional dismantling according to building law. Thus, the complete dismantling of a nuclear power plant was performed for the first time in Europe. The site restoration was celebrated on the 17th August 1995. The radioactive waste amounted to about 2% of the overall amount of decommissioning wastes.

The units 1 to 4 of the **Greifswald Nuclear Power Plant (KGR, WWER type, W-230 reactor)**, were shut down in 1990.

The dismantling of all five units will be achieved without preceding safe enclosure. An application for decommissioning and dismantling of plant units was submitted on 17th June 1994. The first licence for decommissioning was granted by 30th June 1995. Demolition of the facility has started.

Adjacent to the Greifswald site, an intermediate storage and waste treatment facility is under construction (Zwischenlager Nord, ZLN).

The **Kompakte Natriumgekühlte Kernreaktoranlage (KNK II, a sodium cooled Fast Breeder Research Reactor)** was finally shut down in 1991, after finishing its test programme. The shut-down was started with the removal of the fuel elements. The decommissioning concept provides for a stepwise disassembly up to the full dismantling of the plant. The first licence for decommissioning of the facility was granted on 26th August 1993, the second one on 30th May 1994. Since 26th May 1994, the nuclear fuel is completely removed . The third licence for decommissioning was granted on 21st February 1995 approving, among other points, the taking out of operation of the secondary coolant circuit as well as construction, operation and dismantling of a drumming station for the disposal of the secondary natrium. An application for granting the fourth licence for decommissioning has already been submitted.

The **Thorium Hochtemperaturreaktor (THTR-300, a gas cooled high temperature reactor)** was shut down for being decommissioned in 1989. For the facility a period of safe enclosure is planned. On 17th March 1992, the Federal Office for Radiation Protection granted the licence for the storage of irradiated fuel elements from THTR-300 in the **Ahaus Fuel Element Interim Storage Facility (BZA)**.

The first licence for decommissioning, unloading of the reactor core and dismantling of equipment components was issued on 22nd October 1993. Since then, the spherical fuel elements have continuously been removed from the core. The core content had fully been removed by the end of 1994. All 305 Castor containers with fuel elements have been stored in the Ahaus Interim Storage Facility until April 1995.

In 1995, it was decided to finally shut down the Würgassen NPP, a BWR with an electrical power of 670 MW, which had been in operation from 1971 to 1994. Planning for decommissioning is underway.

Obviously, there is a substantial amount of decommissioning experience in Germany. It covers all stages of decommissioning like immediate dismantlement, safe enclosure and dismantlement after safe enclosure and combinations of these basic patterns.

III. Decommissioning operations creating airborne radioactivity

III.I General

Before decommissioning commences, it is assumed that the nuclear fuel and other media not required during decommissioning are removed from the plant in the frame of the operating license. In real cases of decommissioning, however, this is not always fulfilled.

In a nuclear power plant, the remaining inventory of radioactivity is then given by activated RPV and RPV-internals, the activated part of the biological shield, contaminated systems and components and, finally, contaminated building structures.

Decommissioning operations can be roughly divided into dismantling, decontamination, handling and waste management. Each of these areas of activities consists of numerous subtasks characterized by technology and application. During practically all of them airborne radioactivity is created. Thermal cutting techniques like plasma arc cutting or oxy-acthylene cutting for example procuce significant amounts of aerosols. Practically relevant examples of decommissioning operations and aspects of airborne radioactivity are discussed in chapter 4.

III.II Study results

In a study, [2] this has been assessed on a generic basis for the case of the total dismantlement of a modern 1300 MWe PWR. Essential results obtained for the atmospheric discharges and the resulting exposure to the public are summarized in table 1. Even if the variability in generically postulated methods and data is taken into account, the central finding that public exposure is substantially below the prescribed limits given in the next chapter remains valid.

Table 1: Dismantlement of a modern 1300 MWe PWR;
estimates of atmospheric discharges and dose calculations as given in a generic study [2]

Radionuclide	Atmospherically discharged radioactivity (Bq)	Calculated effective dose (µSv)
Co-60	$5{,}4 \cdot 10^{6}$	$1{,}4 \cdot 10^{-2}$
CS-137	$1{,}7 \cdot 10^{7}$	$7{,}8 \cdot 10^{-2}$
Cs-134	10^{4}	$6{,}4 \cdot 10^{-5}$
Mn-54	10^{5}	$1{,}5 \cdot 10^{-5}$
Eu-152	10^{4}	$2{,}4 \cdot 10^{-6}$
Ni-59	10^{3}	$7{,}3 \cdot 10^{-9}$
Ni-63	10^{5}	$1{,}4 \cdot 10^{-6}$
Nb-94	10^{3}	$1 \cdot 10^{-5}$
Fe-55	$3 \cdot 10^{5}$	$4 \cdot 10^{-6}$

IV. Regulatory aspects

According to section 7 para 3 of the Atomic Energy Act the decommissioning of a nuclear installation as well the safe enclosure of a finally decommissioned installation or the dismantling of the installations or of parts thereof require a license.

The level of protection against exposure of the public from discharges in air or water is defined in section 45 of the Ordinance on Radiological Protection (ORP). The dose limits per calendar year are:

1.	Effective dose, partial body dose for gonads, uterus, red bone marrow	0.3 mSv
2.	Partial body dose for all organs and tissues unless specified in 1. or 3.	0.9 mSv
3.	Partial body dose for bone surface, skin	1.8 mSv

In section 28 of the ORP it is furthermore required to keep exposures even below these limits as low as practicable.

In the licensing procedure for decommissioning discharge limits are defined in compliance with these requirements.

V. Selected information on decommissioning projects

V.I General Remarks

For the retention of the airborne radioactive particulates, which are released in dismantling operations in shut down nuclear power plants, firstly the filter systems installed during power operation and still operated at present are available [3]. These are filter trains of the vent air filter system, the system exhaust air filter system and the subatmospheric pressure maintenance system which, for particulate removal, are provided with a prefilter, two category C particulate air filters, and one high-efficiency particulate air (HEPA) filter. The effective removal efficiencies of these filter trains with respect to the spectrum of particulates reaching them are well above the decontamination factor of 3×10^3 which is guaranteed solely for the new HEPA filter for the particles of the most penetrating size. On account of the series connection with the prefilter, the two category C particulate air filters, growing dust loading as well as the actual spectrum of particulates taken into account, total decontamination factors > 10^6 can be anticipated. So, these filter systems alone offer an effective protection against inadmissible emissions of radioactive particulates arising in decommissioning operations.

In the course of dismounting work additional measures are taken with the goal to support the air filter systems mentioned above and to further reduce discharges to the environment. These measures consist in

- keeping as low as possible the source term,
- retaining the released particulates by exhausting them where they are produced, and
- removing most of them in filter units installed in addition.

the goal pursued is not only to minimize the emission of radioactivity, but, at the same time, to avoid the spread of contaminations from dismounting work and, besides, to reduce internal exposure of the dismounting staff resulting from inhalation. Attaining these goals justifies additional expenditure which, in some cases, might be quite considerable.

The extent of additional measures required is quite different in the three most important dismantling phases, namely dismounting of the contaminated primary system, of the activated reactor pressure vessel with internals, and of the reinforced concrete of building structures, especially the biological shield. A great volume of coarse dust with low specific activities and easily to manage arises in dismantling concrete structures, whereas the most stringent requirements have to be met in dismantling the reactor pressure vessel and ist internals. In the latter case specific activities on the order of 10^8 Bq/g might have to be expected [4]. The requirements to be fulfilled in dismantling contaminated systems are on a level between the two cases mentioned above. It should be taken into account also that dismounting of the primary loops is often preceded by chemical decontamination as practiced for instance under the MZFR decommissioning project [5]. The primary objective pursued is to allow for manual dismounting with acceptable low radiation exposure of the staff. At the same time, smaller source terms will arise from dismounting work and hence a positive effect on the emissions to the atmosphere is

achieved as well.

V.II Engineering Measures for Minimizing Radioactive Particulate Emissions

Emission control starts already with the minimization of the source term resulting from cutting operations. This means that to the extent feasible by the respective dismounting work cutting techniques will be applied which will produce no or only very few aerosols. Thus, preference will for instance be given to techniques such as mechanical cutting, shearing, and abrasive cutting. In cases where the application of thermal cutting techniques cannot be avoided, the relevant parameters will be optimized such that the least possible amount of aerosols is produced [6].

In order to remove the radioactive particulates released, the atmosphere has to be exhausted and filtered. In standard cases it will be sufficient to install a hood above the workstation. However, in this way only about 90% of the particulates are normally safely retained which is equivalent to a decontamintion factor of as little as 10. It is known that subsequent filtration produces much higher efficiencies. Consequently, in order to improve primary dust removal, the completest possible exhaust has to be aimed at. This is feasible by setting up a tent or housing around the workstation which is frequently practiced. This concept was implemented in a very sophisticated manner in the course of the meanwhile completed dismounting of the Niederaichbach Nuclear Power Plant (KKN). For remotely cutting up the pressurized tube reactor with its highly complex core structure an additional containment within the reactor containment was installed around the reactor tank [7, 8]. Existing structures of the building were used for construction. In this additional containment kept at a negative pressure with respect to the containment atmosphere directed air flow was maintained. The vent air was cleaned in a purpose-built filter bench, 30,000 m^3/h through-put, and then carried into the vent air system of the containment for secondary cleaning. This solution to the problem is represented schematically in Fig. 1. It allowed to avoid the very expensive dismounting under water and thus helped saving a considerable amount of costs. In this context, operations were facilitated by the fact that the maximum specific activations were on the order of 10^5 Bq/g only due to the short operation period of the plant.

By contrast, the highly activated reactor pressure vessel with internals will normally be dismounted under water using remotely handled tools [9]. This necessitates, as a rule, installation of a suitable water tank around the reactor pressure vessel. Water in that case does not only serve to remove the aerosols generated in the cutting operations but it acts also as a shield protecting the operating staff. Typical experiments have made evident that 10^{-3} to 10^{-4} of the kerf material removed in the cutting operations is released as aerosols above the water surface [10, 11]. As a rule, these aerosols will be exhausted above the water surface and removed in particulate air filters as for instance practiced in the course of decommissioning of the Gundremmingen Nuclear Power Plant, Unit A [12].

A great variety of commercial filter techniques are suited for removal of the dusts and aerosols, respectively, released in cutting up operations. Experience accumulated in the recenlty completed demolition of the Niederaichbach Nuclear Power Plant proved that cleanable particulate air filters should be best suited for this purpose. They comprise two series-connected particulate air filters operated at reduced volume flow rate of approx. 1000 m^3/h per standard sized filter element. The first filter is cleaned by cyclic backflushing whereas the second serves as a safety device. Since the late seventies the successful application of particulate air filters provided with cleanup device has been reported in Germany [13, 14]. Cleanable particulate air filter systems are available on the market. Work on their improvement is under way [15, 16].

It is generally known that the outstanding feature of such a filter combination are extremely high decontamination factors. Besides, very great amounts of dust can be removed. Consequently, the operating costs are justified which are caused mainly by filter changeout and disposal of the loaded filters [17]. Finally, cleanable particulate air filter systems are suited to remove all particles of the spectrum encountered in decommissioning work.

During decommissioning of KKN several small mobile particulate air filter systems were used as well as the already mentioned stationary system with a throughput of 30,000 m^3/h. It was possible by these additional filter devices to keep extremely low the monthly emissions of particulate ß-radioactivity during the whole period of decommissioning from July 1988 until June 1994. Figure 2 shows the respective values of releases [18]. As a rule, they range from 10^3 to 5×10^4 Bq, with the maximum values measured during the phase of dismounting of the activated pressurized tube reactor. The radiation burdens resulting from these emissions at the point of maximum deposition are negligible compared with exposure to natural radiation, a finding that is consistent with the general estimate provided in chapter 3.2. This experience shows that particulate removal during dismounting of nuclear power plants can be very effectively controlled with the engineering tools presently available.

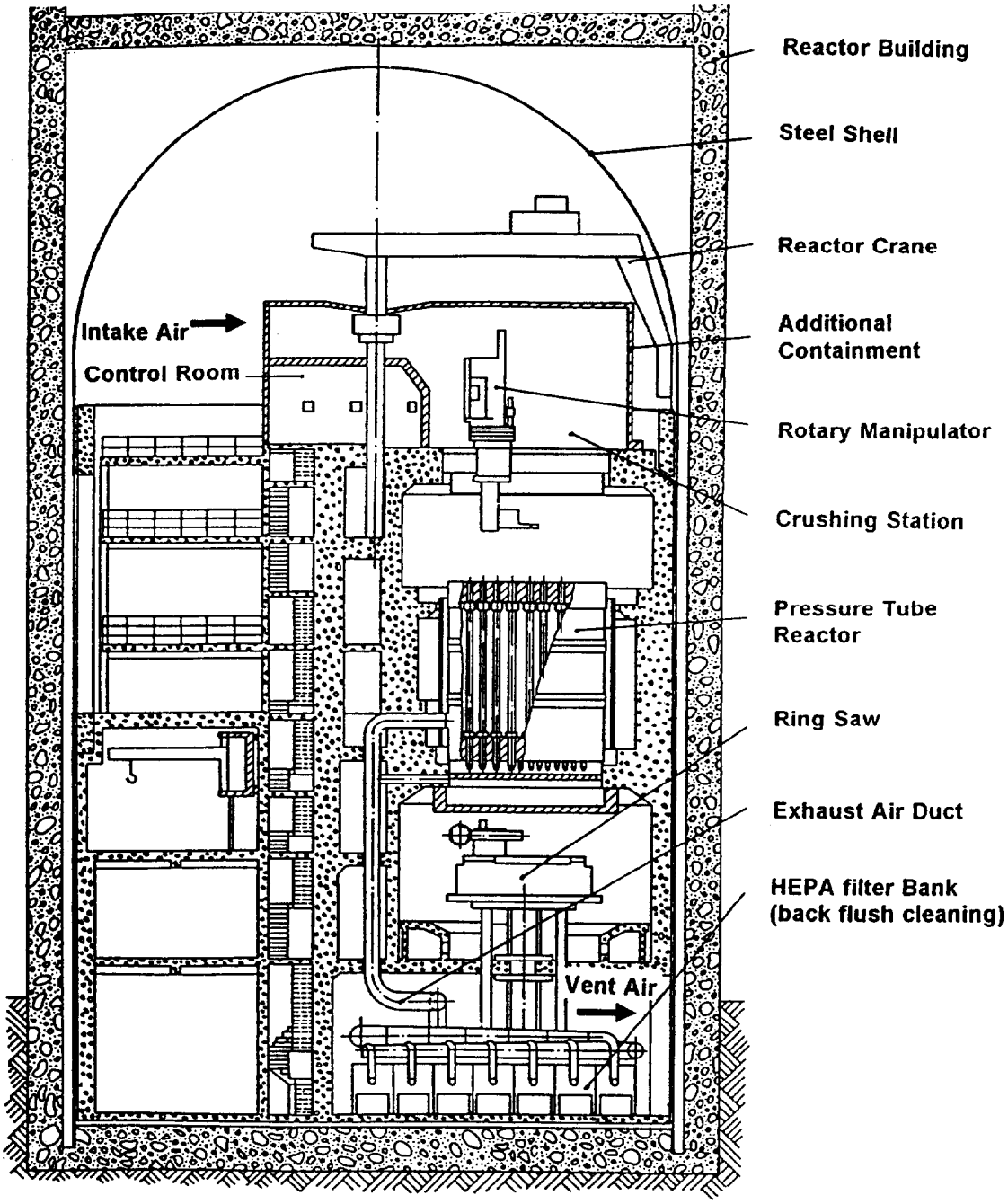

Fig. 1: Additional containment for the dismantling of the activated pressure tube reactor of KKN.

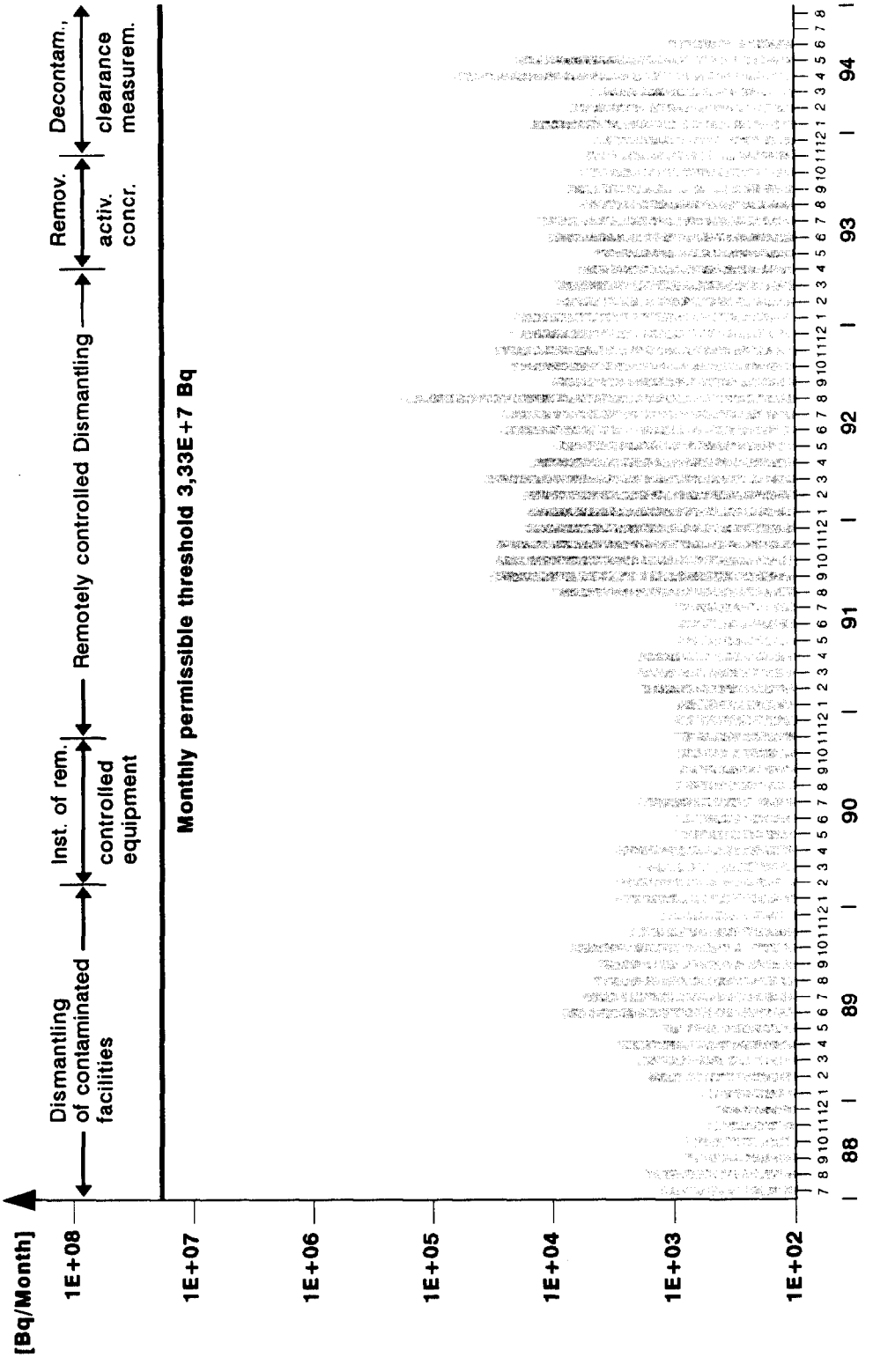

Fig. 2: Monthly emissions of particulate radioactivity during the decommissioning of KKN.

VI. Summary and conclusions

Atmospheric discharges from nuclear facilities finally shut-down are subject to regulation and control as during operation.

The nature of the discharges during decommissioning are in general different. Short-lived radionuclides have decayed and media (nuclear fuel, coolant, operational waste) no longer required are removed from the site and treated or stored elsewhere. In general, long-lived radionuclides in aerosol form are the most relevant group governing the atmospheric discharges during decomissioning.

The processes that lead to the formation of airborne radioactivity during decommissioning operations are quite well known. Generally speaking, they are segmentation, decontamination, handling and conditioning of radioactive parts and components. Thermal cutting of metal components is of special relevance.

As confirmed by the substantial amount of decommissioning experience in Germany, the technology is available for control and retention of airborne radionuclides. It generally consists of a combination of in-situ exhaust with prefiltering and aerosol filters for the overall atmospheric discharges.

Experience shows that in actual decommissioning projects the legal requirements of observing dose limits and keeping exposures below these limits as low as practicable are met. Public exposure due to atmospheric discharges is negligable. Theoretical studies demonstrate that this can be achieved as well in the substantial amount of decommissioning work that will be faced in the decades ahead, when the modern nuclear power plants approach the end of their projected life time and might be taken out of service.

Acknowledgement

The authors gratefully acknowledge the support provided by Mr. V. Rüdinger from KBG (Kernkraftwerk Betriebsgesellschaft mbH) in terms of technical information on decommissioning projects.

References

(1) F. Philippczyk, J. Hutter
"Stand und Entwicklung der Kernenergienutzung 1994 in der Bundesrepublik Deutschland" Bundesamt für Strahlenschutz/Fachbereich Kerntechnische Sicherheit (BfS-KT-10/95)

(2) R.Görtz, R.Graf, S.Kistinger, A.G.Knaup
Genehmigungsrelevante Aspekte der Nachbetriebsphase kerntechnischer Anlagen
Schriftenreihe Reaktorsicherheit und Strahlenschutz
BMU-1991-324, ISSN 0724-3316

(3) V. Rüdinger; C.I. Ricketts; J.G. Wilhelm;
HEPA Filters of High Structurals Strength for Nuclear Air Cleaning Systems;
ASHRAE TRANSACTIONS V.95 (1989), Pt. 2.

(4) V. Massaut; et al.;
Pilot Dismantling of the BR3 Pressurized Water Reactor;
in: R. Wampach et al (Editors), Decommissioning of Nuclear Installations, Luxembourg 1995, pp. 32.

(5) W. Demant;
Stand der Stillegungsaktivitäten des Mehrzweckforschungsreaktors;
3. Statusbericht Stillegung und Rückbau kerntechnischer Anlagen,
Bad Dürkheim, 8.-10. November 1995, pp. 123.

(6) H. Stoiber; G. Hammer; H. Schultz;

Emissionsreduzierung bei der Anwendung thermischer Trennverfahren zur Zerlegung kerntechnischer Anlagen - Autogen- und Plasmatrennen;
ibid. pp. 251.

(7) V. Rüdinger; G. Engelhardt;
Beseitigung des Kernkraftwerkes Niederaichbach (KKN), Atw 36 (1991),
pp. 555.

(8) G. Engelhardt; K. Grabenstätter; L. Valencia;
Über die prototypische Stillegung des KKN - Ablauf, Erfahrungen und Stand der Arbeiten; KfK-Nachrichten 24 (1992), pp. 95.

(9) G. Engelhardt;
Technische Lösungen zur RDB-Zerlegung; Atw 40 (1995), pp. 619 - 623.

(10) B. Waldie; et al.;
Solid and Gaseous Secondary Emissions from Underwater Plasma Arc Cutting;
in: K. K. Pflugrad; et al. (Editors), Decommissioning of Nuclear Installtions, EUR 12690 (1990), pp. 239.

(11) J.P. Dufayet; et al.;
Underwater Thermal Cutting Techniques and Associated Remote-Controlled Manipulator Systems;
Ref. 2; pp. 227.

(12) N. Eickelpasch; H. Steiner; A. Fischer;
Pilot Dismantling of the KRB A Boiling Water Reactor;
Ref. 2; pp. 47.

(13) I. Gail;
Neues wirtschaftliches Verfahren zur Feinstaubabscheidung von staubbeladenen Gasströmen;
Staub Reinh. Luft 37 (1977), pp. 175.

(14) W. Zwanzig;
Hochleistungsschwebstoffilter zur großtechnischen Feinstreinigung von Gasen;
Chem. Techn. 7 (1978), pp. 101.

(15) H. Leibold; T. Leiber; I. Döffert; J.G. Wilhelm;
Grundlagen und Technik der Abreinigung von Schwebstoffiltern durch Rückspülung;
KfK-PEF 109 (1993).

(16) M. Fronhöfer; H. Leibold;
Abreinigungstechnik für Schwebstoffilter zur Entstaubung großer Volumenströme bei hohen Staubkonzentrationen;
FZK-PEF 135 (1995).

(17) P. Böhm; V. Girod;
Effectiveness and Long-Term Behaviour of Automatically Cleanable High Efficiency Aerosol Filters;
EUR 15463 EN (1995).

(18) L. Valencia;
Progress Report for the Niederaichbach Nuclear Power Plant (KKN);
OECD/NEA Co-operative Programme on Decommissioning;
18th. Meeting of the Technical Advisory Group, April 1995, Mito, Japan.

DISCUSSION

BERGMAN: What is the experience with the cleanable HEPA filter? Has there been any damage to the media? Is the media the reinforced type?

WILHELM: Often cleanable HEPA filters are used in Germany without prefilters to remove industrial dust in the g/m^3 range. On the downstream side the medium of the cleanable HEPA filters is reinforced with a glass fiber web, such as the medium of the Lydair 3255 LW 1, or with a web from organic fibers, for example of polycarbonate fibers. It is also important that the pleats be round at the edge. We tried cleanable HEPA filters in different factories including the production of cement. They operated well and had long services lives. Using optimized HEPA fillers and cleaning methods, even the loss of removal efficeincy down to around 99% after large numbers of cleaning cycles could be avoided

BERGMAN: A couple of conferences ago we presented a comparison of cleanable steel HEPA filters and standard glass HEPA filters. With a standard very gentle reverse pulse, we had dozens and dozens of holes; all the bottom pleats were blown out. Is the reason your filter survives the reverse air blast because it is a very, very slow and gentle reverse flow?

WILHELM: The method and the flow velocity during loading and cleaning of the HEPA filter are optimized. The flow velocity is not very slow during the reverse air blast. The larger particles should not be removed upstream of the HEPA filters because they produce the removable filter cake on the surface of the medium and thus prevent the very small particles from penetrating deeper into the medium. Small particles, deposited in the depth of the medium, normally will not cause the formation of a removable filter cake. Therefore, also the filtration speed should be limited. With a loading of particles only with diameters around $1\mu m$ we did not have good results with cleaning cycles.

FUKASAWA: Which nuclides were easy to be discharged to the atmosphere? Did you estimate the discharged ratio i.e., the discharged radionuclides/total amount of the facility?

WILHELM: According to the paper Co-60 and Cs-137 are the most important radionuclides for airborne discharge during decommissioning. The data for the ratio of discharged radionuclides in relation to the inventory are not available.

HEATING, VENTILATING, AND AIR CONDITIONING DEACTIVATION THERMAL ANALYSIS OF PUREX PLANT

William W. Chen and Robert A. Gregonis
Westinghouse Hanford Company
Richland, Washington

ABSTRACT

Thermal analysis was performed for the proposed Plutonium Uranium Extraction Plant exhaust system after deactivation. The purpose of the analysis was to determine if enough condensation will occur to plug or damage the filtration components. A heat transfer and fluid flow analysis was performed to evaluate the thermal characteristics of the underground duct system, the deep-bed glass fiber filter No. 2, and the high-efficiency particulate air filters in the fourth filter building. The analysis is based on extreme variations of air temperature, relative humidity, and dew point temperature using 15 years of Hanford Site weather data as a basis. The results will be used to evaluate the need for the electric heaters proposed for the canyon exhaust to prevent condensation.

Results of the analysis indicate that a condition may exist in the underground ductwork where the duct temperature can lead or lag changes in the ambient air temperature. This condition may contribute to condensation on the inside surfaces of the underground exhaust duct. A worst case conservative analysis was performed assuming that all of the water is removed from the moist air over the inside surface of the concrete duct area in the fully developed turbulent boundary layer while the moist air in the free stream will not condense. The total moisture accumulated in 24 hours is negligible. Water puddling would not be expected. The results of the analyses agree with plant operating experiences.

The filters were designed to resist high humidity and direct wetting, filter plugging caused by slight condensation in the upstream duct is not a concern.

I. INTRODUCTION

This paper documents the results of a thermal analysis that was performed for the proposed Plutonium Uranium Extraction (PUREX) Plant exhaust system after deactivation. The analysis was performed to determine if enough condensation will occur in the concrete duct to raise a concern and to plug or damage the filtration components. A thermal and fluid flow analysis was performed to evaluate the temperature characteristics of the underground duct system, the deep-bed glass fiber (DBGF) filter No. 2, and the high-efficiency particulate air (HEPA) filters in the fourth filter building (Figure 1). The analysis is based on the extreme variations of air temperature, relative humidity, and dew point temperature using 15 years of Hanford Site weather data as a basis. The results will be used to evaluate the need for the electric heaters being considered for the PUREX canyon exhaust to prevent condensation.

The pressure drop of moist air through the filter media because of the Joule-Thomson effect is addressed. Calculations that demonstrate the effect are presented.

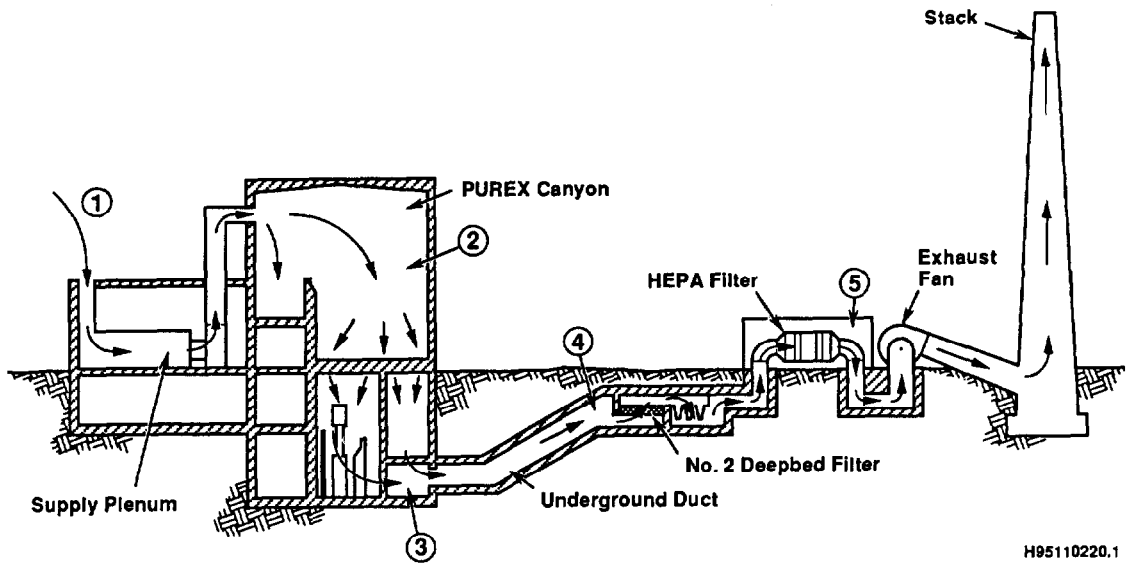

Figure 1. Operating System.

II. SYSTEM BACKGROUND

The ventilation system for the deactivated PUREX plant will consist of a draw-through system as shown in Figure 1. One of 3 canyon exhaust fans with a capacity of 40,000 ft^3/min (18.88 m^3/sec) will maintain negative pressure on the canyon, which provides the motive force to bring outside air into the plant. The proposed design cascades ventilation air through various zones within the plant to the PUREX canyon where it exits through the air tunnel to the underground duct work. The exhaust air passes through the DBGF filter No. 2, the fourth filter building containing HEPA filters, and the main stack to the atmosphere.

III. OPERATING EXPERIENCES

Before 1982, air washers in the supply air inlet plenums were used throughout the year. Large quantities of moisture were added to the air stream providing a mechanism for condensation far greater than what will occur during the surveillance and maintenance period. Available operating history shows no record of filter plugging or large accumulations caused by water condensation. Drains in the underground filter plenums eliminated condensate water that may have formed, but no water was entrained into the air stream to plug the deep bed or HEPA Filters.

The east and west sample gallery hood exhaust system exhausts to underground HEPA filter housings. The cover blocks of the filter housings are exposed to the ambient temperature. During HEPA filter replacements in 1987 and 1992, no high water marks or water damage were observed on any of the filters or plenum walls.

On several occasions in 1992, contamination was found to be dripping from the exhaust duct of the sample gallery hood when the spray washers were turned on. The dripping was attributed to a chemical compound in the ductwork that had an affinity for water. Since 1992, the spray washers have been left off from early spring until late fall. This eliminated the contamination dripping from the duct work. It also provided a 3-year spring/summer operating history that duplicates the sample gallery exhaust (SGE) ventilation during deactivation. No dripping or wetting of the ductwork, piping, and walls has been detected or reported.

During the winter, the sample gallery reheat coil supplies 70 °F (21.11 °C) air to the sample gallery. The walls, which maintain a temperature of 55 °F (12.78 °C), because of the earth's insulating effect, have shown no condensation or dripping. This provides the confidence necessary to predict that the sample gallery will not experience any condensation throughout the year.

IV. ANALYSIS PROCEDURES

The thermal and fluid flow characteristics were evaluated to determine the worst case variations at different locations along the flow path from the PUREX canyon to the 291-AE building (Figure 1). The basic mechanisms for condensation and frost formation were evaluated. The effects of heating and cooling in the underground portions of the ductwork were also described and evaluated. The temperature variations between the duct and exhaust air are investigated to determine if condensation and/or frost formation are likely under these conditions.

Condensation or Moisture Formation

Condensation Principle

Condensation or moisture formation may occur from the humid air under certain flow and thermal conditions. When moist air is exposed to a surface that is colder than the dew point temperature of the air, a trace of moisture film will appear on the surface (McQuiston and Parker 1988). This phase change is called condensation. The dew point (DP) temperature on the wall surface is the controlling factor for condensation to occur. The following conditions prevent condensation from forming:

- The unsaturated air temperature equals the duct surface temperature.
- The unsaturated air temperature is colder than the duct surface temperature.
- The air dew point temperature is colder than the duct surface temperature.

The thermodynamic process of atmospheric air flowing through the PUREX exhaust system is essentially a heating and cooling process without changing the humidity ratio; only sensible heat is added or removed. Therefore, the moist air that flows through the cold duct does not necessarily produce condensation.

Condensation Rate

Based on the Hanford Site weather data for 24 hours on December 11, 1994, the data indicated the dry-bulb temperature in the range of 30 to 33 °F, while the relative humidity was between 95 and 99 percent. The cumulative condensate was calculated based on persistent air temperature of 33 °F (0.56 °C) and relative humidity of 98 percent, for 24 hours, while the duct wall temperature (32 °F or 0 °C) was assumed to fall below the air dew point temperature of 32.5 °F (0.28 °C).

Because the condensation rate was calculated based on the variation of the humidity ratio, a worse Δw = 0.000325 lb of H_2O per lb of dry air was calculated for 24 hours.

The average specific volume of the air was determined at 12.5 ft^3/lb (0.78 m^3/kg), the mass flow rate was calculated as 3,200 lb/min (1,451.5 kg/min).

Because moist air condensation occurs only during contact with the cool wall surface, most of the free-stream air flows through the duct without producing

condensation. The actual condensation occurs only for the moist air inside the laminar sublayer in a fully developed turbulent boundary layer. However, it is conservatively assumed that the moist air inside the fully developed turbulent boundary will be condensed.

For the fully developed boundary layer, the Reynolds number is calculated based on boundary layer length of 50 ft (15.24 m) at 3,787,698. The boundary layer thickness, δ, was calculated at 11 in. (27.94 cm). The total volume for condensation is 3,200 ft^3 (90.6 m^3). The total condensation rate for all the air moisture in 24 hours is 608 lb (275.8 kg).

The total surface area that this amount of condensate will cover in 24 hours is 1,600 ft^2 (148.6 m^2). Therefore, the condensate rate over unit duct surface area is 0.016 lb of $H_2O/hr\text{-}ft^2$ (0.078 kg of $H_2O/hr\text{-}m^2$) or a total of the moisture at 0.38 lb H_2O/ft^2 (1.85 kg H_2O/m^2) per day on the duct wall surface.

The remaining non-condensed moist air outside the boundary layer will flow through the duct. The condensate on the wall surface causes no concern because the accumulated quantity is small; dripping or puddling is not expected.

If the Amercoat on the concrete has deteriorated or the concrete interior is not in a saturated state, the sorption characteristics, capillary suction, and moisture transfer capabilities of the concrete may be able to absorb a small amount of moisture (Jonasson 1985).

For the concrete surface in the air duct, this rate of condensation cannot produce dropwise condensation. The moisture will be spread over the concrete surface with a thin layer of film with no dripping or puddling.

As a result of the assumed condensation, the humidity ratio or moisture contents in the flowing air will be reduced when the air flows through the DBGF filter No. 2.

Fog and Frost Formation

Fog is a disperse system consisting of liquid drops suspended in a gas. The conversion of vapor to fog is a discontinuous process occurring under critical conditions when vapor reaches the supersaturation state (Amelin 1967). The air flow in this study has not experienced any isentropic expansion into the wet region in the enthalpy/entropy diagram (Obert 1960) and the supersaturation condition has never been attained. Thus, fog formation inside the air duct is not possible.

If the fog or gaseous suspensions are flowing from the environment into the plant with the moist air, the warming effect inside the building and air duct will evaporate the moist fog. The fog can be sustained only if a source within the plant continuously supplies the moisture and the temperature in the duct is much colder than the outside air. As the moist air flows through a complicated and winding path inside the plant, the moist drops may impact a surface and deposit along the pathway. Because the fog conditions at the Hanford Site lasted only few hours, a limited amount of moisture was deposited in the air duct.

Frost forms when the moist air is exposed to a surface that is colder than the dew point temperature of the air, which must be far below 32 °F (0 °C). Under this condition, the moisture content of the air passes directly from the gaseous state to the solid state forming a porous layer of frost on the cooled surface. The rates of increase of the frost thickness require a continuous cooler temperature and high-humidity environment. Otherwise, the frost begins to melt and evaporates into the air stream. When the air/frost interface temperature temporarily warms back to 32 °F

(0 °C), even in a high-humidity environment, the frost layer will occasionally undergo cycles of melting and refreezing (Trammell 1968). Considering the high affinity the air has for moisture, the frost melts and is evaporated by the dry air.

Air and Duct Temperature

The worst temperature variations contained in the Hanford Site weather data for the past 15 years were reviewed. The two wettest years, and the two coldest years, and the 1994 winter data were used as the basis for performing the heat transfer analyses. Heat transfer calculations and numerical examples for the conditions described are presented in the following paragraphs.

Transient Heat Conduction

Based on the weather data for the coldest and wettest years at the Hanford Site, transient heat conduction calculations were performed to determine the worse environmental temperature conditions and the depth the freezing layer penetrates into the soil resulting from the worst weather scenario (Schneider 1955).

Two examples are used to demonstrate the depth the frozen layer penetrates into the underground soil under extreme weather conditions.

Example 1: On a cold winter day, after a sudden change in weather conditions, the surface temperature of the plant environment drops to 18 °F (-7.8 °C). These cold conditions continue for 14 days. The temperature of the ground before the weather change is assumed to be 35 °F (1.7 °C). After this period, the temperature is calculated at different distances from the surface (Schneider 1955):

x = 4 ft (1.220 m), T = 32.1°F (0.08 °C).
x = 5 ft (1.524 m), T = 33.6°F (0.89 °C).
x = 6 ft (1.829 m), T = 34.3°F (1.28 °C).

Example 2: During the winter, a sudden cold wave reduces the ambient air temperature to 0 °F (-17.8°C). If the earth was at a uniform temperature of 40 °F (4.4 °C) before the onset of the cold wave, the freezing temperature penetrations were calculated to different depth after various hours,

6 hours, $x = 0.9 \times 2\sqrt{1.8 \times 6} = 5.9$ in (14.98 cm).
12 hours, $x = 0.9 \times 2\sqrt{1.8 \times 12} = 8.4$ in (21.34 cm).
24 hours, $x = 0.9 \times 2\sqrt{1.8 \times 24} = 11.8$ in (29.97 cm).

This indicates that the frozen layer penetrates less than 1 ft (0.3048 m) in 24 hours.

Flowing Air Temperature

The winter atmospheric air flows from the PUREX canyon building and enters the inclined air duct system. The wall surface temperature of the air duct was assumed to be 55 °F (12.8 °C) at 30 ft (9.144 m) below grade and cooled to near the environment temperature at the upper section close to the grade level. Heat transfer calculations were performed to determine the temperature increase of the flowing air at the turbulent boundary layer because of the warmer wall.

This section calculates the moist air temperature change caused by the effect of the warm concrete duct wall. The underground concrete duct cross-section area varies from the lower portion of 11 ft x 5 ft-9 in. (3.35 m x 1.75 m) to the upper portion of 8 ft

x 8 ft (2.44 m x 2.44 m). The upper section is near the grade level, so its temperature is closer to the environmental temperature.

Consider a 40,000-ft^3/min (1,132 m^3/min) flow rate, the flow velocity through an 11 ft x 5 ft-9 in. (3.35 m x 1.75 m) duct is 10.54 ft/sec (3.21 m/sec). The equivalent hydraulic diameter is 90.6 in. (2.3 m). The Reynolds number is 578,529, which falls within the turbulent flow region. Assume that the Prandtl number is 0.7 for air. The heat transfer coefficient was calculated at 0.0196 Btu/hr-in^2-°F (16.02 W/m^2-K) using the correlation (Lancet 1959) $Nu = 0.042 (Re)^{0.8} (Pr)^{1/3}$.

Assuming that the moist air at 32 °F (0 °C) flows through the concrete duct section at 55 °F (12.8 °C), the heat balance equation may be applied to calculate the flowing-air temperature at 34.4 °F (1.33 °C). This demonstrates that the air temperature in the boundary layer will be warmed up to 34.4 °F (1.33 °C), while the air temperature outside of the thin boundary layer remains at 32 °F (0 °C).

Duct Wall Temperature

Another calculation shows the cooling effect on the wall surface if cool air is flowing continuously through the duct. The convective cooling from the wall requires temperature gradient in the concrete wall to initiate the conduction heat flow. Hand calculations appeared to be fairly involved. A transient heat transfer analysis using a simplified finite-element model (ANSYS 1993) was performed to determine the temperature distributions throughout a concrete section.

The warm wall surface of the underground duct may be cooled if air at 32 °F flows through continuously. However, at a great distance from the surface, the duct surrounding remains at 55 °F (12.8 °C).

The finite-element mesh denoting the node and element numbering is shown in Figure 2. The three-dimensional thermal solid elements (solid70) have eight nodes with a single degree of freedom, temperature, at each node was used. Convective boundary condition, with heat transfer coefficient of 0.0196 Btu/in^2-hr-°F (16.02 W/m^2-K), was applied at the inside wall surface. Concrete material properties were used.

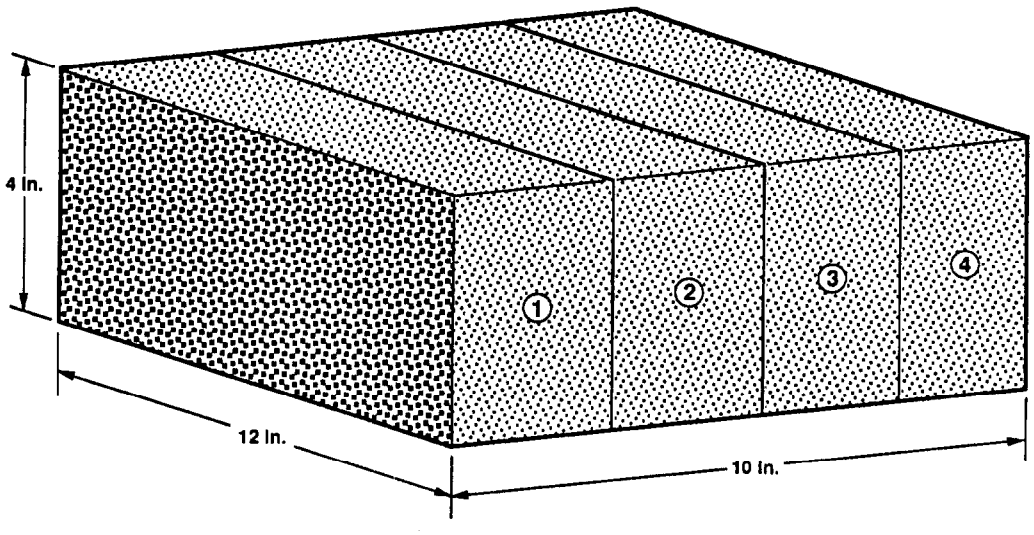

Figure 2. ANSYS Finite-Element Model.

A small initial temperature gradient was applied to start the transient solution. Results indicate that the temperature distribution throughout the section of the wall reached a steady-state temperature of approximately 42 °F (5.56 °C) after 4 hours.

Filter System Condensation

This section describes possible condensation and moisture effects on the filter systems.

Prefilter (Deep Bed Filter No. 2)

If condensation were assumed to have occurred at the cold wall surfaces in the upper portion of the inclined air duct system, the moisture content of the air would be reduced and further effect of condensation on the deep bed filter would be decreased because the air entering the filter is dryer.

Generally, sufficient moisture in droplet form is hazardous to a filter system. However, the filters are designed to resist moisture as long as plugging does not occur. Filtration is achieved by various mechanisms depending on the particle size and flow velocity (Davies 1973). The penetration mechanism is controlled by either molecular diffusion, interception, Brownian motion, or inertial impacting depending on the air flow velocity.

In good-quality filters with low resistance and high efficiency against submicron particles, the air flow obeys Darcy's law, which is usually considered to be valid for creeping flow with low Reynolds number. The low-Reynolds-number flow is dominated by viscous force. The viscous effect between the air particles and the filter fibers may keep the filter surface temperature from decreasing below the air temperature. As a result, the filter surface temperature is generally close to the air flow temperature.

High-Efficiency Particulate Air Filter

If condensation occurs in the underground duct work, the air flowing through the HEPA filters in the 291-AE building will be dryer.

Before the air reaches the HEPA filters, it has to flow through the concrete duct that has a wall surface temperature close to that of the inlet plenum wall located at the entrance to the HEPA filter. The temperature of the plenum wall should be the same as or colder than that of the HEPA filter. If the plenum wall temperature is at or colder than the dew point of the flowing air, condensation will occur at the plenum.

Condensation will not take place in the filters whether or not condensation occurs at the plenum. The air will simply flow through the filters. The HEPA filter media is treated with a water-resistant binder and will tolerate both high humidity and direct wetting (Flanders 1988). Several tests (First and Leith 1976) indicated that no degradation in filtering ability occurs after exposure to a steam-droplet atmosphere.

Joule-Thomson Effects

The Joule-Thomson experiment (Jones and Hawkins 1960, Kestin 1979) may resemble the moist air flowing through filter media and produce condensation. The basic condition for the Joule-Thomson effect to cause cooling is that the initial temperature of the gas must be below the maximum inversion air temperature, which is 628 °F (331 °C). The temperature of the flowing air is below the maximum inversion temperature.

If air is compressed to a pressure of 200 atm (2,940 psi or 20,265 KPa) and a temperature of 126 °F (52 °C), after throttling to a pressure of 1 atm (14.7 psi or

101.325 KPa), it will be cooled to 73 °F (23 °C). For a small pressure drop of few inches or centimeters, such as flow through porous media, the temperature drop and the air cooling effect of the Joule-Thomson phenomenon are negligible.

Frost Formation on HEPA Filters

The possible frost conditions in the HEPA filter building are evaluated under the assumed frozen temperature in the environment. Two conditions may subject a cool surface to frost formation: when the surface has been exposed to nocturnal radiation and when a surface that has cooled below 32 °F (0 °C) contacts the moist air with a dew-point temperature higher than the surface temperature.

The first condition is unlikely to occur because the HEPA filters are housed in a building and not exposed to nocturnal radiation. Therefore, the cooling will not be present inside the building.

The second condition becomes possible when a surface cools to a subzero temperature that is below the dew point of the moist air. If the wall surface temperature of the HEPA filter building is cooled down well below the freezing point, the concrete duct and inlet plenum surface temperature will be near or at the freezing point temperature. Under this condition, the water vapor leaving the air and attaching to the surface may pass directly from gaseous to solid state forming a porous layer of frost.

Tests (Brian et al. 1970) indicate that continuous frost formation requires a subzero temperature and high specific humidity. After the frost formation, frost growth requires a sustained cooling mechanism, a continuous temperature decrease of the cooled surface, and an increase of the specific humidity of the air stream. In the absence of this persistent cooling phenomenon, frost buildup is not possible (Trammell 1968). If at any time the surface temperature reaches 32 °F (0 °C), melting will occur (Jones and Parker 1975). Based on temperature fluctuations from the Hanford weather data, frost may have formed on cold surfaces as a transient condition.

If condensation has already occurred as the cold air flows through the concrete duct or inlet plenum, the same amount of air that flows into the HEPA filters would have reduced the moisture content or humidity ratio. With a reduced humidity ratio because moisture is lost in the duct, the effect on the filters is not a concern.

V. RESULTS AND DISCUSSIONS

The results of a transient heat conduction analysis show that the depth of frozen soil, resulting from a subfreezing surface temperature of 18 °F (-7.78 °C) penetrates 6 ft (1.83 m) below grade after 14 days. These results agree with the publications from the U.S. Weather Bureau map that show the average and maximum depths of frost penetration as 12 and 36 in. (30.48 and 91.44 cm), respectively, in southeastern Washington State (Strock 1965). This indicates that only a small upper section of the air duct perimeter near the grade level may temporarily come close to the freezing temperature under the possible worst environmental condition.

An extreme weather condition that may never occur at the Hanford Site also was analyzed. A plant environmental surface temperature of -27 °F (-32.8 °C) lasting for 60 days was assumed. Results indicate that the frozen layer may penetrate into the soil to a depth of 7 ft (2.134 m).

The earth has been shown to maintain a constant temperature of 55 °F (12.78 °C) throughout the year at the lower section of the air duct. Cool moist air at 32 °F (0 °C) flowing through the 55 °F (12.78 °C) air duct can warm up only 2 °F (1.11 °C)

near the boundary layer, while a large quantity of air at the free stream remains at 32 °F (0 °C). A continuous flow of cold air at 32 °F (0 °C) may lower the wall temperature to 42 °F (5.56 °C) when reaching a steady-state condition in 4 hours. The 42 °F (5.56 °C) temperature is above the dew point of the air.

If the air flows at a velocity of 10.54 ft/sec (3.213 m/sec), the time for air to travel from the duct entrance to deep bed filter no. 2 takes approximately 25 seconds. The duct wall temperature cannot be cooled much lower than the steady-state temperature. Condensation in the lower section of the air duct during the winter is not possible.

A condition may exist in the underground ductwork where the duct temperature can lead or lag the changes in the ambient air temperature because of the thermal storage characteristics of the underground duct. This condition may contribute to condensation on the inside surfaces of the underground exhaust duct.

The coldest and wettest weather data for the past 15 years have shown that only short periods in the early spring and winter of 1994 could contribute to some slight condensation that is barely enough to dampen the duct wall surfaces.

However, the condensation rate was conservatively calculated based on the worst recorded data during the 1994 winter. The dry-bulb temperature occurred between 30 to 33 °F (-1.1 to 0.56 °C), while the relative humidity was between 95 and 99 percent for 24 hours, assuming that the moist air flowing through the boundary layer in the concrete duct is condensed during the 24 hours. Results indicated that only 0.38 lb (0.172 kg) of moisture may be accumulated on 1 ft^2 (0.093 m^2) in 24 hours. A large amount of flowing air in the free stream does not condense.

This small amount of moisture may be evaporated under the condition of temperature variations without producing significant wetting. From the plant operating histories, no significant condensation has been observed, even when the water spray system was in operation.

If condensation occurs on the concrete duct-wall surfaces, the humidity ratio for the air downstream is reduced. As a result, the filter housing temperature is above the dew point temperature of the air; therefore, condensation does not take place. The potential for condensation on the HEPA filter housing surfaces will be less of a concern.

The pressure drop through the filter system is not sufficient to cause any temperature drop and condensation. In addition, the filters are designed to resist high humidity and direct wetting (Burchsted 1978, Flanders 1988), so a small amount of moisture would be of no concern.

Frost formation on the HEPA filters is not possible because frost forms only on much colder surfaces, such as the duct wall or inlet plenum, before the cold air flows into the filters. No enduring mechanisms, such as continuous cooling and a high-humidity environment, exist to build up such effects on the HEPA filters.

VI. CONCLUSION

Condensation heat transfer and fluid flow analyses were completed to evaluate the effects of condensate in the underground duct and filters in the PUREX plant. The results of the analysis indicate that the ductwork upstream of the DBGF filters bed No. 2 is the most likely place for condensation to form.

A worst case conservative analysis was performed assuming that all of the water is removed from the moist air over the inside surface of the concrete duct area in the fully developed turbulent boundary layer while the moist air in the free stream will not condense. The total moisture accumulated in 24 hours is 0.38 lb H_2O/ft^2 (1.85 kg H_2O/m^2), which is barely enough to dampen the concrete wall surfaces. Water dripping and puddling is not expected.

Turbulent heat transfer analysis has shown that 32 °F (0 °C) air flowing through the duct will be warmed to 34.4 °F (1.33 °C) inside the thin laminar sublayer, while the air in the free stream remains at 32 °F (0 °C). Further analysis has indicated that the surface of the duct wall may be cooled to 42 °F (5.56 °C) after reaching a steady state condition in 4 hours.

Based on an air flow velocity through the concrete duct at 10.54 ft/sec (3.213 m/s), the air has a resident time of approximately 25 seconds traveling from the underground duct entrance to the DBGF No. 2 filter. Therefore, the lead/lag temperature characteristics of the underground duct are of short duration allowing the duct to follow changes in air temperature rather closely. This reduces the condition for possible condensation. On the other hand, condensation occurring in the ductwork upstream of the DBGF No. 2 filter will provide dryer air in the downstream duct and filters.

If no condensation occurs before the deep bed filters, the same moist air flows through the concrete duct, the HEPA filter building, and the exhaust system without further condensation. The pressure drop through the filter system is not sufficient to cause any temperature drop that will initiate condensation. However, the filters were designed to resist high humidity and direct wetting (Burchsted 1978, Flanders 1988), filter plugging caused by condensation is not a concern. Tests (First and Leith 1976) indicated no degradation in filtering ability after exposure to a steam-droplet atmosphere. The results of the analyses also agree with the operating experiences. Therefore, it is concluded that no electrical heating system is required for the PUREX canyon exhaust to prevent condensation.

VII. REFERENCES

Amelin, A. G., 1967, *Theory of Fog Formation*, 2nd ed., Israel Program for Scientific Translation Ltd., Jerusalem, Israel.

ANSYS, 1993, *"Engineering Analysis Computer Program,"* Version 5.0A, Swanson Analysis Systems, Inc., Houston, Pennsylvania.

Brian, P. L. T., and R. C. Reid and Y. T. Shah, 1970, *Frost Deposition on Cold Surfaces*, Ind. Eng. Chem. Fundamental, Vol. 9, No. 3, pp. 375-380.

Burchsted, C. A. and J. E. Kahn and A. B. Fuller, 1978, *Nuclear Air Cleaning Book*, ERDA 76-21, Oak Ridge National Laboratory, Oak Ridge, Tennessee.

Davies, C. N., 1973, *Air Filtration*, Academic Press, New York, New York.

First, M. W. and D. Leith, 1976, *Entrainment Separator Performance*, Paper No. 101, Proceedings of the 14th ERDA Air Cleaning Conference, pp. 694-710.

Flanders, 1988, *Nuclear Grade HEPA Filters*, Bulletin No. 812E, Flanders Filters Inc., Washington, North Carolina.

Jonasson, J. E., 1985, *Moisture Fixation and Moisture Transfer in concrete*, Paper No. H5/11, 8th International Conference on Structural Mechanics in Reactor Technology, August 19-23, 1985, Brussels, Belgium.

Jones, J. B., and G. A. Hawkins, 1960, *Engineering Thermodynamics*, John Wiley & sons, Inc., New York, New York.

Jones, B. W. and J. D. Parker, 1975, *Frost Formation With Varying Environmental Parameters*, J. of Heat Transfer, May, 1975, pp. 255-259.

Kays, W. M. and M. E. Crawford, 1993, *Convective Heat and Mass Transfer*, 3rd ed., McGraw Hill Book Company, New York, New York.

Kestin, J., 1979, *A Course in Thermodynamics*, Revised Edition, Volume One, Hemisphere Publishing Corporation, New York, New York.

Lancet, R. T., 1959, *The Effect of Surface Roughness on the Convection Heat-Transfer Coefficient for Fully Developed Turbulent Flow in Ducts With Uniform Heat Flux*, J. of Heat Transfer, May, 1959, pp. 168-174.

McQuiston, F. C. and J. D. Parker, 1988, *Heating, Ventilating, and Air Conditioning, Analysis and Design*, 3rd ed., John Wiley & Sons, Inc.

Obert, E. F., 1960, *Concepts of Thermodynamics*, McGraw Hill Book Company, New York, New York.

Schneider, P. J., 1955, *Conduction Heat Transfer*, Addison-Wesley Publishing Company, Inc., Reading, Massachusetts.

Strock, C and R. L. Koral, 1965, *Handbook of Air Conditioning Heating and Ventilating*, 2nd ed., Industrial Press Inc., New York, New York.

Trammell, G. J., and D. C. Little and E. M. Killgore, 1968, *A Study of Frost Formed on A Flat Plate Held at Sub-Zero Temperatures*, ASHRAE Journal, July 1968, pp. 42-47.

The Trane Company, 1977, *Trane Air Conditioning Manual*, 53rd Printing, The Trane Company, La Crosse, Wisconsin.

DISCUSSION

FRETTHOLD: Are you planning on changing out all of your filters prior to going into this condition, so you start with new filters?

GREGONIS: No, we are not. We test our HEPA filters annually and we have recently replaced up to five banks. Because the system for our filter building was built for 120,000 CFM we have ten banks. Five will be available on-line and five will be off-line. If we have a problem we will just valve in another bank and then replace them during that time.

FRETTHOLD: You are running your filters at your 40,000 CMF instead of 120,000?

GREGONIS: That is correct.

FRETTHOLD: You plan to down rate the filter by going to twice the number of filters?

GREGONIS: That is the plan. This system has been online since '83. Based on its' history has been pretty reliable. Have not had a major problem. So the thought is that it will continue.

FRETTHOLD: Where will supply air come from? It is not supplied with a fan, is it just drawn in through the supply?

GREGONIS: It is drawn through the system by the negative pressure in the canyon, basically it is infiltration. We will have prescribed paths for the air to enter.

BERGMAN: I was looking through your references and I did not see any reference to the excellent work done by Dr. Wilhelm and his group at KfK about moisture accumulation on filters. If I recall right, just a little bit of particle deposition will literally suck the moisture out of the air, even when it is below saturation and when you have a powerful enough fan it will suck the innards out of the filter. That is one thing. A second item is that we were shown at a prior conference that even when you leave a HEPA filter sit in storage, it loses all its water repellency after about ten years. In that case, the image of the filter is not that of a water repellant substance, but a sponge that will literally soak up the water. My question is, have you considered any of these facts from previous literature reports?

GREGONIS: We have a extensive list of research on that. There was a paper presented by Dr. First that showed a case where they were testing a droplet retrainer, I believe, and that paper pretty much showed that water was not a problem. In addition, we go through a deep bed before we go through the HEPA filter. So the dust loading on the HEPA filters is basically nil.

BERGMAN: All studies before the KfK studies during the mid-80's had been done with brand new filters. Again I point out, it does not take a lot of dust, just a little bit of dust immediately changes the characteristics from a brand new filter to an aged filter. And again, the image is a sponge even though you have a very clean environment, the fact that you lose the organic water repellency characteristic transforms the filter into a sponge. And so I would recommend you to refer to some of the pioneering work in Germany, and include that in your references because by not doing so, you may have a little surprise.

GREGONIS: Just a comment based on our operating experience. They used to run the spray washers

year-round and the mechanism for condensation was that the filter housings are out in the ambient temperature. I have been in almost all the filter housings, and been involved in filter changes. We did not see any degradation or ruptures. Therefore, in our deactivation state, where we are not putting any water in, but are just taking ambient air and running it through the plant and out again, I feel we have a pretty good basis for utilizing these filters. However we will study the matter you presented.

ENGELMANN: Whether there can be condensation on the filter depends almost entirely upon the absolute humidity of the air and the filter temperature. A simple and adequate approach is to estimate or measure the absolute humidity within the building and that of the makeup air to calculate what is presented to the filter. A simple solution (if there is a problem) is to add more makeup air which at Hanford, has low humidity. Heating of the air did not merit consideration as a solution, unless there are expected to be major activities with much evaporation within the building.

SESSION 9

COMPUTER MODELING APPLICATIONS & ADSORPTION

Wednesday July 17, 1996
Co-Chairmen: R. Lee
D.W. Moeller

COMPUTER MODELING APPLICATIONS

ADSORPTION

FILTRATION THEORY USING COMPUTER SIMULATIONS*

by

Werner Bergman and Ivan Corey
Lawrence Livermore National Laboratory
Livermore, CA 94550

Abstract

We have used commercially available fluid dynamics codes based on Navier-Stokes theory and the Langevin particle equation of motion to compute the particle capture efficiency and pressure drop through selected two- and three-dimensional fiber arrays. The approach we used was to first compute the air velocity vector field throughout a defined region containing the fiber matrix. The particle capture in the fiber matrix is then computed by superimposing the Langevin particle equation of motion over the flow velocity field. Using the Langevin equation combines the particle Brownian motion, inertia and interception mechanisms in a single equation. In contrast, most previous investigations treat the different capture mechanisms separately. We have computed the particle capture efficiency and the pressure drop through one, 2-D and two, 3-D fiber matrix elements.

I. Introduction

Developing an accurate theoretical model of particle filtration is extremely difficult because of the complex nature of the filtration process, which involves particle transport in a fluid moving through a complex filter geometry. Figure 1 illustrates the complicated structure of a typical filter medium made from glass fibers. The fluid and suspended particles flowing through this fiber maze follow an extremely tortuous path controlled by the fluid dynamics and the particle equations of motion. Other type of filter structures such as spheres or granules and irregular porous structures are also frequently used in filtration.

The previous approach for modeling the particle filtration process has been to represent the complicated filter structure by a single element and then compute the fluid flow and particle transport around the one element.[1,2] The particle transport was computed by separately adding the contributions due to diffusion and inertia to the integrated trajectory. More recently, investigators have begun to model filtration in terms of parallel fibers arranged in a symmetric two-dimensional configuration.[3] Although this is an improvement over the single collector model, the filtration is still limited to 2-D flows through overly simplistic filter geometries.

---

*This work was performed under the auspices of the U.S. Department of Energy by Lawrence Livermore National Laboratory under contract no. W-7405-ENG.48.

Figure 1. Scanning electron micrograph of glass fiber media used in high efficiency particulate air (HEPA) filters.

The problem with these previous approaches is that only general trends can be obtained from the computations, and considerable amount of experimental studies are still needed to substantiate the computations for specific filter designs and operating parameters. For that reason, filter designs and operational parameters generally are established through extensive experimental studies. This approach is both costly and time consuming. Perhaps even more important, the previous theoretical models restrict the development of new filters to existing production designs and available materials rather than what is theoretically possible. To overcome these deficiencies we have developed a filter simulation model that can simulate the filtration of suspended particles through more realistic filter structures, although not yet as complicated as that shown in Figure 1. The complexity of the fluid flow and particle trajectories through the filter media shown in Figure 1 greatly exceed present computer hardware and software capabilities, even when using advanced mainframe computers.

II. Development of Filtration Simulation Model

We have used commercially available fluid dynamics codes, NEKTON version 2.85, (Fluent Inc. 10 Cavendish Ct. Lebanon, NH 03766) and FIDAP version 6.0, (Fluid Dynamics International, Inc. Evanston, Il, 60201) and the particle equation of motion to compute the particle capture efficiency and pressure drop through selected two- and three-dimensional fiber arrays. The approach we used was to first compute the air velocity vector field throughout a defined region containing the fiber matrix. This was the most difficult and time consuming task in our study. Each combination of inlet air velocity and fiber matrix required a significant effort to set up the fluid problem and to compute the velocity field. All of the air flow calculations in this report were conducted with a uniform inlet velocity directed at the fiber matrix, and we allowed the exit velocity to vary. We did not force the fluid to be periodic (equal velocity fields at the inlet and exit) through the fiber matrix because of the additional work required to establish periodic flow.

The most difficult and time consuming step of the simulation is computing the velocity and pressure fields using computational fluid dynamics (CFD) computations. We have used the commercial CFD solvers, NEXTON and FIDAP, which are based on Navier-Stokes equations. The large memory requirements (50MB) and the long processing times (20 hours) for the CFD computations limit the size of the filter model that can be studied to filter structures with about 100 fibers when using computer workstations. Using PCs would restrict the filter to about 10 fibers, while a supercomputer could compute structures with up to 1,000 fibers.

The filtration computer simulations require a UNIX based hardware platform with a minimum of 48MB of memory to run. We computed the filtration simulations that are shown in this report using the SGI Indigo platform from Silicon Graphics. The following are the software and hardware requirements:

Table 1. Hardware and Software Requirements For Computer Simulations

COMPONENT	REQUIREMENT
Graphics	Requires open/GL Graphics. 8 bit -planes is adequate
CFD Solver	A CFD solver is required. Any 3D CFD solver can be used, e.g. NEKTON or FIDAP. A mesh generator may also be required, e.g. TrueGrid.
Visualization	SGI's Explorer was used
Main Memory	48MB
Disk Storage	10MB minimum, primarily for flow fields

Figure 2 shows an example of the two-dimensional air flow calculations through a matrix of 2μm and 4μm diameter fibers. The inlet flow velocity was 20 cm/s. We were also able to compute the three-dimensional flow fields through the staggered hexagonal array in Figure 3 and the crossed fiber array in Figure 4. The direction of flow is in the X-direction. Once the air flow velocity field is determined, the differential pressure is also fixed and is read directly from the computer output.

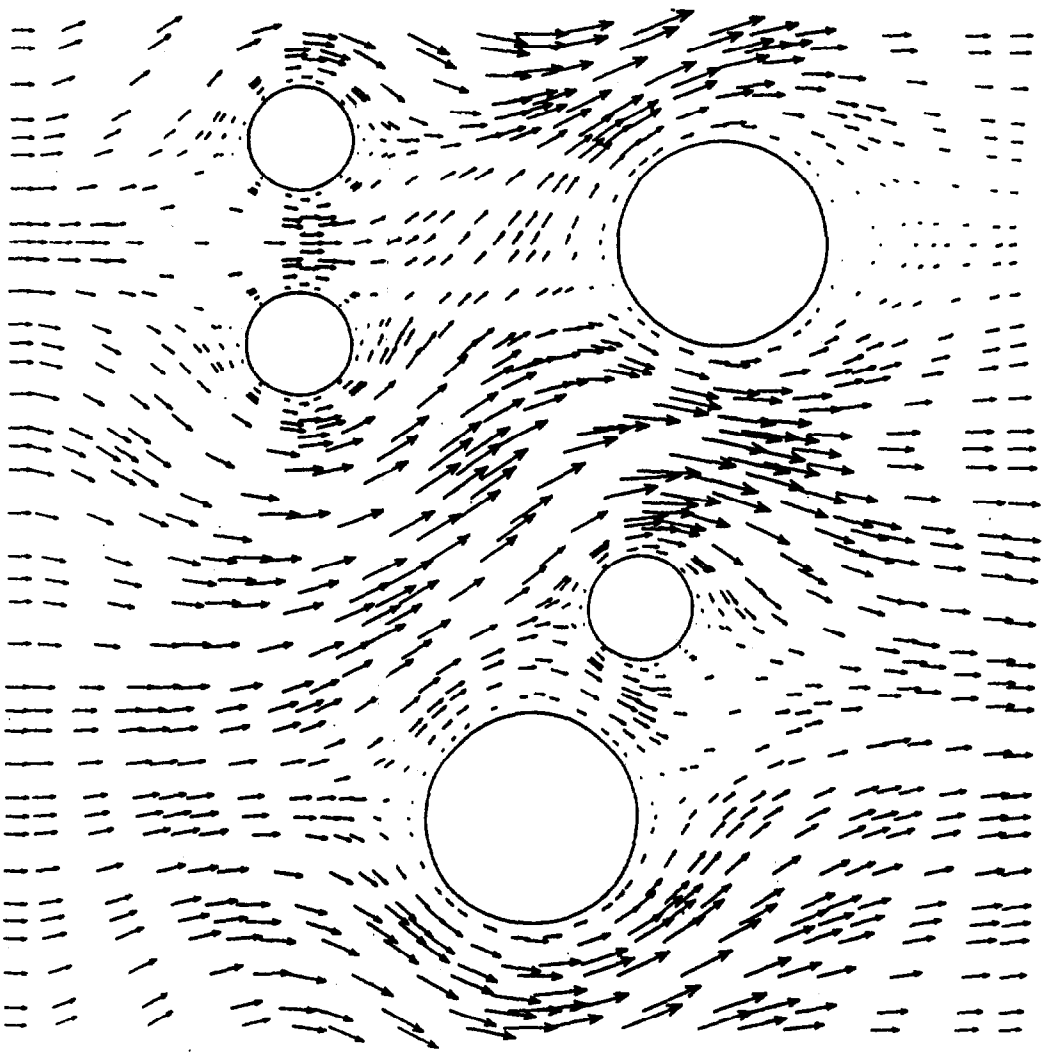

Figure 2 Air velocity vector field through 2-D fiber matrix at 20 cm/s initial velocity. The fiber matrix is 20μm x 20μm with 2 μm and 4μm diameter fibers. The fiber volume fraction is 0.0864.

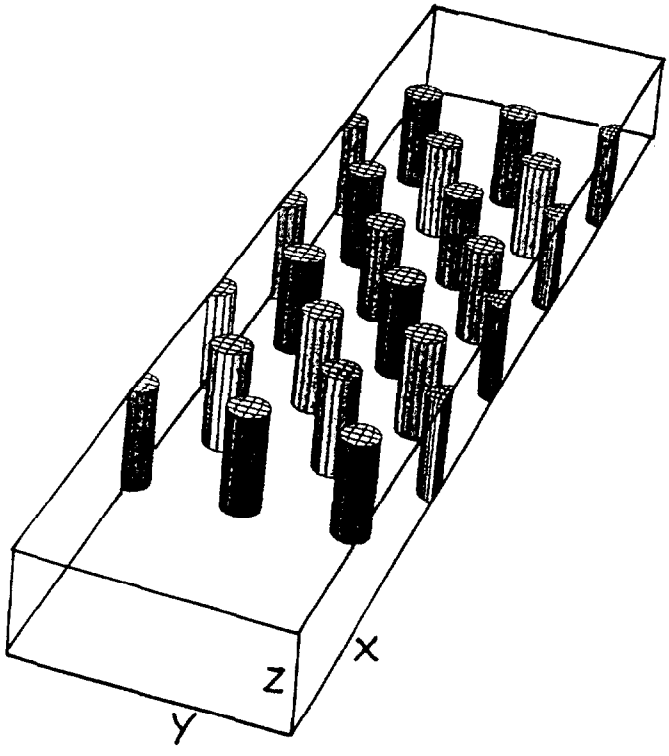

Figure 3 3-D fiber matrix with 1μm diameter fibers arranged in a staggered hexagonal array. The fiber matrix L x W x H is 23.0μm x 6.5μm x 5.0μm. The fiber volume fraction is 0.0825, and air flow is in X direction.

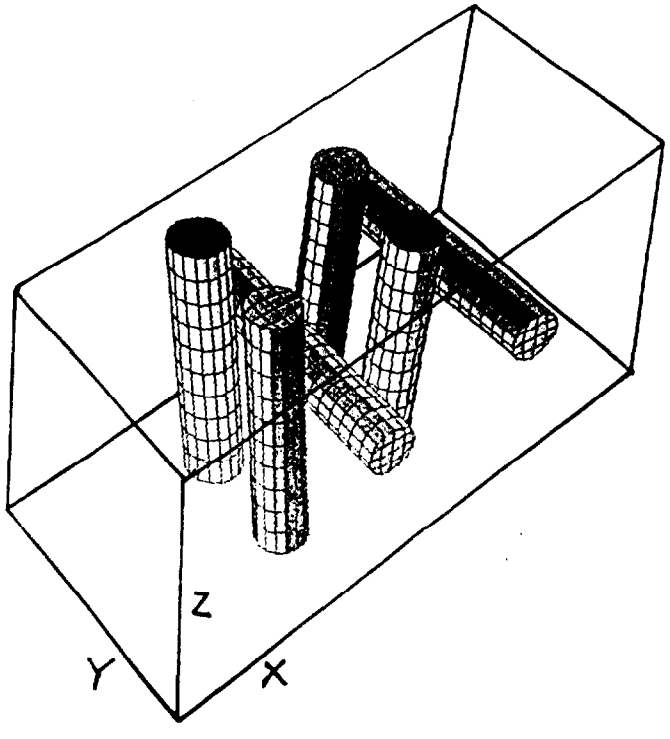

Figure 4 3-D fiber matrix with 1μm fibers arranged in a crossed fiber array. The fiber matrix L x W x H is 11μm x 5μm x 5μm. The fiber volume fraction is 0.0843 and air flow is in X direction.

The particle capture in the fiber matrix is then computed by superimposing the particle equation of motion over the flow velocity field. The resulting particle dynamics is given by:

$$\frac{d\underline{v}}{dt} = B(\underline{u}-\underline{v}) + \underline{A}(t) \qquad (1)$$

where,

$\underline{v}$ = particle velocity vector
$\underline{u}$ = fluid velocity vector
B = friction coefficient
$\underline{A}(t)$ = random Brownian acceleration, time dependent
t = time

The friction coefficient B is defined as

$$B = \frac{6\pi\ \mu a_p}{C_s\ m} \qquad (2)$$

where,

μ = fluid viscosity
a_p = particle radius
m = particle mass
C_s = Cunningham slip correction factor

The solution of Equation 1, called the Langevin equation, can be obtained assuming a constant fluid velocity and a constant value of B.

Ramarao et al have solved Equation 1 using the method proposed by Chandrasekhar for two-dimensional particle trajectories.[4,5] We have extended this method to three dimensions in the present study. The principle of superimposing particle motion over the flow field is illustrated in Figure 5, where the net particle motion is the sum of a deterministic term and a probabilistic term.

Figure 6 shows the results of three, two-dimensional particle trajectories computed for the flow field in Figure 2 using Equation 1. Figure 7 shows the results of three, three-dimensional trajectories computed for the crossed fiber matrix. The inlet air velocity in both figures is 20 cm/s. The particle size in each of the three trajectory calculations was chosen to represent what is generally treated as three separate particle capture mechanisms: Brownian motion, interception and inertia. This artificial separation is not required for the general approach in Equation 1. Particle capture by the filter fiber only occurs if the particle trajectory contacts the fiber surface. Once particle contact is made, we assume the particle is captured and held tight. This assumption is valid for particles smaller than 5 μm at lower air flows.

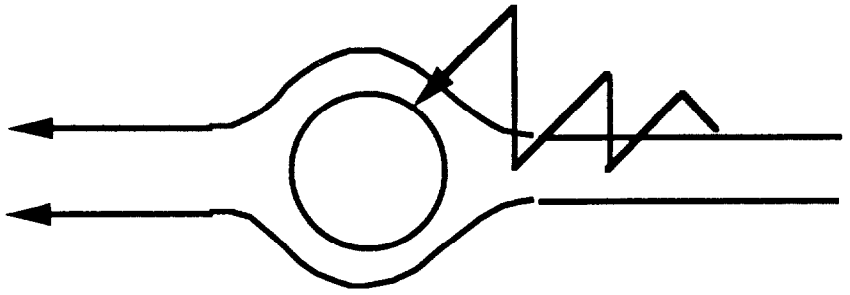

Brownian or probabilistic

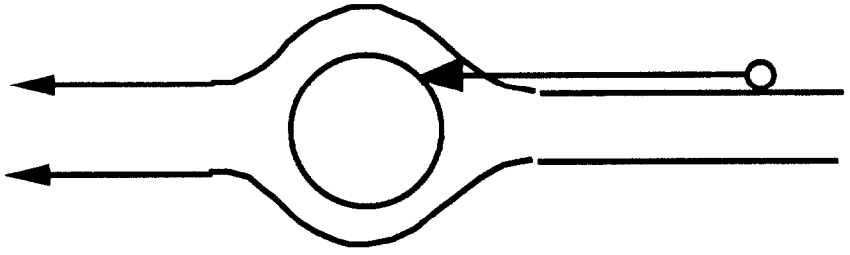

Inertial or deterministic

$$\underbrace{\frac{d\vec{u}}{dt}}_{\text{particle motion}} = \underbrace{B(\vec{v}-\vec{u})}_{\text{deterministic}} + \underbrace{\vec{A}(t)}_{\text{probabilistic}}$$

Langevin eq.

Figure 5. Particle motion is determined by the superposition of the Brownian (probabilistic) motion and the inertial (deterministic) motion over the flow field.

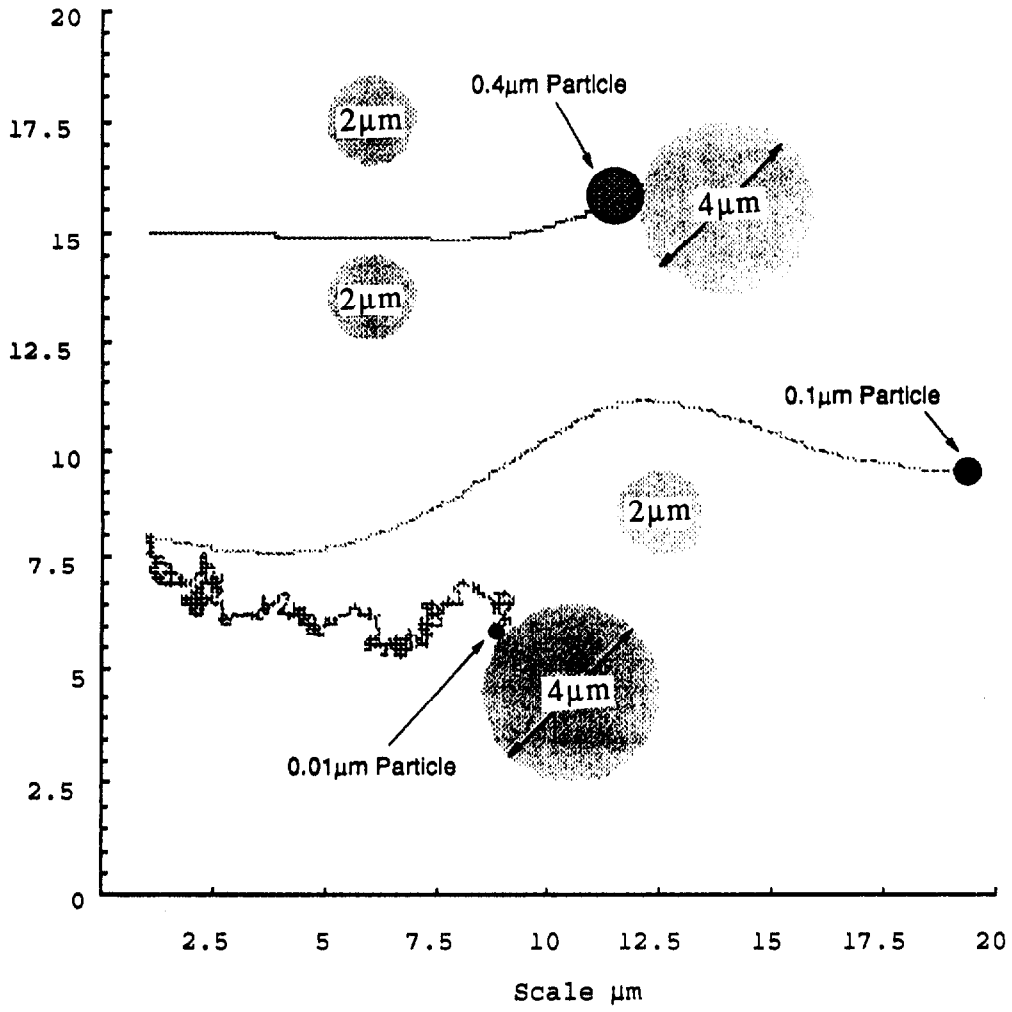

Figure 6 Trajectories of three different diameter particles through the fiber matrix in Figure 2. Particle diameters were selected to illustrate conventional mechanical collection mechanisms: 0.01μm for Brownian motion, 0.1μm for interception, and 0.4μm for inertia.

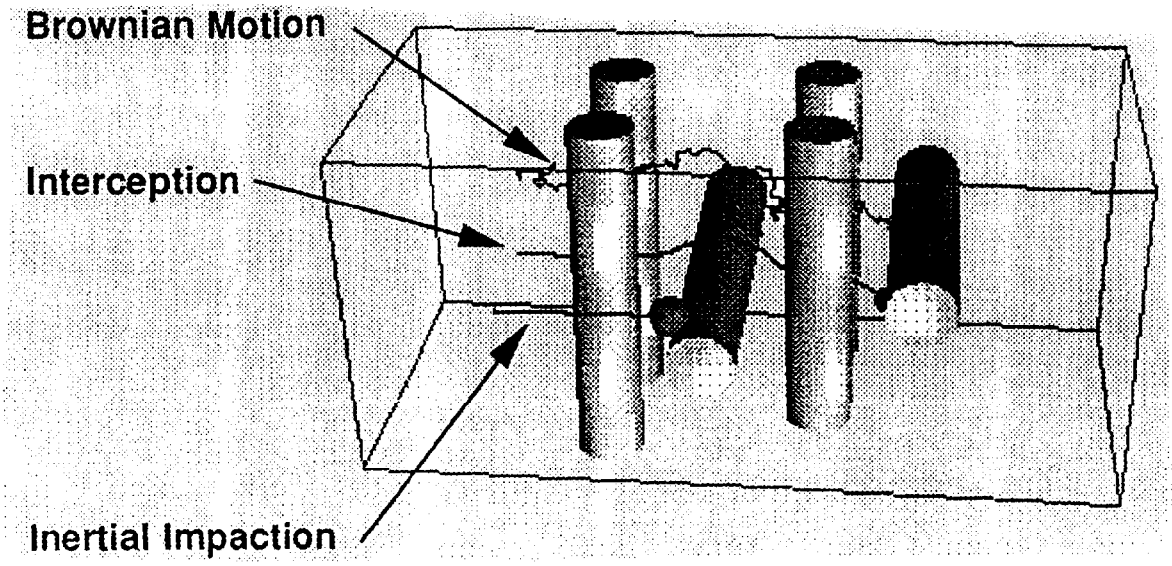

Figure 7 Trajectories of three different diameter particles through the fiber matrix shown in Figure 4 with the inlet air velocity at 20 cm/s. The diameter of the particles were selected to illustrate the conventional collection mechanisms due to Brownian motion, interception and inertial impaction. Note that the particle sizes are not to scale to allow visualization.

To determine the particle capture efficiency of a given fiber matrix for comparison with experimental measurements, it is necessary to compute thousands of trajectories for each particle size. For each trajectory calculation, the initial starting location is determined by a random number generation in the Y-Z plane. Figure 8 shows the cumulative efficiency of 0.3 μm diameter particles (density 1 g/cm^3) passing through the crossed fiber matrix as illustrated in Figure 7 with an inlet air velocity of 20 cm/s. Performing similar calculations at other particle sizes allows us to plot the efficiency versus particle size.

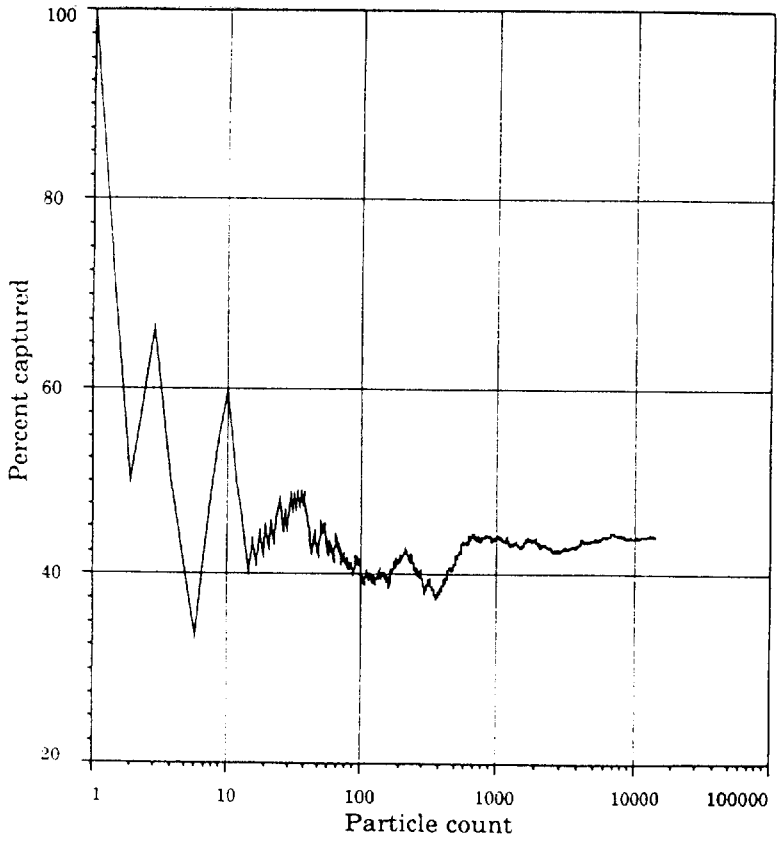

Figure 8 Cumulative efficiency of increasing number of 0.3μm diameter particles (density 1 g/cm^3) passing through the crossed fiber matrix in Figure 4 with a uniform inlet air velocity of 20 cm/s.

III. Sample Computations of Filter Efficiencies

The computation of the filter efficiency for a given fiber configuration and a given air flow requires three sequential steps: (1) compute the fluid flow field using CFD calculations, (2) compute the particle trajectory using Equation 1, and (3) compute the trajectories of many particles at random positions at the filter inlet to obtain an average efficiency. These calculations will yield the efficiency at a given particle size. For filter efficiency as a function of particle size, steps 2 and 3 must be repeated for each particle size. For efficiency at different air flows, all three steps must be computed.

Figure 9 shows the results of the efficiency calculations for the crossed fiber array at 20 cm/s. Figure 10 shows the efficiency of the same crossed fiber array at 2 cm/s. Note that the capture efficiency for the larger particles increases while the efficiency for the smaller particles decreases as the air velocity is increased. Figure 11 shows the particle capture efficiency for the staggered hexagonal array at 3 cm/s.

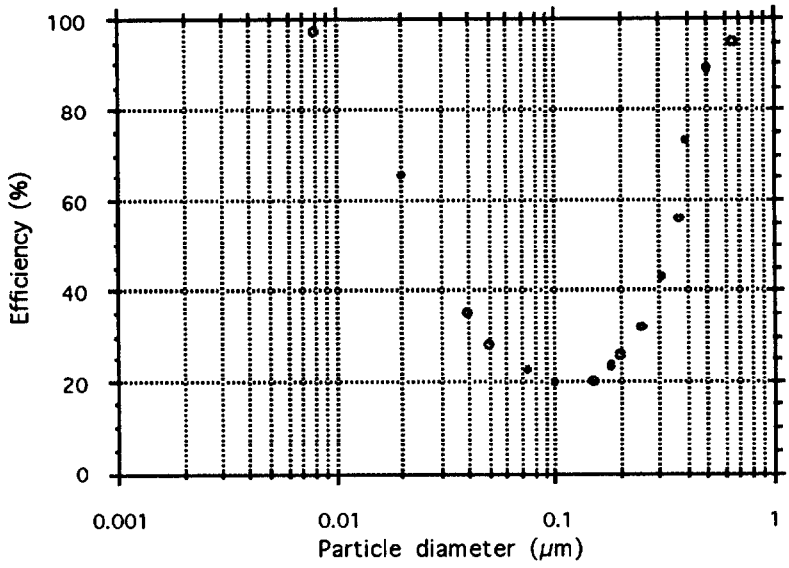

Figure 9 Filter efficiency computed for different particle diameters (density 1 g/cm^3) passing through the crossed fiber matrix in Figure 4 with uniform inlet air velocity of 20 cm/s. The pressure drop across the fiber matrix element is 4.4 x 10^{-5} inches of water.

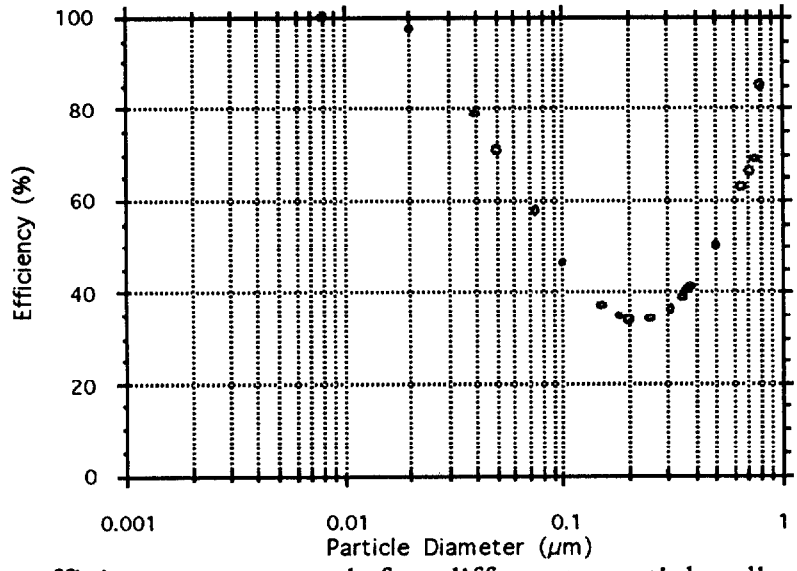

Figure 10 Filter efficiency computed for different particle diameters (density 1 g/cm^3) through the crossed fiber matrix in Figure 4 with a uniform inlet air velocity of 20 cm/s. The pressure drop across the fiber matrix element is 4.4 x 10^{-6} inches of water.

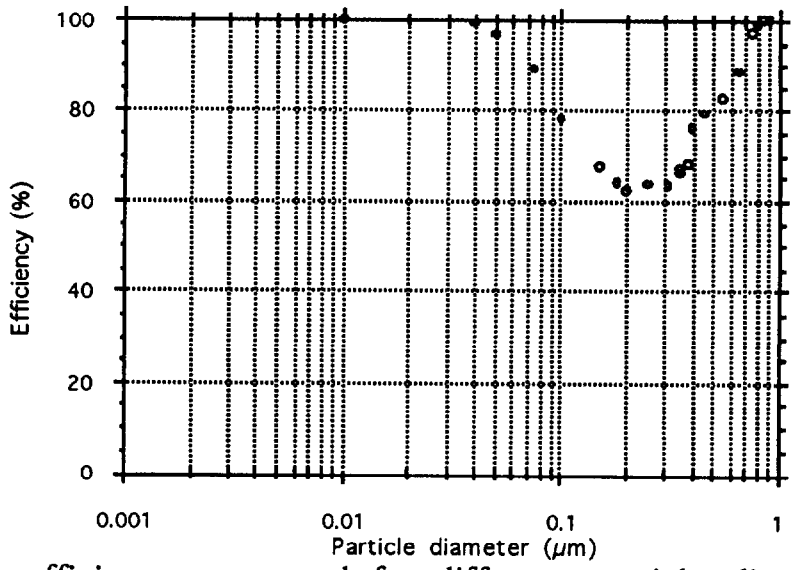

Figure 11 Filter efficiency computed for different particle diameters (density 1 g/cm^3) through the staggered hexagonal array in Figure 3 with a uniform inlet air velocity of 3 cm/s. The pressure drop across the fiber matrix element is 3.2×10^{-5} inches of water.

Although it is feasible to compute the particle capture efficiency and pressure drop across simple fiber matrices as shown in this report, we are a long way from computing the efficiency and pressure drop for commercially available filters. The primary limitation here is an efficient method for computing the fluid flow through the more complicated fiber matrix in real filters.

IV. References

1. Tien, C, Granular filtration of aerosols and hydrosols, Butterworths, Boston, (1989).

2. Brown, Air filtration; an integrated approach to the theory and applications of fibrous filters, Pergamon Press, New York,(1993).

3. Liu, ZG and Wang, PK, "Numerical investigation of viscous flow fields around multifiber filters" J. Aerosol Science and Technology, Vol 25, No. 4, pp 375-391, (1996)

4. Ramarao, BV, Tien, C, and Mohan, S "Calculation of single fiber efficiencies for interception and impaction with superimposed Brownian motion" J. Aerosol Sci., Vol 25, No. 2, pp 295-313, (1994).

5. Chandrasekhar, Rev. Modern Phys. Vol. 15, p 1 (1943).

DISCUSSION

WEBER: I think that the work that Werner is doing is a real service to the industry and I hope that he will be able to carry out his plan to bring it to full fruition. I have a couple of questions for the author. Do you have a way of measuring the fiber diameters in a large assembly?

BERGMAN: We determine fiber diameters from electron micrographs followed by computer scanning and generate histograms of the number of fibers versus size. For three dimensional analysis, we solidity the filter element with an epoxy, take slices of the element at increasing depths and then take SEM photos. For quicker, less expensive analysis, we simply took SEM pictures of the media surface.

WEBER: I noticed that the fiber diameters you cited were greater than 1μm yet we know that the glass fibers optimally used are less than that in many cases. Was there a particular reason for the choice of diameter in your calculations?

BERGMAN: Yes. Below 1μm you have non-continuum fluid dynamics that is often called "slip" flow. All of the conventional fluid dynamics codes are based on a continuum fluids. To address the slip flow, we first compute the flow using continuum mechanics and then close to the fiber, we introduce an empirical term. This approach is not rigorously correct, but it yields better results than ignoring slip. Using a noncontinuous fluid dynamics package in filtration modeling would greatly exceed the capacity of the largest computer.

WEBER: Finally, I am wondering how long through the useful life of a filter it would be until cake build-up or the presence of previously deposited particles would affect the result, or would start to dominate the result?

BERGMAN: We did not do these computations. From the pictures of particle trajectories, you can see that it is possible to model filter clogging. Let me illustrate how this can be done. For the initial particle capture and deposits, we assume the general fluid dynamics flow is not affected by the deposits. However, once the deposits become sizable, you have to recompute the fluid field with the altered filter geometry. Particle trajectories are then computed for the new fluid velocity field and a new increment of deposits formed. The cycle of forming particle deposits and computing new flow fields is repeated many times. Considering that it may take 20-40 hours of computer processing on a silicon graphics workstation to compute the flow field in a 100 fiber filter element, we are a long way from realistic filter clogging simulations.

KOVACH, B: The work you did is great but did you consider the influence of a vibrating fiber due to high velocity airflow? Would it increase or decrease the efficiency? Is your video movie available for use by others?

BERGMAN: As soon the work is finished we will make copies available. With regard to vibrating fibers, I am not aware of any studies. However, if you look at the period of vibration, I suspect the period would be much longer than the effective residence time of a particle in the vicinity of a fiber. I have a difficult time imagining a fiber vibrating at a speed that is comparable to the particle velocity, but then I've been surprised more times than not.

THOMAS: Previously, I tried to use equations by Drs. Liu and Rubo to determine filter efficiency, but I ran into a problem trying to determine their parameter for collector diameter. I used an average fiber diameter, but I was wondering if you have determined any kind of average filter fiber diameter based on information from people that make filter papers?

BERGMAN: Although we can determine fiber size distribution precisely, the problem is that the paper is very heterogeneous. The fiber diameter distribution and fiber volume fraction can vary greatly depending on where the measurments are taken in the filter paper. The common practice is to use an "inhomogeneity factor" and an average fiber diameter derived from SEM pictures in a specific filter equation for pressure drop. The inhomogeneity factor is used to force agreement between the equation and experiment. Since all of the pressure drop theories (Karmen-Kozenly, Kuwabara, etc.) have pressure drop varying inversely proportional to fiber diameter squared, the most common average is the weighted average of diameter squared. The weighting factor generally is a function of the site distribution and the distribution of fiber volume fraction throughout the filter. A more practical approach is to use an "effective" diameter which is the diameter determined from the pressure drop equation with experimental pressure drop data.

DYMENT: Does the speaker consider an attempt should be made to include electrostatic forces? Can the techniques described be used to produce designs of filter media having extended dust capacity?

BERGMAN: We have added electrostatic forces in the computer models but have not run many cases. I should add that any number of additional capture mechanisms can be easily added to the code because once you have established the flow field and the mechanical trajectory, it is a minor step to add additional capture mechanisms. The current stage of computer simulation can be used to investigate extended life, but it is not practical because of the excessive time required to compute. The problem is that each time the morphology of the particle deposits changes it perturbs the air flow and therefore requires a new flow field computation. An entire series of flow computations would be required for each filter media structure. This would require an enormous amount of computation and is not practical at the present time.

DYMENT: I have been fascinated by your demonstration, I think it is a major step forward. Filtration is an extremely complex process. Do you imagine we use the filters that electrical effects are significant because you are studying what we call mechanical effects. Do you think that electrical effects can be important in real filters? That is my first question. My second question concerns the graded papers we were talking about at the last conference which have a somewhat higher dust holding capacity. Do you anticipate that you can use these techniques to give us target designs for filters which will hold larger quantities of particles before their resistance rises to the point at which we have to change them?

BERGMAN: If conditions are favorable for electrical effects, then they will be very important in filtration. Conditions that favor electrical effects are dry air, charged particles, and high filter electrical resistance. Thus I would expect electrical effects would enhance the performance of real filters in dry air powder handling or processing operations. Applications involving aqueous oil mists or ambient aerosols would have little electrical effects. The computer simulations can be used to answer performance and design questions, but only for very simple systems at the present time. Even the simple filtration problems illustrated in this paper require 3-4 days of work. Setting up the basic filter structure represents currently about 10% of the effort. Fluid dynamics represents 80% of the full

effort. The particle trajectories represent 9% and the remaining 1% is the electrostatics. The purpose of this presentation is to begin the process of developing a CAD/CAM system where engineers can sit at their computers and calculate the filter efficiency for graded efficiency filters, unusual structures, filter clogging, whatever it is you want. Major advances in both computer software and hardware will be required this goal.

* * *

STUDY ON COLLECTION EFFICIENCY OF FISSION PRODUCTS BY SPRAY : EXPERIMENTAL DEVICE AND MODELLING

D. DUCRET*, Y. BILLARAND, D. ROBLOT*, J. VENDEL***

* Institut de Protection et de Sûreté Nucléaire
Département de Prévention et d'Etude des Accidents
DPEA/SERAC - CEA/Saclay, Bâtiment 383 - 91191 GIF-SUR-YVETTE Cedex, France

** ECCO Pharmacie et Chimie
5, Bd de Courbevoie - 92523 NEUILLY Cedex, France

ABSTRACT

Consequences of an hypothetical overheating reactor accident in nuclear power plants can be limited by spraying cold water drops into containment building. The spray reduces the pressure and the temperature levels by condensation of steam and leads to the washout of fission products (aerosols and gaseous iodine). The present study includes a large program devoted to the evaluation of realistic washout rates.

An experimental device (named CARAIDAS) was designed and built in order to determine the collection efficiency of aerosols and iodine absorption by drops with representative conditions of post-accident atmosphere. This experimental device is presented in the paper and more particularly :
- the experimental enclosure in which representative thermodynamic conditions can be achieved,
- the monosized drops generator, the drops diameter measurement and the drops collector,
- the cesium iodide aerosols generator and the aerosols measurements

Modelling of steam condensation on drops, aerosols collection and iodine absorption are described. First experimental and code results on drops and aerosols behaviour are compared.

NOMENCLATURE :

C	: concentration	$(mol.m^{-3})$
Cp	: calorific capacity	$(J.kg^{-1}.K^{-1})$
C_{th}	: heat accomodation coefficient	(-)
Cu	: Cunningham correction coefficient	(-)
d	: diameter	(m)
Dif	: diffusion coefficient	$(m.s^{-1})$
dm	: drop mass increase	(kg)
E	: collection efficiency	(-)
h	: heat transfer coefficient	$(W.m^{-2}.K^{-1})$
H_v	: enthalpy of water vaporization	$(J.mol^{-1})$
k	: mass transfer coefficient	$(m.s^{-2})$
L	: free path of gaseous molecules	(m)
m	: mass	(kg)
M	: molar mass	$(kg.mol^{-1})$

N	: mass flux density	$(mol.m^{-2}.s^{-1})$
P	: pressure	(Pa)
Psat	: saturation vapor pressure	(Pa)
q	: heat flux density	$(W.m^{-2})$
T	: temperature	(K)
v	: drop velocity	$(m.s^{-1})$
λ	: thermal conductivity	$(W.m^{-1}.K^{-1})$
ρ	: density	$(kg.m^{-3})$
μ	: dynamic viscosity	(Pa.s)

Dimensionless numbers :

Knusend number : $Kn = \frac{2L}{d_p}$ (-)

Nusselt number : $Nu = \frac{h.d_d}{\lambda}$ (-)

Prandtl number : $Pr = \frac{Cp.\mu}{\lambda}$ (-)

Reynolds number : $Re = \frac{\rho_g.v.d_d}{\mu_g}$ (-)

Schmidt number : $Sc = \frac{\mu}{\rho.Dif}$ (-)

Sherwood number : $Sh = \frac{k.d_d}{Dif}$ (-)

Stokes number : $Stk = \frac{d_p^2.\rho_p.v}{9.\mu_g.d_d}$ (-)

Subscripts :

d	: drop
g	: gaseous
i	: gas-drop interface
I	: iodine
p	: particle
pot	: potential
vis	: viscous
w	: water
diffu	: brownian diffusion
difph	: diffusiophoresis
imp	: impaction
int	: interception
therph	: thermophoresis
tot	: total

I. INTRODUCTION

Consequences of an hypothetical overheating reactor accident in a nuclear power plant can be limited by spraying cold water drops into the containment building. The spray reduces the pressure and the temperature levels inside the containment building by steam condensation on drops. With this thermalhydraulic function, spray leads to the washout of fission products (aerosols and iodine) emitted in the reactor building atmosphere. Today, this spray system is taken into account in different safety codes, using washout rates which have been determined during global experiments. These washout rates provide conservative assumptions. This present study integrates into a large program devoted to the evaluation of more realistic washout rates. First, we develop an experimental device and a modelling in order to determine aerosols collection efficiencies and iodine absorption in severe accident representative conditions.

II. EXPERIMENTAL DEVICE

In order to comply with experimental device design requirements[1], different devices have been developped, tested and set up on CARAIDAS (figure 1) :
- experimental enclosure in which representative thermodynamic conditions could be achieved,
- the monosized drops generator, the drops diameter measurements and the drops collector,
- the cesium iodide aerosols generator, concentration and size distribution measurements.

II.1. Experimental enclosure

Experimental enclosure is a five meters high cylinder with an inner diameter of 0.6 meter. The vessel is heated up by circulating a thermofluid through the double-wall unit. This system is split into three sections to ensure uniform temperatures overall the vessel height. The vessel has 8 windows (100 mm diameter) and several penetrations (50 mm diameter) for instrumentation purposes.
The thermofluid circuit comprises :
- a pump with a flow rate of 12 m^3/h,
- an electric heater (40 kW) using a PID regulation can heat up the thermofluid at a maximum of 160°C. The temperature in the main pipe is monitored by two sensors (Pt100, class A),
- the thermofluid repartition into the three sections is ensured by one valve and one flow meter for each section.

Homogeneous thermodynamic working conditions are obtained by using an air-steam circulation with:
- a varying flow rate fan (0 to 50 m^3/h),
- an electric heater (5 kW), using a PID regulation, can heat up air-steam mixture with a temperature range between 20 to 160°C ; the temperature is monitored by two Pt100 sensors (class A),
- an absolute pressure PID regulation in the range of 1 to 8 bars is carried out by using two valves (one for pressurized air alimentation and one for release),
The steam saturation rate in the vessel is also controlled by a PID regulator. Steam is produced by an electric generator and injected using a valve controlled by the regulator. Steam saturation rate range is between a few per cent and 95 %. Highest saturation limit is 95 % to avoid condensation particularly on windows.
This air-steam circulation ensures a good mixture in the vessel. When nominal working conditions (P, T, S) are reached, air-steam circulation is stopped and then the vessel is isolated by two valves. Several sensors are installed on the vessel to check air-steam mixture homogeneity :
- five gas temperature sensors (Pt100, class A),
- three inner vessel wall sensors (Pt100, class A),

- one pressure transducer (0-10 bars),
- three steam saturation ratio measurements by dew point measurement,
- one steam partial pressure measurement by sampling some gas and condensation by cooling.

All of these experimental data are displayed and saved by using a PC supervisor.

II.2. Drops devices

Drops generator is above the experimental enclosure because this device must be at ambient temperature and this, whatever enclosure temperature. In order to produce monosized drops, the generator (figure 2) is based on a break-up process of a jet into drops by applying a periodic disturbance. This principle of generation induces a one drop diameter spacing. This small drops spacing is not large enough to avoid drops coalescence, so an electrostatic sorting out drops is set up. A stream of uniformly charged drops is shaped by applying a potential difference between a ring electrode and the feeding tube. When a negative impulsion is applied to the ring electrode, an uncharged drop is produced. The deflection plates placed downstream, which are under electrical potential difference, create an electric field. Charged drops passing through this electrical field are deflected and collected. Uncharged drops are not deflected and they are injected in the experimental enclosure. The rate of injection of uncharged drops is variable from 1 to 1/1000. This device is able to produce monosized water drops with a diameter between 100 and 500 μm. Drops injection temperature is measured by a Pt100 sensor on the feeding tube. Drops injection temperature can be set between 20°C to 80°C by a small electric heater.

After injection in the vessel, drops diameter is modified by steam condensation or evaporation as function of thermodynamic conditions. So, three drops diameter measurements are forecast for three falling drops heights: $z=0$, $z=2.51$ and $z=4.39$ meters. These measurements are based on drops shadows axial transmittance. A stroboscopic incoherent light source is placed in front of linear camera (CCD). When a drop comes in front of the CCD camera, analogic signals from photodiodes are obtained and then numerized. Numerical drop shadow is processing in order to calculate the real drop diameter.

At the end of the fall, drops must be collected to measure aerosols mass in drops, so a drops collector ensures three functions :

- drops collection,
- dynamic containment of drops collection surface,
- sample output.

Drops are collected on fiberglass filters, 80 mm diameter, 1.55 mm thickness and temperature proof under 200°C. These filters can soak up water drops volume (a few milliliters). The collected aerosols mass by drops during fall is dissolved in 10 ml of distilled water and measured by fluorimetric method. Aerosols sedimentation on collection surface is avoided by a dynamic containment : clean air is blown throught collection filter and get back by a circular aspiration on the top of the dynamic containment device not to modify aerosols concentration in the experimental vessel. Extraction of several samples during test is been able by a pressure thruster which shifts drops collector from experimental vessel to the SAS where it can be brought out and put a new drops collector in place.

II.3. Aerosols devices

Aerosols generation is based on mechanical spraying by rotative disk, of cesium iodide solution tagged by soda fluorescein. Rotational device is an air turbine because high rotation speed is needful

(3000 rounds per second). Rotation speed is set by air pressure inlet the turbine and monitored by an electromagnetic indicator. Spraying disk (8 mm diameter) is fed up with cesium iodide solution with steady state flow rate. Sprayed droplets diameter which is function of rotation speed and solution flow rate, is about 20 μm. After evaporation, dry aerosols diameter is function of cesium iodide concentration :

$$d_p = d_{droplet}\left(\frac{[ICs]_{solution}}{\rho_{ICs}}\right)^{1/3} \qquad \text{eq.1}$$

With this specific generator, it is possible to produce aerosols with temperature (20-160°C) and pressure (1-7 bars). Aerosols diameter range is between 0.5 and 5 μm with a geometric standard deviation lower than 1.7 and aerosols mass flow rate is roughly 0.1 g/h.

Four aerosols samples are set up on experimental enclosure to check homogeneity of concentration and particles size distribution. Aerosols concentrations are measured on fiberglass filters of 25 mm diameter. Each sample is going on one or two minutes with a 1 l/min flow rate. The filtered aerosols mass is measured by fluorimetric method.

Particles size distribution measurements are given by inertial impactor in vessel pressure and temperature conditions. Aerosols are discriminated among eight size ranges corresponding to aerodynamic diameters from 0.35 to 7.5 μm. Data processing is performed by a classical log-probability graph. This method gives aerosols mass median diameter and geometric standard deviation.

This experimental device allows to measure experimental drops diameter evolution and collected aerosols mass by drops as function of different experimental conditions representative of severe accident scenarios. At the same time we develop a modelling of this experimental device.

III. Modelling

Drops characteristics (temperature, size, iodine and particles concentration) are modified during the fall. Three phenomena of transfer between the gas and the monosized drops are to be modelled :

- heat and steam transfer,
- gaseous iodine transfer,
- particles collection.

Steam condensation, iodine absorption and particles collection are coupled together because some of collection mechanisms depend on steam condensation flow rate.
The basic assumption of these following models is that water drops are supposed independant.

III.1. Steam and heat transfer

Steam and heat transfer from the gaseous phase to the liquid one is modelled by the double film theory (figure 3). Steam mass transfer is located in the gaseous film and heat transfer takes place through the whole double film. Beyond this double film, temperatures and concentrations are supposed steady.

The steam flow rate is the following one : $N_w = k_{g,w} \times \left(\frac{P_w}{RT_g} - \frac{Psat(T_i)}{RT_i}\right)$ eq.2

where $k_{g,w}$ is the ratio between the diffusion coefficient of steam in air and the thickness of the gaseous film. This transfer coefficient is computed thanks to a correlation given by BEARD and PRUPPACHER[2]: $Sh_{g,w} = 1.61 + 0.718 \times Re_d^{1/2} \times Sc_{g,w}^{1/3}$

The heat flow rate through the gaseous film is :

$$q = \underbrace{h_g \times (T_g - T_i)}_{\text{convective exchanges}} + \underbrace{N_w \times H_v}_{\text{condensation contribution}}$$

h_g is also computed by a correlation (BEARD and PRUPPACHER[2]) :

$$Nu_{g,w} = 2 + 0.69 \times Re_d^{1/2} \times Pr_g^{1/3}$$

This flow rate q is equal to the one of the drop side : $q = h_d \times (T_i - T_d)$

h_d is computed by HENDOU's correlations[3].

Finally: $$\underbrace{h_g \times (T_g - T_i)}_{\text{convective exchanges}} + \underbrace{N_w \times H_v}_{\text{condensation contribution}} = h_d \times (T_i - T_d) \qquad \text{eq.3}$$

So coupling equation eq.2 and equation eq.3, T_i and N_W are determined by a numerical method (Newton-Raphson). The knowledge of the steam flow rate and of the convective exchanges value allows to compute the drops growth during a lapse of time called dt :

$$d_d(t+dt) = \left(d_d^3(t) + \frac{6 \times d_d^2(t) \times dt \times N_w \times H_v}{\rho_d} \right)^{1/3}$$

Then drop heating is computed using the heat balance on the drop between t and t+dt :

$$m \times Cp_d \times dT_d = h_g \times (T_g - T_i) \times \pi \times d_d^2 \times dt + dm \times H_v$$

$$\text{with: } dm = \frac{\pi \times d_d^2 \times dt \times N_w \times H_v}{\rho_d}$$

So : $$T_d(t+dt) = T_d(t) + \frac{h_g \times (T_g - T_i) \times \pi \times d_d^2 \times dt + dm \times H_v}{m \times Cp_d}$$

III.2. Iodine transfer

The energetic iodine flow rate contribution is disregarded. Iodine transfer from the gaseous phase to the liquid one is firstable controlled by diffusion through the gaseous film, since by the thermodynamic equilibrium between the both phases which depends on the temperature at the interface, and at least by chemical reactions which take place into the drops.

At low steam flow rates, iodine transfer through the gaseous film is estimated as :

$$N_I = k_{g,I} \times (C_{g,I} - C_{gi,I})$$

This flow is equal to the one through the liquid film : $N_I = k_{d,I} \times (C_{d_i,I} - C_{d,I})$

Finally : $$k_{g,I} \times (C_{g,I} - C_{gi,I}) = k_{d,I} \times (C_{d_i,I} - C_{d,I}) \qquad \text{eq.4}$$

The unknown values are C_{gi} and C_{di}. They are linked by the thermodynamic equilibrium at the interface and by chemical reactions. Hydrolysis of molecular iodine and HOI dissociation are only considered. The other reactions are slow regarding to the fall time of drops (few seconds in CARAIDAS).

- gas-liquid equilibrium : $I_{2,gas} \leftrightarrow I_{2,liq}$ $\quad Ki = \frac{[I_{2\,liq}]}{[I_{2\,gas}]}$ eq.5

- iodine hydrolysis : $I_{2,liq} + H_2O \leftrightarrow HOI + I^- + H^+$ $\quad K_1 = \frac{[HOI] \times [I^-] \times [H^+]}{[I_{2,liq}]}$ eq.6

- hypoiodous acid dissociation : $HOI \leftrightarrow OI^- + H^+$ $\quad K_2 = \frac{[OI^-] \times [H^+]}{[HOI]}$ eq.7

The concentration in protons is supposed to be a constant value. The reaction equilibrium constants are given by GAUVAIN and FILIPPI[4].

Equations eq.5 and eq.6 allow to express $C_{di,I}$ (which is : $[HOI]+[OI^-]+[I^-]+[I_{2,liq}]$) as a function of $C_{gi,I}$:

$$C_{d_i,I} = Ki \times C_{g_i,I} + 2 \times \frac{\sqrt{K_1 \times (K_2 + [H^+]) \times Ki \times C_{g_i,I} \times 1000}}{[H^+]}$$

This expression is used in the place of C_{di} in equation eq.4. Solving equation eq.4 provides C_{di} and so N_I. At least, the updated concentration in iodine into the drop is computed :

$$C_{d,I}(t+dt) = C_{d,I}(t) + \frac{\pi \times d_d^2(t) \times dt \times N_I}{\left(\frac{\pi \times d_d^3(t)}{6}\right)}$$

III.3. Particles collection

Aerosols collection models are completly different than those for iodine absorption. They are based on semi-empirical correlations to calculate collection efficiencies for different mechanisms. Collection efficiency is defined as the ratio of aerosol mass collected by a drop and the aerosols mass in swept out volume. Five mechanisms of particles collection are listed :

- impaction
- interception
- diffusiophoresis
- thermophoresis
- brownian diffusion

Mechanical effects

- *impaction* : drops fall induces fluid flow variations. High inertia particles turn off flow lines around the drop and then are collected on the drop. The efficiency of this mechanism increases with drop velocity and particle mass. POWERS and BURSON[5] suggest :

$$E_{imp} = \frac{E_{vis,imp} + \frac{Re_d\, E_{pot,imp}}{60}}{1 + \frac{Re_d}{60}}$$

if $Stk \le 0.0833$ then $E_{pot,imp} = 0$

if $0.0833 \le Stk \le 0.2$ then $E_{pot,imp} = 8.57\left(\frac{Stk}{Stk+0.5}\right)^2 (Stk - 0.0833)$

if $Stk \ge 0.2$ then $E_{pot,imp} = \left(\frac{Stk}{Stk+0.5}\right)^2$

if $Stk \le 1.214$ then $E_{visc,imp} = 0$

if $Stk \ge 1.214$ then $E_{visc,imp} = \left(1 + \frac{0.75\ln(2\,Stk)}{Stk - 1.214}\right)^{-2}$

- *interception*: this mechanism is only based on a geometric effect. If a particle on a flow line meet the drop, it is collected. POWERS and BURSON[5] propose :

$$E_{int} = \frac{E_{vis,int} + \frac{Re_d\, E_{pot,int}}{60}}{1 + \frac{Re_d}{60}}$$

with $$E_{visc,int} = \left(1 + \frac{d_p}{d_d}\right)^2 \left[1 - \frac{1.5}{1 + \frac{d_p}{d_d}} + 0.5\left(1 + \frac{d_p}{d_d}\right)^3\right]$$

and $$E_{pot,int} = 3\frac{d_p}{d_d}$$

Phoretic effects : the temperature gradient and the steam flow around drops respectively induce thermophoresis and diffusiophoresis.

- *diffusiophoresis* : steam condensation on cold water drops induces a steam flow towards drops. This flow drags along particles. WALDMANN and SCHMITT[6] suggest a formula corrected by the ventilation coefficient of PRUPPACHER[7]:

$$E_{difph} = 4.f_v \frac{\sqrt{M_w}}{x_w\sqrt{M_w} + x_a\sqrt{M_a}} \frac{Dif_w}{V \times d_d} \ln\left(\frac{P - Psat(T_i)}{P - P_w}\right)$$

if $Sc_{g,w}^{1/3}.Re_d^{1/2} < 1.4$ then $\quad f_v = 2.\left(1 + 0.108\left(Sc_{g,w}^{1/3}\,Re_d^{1/2}\right)^2\right)$

if $Sc_{g,w}^{1/3}.Re_d^{1/2} \geq 1.4$ then $\quad f_v = 2.\left(0.78 + 0.308\left(Sc_{g,w}^{1/3}\,Re_d^{1/2}\right)\right)$

- *thermophoresis* : it occurs when particles set in a temperature gradient. Impacts of gas on the warm side are more important than on the cold side of the particle. As a result, this difference creates a force which drags along particles towards cold drops.

$$E_{therph} = \frac{4\,C_{th}\,\mu_g\,f_h\,(T_g - T_d)}{C_g\,T_g\,V.d_d}$$

C_{th} is the dimensionless coefficient of TALBOT[8] and f_h is the heat ventilation coefficient of PRUPPACHER[7]:

$$C_{th} = \frac{2 \times 1.147\left(\frac{\lambda_g}{\lambda_p} + 2.2\,Kn\right) Cu}{(1 + 3 \times 1.146\,Kn) \times \left(1 + 2\frac{\lambda_g}{\lambda_p} + 2 \times 2.2\,Kn\right)}$$

if $Pr_g^{1/3}.Re_d^{1/2} < 1.4$ then $\quad f_h = 2.\left(1 + 0.108\left(Pr_g^{1/3}\,Re_d^{1/2}\right)^2\right)$

if $Pr_g^{1/3}.Re_d^{1/2} \geq 1.4$ then $\quad f_h = 2.\left(0.78 + 0.308\left(Pr_g^{1/3}\,Re_d^{1/2}\right)\right)$

At least, we describe brownian diffusion collection by modelling efficiency as PRUPPACHER[7] suggests :

if $Re_d < 1$ then $\quad E_{diffu} = \dfrac{4 \times Dif_p \times 2\left(1 + 0.5\,Re_d^{1/2}\,Sc_p^{1/3}\right)}{V.d_d}$

if $Re_d \geq 1$ then $\quad E_{diffu} = \dfrac{4 \times Dif_p \times 2\left(1 + 0.3\,Re_d^{1/2}\,Sc_p^{1/3}\right)}{V.d_d}$

The total efficiency is supposed to be the sum of the five elementary efficiencies :

$$E_{tot} = \sum_{i=1}^{5} E_i(d_p)$$

The emitted particles are polydisperse. The efficiency is computed for each particle size class. So, for the whole distribution :

$$E = \sum_{d_p\,min}^{d_p\,max} E_{tot}(d_p) \times f(d_p) \times \log(\Delta d_p)$$

The collected particles mass during a lapse dt is :

$$M_p(dt) = \sum_{d_p\,min}^{d_p\,max} E_{tot}(d_p) \times f(d_p) \times \log(\Delta d_p) \times \frac{\pi d_d^2(t)}{4} \times v \times dt \times C_p$$

Finally, the mass collected during the drop fall is :

$$Mp = \sum_{t=0}^{t_{fall}} \left(\sum_{d_p\,min}^{d_p\,max} E(d_p) \times f(d_p) \times \log(\Delta d_p) \times \frac{\pi d_d^2(t)}{4} \times v \right) dt \times C_p$$

IV CODE RESULTS

From the modelling of the different phenomena involving in the washout of fission products by spraying water drops, the drops and particles behaviours in CARAIDAS are estimated.

IV.1. Drops behaviour

The different evolutions of drops diameter and drops temperature as function of falling height are plotted on the figures 4, 5 and 6. The thermodynamic conditions of gas are steady during the drop fall: 5 bars pressure, 140°C temperature and several steam saturation rates. The initial diameters are 100, 300, and 500 μm.

At the drop fall beginning, the steam flow rate and the heat flow rate induce growth and heating of drops. When the steam saturation rate is equal to 1, this condensation phenomenon occurs on a varying height (3, 20 and 60 centimeters) according to the initial diameter (100, 300 and 500 μm). When the steam saturation decreases, the condensation height also decreases. After, the diameter and temperature of the drops are steady if $S=1$. On the other hand, evaporation phenomenon appears if $S<1$: there is an equilibrium between the heat flow brought to the drop by convective exchanges and the heat flow lost by the drop because of evaporation. Thus, drop temperature is steady but the diameter decreases. We consider that the drop completely disappears when its diameter is smaller than five micrometers.

All these computations show that thermodynamic equilibrium between the drops and the gaseous mixture is quickly reached when the steam saturation rate is equal to 1. On the other hand, when the gas is not saturated ($S<1$), the temperature speedly becomes steady whereas there is no balanced size.

IV.2. Aerosols behaviour

The modelling of drops behaviour coupled with the correlations providing particles elementary collection efficiencies allows to compute the average efficiency on a 5 meters fall. Different experimental conditions and particles diameters are tested for 100 μm diameter drops :

- figure 7 : In this case of atmospheric conditions ($P=1$ bar and $T=20°C$) with $S=1$, phoretic effects are negligible. Impaction and interception are the main mechanisms for the largest aerosols. For the smallest ones, brownian diffusion collection is the main mechanism. As a result, the average total efficiency is minimal (10^{-3}) for the aerosols which the diameter is around 0.5 μm.

- figure 8 : For these conditions, characteristic of spray scenarios (5 bars, 140°C and S=1), phoretic effects are not any more negligible. Thermophoresis is always the minority effect whatever the particles diameter. Diffusiophoresis efficiency which does not depend on particles diameter is slightly higher than the other ones when the total efficiency is minimal. Impaction, interception and diffusion mechanisms efficiencies do not vary a lot as function of thermodynamic conditions.

- figure 9 : The conditions are the same than ones of figure 8 excepted the initial drop temperature which is 80°C in this case. These values square with a scenario of recirculation. Despite lower values, diffusiophoresis efficiency is always the higher effect when the total efficiency is minimal. The decrease is due to the lower difference between gas and drops temperatures at the top of the vessel. The steam flow rate is lower so phoretic effects decrease.

Similary calculations are plotted on figures 10, 11 and 12 for 500 μm diameter drops. For ambient conditions (figure 10), phoretic effects are also negligible. The minimal efficiency (10^{-3}) resulting from impaction, interception and brownian diffusion mechanisms, is placed for aerosols which the size is lower than 0.1 μm.
In conditions characteric of spray scenarios (figure 11 and figure 12), diffusiophoresis is the main effect for aerosols which the diameter is lower than 1 μm. Thus, the minimal efficiency reached 10^{-2} thanks to the phoretic effects.

The previous curves represent the average efficiencies on a five meters fall. But these efficiencies change a lot as function of falling height because of the evolution of the steam flow rate and the temperature gradients around drops.
On figure 13 and figure 14, all the efficiencies and drops temperature are plotted for two particles diameters : 0.1 and 5 μm. We clearly observe that the phoretic effects are very important at the beginning of the fall but stop when temperature becomes steady.
Mechanical effects, do not depend a lot on temperature, are almost steady during the fall. The slight variations are only due to the changing drop size and to the drop velocity evolution. The temperature equilibrium is quickly reached so the efficiencies steady values are close to the average values dropped on figure 11.

V. EXPERIMENTAL RESULTS

Acquisition of experimental results on the device CARAIDAS allows to qualify the modelling of the different phenomena involved in the fission products washout by spray.
We only present the first experimental results. At the moment, an important campaign of tests is going on.

The three falling height drops diameter measurements and drop behaviour modelling are plotted on the figures 15, 16, 17 and 18 for different experimental conditions. Each experimental drops diameter is the average value of about fifty experimental points. Because of the slight decrease of diameter in some tests, the average values are accompanied with a confidence interval. If n is the number of experimental measurements, x_i a measurement i and x_a the average value on the measurements, we obtain :

the estimated standard deviation: $$s = \sqrt{\frac{\sum_{n=1}^{n} (x_i - x_a)^2}{n-1}}$$

the confidence interval on x_a: $i = 2 \times \frac{2s}{\sqrt{n}}$

(there are ninetyfive chances in a hundred that x_a is included in this interval)

Any confidence interval is drawn because it is very small (a few micrometers) in relation to the drops diameter decrease. So we can conclude that experimental measurement decreases are significant.
There is a good agreement between calculations and experiments whatever thermodynamic conditions (figure 15, 16, 17 and 18). Even when the drop evaporates a lot (dry warm air on figure 18), the divergences between the code and the experimental data are low.
More experimental results, with condensation thermodynamic conditions, will be getting but we can expected a good agreement also.

VI. CONCLUSION

The experimental device CARAIDAS is operational for aerosols experiments, so particles collection efficiencies as function of different working conditions representative of severe accident will be determined. Experimental aerosols tests are going on. In the same time, we have developped a model. Experimental collection efficiencies and code results will be used in order to propose qualified collection efficiencies correlations. At the end of this program more realistic washout rates could be computed as function of accident scenarios. Iodine experimental tests will be done after aerosols tests.

REFERENCES:

(1) DUCRET D., VENDEL J. and VIGLA D.
«Etude préliminaire de l'aspersion»
report SERAC/LECEV/93-22, 1993

(2) BEARD K.V. and PRUPPACHER H.R.
«A wind tunnel investigation of the rate of evaporation of small water drops falling at terminal velocity in air»
J. Atmos. Sci., vol. 28, pp 1455-1464, 1971

(3) HENDOU M.
«Contribution à la modélisation des transferts simultanés lors de l'absorption de gaz traces par une pulvérisation»
ENSIGC thesis, TOULOUSE, FRANCE, 1992

(4) GAUVAIN J. and FILIPPI M.
«Iodine transfer in the containment in the event of a severe accident»
Escadre System, Iode Code (release 2), CEA report, 1991

(5) POWERS D.A. and BURSON S.B.
«A simplified model of aerosol removal by containment sprays»
U.S. Nuclear Regulatory Commission, Washington D.C., 1993

(6) WALDMAN L. and SCHMITT Kh.
«Thermophoresis and diffusiophoresis of aerosols»
in «Aerosols Science» edited by C.N. DAVIES

(7) PRUPPACHER H.R. and al.
«Microphysics of clouds and precipitation»
D. REIDEL publishing compagny, 1978

(8) TALBOT L. and al.
«Thermophoresis of particles in a heated boundary layer»
J. Fluid Mech., 101, (4), 737-758, 1980

figure 1: Experimental device scheme

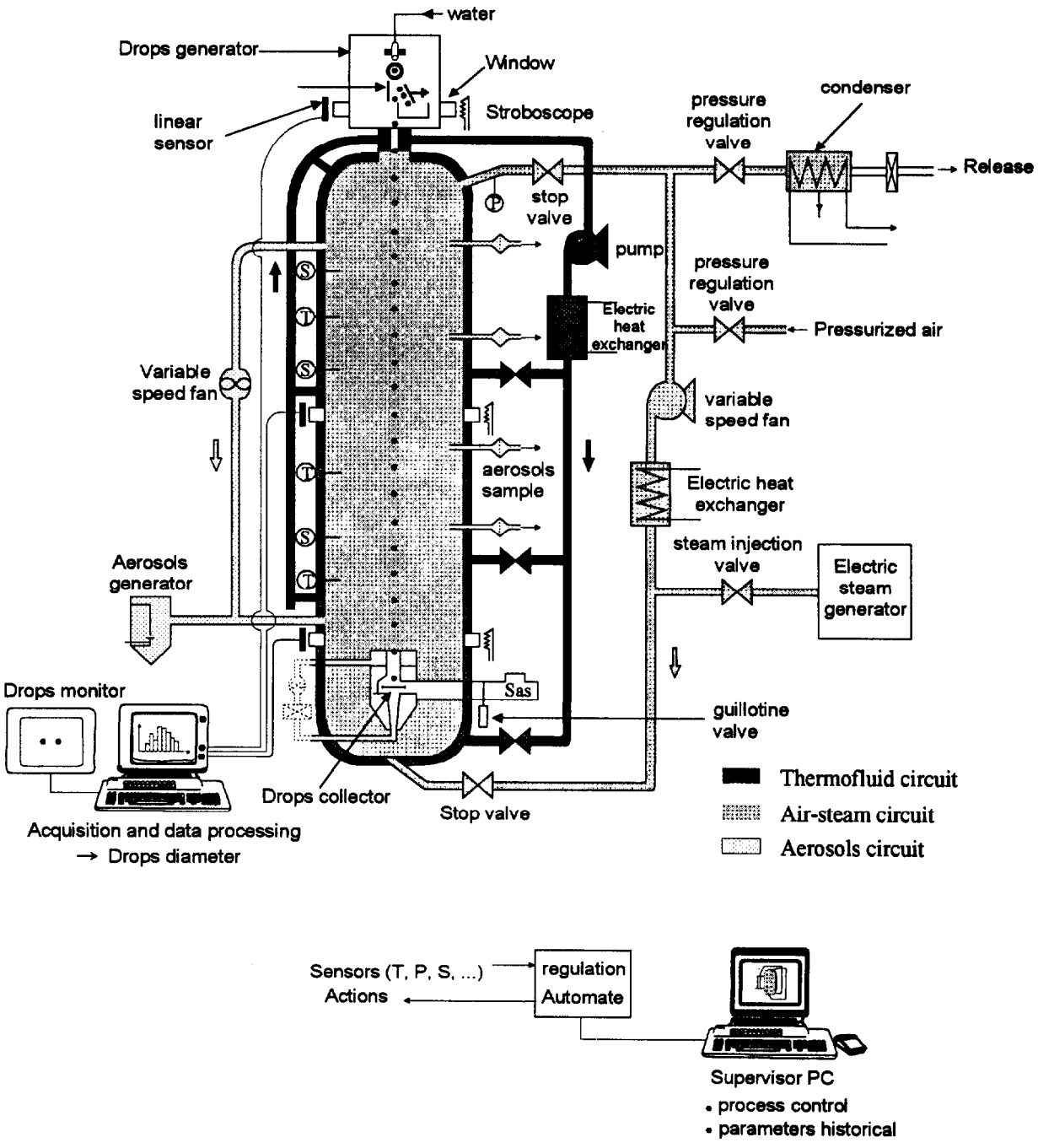

Figure 2 : Electrostatic sorting out drops generator

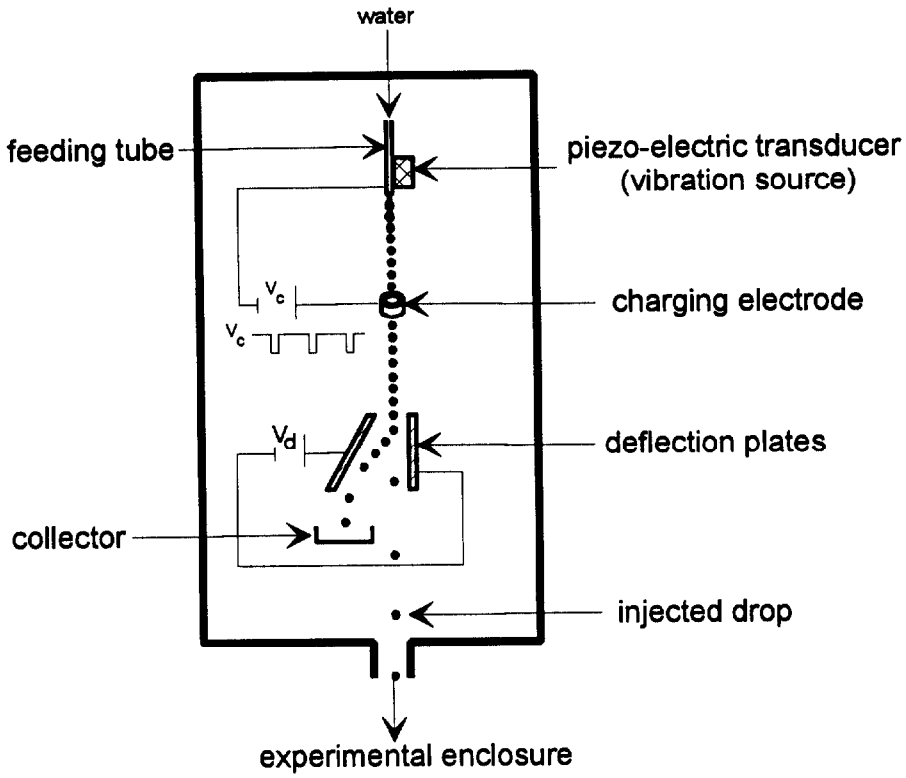

Figure 3: Double-film theory scheme

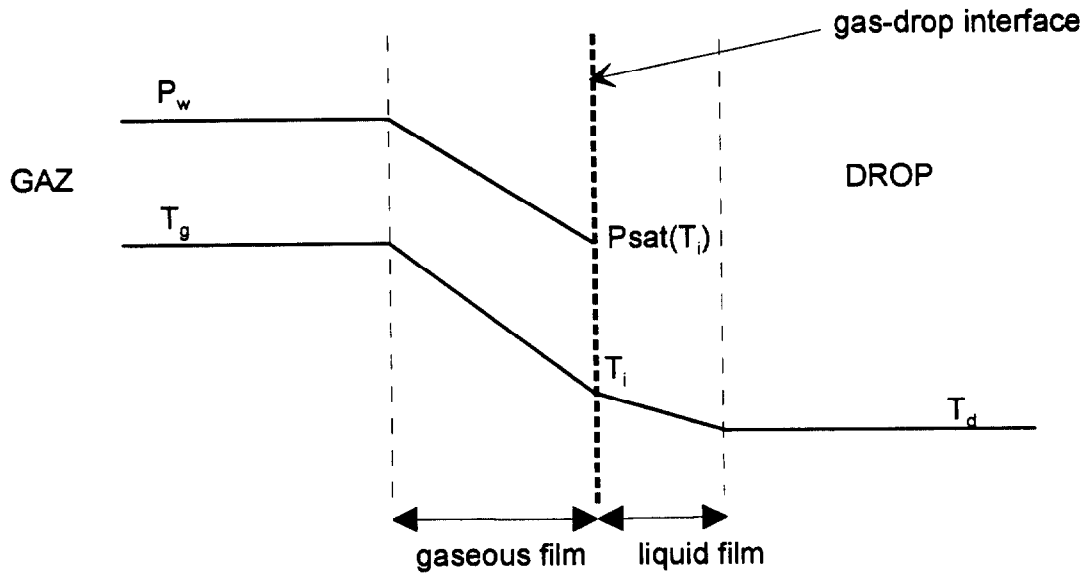

Fig. 4a: Drop diameter versus falling height - Initial drop diameter : 100 µm

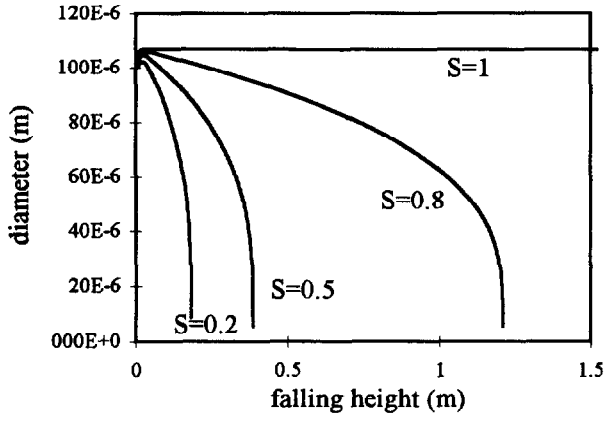

Fig. 4b: Drop temperature versus falling height - Initial drop diameter : 100 µm

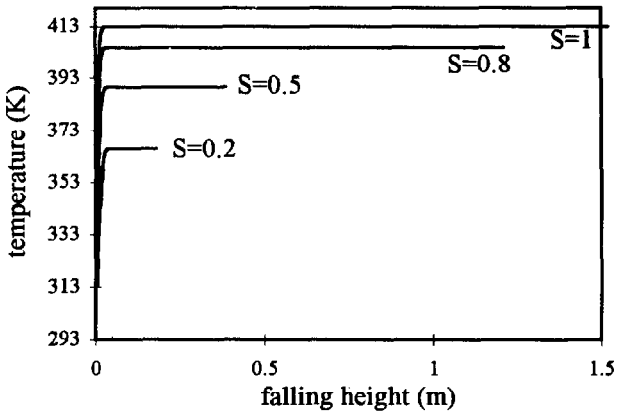

Fig. 5a: Drop diameter versus falling height - Initial drop diameter : 300 µm

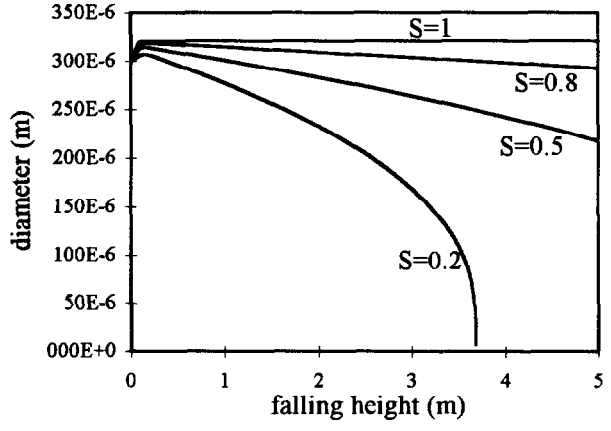

Fig. 5b: Drop temperature versus falling height - Initial drop diameter : 300 µm

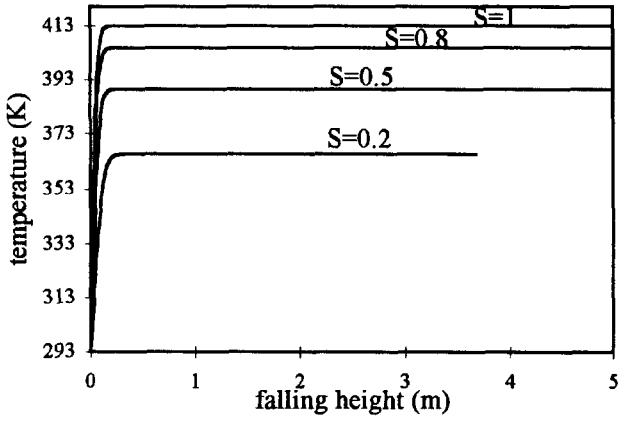

Fig. 6a: Drop diameter versus falling height - Initial drop diameter : 500 µm

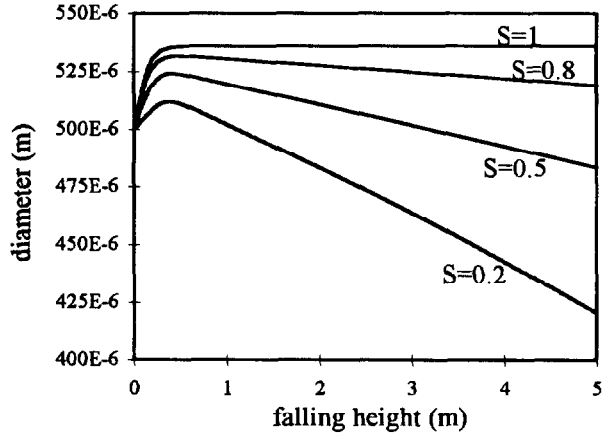

Fig. 6b: Drop temperature versus falling height - Initial drop diameter : 500 µm

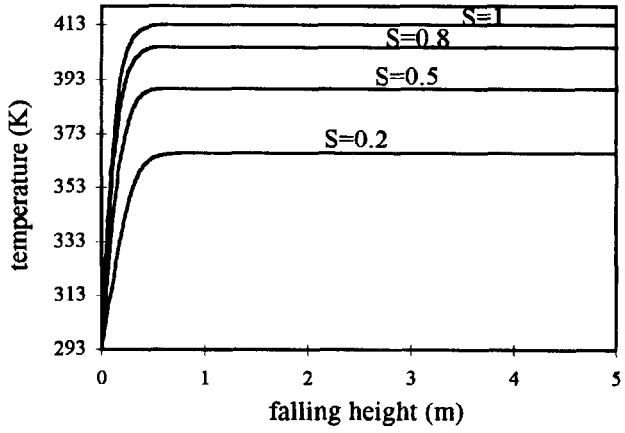

Figure 7: Collection efficiency versus aerosol diameter
P = 1 bar, Tdrop = Tgas = 20 °C, S = 1, Ddrop = 100 µm

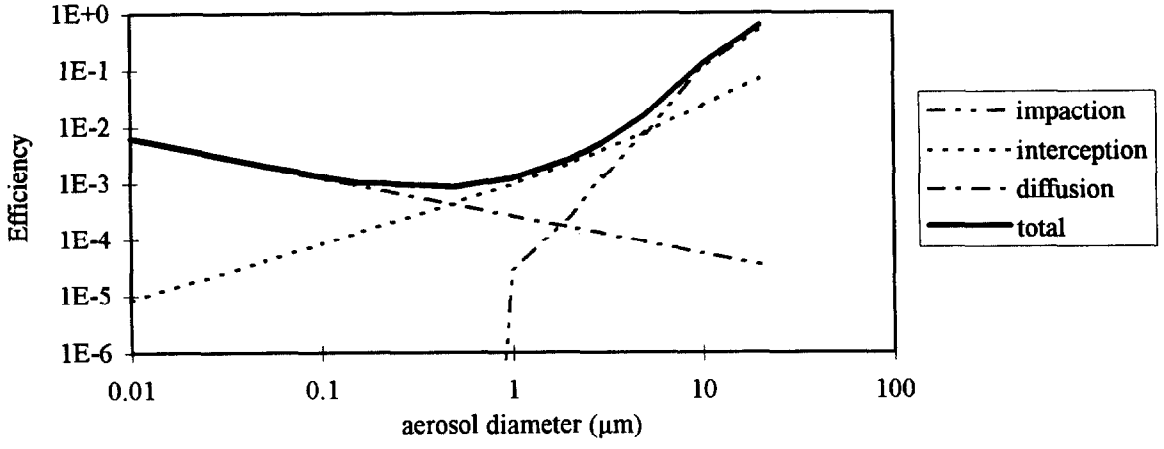

Figure 8: Collection efficiency versus aerosol diameter
P = 1 bar, Tgas = 140 °C, Tdrop = 20 °C, S = 1, Ddrop = 100 µm

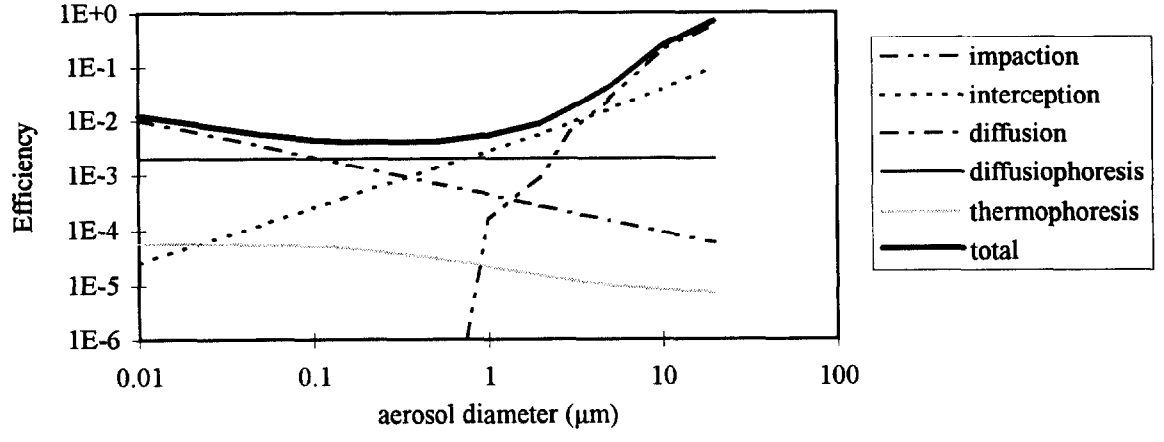

Figure 9: Collection efficiency versus aerosol diameter
P = 5 bars, Tgas = 140 °C, Tdrop = 80 °C, S = 1, Ddrop = 100 µm

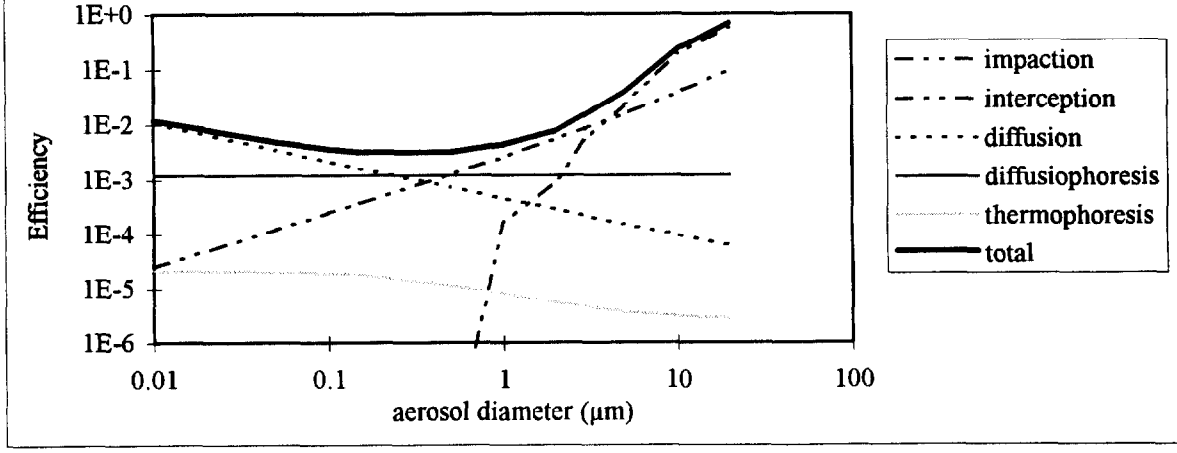

Figure 10: Collection efficiency versus aerosol diameter
P = 1 bar, Tdrop = Tgas = 20 °C, S = 1, Ddrop = 500 µm

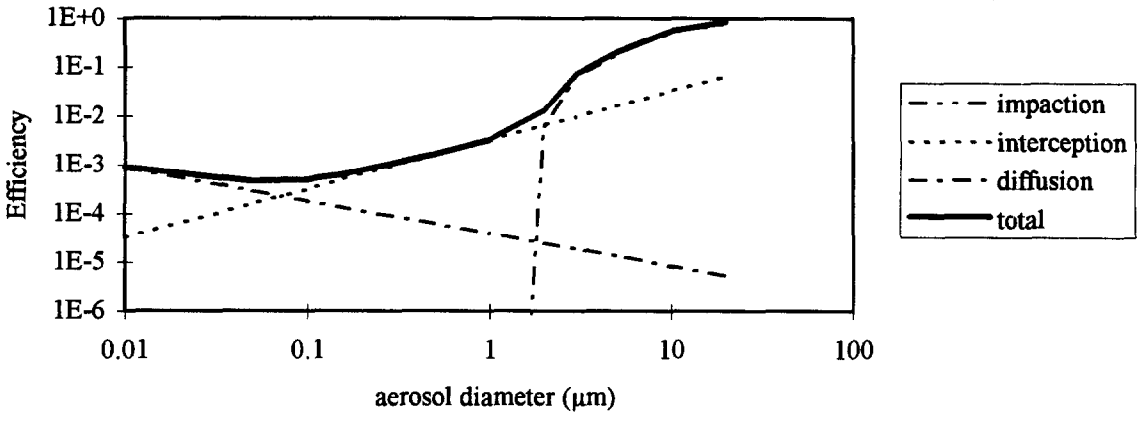

Figure 11: Collection efficiency versus aerosol diameter
P = 5 bars, Tgas = 140 °C, Tdrop = 20 °C, S = 1, Ddrop =500 µm

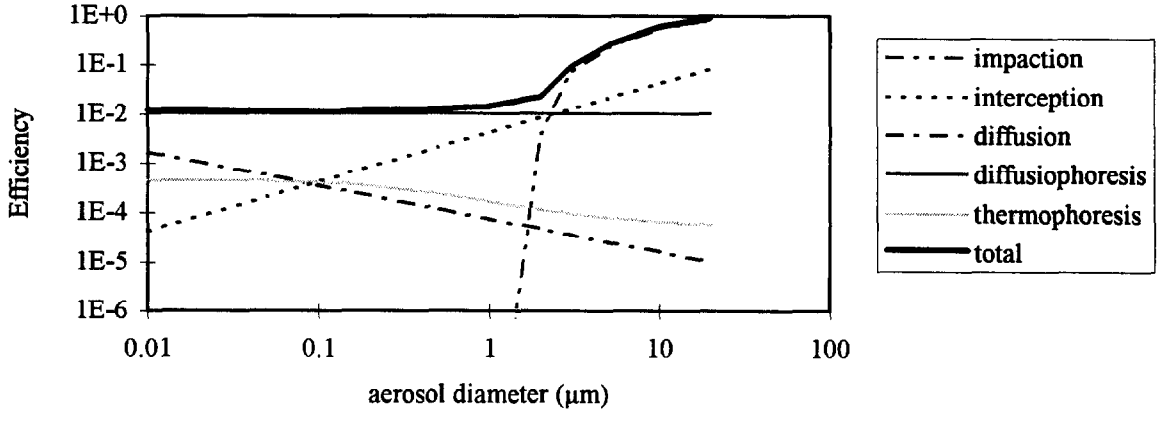

Figure 12: Collection efficiency versus aerosol diameter
P = 5 bars, Tgas = 140 °C, Tdrop = 80 °C, S = 1, Ddrop = 500 µm

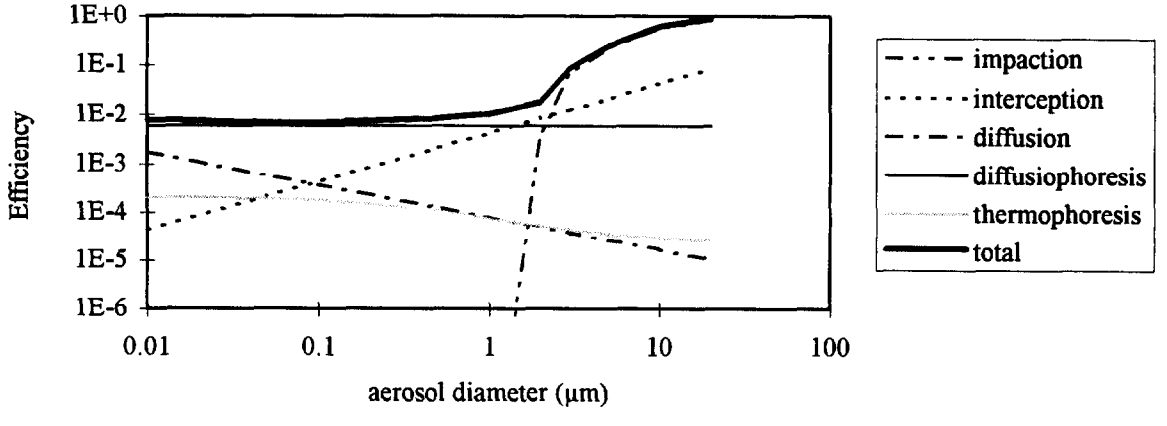

Figure 13: Elementary efficiency versus falling height
P = 5 bars, Tgas = 140 °C, Tdrop = 20 °C, S = 1
Ddrop = 500 µm, Daerosol = 0.1 µm

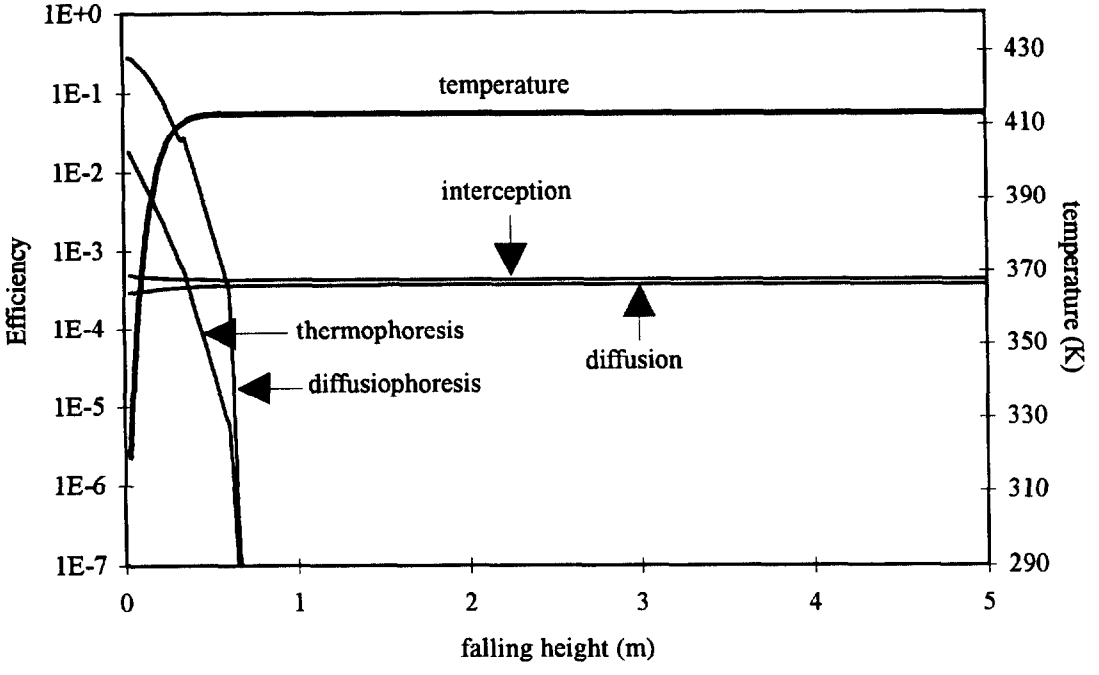

Figure 14: Elementary efficiency versus falling height
P = 5 bars, Tgas = 140 °C, Tdrop = 20 °C, S = 1
Ddrop = 500 µm, Daerosol = 5 µm

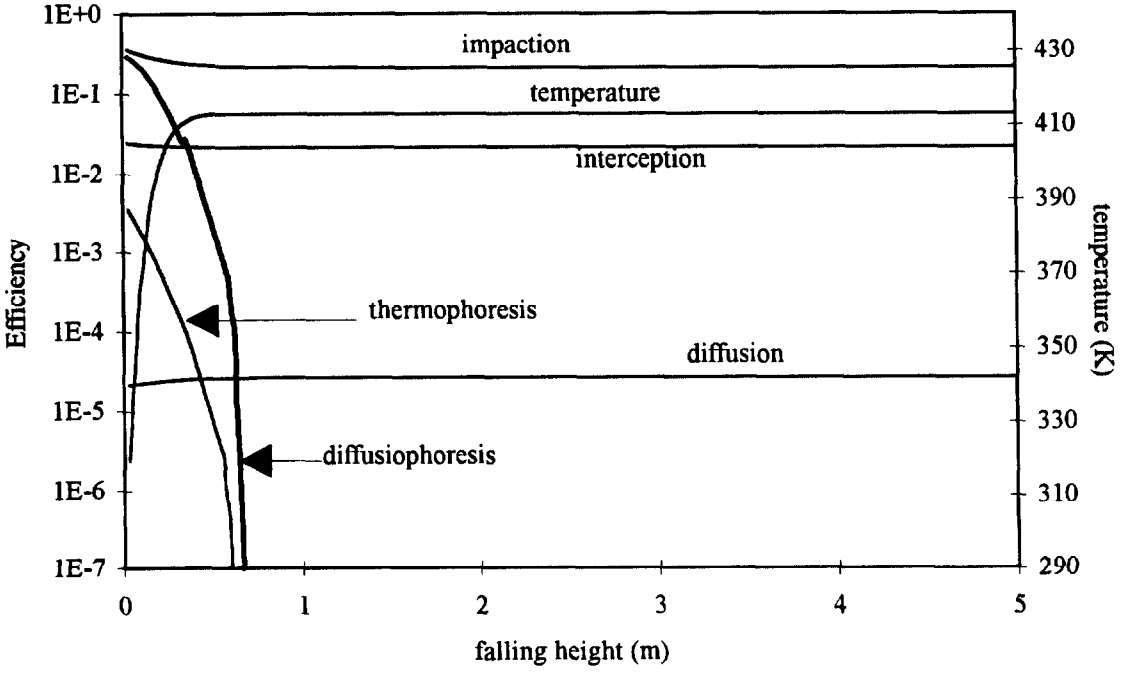

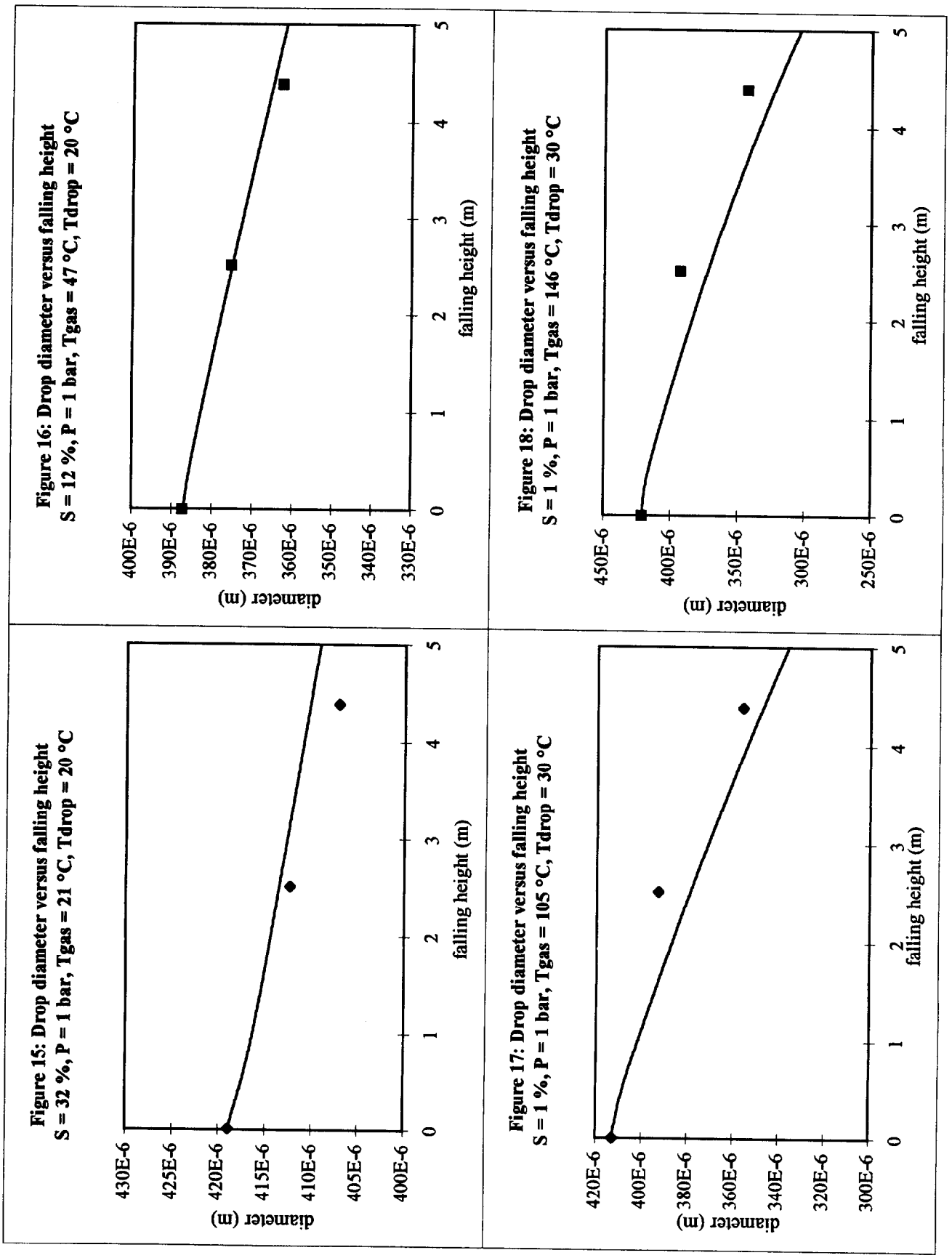
Figure 16: Drop diameter versus falling height
S = 12 %, P = 1 bar, Tgas = 47 °C, Tdrop = 20 °C
diameter (m)
400E-6
390E-6
380E-6
370E-6
360E-6
350E-6
340E-6
330E-6
0
1
2
3
4
5
falling height (m)
Figure 18: Drop diameter versus falling height
S = 1 %, P = 1 bar, Tgas = 146 °C, Tdrop = 30 °C
diameter (m)
450E-6
400E-6
350E-6
300E-6
250E-6
0
1
2
3
4
5
falling height (m)
Figure 15: Drop diameter versus falling height
S = 32 %, P = 1 bar, Tgas = 21 °C, Tdrop = 20 °C
diameter (m)
430E-6
425E-6
420E-6
415E-6
410E-6
405E-6
400E-6
0
1
2
3
4
5
falling height (m)
Figure 17: Drop diameter versus falling height
S = 1 %, P = 1 bar, Tgas = 105 °C, Tdrop = 30 °C
diameter (m)
420E-6
400E-6
380E-6
360E-6
340E-6
320E-6
300E-6
0
1
2
3
4
5
falling height (m)

DISCUSSION

LEE: Are you aware that we requested the Phebus project at Cadarache to install a single drop aerosol experiment (instead of using a spray) during the test in the containment to assess current modeling of spray scrubbing of iodine?

DUCRET: I do not really know the answer because it is on another project.

LEE: Because the containment of Phebus is very small, if they are going to use a spray, the spray cone will practically cover everything in the containment. Therefore, if you look at the cross section (of the spray) versus the surface area and the volume (of the containment) it will be greatly distorted no matter what kind of spray is used, and the results will probably not be useful for validating the models for spray scrubbing of iodine. For this reason, we proposed to the CEA to use a single drop type experiment.

CHARACTERIZATION AND RESTORATION OF PERFORMANCE OF "AGED" RADIOIODINE REMOVING ACTIVATED CARBONS

W. Peter Freeman
NUCON International, Inc.
Columbus, Ohio

Abstract

The degradation of radioiodine removal performance for impregnated activated carbons because of ageing is well established. However, the causes for this degradation remain unclear. One theory is that this reduction in performance from the ageing process results from an oxidation of the surface of the carbon. Radioiodine removing activated carbons that failed radioiodine removal tests showed an oxidized surface that had become hydrophilic compared with new carbons. We attempted to restore the performance of these "failed" carbons with a combination of thermal and chemical treatment. The results of these investigations are presented and discussed with the view of extending the life of radioiodine removing activated carbons.

Introduction

Experience has shown that the performance of activated carbons for radioiodine removal decreases with time by a process known as ageing. This ageing process can occur in storage and has lead to the recommended shelf life of five years currently accepted in the U.S. after which the carbon should be retested for radioiodine removal. Carbons that do not meet the retesting requirements and thus cannot be used though "new" have become known as "spinster" carbons. It is generally believed that these "spinster" carbons fail after prolonged storage due to a change in the surface oxides present on the carbon. NUCON® and others [1,2] have used a combination of thermal and chemical treatments to restore the performance of these "failed" carbons. The results of these investigations are presented and discussed.

Methodology

Except where noted, ASTM D3803-89 [3] was used to determine the methyl iodide removal efficiency at 30°C and 95% relative humidity. Heat treatments were performed using a rotary kiln. Carbon impregnations were performed using the incipient wetness technique.

Presentation of Results

Results of tests performed in the NUCON® laboratory are shown in Table 1 for treatment of "spinster" carbon. Shown in Table 2 are results of treatments of a spent carbon from a German plant[2].

Discussion of Results

The German test results in Table 2 show the methyl iodide removal efficiencies after different types of treatment techniques performed on a spent (i.e., a carbon that has seen service) carbon sample. These treatments included; desorption with steam at 130 °C, with nitrogen at 200, 300 and 450 °C and with carbon dioxide at 180 °C; extraction with hexane and heptane at 25 °C and extraction with supercritical carbon dioxide at 40 and 60 °C; and desorption with nitrogen at 450 °C followed by potassium iodide impregnation. Although their radioiodine test method differs from the ASTM method, the success of their thermal treatment using N_2 at 450°C with or without a following impregnation, prompted similar treatments in our laboratory on "spinster" carbon samples.

The results of these tests with "spinster carbons", shown in Table 1, indicate that desorption at 850°C with nitrogen followed by impregnation with TEDA restores the carbon to a greater than 99% efficiency. This is NUCON®'s lower limit for an acceptable test result using ASTM D3803-89. Hydrazine treatment of spent carbons has also been suggested as a treatment to restore the performance of aged carbons[1]. However, as shown in Table 1, hydrazine gave no improvement over TEDA impregnation.

This high temperature treatment with N_2 has been shown to drive surface oxides off the carbon[4] and, following impregnation, restores the carbon to "new" carbon performance. This treatment method may be a cost-effective way to restore the performance of "spinster carbons"especially when compared with new carbon replacement costs.

References

1. Deitz, V. R., " Charcoal Performance Under Accident Conditions in Light- Water Reactors", NUREG/CR-3990, NRL Memo Rpt 5528 (March 1985)

2. Lasch, M., et al, " Exhaustion of activated carbon for iodine retention in nuclear power plants", VGB *Krartwerkstech*, 1994, 74(11) 988-90

3. ASTM D3803-89, "Standard Test Method for Nuclear-GRade Activated Carbon", *Annual Book of ASTM Sandards*, Vol 15.01

4. Boehm, H. P., "Chemical Identification of Surface Groups", *Institute of Inorganic Chemistry, University of Heidelberg, Germany*

TABLE 1
Methyl Iodide Removal Efficiency After Treament of "Spinster" Carbon

Sample ID	Treatment	Methyl Iodide Removal Efficiency, %
4501	As Is	90.7
4501	N_2, 450 °C, KI+TEDA	98.0
4501	N_2, 700 °C, KI+TEDA	98.4
4501	N_2, 800 °C, KI+TEDA	98.6
4501	N_2, 850 °C, TEDA	99.3
I122	TEDA	97.1
I416	Hydrazine, TEDA	97.0

Radioiodine Test Conditions: ASTM D3803-89, 30 °C, 95% Relative Humidity

TABLE 2
German Studies of Depleted Carbon for Iodine Retention

Sample #	Treament	Methyl Iodide Removal Efficiency, %
1	Steam, 130 °C	98.86
2	N_2, 200 °C	99.27
3	CO_2, 180 °C	98.86
4	Supercritical CO_2, 40 °C	99.97
5	Supercritical CO_2, 60 °C	99.87
6	n-Hexane, 25 °C	99.83
7	n-Heptane, 25 °C	99.90
8	N_2, 300 °C	99.978
9	N_2, 450 °C	99.999
10	N_2, 450 °C, KI	99.999+

Radioiodine Test Conditions: 30 °C, 0.42 m/s, 1.2 sec. Residence Time

DISCUSSION

RICKETTS: I wonder if you could comment about how long these regeneration processes take and whether there are any significant differences between the various processes as far as costs go?

KOVACH, L: Yes, certainly there are differences. I do not know how familiar everybody is with how activated carbon is made. You process activated carbon at high temperature and at best the residence time may be from 1-3 hours in rotary furnaces but you may also be dealing with 10 - 24 hours residence time at these temperatures for some products. In the case discussed in the paper residence times are much shorter, a half-hour at temperature for the nitrogen treatment. If we are looking at supercritical extraction with carbon dioxide it becomes more complicated because there has been a significantly more strict controlled pressure boundary on the system than just a straight rotary furnace with an inert gas. Organic extractions are again more expensive because you have to recover the organic from the material and then you have to dry it again. So the lowest cost products are still made by nitrogen treatment. I would say by almost an order of magnitude lower cost than any of the other ones. Temperature is nothing other than an energy cost, it is really not significant. It is just as easy to run at 850°C as at 450°C, the residence times would be the same for all cases. In the US, straight impregnation cost is probably somewhere in the neighborhood of $0.50/lb for labor and material but excluding the cost of carbon used. The nitrogen treatment is the one that looks most promising, both from a cost and a benefit standpoint.

RICKETTS: Are you passing nitrogen through the carbon during the regeneration process?

KOVACH, L: It is not directly passed through, although we are currently doing some tests where we are passing it through the carbon. In a rotary furnace you are dealing with partial exposure, i.e., carbon is scattered up on the walls and it falls back so there is exposure partly to the nitrogen stream. But it is not continuous, so it is not like a fixed bed with hot nitrogen going through it, it is a rotating bed and it falls back in the tube while it is exposed to nitrogen.

24th DOE/NRC NUCLEAR AIR CLEANING AND TREATMENT CONFERENCE

EFFECTS OF WELDING FUMES ON NUCLEAR AIR CLEANING SYSTEM CARBON ADSORBER BANKS

Philip W. Roberson
Duke Power Company
McGuire Nuclear Station, Huntersville, NC 28078

Abstract

Standard Technical Specifications for nuclear air cleaning systems include the requirement to perform a full battery of surveillance tests following "fire, painting, or chemical release" in areas communicating with the affected system. In order to conservatively implement this requirement, many plants have categorized welding as a chemical release process, and instituted controls to ensure that welding fumes do not interact with carbon adsorbers in a filter system.

After reviewing research data that indicated that welding had a minimal impact on adsorber iodine removal efficiency, McGuire Nuclear Station decided to pursue further testing with the goal of establishing a "welding threshold". It was anticipated that some quantity of weld electrodes could be determined that had a corresponding detrimental impact on iodine removal efficiency for the exposed adsorber. This value could then be used to determine a conservative sampling schedule that would allow the station to perform laboratory testing to ensure system degradation did not occur, without incurring the penalty of a full battery of surveillance tests.

A series of tests was designed to demonstrate carbon efficiency versus cumulative welding fume exposure. Three series of tests were performed, one for each of the three different types of commonly encountered weld electrodes (E7018, E308 and E309). Each test series used a test filter train with a freshly loaded carbon adsorber and 20 pounds of electrode. Welding was performed with all airborne welding by-products directed through the filter train. Carbon sampling was performed at baseline conditions, and every five pounds of electrode thereafter. Two different laboratory tests were performed for each sample; one in accordance with ASTM 3803/1989 at 95% relative humidity and 30 degrees C, and another using the less rigorous conditions of 70% relative humidity and 80 degrees C.

Review of the test data for all three types of electrodes failed to show a significant correlation between carbon efficiency degradation and welding fume exposure. Accordingly, welding is no longer categorized as a 'chemical release process' at McGuire Nuclear Station, and limits on welding fume interaction with ventilation systems have been eliminated.

Introduction

Historically, at McGuire Nuclear Station, the generation of welding fumes has been considered to have a potentially detrimental effect on the carbon adsorbers of nuclear air cleaning system filter packages. Accordingly, their communication with operating filter systems has been administratively controlled; if welding fume exposure for a given system is unavoidable, that system would conservatively be considered inoperable and subject to the full battery of surveillance tests to demonstrate its return to operability.

Normally, these administrative controls do not place an undue burden on coordination between work and system operation. However, upcoming steam generator replacement projects at two of Duke Power Company's nuclear sites led to a re-examination of the welding fume impact issue.

During an outage, the Containment Purge filter trains at McGuire are essentially under continuous operation, either in 100% (dual train), or 50% (single train) mode. There are no designed system bypasses, so it is anticipated that essentially ALL of the gases generated by welding processes in containment will communicate with the operating filters. In order to avoid unnecessarily declaring filter trains inoperable based on 'suspected impact,' a site project was undertaken by the System Engineering and Operations groups to attempt to establish a correlation between the amount of fumes generated by welding and the resulting degradation in filter system methyl iodine removal efficiency.

Project Goal and Scope

The original project goal was to determine the point at which filter system adsorber performance deterioration occurred in a small test system, and then correlate this point to the cumulative weld fume exposure. Conservative extrapolations of this small test filter package data to actual systems would then be developed. It was anticipated that a 'pounds of electrode consumed per filter system flow rate' limit could be devised. This would be analogous to the painting 'rule of thumb' of 100 sqft per 1000 cfm that is widely used in the nuclear industry to perform carbon sampling and laboratory testing.

It was recognized that many hundreds of pounds of welding electrode would be used during the steam generator replacements, (and in the preceding outage, which incorporated as much structural prestaging as possible). Much of this welding would be 'stick', or electrode welding, (more formally called 'shielded metal arc welding', or SMAW). Other welding processes using an inert gas purge (i.e., MIG, TIG) are comparatively insignificant fume producers, and are not generally considered to be 'chemical releases.' Electrode welding was the only issue considered unresolved, and therefore was the sole focus of the project.

Test Method, Execution and Observations

Test Parameter Determination

The McGuire Training Support division has a small test filter train which was made available for use in project. The system is a portable and self-contained filter package manufactured by Charcoal Service Corporation of Bath, NC. This package consists of:

a) an 8" diameter intake duct (including flow orifice and manual throttle damper),
b) a filter housing, containing:
   one 24"x24"x2" prefilter,
   one 24"x24"x12" HEPA filter, and
   one carbon adsorber with approximately 75 pounds of carbon arrayed in 1 and 3/8" thick pleats, and
c) a belt driven centrifugal fan with a 120 VAC, 1.5 HP motor.

The nominal flow rate through the system is 500 cfm; manufacturer's supplied data for the adsorber states a residence time of 0.125 seconds at a flow rate of 1000 cfm (or, 0.25 seconds at 500 cfm).

Each of the two containment purge filter package carbon adsorbers holds approximately 2200 pounds of activated impregnated carbon, and has a nominal individual train flowrate of 14,000 cfm and 0.25 second residence time. A conservative approximation of the actual amount of welding electrode that might be consumed during an outage was 500 pounds. Comparing sizes of the test filter package to an individual containment purge package (based on either flow rate or the roughly equivalent carbon weight ratio) led to the choice of 20 pounds of electrode as the appropriate challenge for the test filter package. This equates to subjecting a single containment purge package to the fumes of approximately 585 pounds of welding electrode. Added conservatism is given by the fact that containment purge train operation is normally rotated during an outage, and routine lab tests of representative carbon samples are required after every 720 hours of system operation..

At McGuire, three different types of electrodes are used in 'stick welding' applications. They are:

1) AWS Classification E7018 for carbon steel to carbon steel welding,
2) AWS Classification E308 for stainless steel to stainless steel welding, and
3) AWS Classification E309 for stainless steel to carbon steel welding.

Due to the questions about the varying chemical compositions of the fluxes and the possibility of differing carbon degradation trends, it was decided that all three types would be tested (20 pounds of each). The carbon adsorber would be reloaded prior to each test series to quantify individual impacts.

Carbon to be used in each test series was the same nuclear grade-adsorbent as used in McGuire's safety filter systems. Purchase specifications state that it shall be impregnated to a range of 4.8 to 5% TEDA, and conform to all the physical and test standards as required by ANSI N509-1980, Table 5.1. The supplier for the carbon used was Carbon Applications, Inc. of Columbus, Ohio.

In order to add further conservatism and fully allow for any interaction between the welding fumes and the adsorber bed, a maximum test filter package flow rate of 250 cfm was established, which translates into a residence time of at least 0.50 seconds. In order to trend and correlate carbon degradation versus welding exposure, a carbon sampling frequency of a) prior to exposing the carbon to fumes, as a baseline, and b) following the consumption of every five pounds of electrode was assigned.

Test Execution

The general approach for each of the three test series was the same. The adsorber was loaded with new carbon, a baseline sample was obtained, and the filter package was started. The flow rate was throttled to a nominal 240 cfm. Welding was performed in the inlet plenum of the 8" ductwork to ensure that all fumes were drawn into the test filter package. The full length of the electrode was used for welding, regardless of whether restriking was required (impurities in the weld beads being generated were of no consequence to the test program). Representative carbon samples were removed from the adsorber following the consumption of each 5 pounds of electrode.

E308 Test Series: The original loaded carbon weight was 79 lbs. A gradually increasing prefilter differential pressure was observed during welding; its affect on flow was offset by adjusting the manual throttle damper in the inlet duct. Flow varied from 236 to 246 cfm. The total weight of E308 electrode was made up of 15 lbs. of 1/8" dia. and 5 lbs. of 3/32" dia.

E309 Test Series: The newly loaded carbon weight was 75 lbs. Prefilter differential pressure continued to rise during the test. Manual throttle damper adjustment was still sufficient to maintain nominal flow. Calculated flow for the series held steady at 242 cfm. E309 electrode weight was comprised of 16 lbs. of 1/8" and 4 lbs. of 3/32" dia.

E7018 Test Series: The test filter package prefilter was changed out along with carbon. Reloaded carbon weight was 80 lbs. The starting position for the throttle damper was further closed to account for the decreased D/P of the new prefilter. Flow varied from 229 to 239 while compensating for the initial particulate loading of the prefilter with damper adjustment. The breakdown of electrode sizes for the E7018 series was 5 lbs. of 3/32" dia., 7 lbs. of 1/8" dia., and 8 lbs. of 5/32" dia.

Test Results

Laboratory analysis of the carbon samples was performed by NCS Corporation of Columbus, Ohio. Each carbon sample was tested under two sets of conditions. The first was the Technical Specification dictated test of 80°C/95% Relative Humidity. The acceptance limit for this test is 99.00 % efficiency. The second test was the more conservative ASTM D3803-1989 test which incorporates a 16 hour pre-equilibration period and 30°C/95% RH test conditions.

The results of the laboratory testing performed at five pound intervals for the three types of electrodes are presented in the following table.

Welding Exposure	Carbon Laboratory Efficiencies (%): Electrode Type / Lab Test Conditions					
(Lbs. of	E308		E309		E7018	
Electrode)	(80C/95%RH)	(3803-1989)	(80C/95%RH)	(3803-1989)	(80C/95%RH)	(3803-1989)
0	99.99	99.59	99.99	99.58	99.99	99.81
5	99.99	99.72	99.99	99.55	99.99	99.72
10	99.98	99.70	99.99	99.59	99.99	99.76
15	99.99	99.68	99.99	99.66	99.99	99.75
20	99.99	99.63	99.99	99.73	99.99	99.79

Review of the above data shows that even under heavy exposure to welding fumes, the ability of the adsorber to filter methyl iodine was not significantly affected. This general observation is applicable to the test results of each of the three types of electrodes.

The graphical presentation of the same data is provided for each electrode test series on the facing page; Graphs 1, 2, and 3.

Graphs 1, 2, and 3

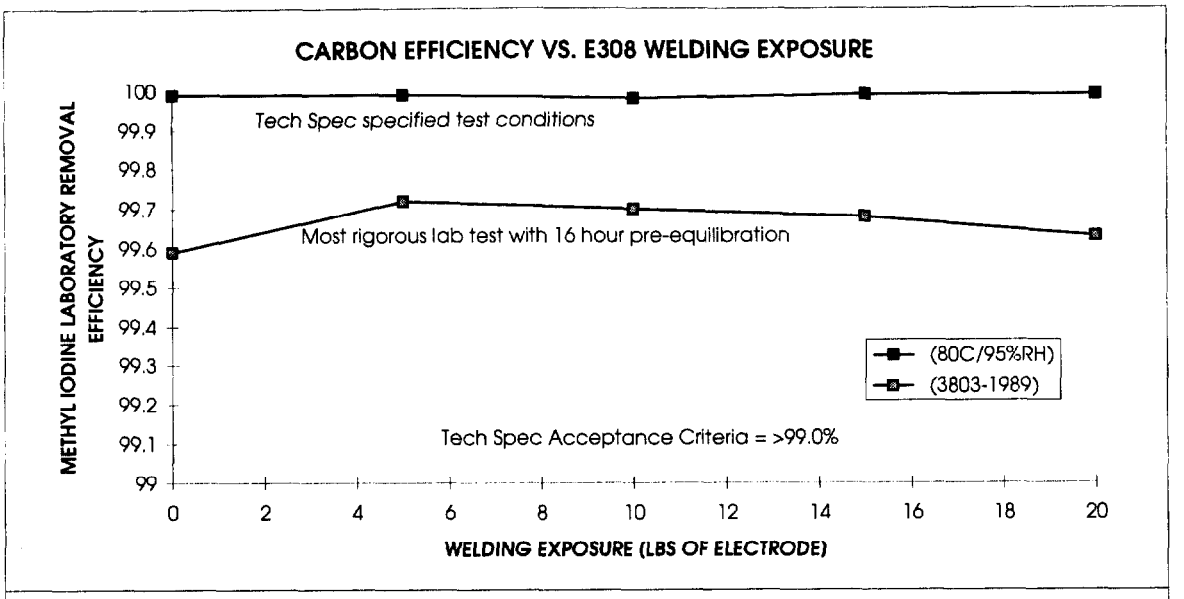

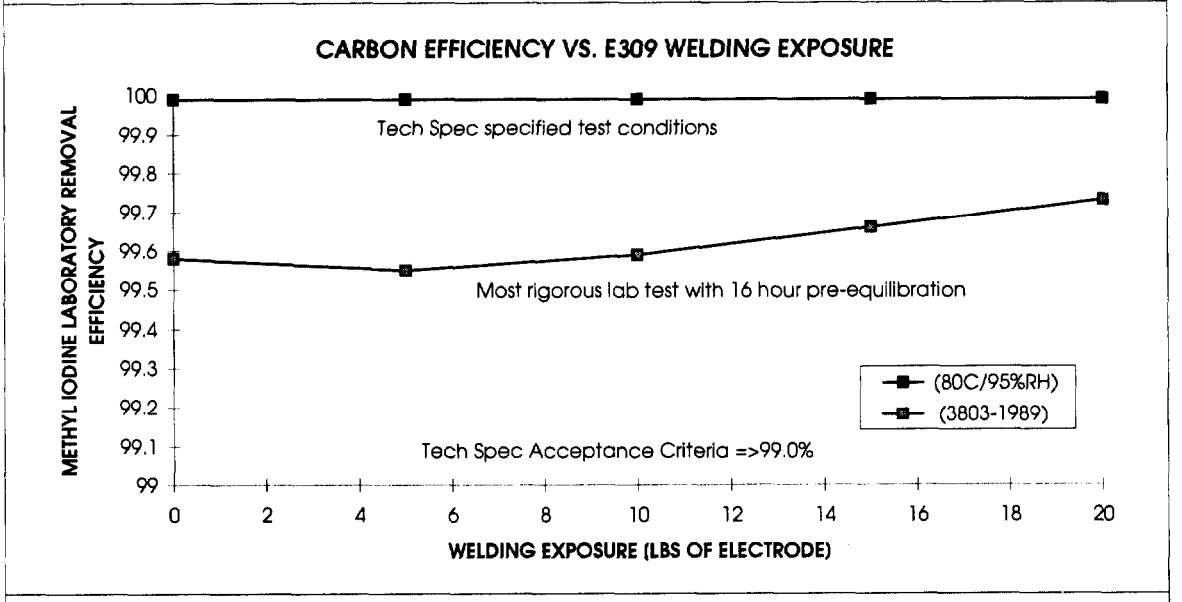

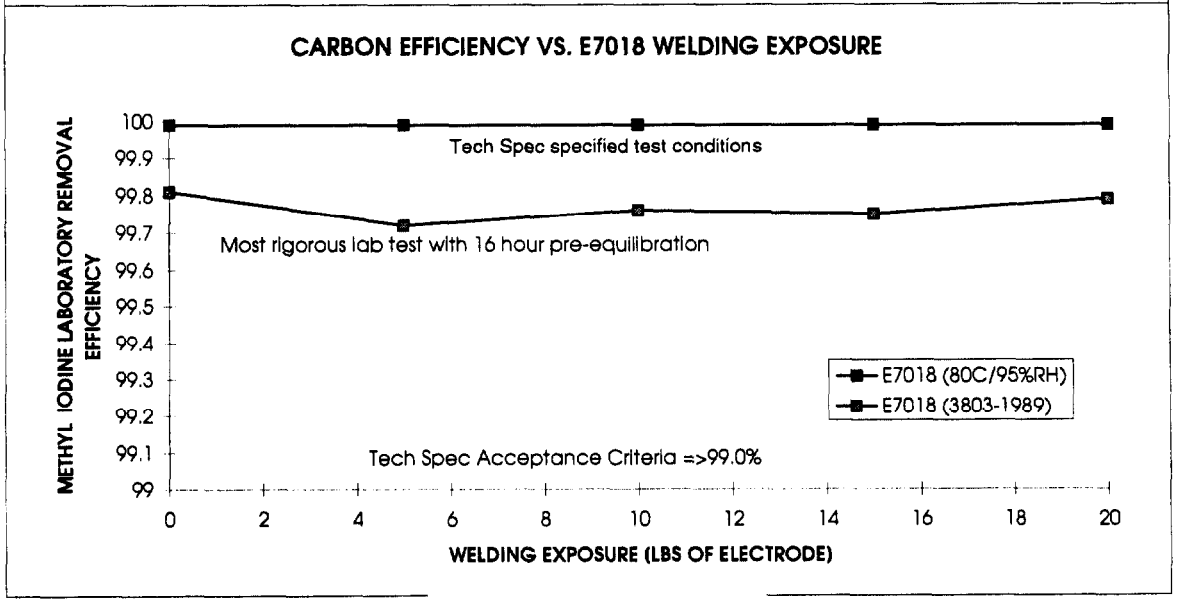

Conclusions

Review of the laboratory test data for the three test series showed uniformly non-existent impact for the methyl iodine penetration tests performed at Tech Spec dictated conditions. With one exception (whose results were 99.98% efficient), all test results following increasing exposure to welding fumes showed the same performance as the baseline. This consistency, and lack of an identifiable deterioration trend, was a pleasant surprise.

Turning to the results for the carbon samples when tested according to ASTM 3803-1989, more variation was noted. An average efficiency for each test series was calculated, along with a standard deviation. For the 15 samples, 10 fell within a single standard deviation of the average, and for the remaining five, the worst "outlier" was 1.5 standard deviations off the average. It is interesting to note that this point (Series E309, Sample #5) showed an increase in efficiency over the baseline test.

Based on the trends established by the sampling and lab results for each test series, it does not appear that the airborne byproducts of electrode welding have a statistically significant impact on the performance of a filter package adsorber. No correlation of adsorber performance degradation vs. welding exposure was established. It was, however, noted that the visible smoke from electrode arcing is a particulate that does have a cumulative effect on prefilters, and therefore, potentially, on total system flow and/or HEPA filter D/P. The routine monitoring of operating filter systems at McGuire is considered adequate to identify any flow impacts of increasing D/P due to welding or other dust/particulate generating activities.

Accordingly, electrode welding is no longer considered a chemical release process at McGuire Nuclear Station.

Acknowledgments

The author would like to acknowledge and extend his appreciation to David G. Davenport for his leadership and coordination efforts in conducting this project. Additional thanks are also extended to John Pearson of NCS, for his usual excellent support.

References

ANSI-N509-1980, "Nuclear Power Plant Air Cleaning Units And Components"

ASTM D3803-1989, "Standard Test Method for Nuclear Grade Activated Carbon".

American Welding Society, "Characterization of Arc Welding Fumes", 1983.

Ghosh, D. "Effects on the efficiency of activated carbon on exposure to welding fumes"; Proceedings of the 23rd DOE/NRC Nuclear Air Cleaning Conference, Conf-940738, Pg. 639, (1994).

DISCUSSION

ADAMS: Was there an interval after you exposed the carbon to the electrode contaminants when there was free flow of air through it? For example, after you exposed it for five electrodes, after you exposed it for ten electrodes, etc. After you completed five electrodes, for example, how much air flowed, or how soon did you pull a sample before you began the next electrode exposure?

ROBERSON: Let me clarify the question; as opposed to five electrodes it is five pounds of electrodes. We are looking in the neighborhood of fifteen electrodes per pound, so it's a little heavier exposure than that. We did not allow any specified amount of time between when the welder finished and we were ready to open the package up and pull the adsorber sample. It did not exceed 15 min.

ADAMS: Did flow continue through the unit while you were pulling the sample?

ROBERSON: Flow continued for an unspecified but relatively insignificant amount of time. The overall consumption of the weld rod, i.e., the number of pounds of weld rod, would take several hours between each sample, but when the welding was completed, sampling was promptly scheduled right after that.

ADAMS: Was the charcoal and filter package unit that you used a qualified ANSI N-509 unit?

ROBERSON: Yes.

ADAMS: How long did air pass through the unit after pulling a sample and beginning the next loading set?

ROBERSON: Unspecified, but in general the run time did not exceed an additional 15 minutes.

HAYES: Was the charcoal that you utilized brand new charcoal?

ROBERSON: Yes.

HAYES: Can you estimate the impact of welding on the charcoal if the test charcoal had not been new but aged for a year or longer?

ROBERSON: Although I would not expect different behavior, the project scope did not focus on carbon age impact. On a practical level, we have applied this relaxed policy on welding through the past outage, which included significant structural pre-staging work for the upcoming S/G outage. Ages of the carbon beds for the two trains of containment purge are approximately one and eight years. Sampling and lab results based on system run time confirmed no degradation on either train, new or old.

HAYES: You indicated that there was a trend that once you got initial degradation the efficiency may have picked up slightly, although within the error that you are talking about, you might even say it was flat. I am wondering if the deterioration, once the charcoal has been exposed, caused the process to somehow speed up one way or the other.

PEST: Can you elaborate on the sampling process? Did you use a grain thief, did you use a test canister?

ROBERSON: We used a grain thief and used a blended sample pulled from a number of pleats to obtain a standard sample.

FRANKLIN: Did you sample the air leaving the filter unit during or after welding?

ROBERSON: No, there was no attempt to quantify what kind of effluent came out of the filter package after all the weld fumes had passed through the pre-filter, HEPA filter, and adsorber.

HARRIS: There is a perceptible dust loading on the pre-filter. Was there an additional loading on the HEPA filter?

ROBERSON: It was minor. There was some but, I do not recall the exact number. From recollection, if the filter pressure drop started at 1.0 in. w., it was 1.1 in. w. at the conclusion.

GOLDEN: Regarding Jack Hayes' question on the aging of charcoal and how that was affected, I want to refer to a paper presented at the last air cleaning conference. The same conclusion was reached.

GHOSH: We did not check into the aging effects of the carbon in the test you are referring to. We used new carbon. We had test canisters and kept pulling the test canisters out. We did a combination of different tests and we tried to use the same type of carbon. The aging effect has not been addressed.

ROBERSON: At a practical level, we have been through one outage while constructing prestaging of structural steel with a lot of welding. We have done the required monthly sampling and continue to see good performance by the containment purge systems with five to seven year old carbon.

BARROW: In both units, we have reloaded carbon on "A" train but the Bravo train of each unit is approximately eight years old. Neither train has shown any degradation by carbon testing.

GHOSH: We use a test to validate that the building fumes had no effect on carbon. We have had two or three tests since we gave our paper and we did not show any degradation of the carbon. That confirms your results. In response to one of the questions somebody asked during my test, we monitored the gases in the inlet and outlet and found that the welding fumes were passing through the bed.

PEST: On the basis of the tests that you have done on your containment purge systems, do they seem to be operating well? What test parameters on your radioiodine test are you referring to, the regulatory required (80°C/70 % RH, or the new D3803-1989?

ROBERSON: We do dual testing with all of our systems. D3803 is used for trending and predicting end-of-life.

CASS: How "clean" was the material that was used as the base for the welding? Burnished, sandblasted clean or oily, dirty, rusty, painted metal, as is usually found in operating plants? Could obscure fumes, i.e. burnt smoke, affect the carbon? Was this considered or evaluated?

ROBERSON: Over the full range of the electrode test series (60#), a variety of welding "base metal" was used, some was painted, some rusty, and (for the stainless steel) some clean. Differences based on different base metal conditions was not specifically identified as a variable, but (by sheer coincidence), a range of base metal conditions was used. Specific documentation (or reconstruction) cannot be provided concerning which 5# increment of electrode consumption used which base metal.

BASIS FOR AND PRACTICAL METHODS OF CONTROLLING PAINTING ACTIVITIES AT THE SEQUOYAH NUCLEAR PLANT

Robert R. Campbell
Tennessee Valley Authority (TVA)
Chattanooga, Tennessee 37402-2801

Abstract

Sequoyah Nuclear Plant (SQN) follows the guidance presented in Regulatory Guide (R.G.) 1.52, "Design, Testing, and Maintenance Criteria for Atmospheric Cleanup System Air Filtration and Adsorption System Units of Light-Water-Cooled Nuclear Power Plants" in protecting its charcoal filter trains from the effects of painting and other chemical releases. SQN, as well as other nuclear facilities around the country, have the problem of how to address the issue of protection of Engineered Safety Feature (ESF) filter systems from degradation due to communication with airborne hydrocarbons (i.e., primarily paints and solvents). R.G. 1.52 (and a similar statement from R.G. 1.140) states in part, "Testing should be performed ... following painting, fire, or chemical release in any ventilation zone communicating with the system...," and requires that a test be performed upon any kind of painting or chemical release. This is considered overly restrictive if the activity is minor and in a location remote from the charcoal filters.

Charcoal filters used in air cleaning systems are required to filter out radioactive iodine from an airstream before its release from the plant to the environment. Charcoal filters will age with time because of their ability to adsorb many different types of material. This aging affects the charcoal by lowering its iodine retention efficiency, and therefore the charcoal needs to be protected from the effects of chemicals such as paint fumes.

An integrated approach was used to determine a basis for and methods of controlling painting (and other chemical releases) for the protection of charcoal filters. The areas investigated were:

1. Test charcoal efficiency after exposure to known contaminants
2. Charcoal and its ability to adsorb contaminants
3. Other utility experience
4. Potential contaminants in paint and their release rates
5. Air change rates
6. Procedural and administrative controls

The TVA SQN testing results supported previous industry papers addressing hydrocarbon effects on charcoal. The results indicated charcoal (TVA uses TEDA and KI impregnated charcoal) can meet its required efficiencies after some exposure to hydrocarbons. Industry information indicates that charcoal may start having lowered efficiencies with as little as 5 percent, by weight, in contaminants absorbed by the charcoal. SQN has chosen 0.5 percent as its administrative limit for charcoal contaminants. The administrative controls, implemented as a result of this effort, have been well received by the plant (craft, operations, management, and engineers) and have not exposed the filters to any excessive amounts contaminants.

Background

SQN follows the guidance presented in R.G. 1.52, "Design, Testing, and Maintenance Criteria for Atmospheric Cleanup System Air Filtration and Adsorption System Units of Light-Water-Cooled Nuclear Power Plants" in respect to the design, operation and maintenance of the installed air cleaning systems. Charcoal filters are an integral part of air cleaning systems and are used to filter radioactive iodine from an airstream before its release from the plant to the environment. Charcoal filters will age with time because of their ability to adsorb many different types of material. Additionally, contaminants such as paint fumes, cleaning solvent fumes, and sealing material offgases will damage and contaminate charcoal which lowers its iodine adsorption efficiency. This aging affects the charcoal by lowering its iodine retention efficiency, and therefore the charcoal needs to be protected from the effects of chemicals such as paint fumes. SQN, as well as other nuclear facilities around the country, have the problem of how to address the issue of protection of Engineered Safety Feature (ESF) air cleaning and non-ESF air cleaning filter systems from degradation due to the effects of painting and other chemical releases (i.e., primarily paints and solvents). One method of addressing this problem is to strictly control painting activities in areas of the plant where such activities could jeopardize the efficiency of charcoal filters installed in air cleaning filter systems.

The NRC recognizes this ability of charcoal filters to adsorb materials and requires testing be performed when filters are exposed to chemicals. NRC R.G. 1.52 (and a similar statement from R.G. 1.140) states in part, "Testing should be performed ... following painting, fire, or chemical release in any ventilation zone communicating with the system...," and requires that a test be performed upon any kind of painting or chemical release. A strict interpretation of this statement requires that a test be performed upon any kind of painting or chemical release. This is considered overly restrictive if the activity that could release chemical fumes (i.e., painting) is minor and in a location remote from the charcoal filters. Therefore, an engineering basis is required addressing the effects of painting activities on charcoal.

SQN has five installed filter systems that contain charcoal filters and hence the need for a process to control paints and other chemicals that may harm the installed charcoal filters. The following are descriptions of the systems affected at SQN:

The Auxiliary Building Gas Treatment System (ABGTS) is used to filter radioactive particulates and iodine from the exhaust airstream and maintain the Auxiliary Building at a negative pressure with respect to outdoors. It is an ESF filter system in standby and only operated occasionally for testing. It performs its function following a LOCA, a fuel handling accident, and an Auxiliary Building isolation. The purpose of maintaining a negative pressure is to prevent unfiltered outleakage. The capacity of the system is 9000 CFM/train.

The Emergency Gas Treatment System (EGTS) is used to filter radioactive particulates and iodine from the exhaust airstream and maintain the Reactor Building annulus at a negative pressure with respect to outdoors. It is an ESF filter system in standby and only operated occasionally for testing. It performs its function following a LOCA. The purpose of maintaining a negative pressure is to prevent unfiltered outleakage. The capacity of the system is 4000 CFM/train.

The Containment Purge (CP) System is used to filter radioactive particulates and iodine from the exhaust airstream before it is released to the atmosphere. It is a non-ESF filter system that is operated continuously during outages and occasionally during plant power operation. It is required during purging activities while at power and during refueling operations although no credit is taken for the filters in calculations of offsite doses. The capacity of the system is 14000 cfm/train.

The Control Building air cleaning system is used to filter out radioactive particulates and iodine from the outdoor pressurizing airstream before its entry into the main control room. It is an ESF filter system in standby and only operated occasionally for testing. It is required for any event in which radioactive particulates and/or iodine can be released (i.e., Fuel Handling Accident, LOCA, and waste gas decay tank rupture). The capacity of the system is 4000 CFM/train.

The Post Accident Sampling Facility (PASF) Ventilation System is used when the sampling facility is utilized or following an accident. It is a non-ESF filter system and is operated for testing and when the sampling facility is being used. The PASF filters radioactive particulates and/or iodine from the exhaust airstream. The capacity of the system is 2000 CFM/train.

Investigation

The investigation utilized an integrated approach to providing an engineering basis. The six areas investigated were:

1. Test charcoal efficiency after exposure to known contaminants
2. Charcoal and its ability to adsorb contaminants
3. Other utility experience
4. Potential contaminants in paint and their release rates
5. Air change rates
6. Procedural and administrative controls

The purpose of the six areas is:

1. To corroborate charcoal's documented efficiency performance following exposure to contaminants
2. To determine the upper limit of contaminants charcoal can adsorb and still fulfill its safety function
3. To determine if the nuclear industry has a common approach
4. To determine the amount of contaminants which will become airborne in paint used
5. To determine minimum time required to purge areas of contaminants before operating ESF filter systems
6. To determine if existing controls are adequate

Test Charcoal Efficiency

Spare charcoal, at the plant site, was intentionally exposed to known quantities of paint to corroborate charcoal's documented efficiency performance following exposure to contaminants. The test setup consisted of a leak-tight enclosure (for the painting and sealing activities), a filter housing capable of containing one Type II charcoal adsorber tray (containing charcoal impregnated with TEDA and KI), and a fan. The test setup was interconnected with flexible ducting and the fan was equipped with a damper to adjust airflow.

The materials chosen for the testing were the two types of paint most commonly used at the plant and the RTV most commonly used at the plant. Five tests were performed with paints and two tests were performed with RTV. This charcoal was then tested in accordance with technical specifications requirements to determine the charcoal efficiency. Testing was conducted in early 1989 in accordance with ASTM D 3803-1979. Test results are contained in Table 1.

The acceptance criteria for charcoals at SQN varies from 90 percent for CP to 99.875 percent for EGTS. The test results show that the charcoal still met all acceptance criteria. The most severe test was PNT-4 using a highly volatile paint. This released approximately 8.76 lb. of volatiles onto the charcoal. Using 55 lbs. of charcoal per tray, this is a percentage of (8.76/55) x (100)) = 15.93 percent. Thus, the testing supports previous literature published and the present limits of the TVA procedure (1/2 of 1 percent by weight).

Table 1 Testing Results

Test #	Material	Contaminants pounds	Charcoal pounds	Percent by Weight	Charcoal Efficiency percent
PNT 1	Low volatile paint	1.08	55	1.96	>99.9
PNT 2	Low volatile paint	2.16	55	3.93	>99.9
PNT 4	Highly volatile paint	8.76	55	15.93	>99.9
PNT 5	Low volatile paint	1.08	55	1.96	>99.9
Seal 1	RTV	0.01	55	0	>99.9
Seal 2	RTV	0.59	55	1.07	>99.9

Test PNT-3 was not performed.

The testing indicated that the charcoal met all acceptance criteria for iodine efficiency. The testing indicated that charcoal can still perform adequately after being exposed to fumes from painting and sealing activities.

Charcoal and Its ability to Adsorb Contaminants

Industry-issued papers were researched and used to determine the amount of material that a charcoal filter can adsorb and still meet its iodine efficiency requirements. Published information indicates that unimpregnated charcoal can handle approximately 6.8 percent to 11.5 percent of its weight, in contaminants, before it will fail its iodine retention test[9]. Other information indicates that charcoal will maintain its efficiency with contaminant loadings of 5 to 30 percent[6, 7]. The papers also indicated that water vapor in conjunction with the hydrocarbon contaminants degrades the charcoal at the highest rate[10]. It also indicated that charcoals impregnated with both TEDA and KI have the greatest resistance to the effects of water vapor and hydrocarbon contaminants[10]. SQN charcoal is purchased with both TEDA and KI. Thus, it follows that a conservative exposure level for known contaminants should be chosen at 5 percent or less by weight of the charcoal.

Other Utility Experience

Experience of utilities, other than TVA, was used in developing the direction and type of controls that are now in place at SQN. Engineers at other nuclear facilities around the country were contacted to determine how they address protecting ESF (and non-ESF) filters from contamination by hydrocarbons which are formed during painting[1,5,11]. It is interesting to note that in a 1989 survey 54 percent of the utilities contacted allowed some exposure of their charcoal filters to paint fumes before a test was required. A 1996 survey indicates that 75 per cent of utilities now allow some exposure (some as much as 2500 square feet)[14]. Industry practices to protect charcoal adsorbers from contamination include the use of painting permits and coordination of use of cleaning solvents and sealing materials with the testing and running of air cleaning systems. No plant contacted allowed any intentional exposure of charcoal filters to paint or other hydrocarbon fumes. Other methods of controlling painting activities included:

a. Painting in tents using a portable sacrificial charcoal bed. The sacrificial charcoal was in service until the paint had cured.
b. Run the normal ventilation system to remove paint fumes from the area prior to operation of a filter system.
c. Allow painting and if the system is operated then test the system within the Technical Specification time limits.

Potential Contaminants in Paint and Their Release Rates

There are many different materials used at a nuclear plant. Material data sheets, supplied by the paint (or chemical) manufacturer were used to determine the amount of material that can offgas from paints as the paint cures. This information can be used to determine the level of exposure of a charcoal filter to contaminants. The materials that were evaluated were the paints and sealants that were most commonly used. The Material Safety Data Sheets (MSDS) for the most common materials used were then obtained as the amount of volatiles are shown in the MSDS. The paints and sealants used range from a high of about 60 percent volatile (8.76 pounds of solvent per gallon of paint) to a low of about 4 percent volatile (approximately 0.54 pounds of solvent per gallon of paint). The paints evaluated have short cure times, however some paints require cure times of approximately 20 hours.

Air Change Rates

Air change rates are useful in determining the time required to remove paint fumes from an area prior to operating a filter system that serves the area. Air changes are easily calculated by using building volumes and ventilation air flow rates. Air change rates for the various elevations of the auxiliary building ranged from 1.9 air changes per hour (ACH) to 6.6 ACH. The air changes for the reactor building were considerably less; however the ACH for the reactor building is moot as all ventilation air must be exhausted through the containment purge air filters.

The ACH can then be used to determine the minimum time for ventilation system operation following completion of paint curing (or other activity that releases hydrocarbons) to remove fumes. ASTM E741 - 83 can be used to determine the time frame. This ASTM standard uses the following equation [eq 1] to determine dilution of a gas:

$$C = Co \exp(-It) \qquad (1)$$

where

C = fume concentration at time t
Co = fume concentration at time (t) = 0 percent
I = ACH, and
t = time, hrs.

Therefore to determine the time required to reduce the concentration of fumes (i.e., hydrocarbons) in the air by 95 percent, the following is calculated:

$$C = 1.0 - 0.95 = 0.05$$
$$Co = 1 \text{ or } 100\%$$
$$I = 1.9 \text{ ACH} \quad \text{chosen as the most conservative value}$$

solving for t renders

$$C = Co \exp(-It)$$
$$0.05 = 1.00 \exp(-1.9t)$$
$$1.58 \text{ hours} = t$$

For conservatism, the number is rounded to two hours and then a margin of two hours is added. This then results in a four hour run time for the ventilation system following completion of the activity.

Procedural and Administrative Controls

Procedures at the plant control activities by requiring permits for activities that can release airborne hydrocarbons into zones served by ESF (and non-ESF) air cleaning systems. Review of the earlier version of the TVA procedure, AI-29, "Aromatic and Ester Hydrocarbon Release Permit" indicated it was adequate for its intended function. The procedure prevented any activities whenever filter systems were operating or could potentially operate. This presented the plant with a multitude of scheduling and coordination problems for the smallest of activities. An example is the painting of a weld on a baseplate (approximate total area of one square foot). This activity would be required to be scheduled several weeks in advance and still may have been cancelled on the day it was scheduled. The permits are issued on a daily basis and require Operations notification prior to issuance. A 24-hour waiting period was required following any activity that released fumes prior to operating any filter system. Review of the permits indicated that the vast majority of permits issued were for areas approximately 10 square feet or less. The permit process did not allow for evaluations of the activity should a filter system be operated while a painting activity was ongoing. Other areas noted for improvement in the permit process were the need for:

a. Clearer identification of the areas where permits were required
b. Identification of areas outside the building that could have an effect on the filters (some filters took suction from the outside atmosphere)
c. Identification of the vent systems operated during any activity

Results

Testing of Charcoal

Testing performed at SQN corroborated industry information on charcoals and the effects of contaminants. The tested charcoal was able to meet required efficiencies after being exposed to as much as 15.9 percent of its weight in contaminants. The tests were not all inclusive but did coincide with previous papers published.

Charcoal and Its ability to Adsorb Contaminants

Previously it was noted that a conservative level of contaminants is 5 percent by weight of charcoal. Based on a 5 percent by weight ratio, the following systems would then have the capacities indicated. Note that there is approximately 55 pounds of charcoal per charcoal tray and three trays per 1000 CFM. Each value is based on one train of equipment.

For conservatism, a safety factor of 10, below the maximum permissible level of contaminants, is used to assure that the charcoal shall not be exposed to amounts of contaminants that can degrade its performance. This accounts for normal aging and spurious system starts that may increase exposures of charcoal to contaminants. Also, with the potential questions of obtaining accurate test results using ASTM D 3803-79, the additional conservatism will help ensure that charcoal will not be exposed to excessive amounts of contaminants. Therefore, the maximum amount of documented exposure to a charcoal filter, conservatively chosen, is 0.5 percent of the weight of the charcoal.

A sample calculation to determine the amount of contaminants permitted on the PASF is:

Procedural Limits, lbs = (2000 cfm) (3 charcoal trays/1000 cfm) (55 lbs charcoal/tray) (.05) (1/10)
= 1.65 lbs

Results are contained in Table 2.

Table 2 Exposure Limits for Charcoal

System	Airflow CFM	Charcoal weight pounds	Maximum Amount of Contaminants pounds	Procedural Limits pounds
ABGTS	9000	1485	74	7.4
EGTS*	4000	660	33	3.3
CP	14000	2310	115	11.5
Cont. Purge	4000	660	33	3.3
PASF	2000	330	16	1.6

*Has two banks of charcoal. Calculation is based on one bank.

Other Utility Experience

The nuclear industry does have a consistent approach in that it does protect ESF charcoal filters in air cleaning systems. However, the degree of protection varies with the utility as seen by the fact that utilities will allow exposure of filters to fumes (some areas as much as 2500 square feet). Incorporated into the procedure is an allowance of up to 10 square feet of area which can be painted (or equivalent area for solvents or other chemicals) without the need for a permit. This is a consistent approach with other utilities in that a small amount of exposure (fumes equivalent to 10 square feet of painted surface area) does not automatically require an efficiency test be performed. Determination of this value (10 square feet) was based on an evaluation of the square foot areas designated on permits issued prior to this allowance. Another feature incorporated into the procedure is use of a tent with a sacrificial bed of charcoal. Painting or other activities are performed inside the tent. Air is exhausted from the tent and passed through the sacrificial charcoal filter to remove contaminants.

Potential Contaminants in Paint and Their Release Rates

It has been previously stated that 20 hours is required to cure paints. Many of the paints used cure in a time frame less than the 20 hours. Solvents evaporate immediately (i.e., in a few minutes) and would be removed from the area by the ventilation system. With the weight of solvents known, conservatively assuming that all solvents are released from the paints, and knowing the coverage area of the paints Table 3, "Permissible Level of Contaminants" is developed. The table shows the relationship between the maximum allowable contaminants and surface area for paints and sealants and the volume for solvents. The paint weights are based on weight of volatiles offgased from paints. Sealants are taken to be the same as low volatile paints.

TABLE 3 Permissible Level of Contaminants

System	Maximum Amount of Contaminants pounds	Maximum Area for Painting Highly volatile Paints, FT2 Note 1	Maximum Area for Painting Low Volatile Paints, ft2 Note 2	Maximum amount of solvent gallons Note 3
ABGTS	7.4	125	685	0.9
EGTS	3.3	55	300	0.4
CP	11.5	200	1050	1.4
Cont. Bldg	3.3	55	300	0.4
PASF	1.6	28	150	0.2

Note 1. Area = (lb. contaminants/8.76 lb/gal) (150 ft2/gal)
Note 2. Area = (lb. contaminants/0.54 lb/gal) (50 ft2/gal)
Note 3. Volume = (lb. contaminants/8 lb/gal)

Air Change Rates

The minimum time to run the Auxiliary Building ventilation is 24 hours. The 24 hours is based on 20 hours for the majority of hydrocarbons to offgas (95 percent) and 4 hours to purge the building. The minimum time to run the ventilation system for solvents is 4 hours after use of the solvent has been discontinued; however for simplicity, the air cleaning systems are not run for 24 hours following any activity. If the system is operated, an evaluation of the effects of the activity is required.

Procedural and Administrative Controls

The improvements in the administrative controls implemented in the work control process are:

a. allowing up to 10 square feet of surface to be painted, cleaned, or weld inspected without the use of a permit
b clearly identifying areas that require permits for the protection of filters
c. requiring an evaluation of the effects of the activity should a filter system be operated during the performance of that activity
d. requiring that an exposure log be kept to record the cumulative amount of exposure for each system
e. defined the use of tents for controlling activities that may release hydrocarbons
f. establishing limits for exposure of the filters
g. integrating Operators in the permit process

Filters are never intentionally exposed to hydrocarbon fumes. Activities are scheduled to operate systems at times when painting or other hydrocarbon releasing activities have ceased. For exposures above the acceptable levels, the unit (charcoal) will be tested, and any further exposure will be prevented or require additional charcoal tests. Prior to making the procedural changes, SQN was issuing approximately 900 permits a year. The number of permits issued per year has dropped to less than 100. An exception to never intentionally exposing filters to contaminants is the Containment Purge system. This system operates during refueling outages to ventilate containment. There is no practical way to protect the filters, and as a result, charcoal tests are scheduled following the outage. The current permit in use at SQN is contained in Attachment 1.

Conclusions

The TVA Sequoyah testing results supported previous industry papers addressing hydrocarbon effects on charcoal. The results indicated charcoal can meet its required efficiencies after exposure to hydrocarbons. Industry information indicates that charcoal may start having lowered efficiencies with as little as 5 percent, by weight, in contaminants absorbed by the charcoal. SQN has chosen 0.5 percent as its administrative limit for charcoal contaminants. The administrative controls, implemented as a result of this effort, have been well received by the plant (craft, operations, management, and engineers) and has not allowed any excessive exposures of contaminants with the filters.

References

1. Sequoyah Nuclear Plant Condition Adverse to Quality Report, CAQR SOP890064, Revision 0.

2. Administrative Instruction AI-29, "Aromatic and Ester Hydrocarbon Release Permit" (replaced by Site Standard Practice SSP-7.4, "Work Permits")

3. Regulatory Guide 1.52, "Design, Testing, and Maintenance Criteria for Atmospheric Cleanup System Air Filtration and Adsorption System Units of Light-Water-Cooled Nuclear Power Plants"

4. Regulatory Guide 1.140, "Design, Maintenance, and Testing Criteria for Normal Exhaust System Air Filtration and Adsorption Units of Light-Water-Cooled Nuclear Power Plants"

5. "Diablo Canyon Power Plant Guidelines for Protection of Carbon Filters" by Ginter, W., paper submitted at the 19th DOE/NRC Nuclear Air Cleaning Conference.

6. "Manufacture, Structure, Properties, and Application in the Nuclear Industry A Presentation for ASTM-D33," April 1986, Aimsworth, D., Sutcliffe Speakman, Inc. Carbon has a capacity of 5 percent-30 percent weight before being exhausted (and therefore failing its test).

7. "Evaluation and Control of Poisoning of Impregnated Carbons Used for Organic Iodide Removal" by Kovach, J. L., and Rankovic, L., paper submitted at the 15th DOE Nuclear Air Cleaning Conference. One case of failed charcoal due to 5 percent by weight of organics present. Testing indicated charcoal can hold up to 260 mg/g (26 percent) organics and still pass testing.

8. Sequoyah Nuclear Plant Site Standard Practice (SSP) 7.4, "Work Permits"

9. KFK 2449 "Iodine Filters in Nuclear Power Stations," Wilhelm, J. G., April 1977. This report indicated that iodine efficiencies were lowered drastically with solvent loadings varying from 6.8 percent to 11.5 percent. The paper noted that impregnated charcoal maintains higher efficiencies when exposed to solvent vapors than does unimpregnated charcoal.

10. "Charcoal Performance Under Accident Conditions in Light-Water Reactors," NUREG/CR-3990 (NRL Memo Rpt 5528), March 1985. This report indicates that charcoal impregnated with TEDA and KI exhibit less penetration than other charcoals. This report also indicates the adverse synergistic effect of high moisture and hydrocarbon contaminants degrading the charcoal when exposed at the same time.

11. David Besse, Procedure ISG-15, Rev. 1. Procedure allows 50 ft2 exposure. There must be three air changes before system runs.

12. ASTM E 741-83 "Standard Test Method for Determining Air Leakage Rate By Tracer Dilution"

13. Sequoyah Nuclear Plant Technical Specifications, T.S. 3.6.1.8, EGTS; 3.7.7, CREVS; 3.7.8 and 3.9.12, ABGTS

14. LIS Survey Regarding Charcoal Filters (#96077), June 10, 1996

Attachment 1

SQN	WORK PERMITS	SSP-7.4 Rev 6 Page 18 of 25

APPENDIX C
Page 1 of 7

PAINTING, CLEANING, SEALING, AND OTHER VOLATILE HYDROCARBON USE PERMIT [C.3]

**Permit Number #_____

**ISSUED BY_____/_____/_____ **Vent. System Affected_____
Tech Support Date Time

NOTE: This permit is valid only for the date and location shown. The original permit is to remain with the work package. A copy of every permit is to be sent to Tech Support for exposure log entries after SOS signoff.

UNIT WORK LOCATION (BUILDING) (ELEVATION)

____ _____

Brief Description of Work:_____

Material:_____

***This permit starts:_____

***This permit expires:_____

*Volume of solvent used or area painted. Estimated_____ Actual_____

- ☐ Solvent
- ☐ Sealant
- ☐ Paint

Affected ventilation system operated during time this permit was in effect.

☐ YES ☐ NO

If system operated, evaluation by System Engineer; otherwise, N/A.

_____/_____ _____/_____ Evaluation Attached ☐
SOS or Designee Date System Engineer Date

NOTE: Touch up painting (less than 10 square feet) or weld inspections do not require a permit.

YES	NO	CERTIFICATION
____	____	All material which may constitute a fire hazard has been removed from the area or adequately protected. Transient fire loads have been evaluated by Fire Operations and specified controls initiated per SSP-12.15, Appendix E. All firefighting equipment is available as required by the program for control of ignition sources and I have instructed my men on how a fire is to be reported.
____	____	As the Foreman (supervisor), I recognize that work areas will require reinspection for fumes which may constitute a hazard and I will personally reinspect the area at least once during the shift for which this permit is valid.

_____ _____
Responsible Foreman or Supervisor (Signed & Printed) Date

NOTE ONLY one permit is needed if using a tent. No exposure is assumed to occur to charcoal filters if a tent is used. The use of a tent still requires a permit.

* Not required if enclosures and portable charcoal filters are used.
** Completed by Tech Support. (See Table C-1)
*** The permit will be valid for one job at one location. It shall be valid for one day, three working shifts. Permits can be obtained up to three days in advance. (Exception see note)
Posting Requirements: Retain with work document during and following work.

DISCUSSION

BARROW: Did you perform a D3803-89 test?

CAMPBELL: The test conditions are 80°C and 70% RH. 70% RH is used as we have humidity control. This is in accordance with the plant technical specifications.

GOLDEN: Prior to implementing this program did you have any failures of your charcoal system test that were directly attributed to painting?

CAMPBELL: No, we did not, but our management is conservative in some of their evaluations. We have had some events from exposure to welding fumes and we have had some small electrical equipment catch fire while running the systems. In each case, we would pull a sample. We would change out the charcoal but we would pull a sample on the charcoal that we were changing out and each time the charcoal that we discarded still passed our Tech. Spec. Test. So, we have not had any failures. The only reasons that we have replaced charcoal in the past eight years, that I know of, is because of permanent sets in the gaskets that prevent us from replacing the tray after we pull the charcoal sample. We cannot pass our bypass leakage test then we change out all the charcoal in the system to maintain the same lot number in the entire system.

ROBERSON: Does the "less than 10" non-permit criterion mean that these fume exposures are not cumulatively tracked?

CAMPBELL: One of the reasons that we chose 10 ft^2 is because of the 0.5% by weight that we allow on our filter systems. Because we are not controlling below 10 ft^2, there can be exposures that occur without knowing it. So we chose an order of magnitude below what has previously been published regarding charcoal failure to allow us a margin so that we will not have to worry whether or not we should test our charcoal. Also, we have looked at the run times when this has happened and we have an ability to call up run times on all our filter systems on our plant computer. If systems have run spuriously, it will be only for 15-30 min., rarely longer than an hour. That does not always happened with containment isolation so there are factors that go into whether or not the systems are exposed. In addition to choosing 10 ft^2 we looked at number of square feet that were allowed on previous permits and the vast majority were for 3 - 4 ft^2. We also talked to our maintenance department and our chemistry people. The result was that we chose 10 ft^2 as a reasonable value. It has been very well received.

ROBERSON: Does the paint accumulation log only update based on the system being in service?

CAMPBELL: Yes. The systems have isolation dampers and exposure can only occur when the system is running.

HARRIS: We have a painting program in which we track the volatile organic content of each of the coatings and adhesives on the filter beds. We have noticed that even when relying on only 10 ft^2 to be painted, very few coatings come out without a one gallon kit, or a five gallon kit. If that paint is still in the ventilation zone, do you still assume that the volatiles are coming out and tracking it on your charcoal loading as well?

CAMPBELL: This is a good question. What we have implemented at in our Sequoia plants is a chemical control. Again, our Rad Con people will not allow anyone to take anything into the RCA's unless they are going to use that material. So we have controls over what is taken in. If they say they intend to paint a hundred square feet but when they give the permits back to us they report only painted ten square feet, the instructions given to our maintenance people is to show the total volume of paint they took in. We then consider making an adjustment, but as a rule, we do not. What you take in you use up because what is left is rad waste. There is no way you can really prove that it is not.

GOLDEN: You said you did your testing to the 1979 or 1980 standard. I assume, because that is what your Tech Specs called for, the 80°C test. Did you also do any parallel testing to the 1989 standard or anything more stringent like a 30°C test?

CAMPBELL: No. The testing we did was several years ago, and the ASTM 89 version was not available at that time. I was aware of the controversy around 1979 and that is another reason why we chose an order of magnitude less than what the lowest recorded values were. At every step along the way we tried to be conservative in what we were doing but maintain some flexibility. We did not have any flexibility to begin with, but we wanted something reasonable that we would not have to come back and change again in three or four years. Knowing the controversies, we tried to stay very conservative on what we are doing.

CASS: Did you considered different methods of application, roller, brush, or spray? Did you take in preparation; sandblasting, grinding, what have you?

CAMPBELL: No, we did not look at different application methods. As far as grinding or chipping away the paint, that is dust and we did not consider it.

GHOSH: Did you consider the drying time of the solvent? The solvent time varies exponentially, between two and four hours during which time most of the solvent may be reduced from 100 to 50%. In four hours it may go to 10 or 5%. Using that method, did you check how much loading is taken back from the carbons?

CAMPBELL: No, we did not check into that . The way we are looking at it is that the paints will cure exponentially. Most of the offgases will occur during the first hour and then it will decrease. We look at the run times at the end of the painting activity and we assume the paint is totally cured according to what the vendors tell us on the paint. At that point, everything that is going to offgas should have offgassed. We assume 100% for the purpose of calculating run time. We say 100% is still in the area and we run four more hours. In reality, the stuff is going to be removed continuously, it is going to be less and less over a period of time and probably at the time the paint cures there is probably very, very little fume in the area.

GHOSH: Yes, 24 hours is very safe.

CAMPBELL: Definitely. It is an easy value to remember.

GHOSH: One more thing, you use 10 square feet. Did you equate it in terms of limiting the amount in terms of gallons? That is what we did.

CAMPBELL: Yes we have, but that is not covered in the paper. We did equate it when we were talking to our maintenance people. We asked what do you want, and they said square feet. We looked at high and low volatile paints (we considered sealants the same as low volatile paints) and we agreed that 10 square feet was acceptable based on the paints we use at the plant.

GHOSH: It varies with how much thickness, how many mills.

CAMPBELL: It depends on the thickness. It doesn't show in the paper, but a low volatile paint that we use is a Keylor and Long 4500 paint, for example, that will cover 64 square feet per gallon, we say it will cover 50 square feet rather than the recommended 64 square feet and we base our calculations on that number.

SESSION 10

IODINE TREATMENT: CHEMICAL OPERATIONS AND REACTOR ACCIDENT SCENARIOS

Wednesday July 17, 1996
Co-Chairmen: R.T. Jubin
T. Fukasawa

BEHAVIOR OF IODINE IN THE DISSOLUTION OF SPENT NUCLEAR FUELS
T. Sakurai, K. Komatsu, and A. Takahashi

INFLUENCES OF IMPURITIES ON IODINE REMOVAL EFFICIENCY OF SILVER ALUMINA ADSORBENT
T. Fukasawa, K. Funabashi, and Y. Kondo

DIFFUSIONAL ANALYSIS OF THE ADSORPTION OF METHYL IODIDE ON SILVER EXCHANGED MORDENITE
R.T. Jubin and R.M. Counce

REMOVAL EFFICIENCY OF SILVER IMPREGNATED FILTER MATERIALS AND PERFORMANCE OF IODINE FILTERS IN THE OFF-GASES OF THE KARLSRUHE REPROCESSING PLANT WAK
F.J. Herrmann, B. Herrmann, V. Hoeflich, Ch. Beyer, and J. Furrer

CONTROL OF RADIO-IODINE AT THE GERMAN REPROCESSING PLANT WAK DURING OPERATION AND AFTER SHUT DOWN
F.J. Herrmann, B. Herrmann, K.D. Kuhn, A. van Schoor, M. Weishaupt, J. Furrer, and W. Knoch

OPENING COMMENTS OF SESSION CHAIRMAN

We have an important subject to discuss. This is a series of presentations on the treatment of iodine for the nuclear industry. It has been one of the mainstays of Air Cleaning Conferences in the past. A great deal of work has been reported in this area and we have five important papers that will contribute to the overall collection of literature on this subject.

BEHAVIOR OF IODINE IN THE DISSOLUTION OF SPENT NUCLEAR FUELS

by

Tsutomu Sakurai, Kazunori Komatsu, and Akira Takahashi
Physical Chemistry Laboratory
Japan Atomic Energy Research Institute
Tokai-mura, Ibaraki-ken, 319-11, Japan

Abstract

The results of laboratory-scale experiments concerning the behavior of iodine in the dissolution of spent nuclear fuels, which were carried out at the Japan Atomic Energy Research Institute, are summarized. Based on previous and new experimental results, the difference in quantity of residual iodine in the fuel solution between laboratory-scale experiments and reprocessing plants is discussed. Iodine in spent fuels is converted to the following four states: (1) oxidation into I_2 by nitric acid, (2) oxidation into I_2 by nitrous acid generated in the dissolution, (3) formation of a colloid of insoluble iodides such as AgI and PdI_2, and (4) deposition on insoluble residue. Nitrous acid controls the amount of colloid formed. As a result, up to 10% of iodine in spent fuels is retained in the fuel solution, up to 3% is deposited on insoluble residue, and the balance volatilizes to the off-gas. Contrary to earlier belief, when the dissolution is carried out in 3 to 4 *M* HNO_3 at 100°C, the main iodine species in a fuel solution is a colloid, not iodate. Immediately after its formation, the colloid is unstable and decomposes partially in the hot nitric acid solution through the following reaction:

$$AgI(s) + 2HNO_3(aq) = \tfrac{1}{2}I_2(aq) + AgNO_3(aq) + NO_2(g) + H_2O(l).$$

For high concentrations of gaseous iodine, $I_2(g)$, and NO_2, this reaction is reversed towards formation of the colloid (AgI). Since these concentrations are high near the liquid surface of a plant-scale dissolver, there is a possibility that the colloid is formed there through this reversal. Simulations performed in laboratory-scale experiments demonstrated this reversal. This phenomenon can be one reason the quantity of residual iodine in spent fuels is higher in reprocessing plants than in laboratory-scale experiments.

I. Introduction

Long-lived ($T_{1/2}$ = 1.57 × 10^7 y) and hazardous, radioiodine, ^{129}I, generated in the dissolution of spent nuclear fuels should be strictly controlled in reprocessing facilities. For gaseous iodine, various kinds of silver-impregnated adsorbents have been developed to very efficiently remove it from the off-gas. Therefore, it is desirable for environmental safety that all possible iodine be expelled from fuel solutions to the dissolver off-gas (DOG) where it will be fixed on an adsorbent such as silver-impregnated silica gel (AgS). The remaining iodine, that not expelled to the DOG, migrates into the Purex process which allows its escape to the environment. Therefore, understanding the chemical species and amounts of iodine in fuel solutions as well as developing a way of expelling it therefrom are important. Extensive work has been performed by many researchers.[1]-[3]

Before our research, the main iodine species in fuel solutions was postulated to be iodate (IO_3^-) from the chemical reaction of iodine in

hot nitric acid solution or uranium-nitric acid solution or both. Sparging with NOx has been recommended for iodate removal from these solutions. More than 99% of input iodine was expelled to the DOG in both laboratory- and plant-scale experiments.[1),(2),(4)] According to the reports from an actual reprocessing plant, however, considerable amounts of iodine (up to 5%) remained in spent-fuel solutions and migrated to the Purex process.[5),(6)] Although the causes were not clarified, this finding suggests the presence of other iodine species in spent-fuel solutions and/or the presence of some factors that influence the behavior of iodine between laboratory-scale experiments and actual reprocessing plants.

Japan has been constructing a commercial reprocessing plant having a throughput of 800 t/d. Since the release of ^{129}I into the environment is strictly regulated, we began to restudy the iodine species in spent-fuel solutions and the methods of expelling this iodine to the DOG. In beginning this study, we labeled other fission products (FPs) in spent-fuel solutions. The interactions of iodine with other FPs were examined for the first time with simulated spent-fuel solutions. These interactions had not been questioned by earlier researchers. It was found that colloids of such insoluble iodides as silver iodide (AgI) and palladium iodide (PdI_2) played an important role in the behavior of iodine in the dissolution stage.

This paper first summarizes the results of our laboratory-scale experiments. The difference in behavior of iodine in the dissolution stage between laboratory-scale experiments and the dissolution process that occurs in reprocessing plants is then discussed.

II. Main Iodine Species in Spent-Fuel Solutions

2.1 Preliminary Study with a Simulated Spent-Fuel Solution

To obtain preliminary information about iodine species in spent-fuel solutions, experiments were performed using a uranyl nitrate-nitric acid solution and a simulated spent-fuel solution that contained uranium and simulated FPs equivalent in composition to a solution of spent fuel with a burnup of 40 GWd/t. Varying amounts of potassium iodide labeled with ^{131}I were added to these solutions (30 to 50 mℓ) at 100°C and the iodine species produced were analyzed using the carbon tetrachloride extraction method. This analysis determined the quantities of dissolved iodine ($I_2(aq)$), I^-, IO_3^-, and organic iodine using an analytical scheme and considered the remaining species in the aqueous phase as non-ionic submicroparticles.[7)] The following results were obtained concerning the main iodine species in the solutions.[8),(9)]

(1) The main iodine species in the simulated spent-fuel solution was submicroparticles, while iodate was the main species in uranium-nitric acid solution.

(2) The quantity of iodine in the submicroparticles increased with increasing concentrations of Ag^+ and Pd^{2+}. When heated in 3 to 4 *M* HNO_3, the submicroparticles released molecular iodine (I_2).

(3) When the simulated spent-fuel solution containing the submicroparticles was subjected to ultracentrifugation of 65,000 rpm, a decrease of ^{131}I radioactivity was observed in the upper portion of the solution.

(4) A thermochemical calculation indicated that iodate cannot be the main iodine species because it is reduced to I_2 by NOx produced in dissolution of fuels.[9)]

From these results, it was concluded that the submicroparticles, the main iodine species, were colloids of AgI and PdI_2. The measured solubilities of these iodides also supports this conclusion.[10]

The colloidal iodine is unstable in hot nitric acid solution immediately after its formation so it decomposes into molecular iodine:

$$AgI(s) + 2H^+ + NO_3^- = \tfrac{1}{2}I_2(aq) + Ag^+ + NO_2(g) + H_2O(l), \quad (1)$$

$$PdI_2(s) + 4H^+ + 2NO_3^- = I_2(aq) + Pd^{2+} + 2NO_2(g) + 2H_2O(l). \quad (2)$$

Concurrently with this process, however, the remaining colloidal iodine ages and changes to stable species. For decomposition of the stabilized colloidal iodine, it was found that the addition of an excess amount of iodate (e.g., HIO_3) was effective:

$$5AgI(s)+HIO_3(aq)+5HNO_3(aq) = 3I_2(aq)+5AgNO_3(aq)+3H_2O(l), \quad (3)$$

$$5PdI_2(s)+2HIO_3(aq)+10HNO_3(aq) = 6I_2(aq)+5PdNO_3(aq)+6H_2O(l). \quad (4)$$

These reactions are illustrated in Fig. 1 and essentially refer to the following reaction:

$$5I^-(^{129}I^-) + IO_3^- + 6H^+ = 3I_2(I_2^*) + 3H_2O, \quad (5)$$

where the asterisk denotes radioactive iodine, ^{129}I. Based on these results, the following two-step process for expulsion of the iodine remaining in spent-fuel solutions was proposed.[10],[11]

Step One - Heat the fuel solution without supplying NOx to decompose the colloidal iodine. When aging of colloidal iodine has proceeded after dissolution, an excess amount of iodate should be added.

Step Two - Sparge (bubble) NOx through the solution while heating to reduce the iodate($^{129}IO_3^-$) to form volatile I_2. This process is necessary because there is a possibility of formation of the iodate during Step One.

The same process was proposed by Boukis and Henrich for decomposition of non-volatile organic iodides that originated from organic impurities in nitric acid.[12]
In our experiments, however, the amounts of organic impurities were negligibly small.

2.2 Demonstration of the Main Iodine Species Using Actual Spent-Fuel Solutions

Expulsion of iodine from solutions of spent PWR-fuel with burnups of 21 to 39 GWd/t was performed to identify the main iodine species in actual spent-fuel solutions. Two procedures were used and their efficiencies were compared.[8],[9] One procedure was conventional NOx sparging to reduce iodate to volatile iodine (I_2) through the following reaction:

$$2IO_3^- + 10NO_2 + 2H^+ + 4H_2O = 10HNO_3 + I_2. \quad (6)$$

The other procedure was as described above, viz., the addition of iodate to decompose colloidal iodine through Reactions (3) and (4). This process was also applied to the solution subjected to the NOx sparging to determine the amount of iodine remaining after NOx sparging.

The results showed that, while 27.4 to 45.7% of the initial iodine quantity in the solutions remained after NOx sparging, the iodine was completely removed by the process of adding iodate. This clearly indicates that the main iodine species in actual spent-fuel solutions is colloidal iodine, not iodate.

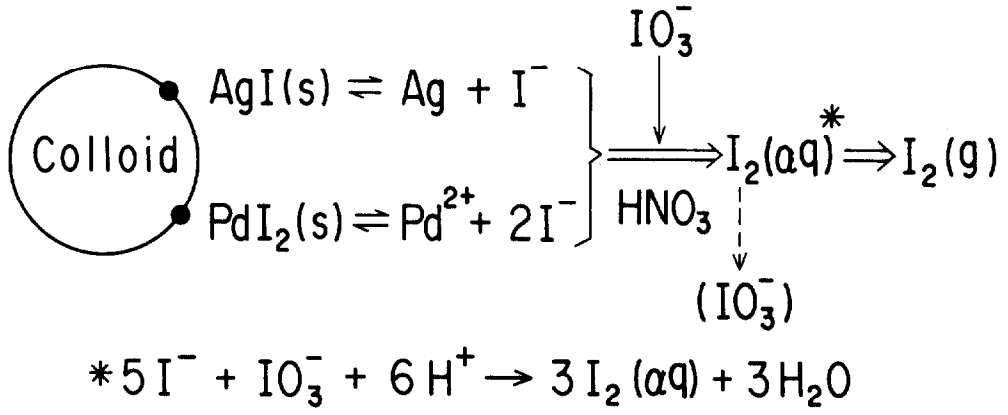

Figure 1 Mechanism for decomposition of colloids of AgI and PdI_2 by addition of iodate

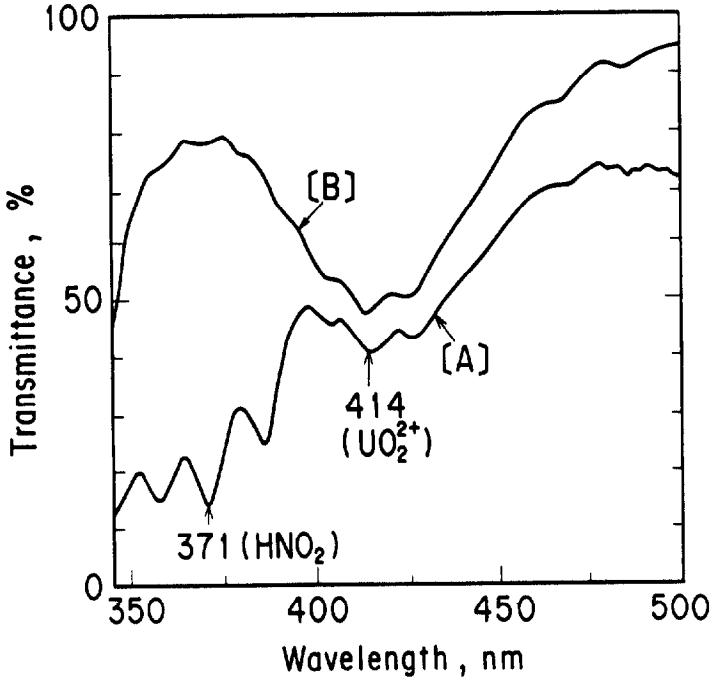

Figure 2 Influence of the dissolution rate of UO_2 on the concentration of HNO_2 produced during UO_2 dissolution in 3.5 *M* HNO_3 at 100°C
Production of HNO_2 was observed spectrophotometrically. Dissolution rate was [A] about 2 min for 0.909 g UO_2 powder and [B] 2.5 h for a 0.9321 g UO_2 pellet.

III. Distribution of Iodine in Spent-Fuel Dissolution

In the dissolution of spent fuels in laboratory-scale experiments, radioiodine in spent fuels (assumed as CsI) was distributed among the off-gas, fuel solution, and insoluble residue as follows.[11]

3.1 Volatilization into DOG

The majority of the iodine (90% or more) was expelled to the off-gas through its oxidation by HNO_3 and by the nitrous acid (HNO_2) produced in the dissolution (Figure 2):

$$I^- + 2H^+ + NO_3^- = \tfrac{1}{2}I_2(aq) + NO_2(g) + H_2O(l), \quad (7)$$

$$I^- + 4H^+ + NO_2^- + 2NO_3^- = \tfrac{1}{2}I_2(aq) + 3NO_2(g) + 2H_2O(l). \quad (8)$$

The dissolved iodine, $I_2(aq)$, then volatilizes and is expelled to the off-gas, leaving a small fraction as iodate in solution:

$$I_2(aq) = I_2(g), \quad (9)$$

$$I_2(aq) + 8H^+ + 10NO_3^- = 2IO_3^- + 10NO_2(g) + 4H_2O(l). \quad (10)$$

Since the iodate is reduced to I_2 by the NOx and HNO_2 produced in fuel dissolution, only small quantities of iodate can be produced in fuel dissolution occurring in 3 to 4 *M* HNO_3.

Of the iodine volatilized to the off-gas, 7% or less consisted of organic iodides, which were probably produced through the reactions of I^- or I_2 or both with organic impurities in the fuel solutions.[9]

3.2 Retention of Iodine Species in Spent-Fuel Solutions

Besides I_2 and a small amount of IO_3^-, colloidal iodine is produced in spent-fuel dissolution by the following reaction:

$$3I^- + Ag^+ + Pd^{2+} = AgI(s) + PdI_2(s). \quad (11)$$

Since this reaction competes with Reaction (8), the amount of colloids produced decreased for high dissolution rates, even with high burnup fuels.[11] This occurs because high dissolution rates result in high concentrations of NOx and HNO_2. On the other hand, when the concentrations of NOx and HNO_2 are too high, secondary formation of colloidal iodine may result. In high concentrations, NOx and HNO_2 react with the iodine produced in Reactions (7) and (8) reversing Reaction (1) and forming AgI. Details are discussed below.

In experiments with simulated spent-fuel solutions, the iodine species in the solutions consisted of 60% colloidal iodine, 20% I_2, and 20% iodate.

3.3 Deposition onto Insoluble Residue or to a Precipitate or both

Part of the iodine in spent fuels is transferred to insoluble residue or to a precipitate or both via. formation of colloidal iodine. Of the iodine in spent PWR-fuels, 3% or less was deposited onto insoluble residue.[10]

In dissolution of simulated spent-fuel pellets, an increase in UO_2^{2+} concentration in the solution beyond 170 g U/ℓ resulted in the precipitation of large quantities of metal molybdates on which iodine was deposited.[13] The causes have not yet been clarified.

The behavior of iodine in the present laboratory-scale dissolution at JAERI (the Japan Atomic Energy Research Institute) with the results earlier researchers have reported is summarized in Fig. 3. The differences noted are partially attributed to differences in the concentration of nitric acid used.

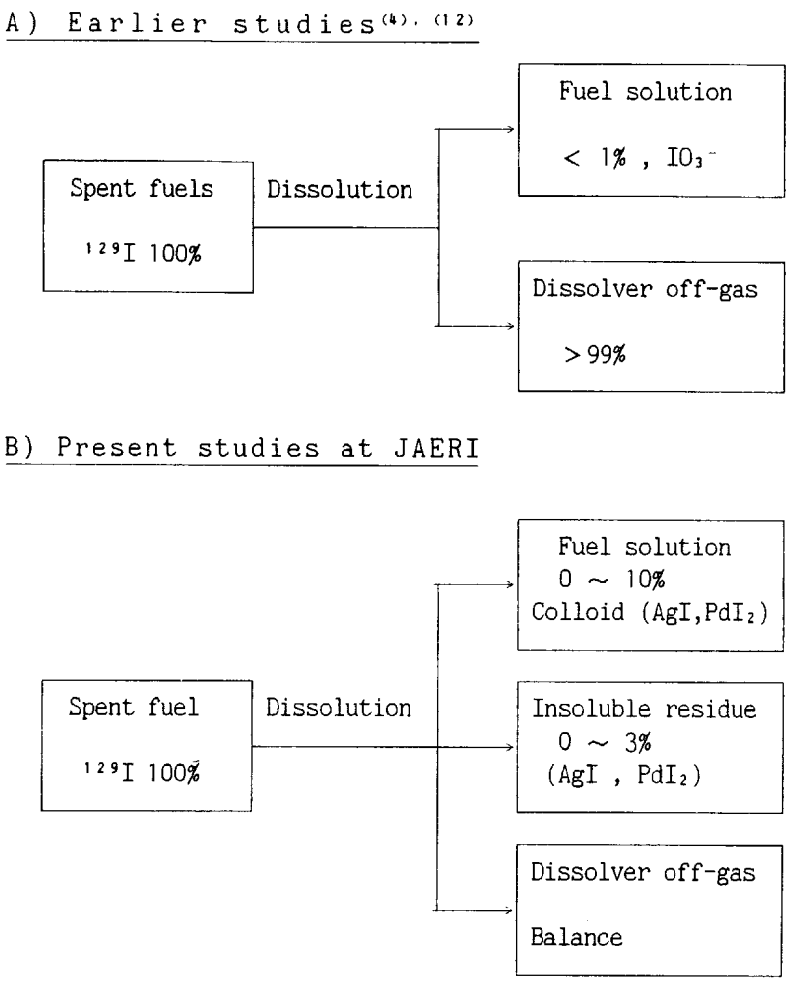

Figure 3 Distribution of iodine (^{129}I) from dissolution of spent fuels in laboratory-scale experiments

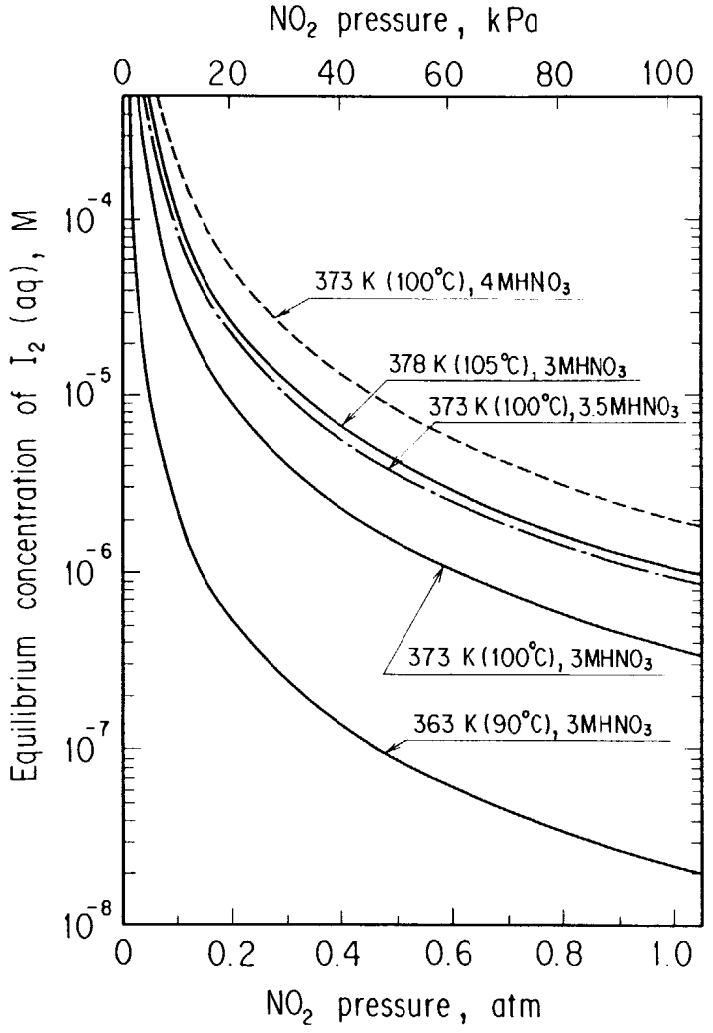

Figure 4 Relationship between dissolved iodine, $I_2(aq)$, and NO_2 in the chemical equilibrium, $AgI(s) + 2H^+ + NO_3^- = \frac{1}{2}I_2(aq) + Ag^+ + NO_2(g) + H_2O(l)$
Concentration of Ag^+ was assumed to be 2.37×10^{-4} *M* for a spent-fuel solution with a burnup of 40 GWd/t.

Table 1 Comparison of the amount of iodine in spent-fuel solutions

Scale	Literature	Burnup of fuel, GWd/t	Wt. of fuel dissolved	^{129}I in the fuel solution, %	Conditions of the dissolution
Laboratory	N.Boukis and E.Henrich (1991) [12]	45	80 g	0.7	7.5 M HNO_3 (0.22 ℓ), 97℃, 2h
	A.Leudet et al., (1983) [6]	32	Half of a fuel pin	< 1	Boiling
Plant	F.J.Herrmann et al., (1993) [5]		15 ~20t/y (WAK plant)	≦ 5	

Table 2 Calculation for secondary formation of colloid(AgI) at the liquid surface of an assumed plant-scale dissolver

Conditions of the dissolver: Size, 5 × 0.3 × 2 m;
Liquid surface, 1.5 × 10^4 cm^2 ; 3.5 M HNO_3 3 m^3(100℃);
Bottom air supply, 40 Nm^3/h;
Throughput of spent fuels, 5 t/d (burnup 40 GWd/t).

Concentrations at the liquid surface	Chemical equilibrium concerned	Equilibrium concentration of I_2(aq)	
I_2(g) 88 ppm	I_2(g) = I_2(aq)	2.3 × 10^{-5}M …(a)	Since (a) > (b), AgI will be formed.
NO_2 36%	AgI(S)+2 HNO_3(aq) = 1/2 I_2(aq) + $AgNO_3$(aq) + NO_2(g) + H_2O(l)	7.2 × 10^{-6}M …(b)	

IV. Iodine Behavior Differences between Laboratory-Scale Experiments and Reprocessing Plants

Table 1 cites an instance where the quantity of iodine remaining in a spent-fuel solution is greater in a reprocessing plant than in several laboratory-scale experiments. While laboratory-scale dissolution of high burnup fuels left only 1% or less of the iodine in spent-fuel, up to 5% of the iodine remained in spent-fuel solutions at the WAK reprocessing plant. Several factors may cause this difference. Through our studies, however, we noted the possibility that colloidal iodine (AgI) is formed secondarily at the liquid surface of a plant-scale dissolver. The reasons are discussed below.

4.1 Chemical Equilibrium

As already described, colloidal iodine is partially decomposed in hot nitric acid solution through Reactions (1) and (2). However, Reaction (1) can be reversed near the liquid-gas interface of a plant-scale dissolver. The liquid surface may have high concentrations of $I_2(g)$ and NO_2 because bubbles containing these gasses rise through the liquid after formation. When dissolution of fuel proceeds continuously at a constant rate, the concentrations of $I_2(g)$, $I_2(aq)$, NO_2, Ag^+, and HNO_3 remain constant with time at the liquid surface. This condition is regarded as a state of quasi equilibrium among these species; thus, an approximate chemical equilibrium treatment is appropriate for the system. Figure 4 shows the chemical equilibrium relationships of Reaction (1), in which the abscissa denotes NO_2 pressure and the ordinate represents the corresponding concentration of dissolved iodine, $I_2(aq)$. These relationships were derived from the following commonly accepted set of thermochemical equations:[14]

$$\ln\left(K(T_2)/K(T_1)\right) = \int_{T1}^{T2} (\Delta H^\circ_T/RT^2)\, dT, \qquad (a)$$

$$H_T^\circ = H_{T1}^\circ + \int_{T1}^{T} \Delta C_p\, dT, \qquad (b)$$

$$C_p = A + B\,10^{-3} + C\,10^{5}\,T^{-2} + D\,10^{-6}\,T^2, \qquad (c)$$

where H_T° is the standard enthalpy of formation at T K, C_p is the heat capacity, and A, B, C, and D are constants specific to each substance. The equilibrium constant $K(T_1)$ = 298 K; H_{298}° and C_p were adopted from the literature.[15]-[17]

In a fuel solution, when the concentration of $I_2(aq)$ increases beyond the curve corresponding to its temperature and HNO_3 concentration under a specific value of P_{NO2}, colloidal AgI is formed through the reversal of Reaction (1). By assuming a simplified continuous dissolver, the concentrations of NO_2 and I_2 near the liquid surface were estimated (see below).

4.2 Concentrations of NO_2 and I_2 in a Plant-Scale Dissolver

The assumed dissolver, similar to a continuous dissolver in a reprocessing plant described in the literature,[2],[3] is 5 × 0.3 × 2 m with a liquid-gas interface of 1.5 × 10^4 cm^2. To stir the solution in this dissolver, 40 Nm^3/h of air is fed from the bottom. Spent fuels with a burnup of 40 GWd/t are dissolved at a rate of 5 t/d in 3 m^3 of 3.5 *M* HNO_3 at 100°C. The NOx produced consists of 80% NO_2 and 20% NO for the chemical equilibrium

$$NO(g) + 2HNO_3(aq) = 3NO_2(g) + H_2O(l)$$

at 100°C. Fuel solution containing 250 g U/ℓ overflows toward downstream processes. Calculations indicate that gaseous iodine, $I_2(g)$,

and NO_2 volatilize at rates of 4.1×10^{-3} mol I_2/min and 16.6 mol NO_2/min, respectively. The bottom fed air increasingly collects these gasses as it rises through the solution. At the liquid surface, the air consists of 35.8% (0.358 atm) of NO_2 and 88.4 ppm of $I_2(g)$. The concentration of dissolved iodine, $I_2(aq)$, corresponding to 88.4 ppm $I_2(g)$, was calculated to be 2.3×10^{-5} *M* using the equilibrium constant

$$K(373) = P_{I2}/[I_2(aq)] = 3.798$$

of Reaction (9) where P_{I2} is in atm. Figure 4 shows that the concentration of $I_2(aq)$ (in 3.5 *M* HNO_3) in equilibrium with 0.358 atm NO_2 (36 kPa) is 7.2×10^{-6} *M*, which is lower than the foregoing value (2.3×10^{-5}) in equilibrium with 88.4 ppm $I_2(g)$. This excess $I_2(aq)$ causes the reversal of Reaction (1) and the secondary formation of colloids of AgI at the liquid surface of the plant-scale dissolver (Table 2).

4.3 Experiments to Reverse Reaction (1)

To verify the progression of the reversal of Reaction (1) under conditions similar to those at the liquid surface of the assumed dissolver, laboratory-scale experiments were performed using the apparatus shown in Fig. 5. A 30 mℓ volume of 3.5 *M* HNO_3 solution containing 7.5 g U/30 mℓ (250 g U/ℓ) and 0.8 mg Ag^+/30 mℓ was heated to 100°C and bubbled with nitrogen flow (22 mℓ/min) containing 88 ppm $I_2(g)$ labeled with ^{131}I and 36% NO_2 for 1 h (Run 1). After its radioactivity was measured, 20 mℓ of the solution was transferred to a centrifuge tube (solution depth, 4 cm) and subjected to centrifugation of 4,500 rpm for 5 min. The top 10 mℓ was then examined by gamma spectrometry. Table 3 lists the results. The radioactivity of the solution decreased to 8% of the initial value and a whitish yellow sediment was observed on the bottom of the centrifuge tube. This confirmed that supplying 88 ppm $I_2(g)$ and 36% NO_2 produced a colloid of AgI at 100°C; that is, Reaction (1) was reversed. In Run 2, also listed in Table 3, a higher concentration of $I_2(l)$ (263 ppm) and 38% NO_2 was fed to 30 mℓ of 3.5 *M* HNO_3 solution containing 12 mg Pd^{2+}/30 mℓ, 7.5 g U/30 mℓ, and 0.8 mg Ag^+/30 mℓ for 1 h. In this case, precipitate was observed on the bottom of the dissolver flask before centrifugation. The same sedimentation as in Run 1 was produced by the centrifugation.

The foregoing assumed dissolver is a simplified one. In actual (plant-scale) dissolvers, however, concentrations of I_2 and NO_2 would be higher near the liquid-gas interface because these gasses rise through the liquid after their formation. Due to the difference in fluid depth of spent-fuel solutions, the concentrations of these gasses at the liquid surface would be higher in a plant-scale dissolver than in a laboratory-scale dissolver. The experiments suggest that when their concentrations increase beyond the equilibrium conditions shown in Fig. 4, colloidal iodine is formed. This phenomenon can be one reason for the residual iodine quantity in spent-fuel solutions being greater in reprocessing plants than in laboratory-scale experiments.

V. Conclusions

(1) In the laboratory-scale dissolution of spent-fuels with burnups of 21 to 39 GWd/t, up to 10% of the ^{129}I in the spent fuel remains in fuel solutions, up to 3% deposits on insoluble residue, and the balance volatilizes and is expelled to the DOG.

(2) Of the iodine in the DOG, 7% or less is organic.

(3) The main iodine species in fuel solution are the colloids of

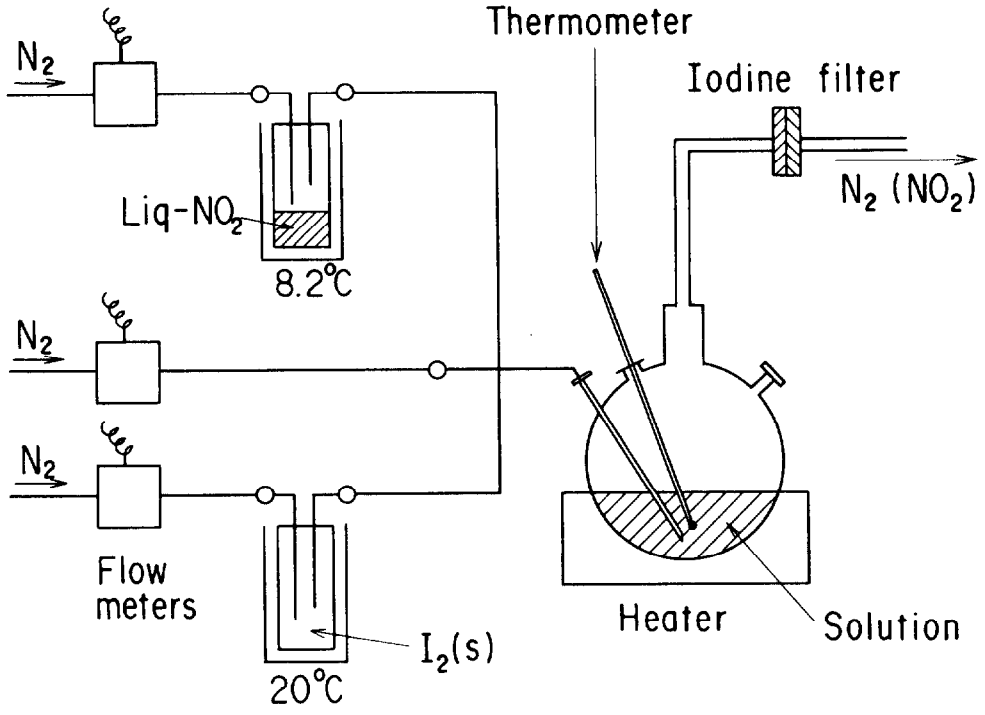

Figure 5 Experimental apparatus used for demonstrating the reversal of Reaction (1)

Table 3 Evidence of the formation of colloid by the reaction of I_2(g) with NO_2 in simulated spent-fuel solutions at 100℃

[Run 1] 30 mℓ-3.5 M HNO_3 solution containing 7.5 g-U/30 mℓ and 0.8 mg-Ag^+/30 mℓ
[Run 2] 30 mℓ-3.5 M HNO_3 solution containing 7.5 g-U/30 mℓ, 0.8 mg-Ag^+/30 mℓ and 12 mg-Pd^{2+}/30 mℓ.
Time period of the supply of I_2(g) and NO_2, 1h
Centrifugation, 4,500 rpm for 5 mm.

Run No.	I_2 supplied	NO_2 supplied	N_2 flow rate	Iodine remaining in the solutions		
				① Before centrifugation	② After centrifugation	Ratio of the decrease, ②/①
1	88 ppm (1.8 mg)	36 % (12 ml/min)	22 ml/min	417 μg/30 mℓ (1.1×10^{-4}M-I)	32 μg/30 mℓ (8.4×10^{-6}M-I)	0.08
2	263 ppm (3.3 mg)	38 % (13 ml/min)	20 ml/min	216 μg/30 mℓ* (5.7×10^{-5}M-I)	13 μg/30 mℓ (3.4×10^{-6}M-I)	0.06

* Before centrifugation, precipitate was observed on the bottom of the dissolver flask.

insoluble iodides, such as AgI and PdI_2.

(4) The amount of colloidal iodine tends to decrease with increasing concentrations of nitrous acid (HNO_2) and NOx produced in the dissolution. So, for spent fuels with high dissolution rates, the amount of colloidal iodine is small, even if the fuel is high burnup fuel.

(5) High concentrations of I_2 and HNO_2 (or NOx) cause formation of colloidal AgI. This is because the following reaction is reversed by conditions described above:

$$AgI(s) + 2H^+ + NO_3^- = \tfrac{1}{2}I_2(aq) + Ag^+ + NO_2(g) + H_2O(l). \quad (1)$$

The reversal of this reaction has been confirmed experimentally.

(6) This reaction can also be reversed at the liquid surface of plant-scale dissolves where the concentrations of NO_2 and I_2 are higher than in laboratory-scale experiments. This phenomenon can be one reason the residual iodine in spent-fuel solutions is higher in a reprocessing plant than in laboratory-scale experiments.

Acknowledgements

The authors wish to express their thanks to Drs. Michio Hoshi (Director of the Department of Chemistry and Fuel Research) and Takeo Adachi (Head of Analytical Chemistry Laboratory), Japan Atomic Energy Research Institute (JAERI), for their advice and support. We also thank Mr. Haruka Shinohara (Physical Chemistry Laboratory of JAERI) for his assistance in preparation of this manuscript.

References

(1) Henrich, E., Hufner, R., and Sahm, A., "Improved procedures for efficient iodine removal from fuel solutions in reprocessing plant," IAEA-SM-245/16, p. 139, International Atomic Energy Agency, Vienna (1989).

(2) Auchapt, P., Patarin, L., and Tarnero, M., "Development of a continuous dissolution process for the new reprocessing plant at La Hague," Proc. Int. Topl. Mtg. Fuel Reprocessing and Waste Management, Jackson Hole, Wyoming, August 26-29, 1984, American Nuclear Society (1984).

(3) Poncelet, F.J., Hugelmann, D., Saudray, D., Mukohara, S., and Cho, A., "Head-end process technology for the new reprocessing plants in France and Japan," Proc. 3rd Int. Conf. Nuclear Fuel Reprocessing and Waste Management," Sendai, Japan, April 14-18, 1991, Vol. 1, p. 55 (1991).

(4) Leudet, A., Miquel, P., Goumondy, P-J., and Charrier, G., "Balance and behavior of gaseous radionuclides released during initial PWR fuel reprocessing operation," Proc. 17th DOE Nuclear Air Cleaning Conf., Denver, Colorado, August 1-6, 1982, CONF-8208-33-V1, p. 639 (1983).

(5) Herrmann, F.J., Motoi, V., Herrmann, B., Fang, D., Finsterwalder, L., Kuhn, K.D., van Shoor, A., Beyer, Ch., Furrer, J., and Knoch, W., "Minimizing of iodine-129 release at the Karlsruhe reprocessing plant WAK," Proc. 22nd DOE/NRC Nuclear Air Cleaning and Treatment Conf., Denver, Aug., (1992); NUREG/CP-0130, CONF-902083-V1, p. 75 (1993).

(6) Weinlaender, W., Huppert, K.L., and Weishaupt, M., "Twenty years of WAK reprocessing pilot plant operation," Proc. 3rd Int. Conf. Nuclear Fuel Reprocessing and Waste Management (RECOD' 91)," Sendai, Japan, April 14-18, Vol. 1, p.55 (1991).

(7) Castleman, A.W. Jr., Tang, I.N., and Mulkelwitz, H.R., "The chemical states of fission-product iodine emanating into a high

temperature aqueous environment," J. Inorg. Nucl. Chem., **30**, 5 (1968).
(8) Sakurai, T., Takahashi, A., Ishikawa, N., and Komaki, Y., "The behavior of iodine in a simulated spent-fuel solution," Nucl. Technol., **85**, 206 (1989).
(9) Sakurai, T., Takahashi, A., Ishikawa, N., Komaki, Y., Ohnuki, M., and Adachi, T., "Thermochemical and experimental consideration of NOx composition and iodine species in the dissolution of spent PWR-fuel specimens," J. Nucl. Sci. Technol., **30**, 533 (1993).
(10) Sakurai, T., Takahashi, A., Ishikawa, N., Komaki, Y., Ohnuki, M., and Adachi, A., "The iodine species and their behavior in the dissolution of spent-fuel specimens," Nucl. Technol., **99**, 70 (1992).
(11) Sakurai, T., Takahashi, A., Ishikawa, N., Komaki, Y., Ohnuki, M., and Kato, K., "A study on the expulsion of iodine from spent-fuel solutions," Proc. 23rd DOE/NRC Nuclear Air Cleaning Conf., NUREG/CP-0141, CONF-940738, 321 (1995).
(12) Boukis, N., and Henrich, E., "Two-step procedure for the iodine removal from nuclear fuel solutions," Radiochim. Acta, **55**, 37 (1991).
(13) Sakurai, T., Takahashi, A., Ishikawa, N., and Komaki, Y., "The interaction of iodine with insoluble residue in the dissolution of simulated spent-fuel pellets," Nucl. Technol., **94**, 99 (1991).
(14) Moore, W.J., "Physical Chemistry," 3rd ed., p. 167, Prentice-Hall, Englewood Cliffs, New Jersey, 1962.
(15) Lemire, R.J., Paquette, J., Torgerson, D.F., Wren, D.J., and Fletcher, J.W., "Assessment of iodine behavior in reactor containment buildings from a chemical perspective," AECL-6812, Atomic Energy of Canada Limited, 1981.
(16) Criss, C.M., and Cobble, J.W., "The thermodynamic properties of high temperature aqueous solutions. V. The calculation of ionic heat capacities up to 200°C. Entropies and heat capacities about 200°C," J. Amer. Chem. Soc., **86**, 5390 (1964).
(17) Pourbaix, M. "Atlas of electrochemical engineering in aqueous solutions," Pergamon Press, Oxford, 1966.

DISCUSSION

HERRMANN: I have a question about Point B . You have marked 0-10% in the fuel solution, 0-3% in insoluble residue. Is the value of 0% not too low? Does this mean that the rest, 87%, is in the offgas?

SAKURAI: In our laboratory-scale dissolutions, iodine quantities in the fuel solution and in the insoluble residue varied in the range of 0 to 10% and 0 to 3%, respectively, largely depending upon the rate of dissolution of the spent-fuel specimens. The fuel specimen with a burnup of 39GWd/t dissolved quickly, leaving little iodine in the solution and 0.6% in the residue. But the fuel-specimen with a low burnup of 21GWd/t took a long time to dissolve and 9.7% of the iodine remained in the fuel solution, and 2.3% in the residue. As a whole, the iodine quantity volatilized into the off-gas varied between 88 and 100%.

JUBIN: I found this very interesting and I have one additional question. In your laboratory studies, have you had an opportunity to try to identify the iodine in the dissolver solution? Have you identified through your centrifugation at the end a reduction in the iodine concentration? Have you been able to conduct any experiments using spent fuel to see if it does the same? Have you had an opportunity to look for the formation of iodine in the form of the colloid in actual dissolver solution?

SAKURAI: Not directly. However, iodine species in spent-fuel solution
showed the same behavior in the expulsion process as the colloid of AgI and PdI_2 did. It is almost impossible to directly identify iodine species in spent-fuel solutions because of the extremely high radioactivity of the solution and the weak radioactivity of ^{129}I. We had to identify them through their behavior in separating from the fuel solution. The expulsion of iodine was performed in two different ways for the fuel solution. The insoluble residue had already been separated by centrifugation. From their behavior in the two expulsion processes, the main iodine species in the actual spent-fuel solution was concluded to be the colloidal iodine already mentioned.

INFLUENCES OF IMPURITIES ON IODINE REMOVAL EFFICIENCY OF SILVER ALUMINA ADSORBENT

Tetsuo FUKASAWA*, Kiyomi FUNABASHI*, and Yoshikazu KONDO**

* Power & Industrial Systems R & D Division, Hitachi, Ltd.
7-2-1 Omika, Hitachi, Ibaraki, 319-12 Japan

** Hitachi Works, Hitachi, Ltd.
3-1-1 Saiwai, Hitachi, Ibaraki, 317 Japan

Abstract

Silver impregnated alumina adsorbent (AgA), which was developed for iodine removal from off-gas of nuclear power and reprocessing plants, has been tested laying emphasis on investigation of the influences gaseous impurities have on adsorbent chemical stability and iodine removal efficiency. The influences of the major impurities such as nitrogen oxides and water vapor were checked on the chemical state of impregnated silver compound ($AgNO_3$) and decontamination factor (DF) value.

At 150℃, a forced air flow with 1.5% nitrogen oxide ($NO/NO_2=1/1$) reduced silver nitrate to metallic silver, whereas pure air and air with 1.5% NO_2 had no effect on the chemical state of silver. Metallic silver showed a lower DF value for methyl iodide in pure air (without impurities) than silver nitrate and the lower DF of metallic silver was improved when impurities were added.

At 40℃, a forced air flow with 1.5% nitrogen dioxide (NO_2) increased the AgA weight by about 20%, which was caused by the adsorption of nitric acid solution on the AgA surface. AgA with 10wt% silver showed higher weight increase than that with 24wt% silver which had lower porosity. Adsorption of acid solution lowered the DF value, which would be due to the hindrance of contact between methyl iodide and silver.

The influences of other gaseous impurities were also investigated and AgA showed superior characteristics at high temperatures.

I. Introduction

Uranium and plutonium are important energy sources, and can be utilized more effectively by recycling them in the nuclear fuel cycle. In Japan, the first light water reactor started commercial operation in 1969. Now there are 47 reactors in operation and their total power generation capacity is 38 GW. Reprocessing of spent nuclear fuel is carried out at Tokai Reprocessing Plant

where 812.9 tons of uranium was treated by the end of FY 1994. Commercial reprocessing will start at Rokkasho Plant at the beginning of the next century.

The nuclear energy industry adopts multibarrier protection towards radioactivity exposure for human beings and the environment. In particular, radioactive iodine release to the atmosphere must be surpressed because iodine is volatile and apt to concentrate in the thyroid gland. Therefore nuclear facilities, such as nuclear power plants and reprocessing plants, remove radioactive iodine from their off-gas streams.

Iodine removal methods are generally classified into two types, wet ones which absorb iodine into a solution and dry ones which adsorb iodine onto a solid material.[1-3] Both wet and dry methods must take into account the effects of impurities. For example, wet scrubbing with an alkaline solution absorbs not only iodine, but also various impurities, which sometimes leads to drops in the pH value and iodine absorption capacity of the solution. Impurities also sometimes interfere with the reaction of iodine and solid adsorbent.

The authors have been developing an inorganic adsorbent, silver impregnated alumina (AgA) for about 15 years.[4-14] This adsorbent can be applied to off-gas systems of both nuclear power plants and spent fuel reprocessing plants. The influences of impurities were checked on AgA under the various conditions possible in the above systems. This paper reports experimental results of the investigation which laid emphasis on the changes of chemical stability and iodine removal efficiency of AgA in the presence of gaseous impurities. Iodine removal efficiency was evaluated using adosorption capacity and decontamination factor (DF) which is defined as the iodine concentration at the inlet of the adsorbent column divided by that at the outlet.

II. Off-Gas Systems

The adsorbent AgA is intended for application to the tank vent system for the waste solution of boiling water reactors (BWRs), standby gas treatment system (SGTS) of BWRs, and dissolver off-gas (DOG) system of reprocessing plants. A schematic and conditions of these systems are summarized in Fig. 1 and Table 1. Systems characteristics are as follows. The tank vent filter (adsorbent) removes iodine from the off-gas which contains many contaminants and has a high humidity. The SGTS filter removes iodine over a wide range of concentrations during an accident. The DOG filter removes high concentrations of iodine in the presence of nitrogen oxides. Stability of the adsorbed iodine is an important factor for the DOG system because the main radioactive iodine isotope is I-129 (half life: $1.57 \cdot 10^7$y), whereas I-131 (8.02d) is the main radioisotope for the tank vent system and SGTS. Furthermore, iodine concentration is high (~30ppm) for the DOG, whereas it is below 0.1ppm for power plants (tank vent and SGTS). So two types of AgA were prepared, AgA with 24wt% Ag and 10wt% Ag for DOG and power plants, respectively. Operation temperatures differ for the

three systems. The most severe situation seems to be that of the tank vent because of the low temperature and high humidity. Water vapor clogs the adsorbent pores. Other systems may have low temperature conditions would be exist such as during storage before and after use, and at operation standby. Nitrogen oxides of high concentration also can interfere with the reaction of iodine and impregnated silver, and change the chemical form of impregnated silver. All these factors must be considered in order to apply AgA to actual systems.

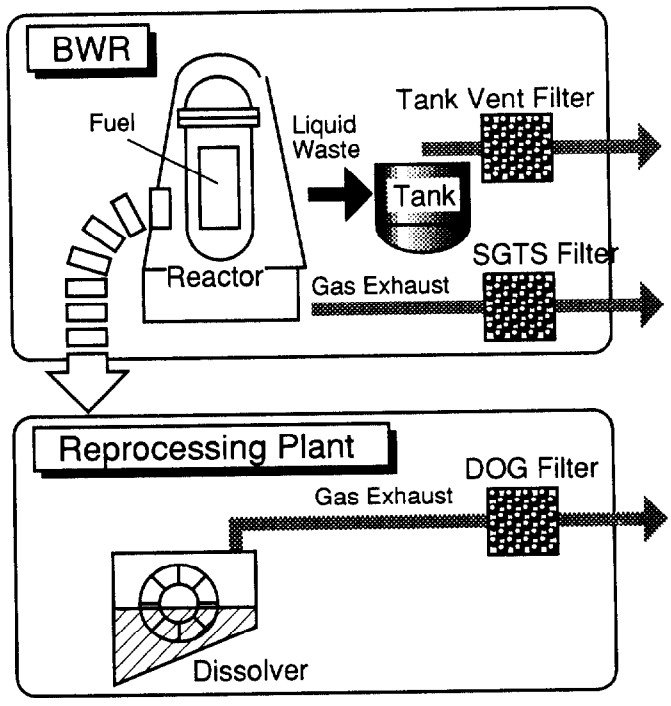

Fig. 1 Off-Gas Treatment Systems

Table 1 Off-Gas Conditions of Each System

System	Off-Gas Conditions				Requirement *filter bed depth
	Temp.	RH	[I]	[NOx]	
(1)Tank Vent Off-Gas → Demister HEPA Iodine HEPA Filter → Stack Waste Tank	30℃	50-90%	1ppb (10^{-3} ppm)	10ppb (10^{-2} ppm)	· High removal efficiency (DF>10 at 5cm*)
(2)SGTS Demister HEPA Iodine HEPA Filter → Stack Reactor Building	66℃	<70%	1ppt–0.1ppm (10^{-6} -10^{-1})	10ppb (10^{-2})	· High removal efficiency (DF>34 at 5cm*)
(3)Dissolver Off-Gas Off-Gas → Mist Filter HEPA Iodine Filter HEPA → Stack Dissolver	150℃	~1%	30ppm	1.5% (1.5×10^{4})	· High removal efficiency (DF>250 at >85cm*) · High adsorption capacity

III. Experimental

The preparation of AgA was described previously.[14] Both types of AgA tested here had particle diameter of about 2mm and pore diameter of from 10 to 100 nm. Specific surface areas of 24 and 10 wt% AgA were about 10 and 40 m^2/g,

and bulk densities were about 1.5 and 1.2 g/cm³, respectively.

The test apparatus is schematically shown in Fig. 2. The iodine species were methyl iodide and molecular iodine. Concentrations of iodine and NOx, ratios of NO to NO_2 of simulated off-gas, the gas temperature and adsorbent bed depth were adjusted to get a desired condition. Iodine concentrations at the inlet and outlet of the column were measured by three methods depending on the form and concentration of iodine, that is gas chromatography with an FID or ECD detector after gas sampling, spectrophotometry using ferric thiocyanate, and inductively coupled plasme mass spectrometry after absorbing the iodine in an alkaline solution.

In order to simulate the standby condition for the DOG system, pre-blow tests were carried out. Pre-blow meant blowing of simulated off-gas without iodine through the AgA column in this study. The weight change of AgA and chemical form of silver were measured during and after pre-blow. The tests of iodine removal were carried out after pre-blow. The breakthrough test was also conducted to confirm the adsorption capacity of AgA with the 10 cm bed depth.

The influences on AgA of other gaseous impurities such as SO_2, NH_3 and CO_2 were investigated with 10 wt% Ag at relatively low temperatures and long times.

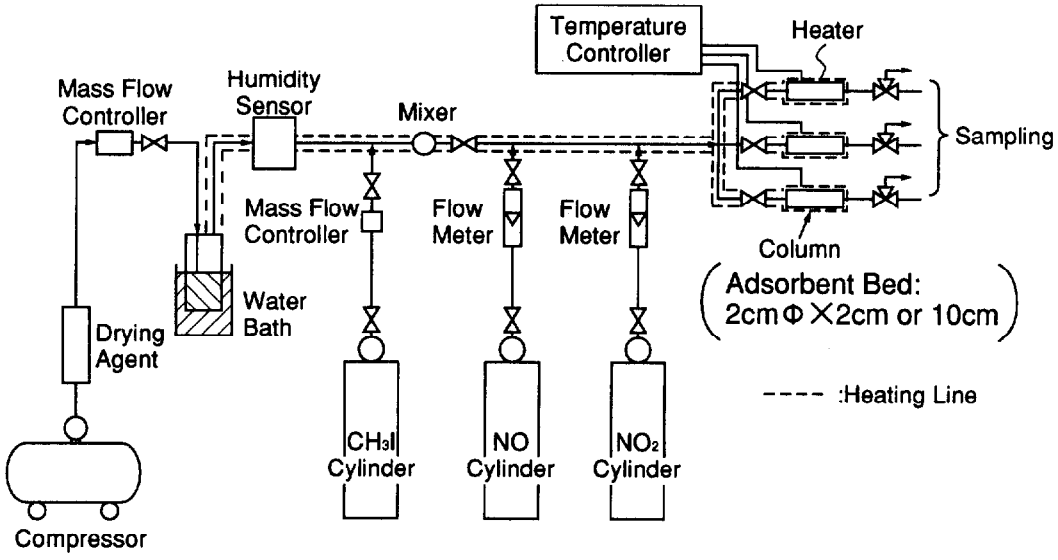

Fig. 2 Outline of the Test Apparatus

IV. Influence of NOx and H_2O on AgA

Before the iodine removal tests, pre-blow tests without iodine were carried out to clarify the influence of only gaseous impurities on the chemical form of impregnated silver. Figure 3 shows the relative weight change of AgA when 1.5% NOx (NO/NO_2=1/1) was blown in at 40 and 150℃. A forced air flow without NOx was carried out as a reference. A slight increase at 40℃ and a decrease at 150℃ were observed in the reference data, which is due to adsorption of H_2O in

the air at 40℃ and desorption of H_2O adsorbed on AgA before the test at 150℃. AgA with 10% silver showed a higher weight increase than AgA with 24% silver at 40℃, which is attributable to the higher surface area of the former. For the NOx pre-blow, weight changes were more notable than the reference case. At 40℃, NOx (NO_2) would be absorbed in the adsorbed H_2O, which would dissolve impregnated $AgNO_3$ and enhance the H_2O adsorption. Nitrate presence which was observed in the 1.5% NO_2 pre-blow supports this mechanism. At 150℃, the weight decrease could not be explained only by the H_2O desorption. In this case, NOx (NO) reduced the impregnated $AgNO_3$ to Ag and decreased the AgA weight. X-ray diffraction (XD) patterns are shown in Fig. 4 for 24% AgA before and after the NOx pre-blow, which indicated the conversion of $AgNO_3$ to Ag by Eq. (1).

$$AgNO_3 + NO \rightarrow Ag + 2NO_2 \quad (1)$$

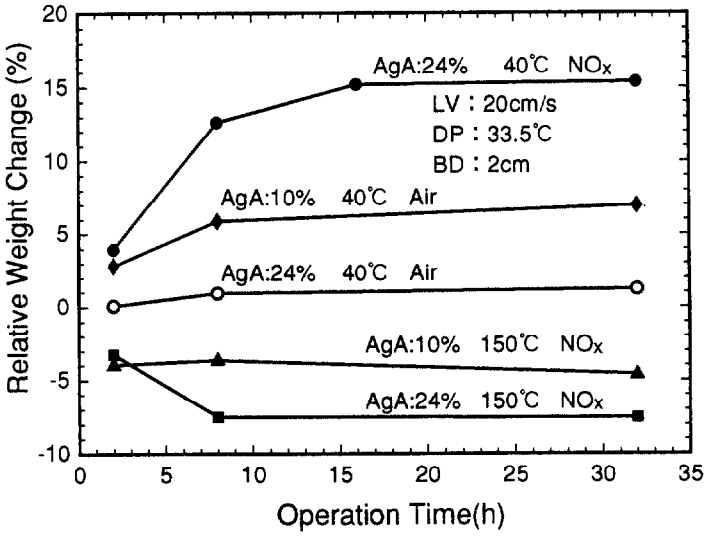

Fig. 3 Relative Weight Change of AgA during NOx Pre-Blow

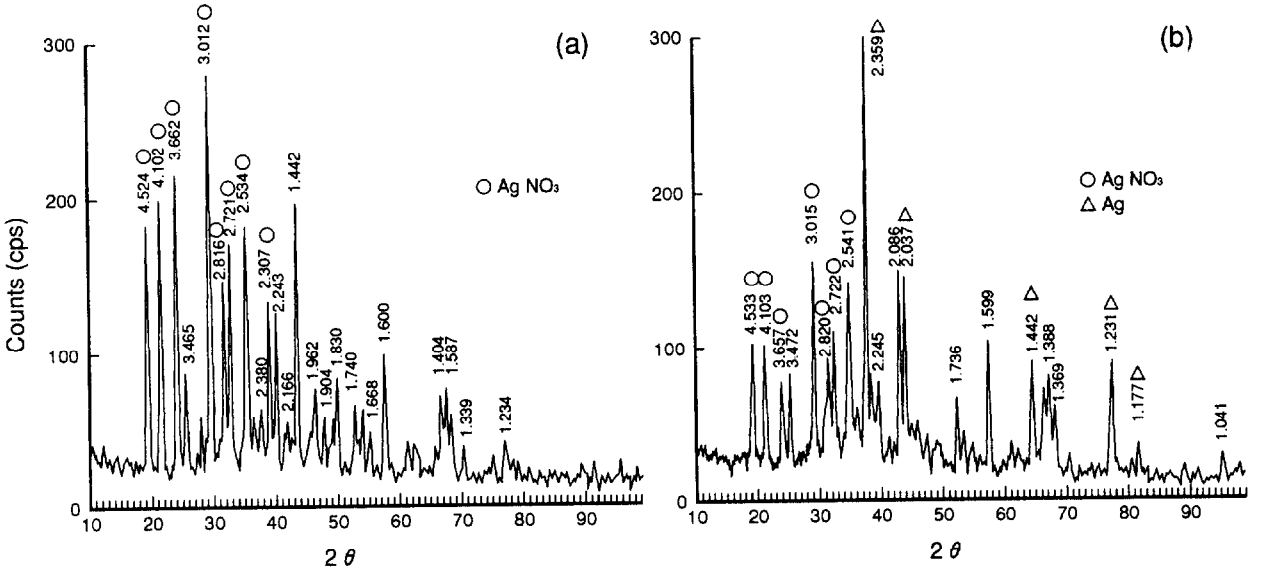

Fig. 4 XD Pattern of AgA before(a) and after(b) NOx Pre-Blow at 150℃

Figure 5 shows the weight change ratio of AgA during the 1.5% NO_2 pre-blow. The data showed that a larger increase was observed for 10% AgA than 24% AgA due to the larger surface area of the former. Compared with the data for 24% AgA in Fig. 3, NO_2 pre-blow had a larger weight increase than NOx pre-blow, which would be due to the easier solution of NO_2 into water than NOx.

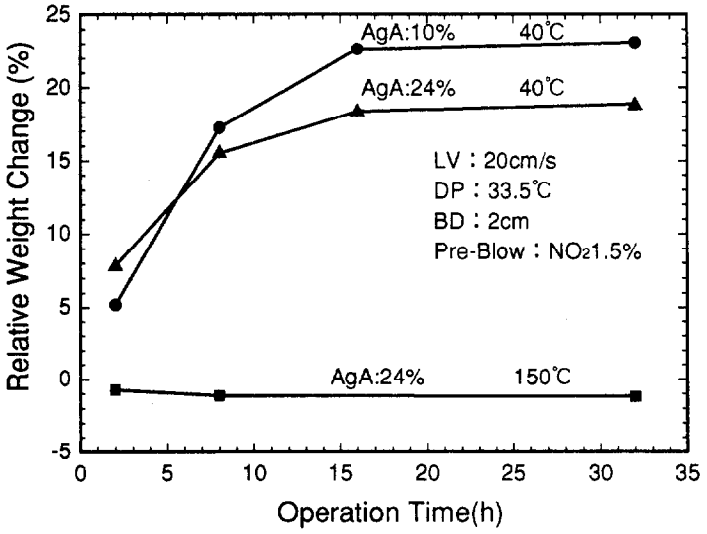

Fig. 5 Relative Weight Change of AgA during NO_2 Pre-Blow

V. Iodine Removal Efficiency after NOx Pre-Blow

Iodine removal experiments were carried out after pre-blow of simulated off-gas without iodine. Iodine was mixed with air without and in same cases with impurities. Typical iodine forms selected here were methyl iodide (CH_3I) and molecular iodine (I_2). CH_3I is the most difficult species to separate from simulated off-gas among the major organic iodines, and I_2 is the main form in the dissolver off-gas of spent fuel reprocessing[1,13]. In the experiments done here, the bed depth was quite small (2cm) to allow sensitive assessment of the change in decontamination factor (DF). It is known that the iodine adsorption band is about 5cm for AgA and a bed depth of 5cm is necessary for good iodine removal. So some cases showed rather rapid iodine breakthrough due only to the insufficient bed depth.

The DF values for CH_3I with 24% AgA are shown in Fig. 6 after various gases were pre-blown as a function of operation time. When the iodine concentration at the column outlet was under the detection limit, a DF value was calculated by substituting the detection limit for the outlet iodine concentration; these values are indicated with an upward pointing arrow in Figs. 6 and 7. The DF value was high after 1.5% NO_2 and air pre-blows. No gaseous impurities were added during the iodine removal test in these two cases. The DF values were low after 1.5% NOx ($NO/NO_2=1$) pre-blow (no NOx during iodine removal), and they

were raised by the addition of NOx during iodine removal. The reactions of CH_3I with silver impregnated on AgA could be written as follows.

$$CH_3I + AgNO_3 \rightarrow AgI + CH_3NO_3 \quad (2)$$

$$CH_3I + Ag \rightarrow AgI + CH_3- \quad (3)$$

$$CH_3I + Ag + NO_2 + 1/2O_2 \rightarrow AgI + CH_3NO_3 \quad (4)$$

Reaction (2) is the normal iodine adsorption reaction which has a high DF. As described in the previous section, NOx pre-blow reduced $AgNO_3$ to Ag. It would be difficult for Reaction (3) to proceed because no couter ions are present for CH_3-, whereas gaseous impurities could act as couter ions as described in Reaction (4).

Figures 7 and 8 show the DF values of 10% AgA after 1.5% NOx and air pre-blows, respectively. Iodine forms of CH_3I and I_2 were examined in both figures. Temperature dependency is summarized in Fig. 8. Molecular iodine (I_2) showed no apparent DF decrease with lower temperature because the reactivity of I_2 with silver would be high. Methyl iodide (CH_3I) showed a lower DF especially at low temperatures and after NOx ($NO/NO_2=1$) pre-blow. This is because of the low reactivity of CH_3I with $AgNO_3$ and the much lower CH_3I reactivity with Ag metal at low temperatures. DF values of over 500 could be obtained for 30ppm CH_3I at 150℃ with 10% AgA in a 2cm bed depth after air pre-blow. AgA with 24% silver showed DF of over 500 even after 1.5% NOx pre-blow.

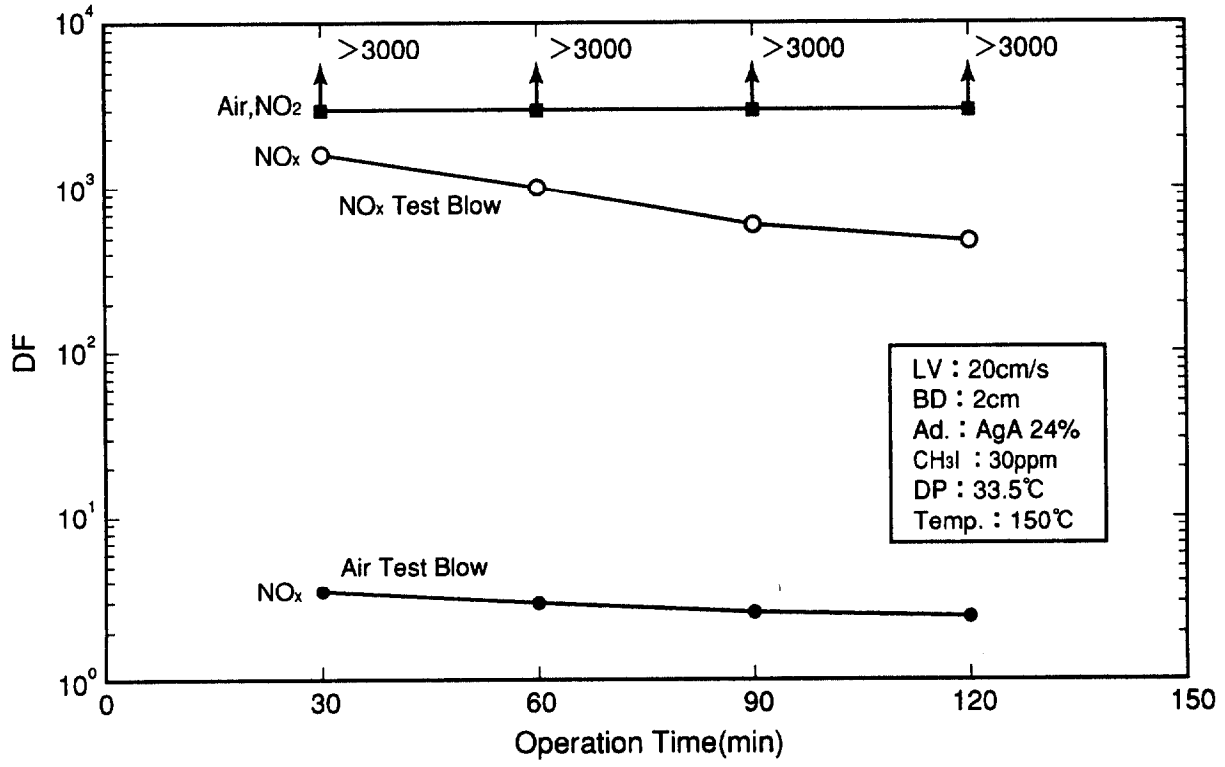

Fig. 6 DF of 24% AgA for CH_3I after Various Gases Were Pre-Blown

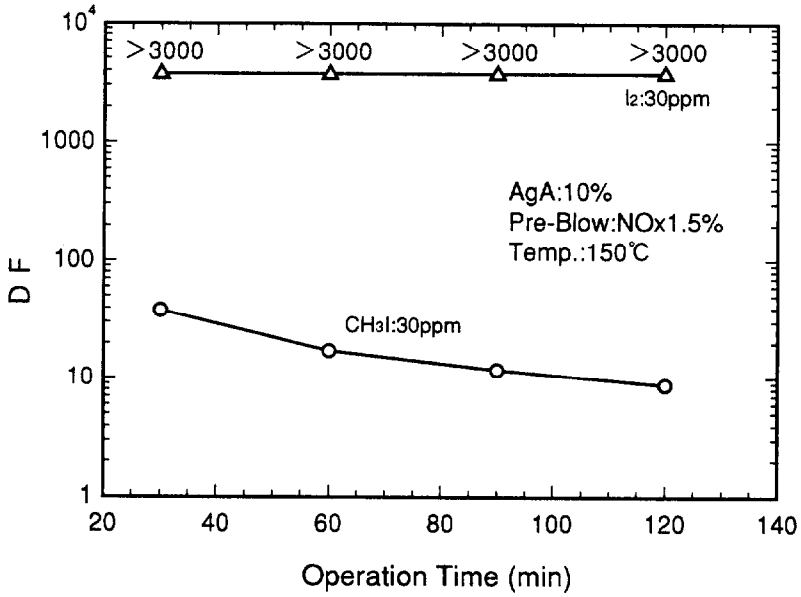

Fig. 7 DF of 10% AgA for CH_3I and I_2 after 1.5% NOx Pre-Blow

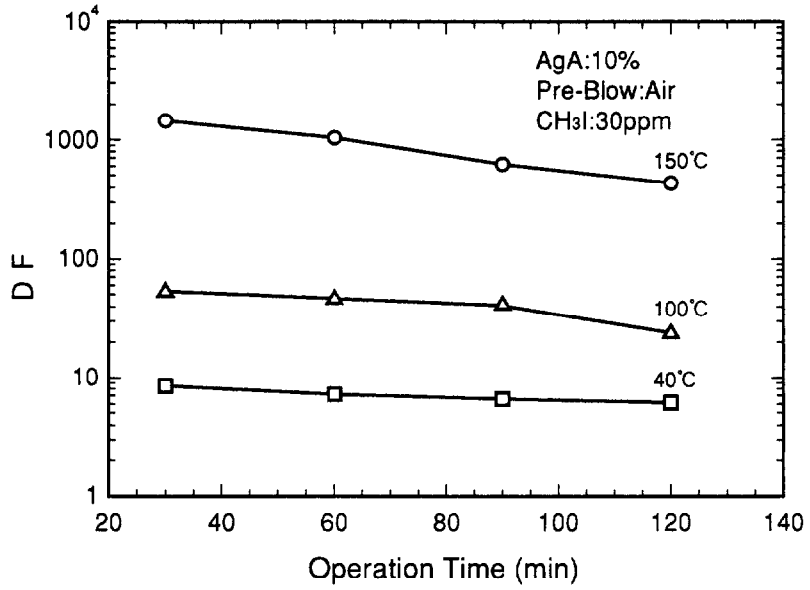

Fig. 8 DF of 10% AgA for CH_3I after Air Pre-Blow

VI. Breakthrough Property of AgA

Iodine breakthrough property was checked in order to get the iodine adsorption capability of AgA in a column. The results are shown in Fig. 9 for AgA with silver contents of 10wt% and 24wt% and CH_3I concentrations of 30 and 300ppm with air blowing. The bed depth of AgA was set at 10cm. Iodine concentration of 300ppm simulated an accelerated condition. AgA is known to show almost the same adsorption capacity for both CH_3I and I_2, and was expected to show a similar breakthrough curve.

The breakthrough point was defined in this study as the operation time

where the DF value decrease was first observed. The breakthrough point depends on the iodine flow rate, and bed volume and silver content of AgA. This could be qualitatively understood by the data in Fig. 9. Iodine adsorption capacity of AgA was about 0.12 g-I/cm³-AgA(10wt%) and 0.35 g-I/cm³-AgA(24wt%). Iodine reacts with the same number of moles of silver in AgA and capacity data obtained indicated about 80% silver utilization. As mentioned before, adsorption band length is around 5cm, so breakthrough point would be full adsorption to 5cm of AgA in this experiment. Calculated breakthrough points of 24% AgA were about 140h and 14h, and those of 10% AgA were about 50h and 5h for 30ppm and 300ppm CH_3I, respectively. Corresponding experimental breakthrough points were 90h, 24h, 48h and 4h, which were not so different from the calculated points. High DF values were obtained for AgA before the breakthrough points which could be predicted by iodine adsorption capacity.

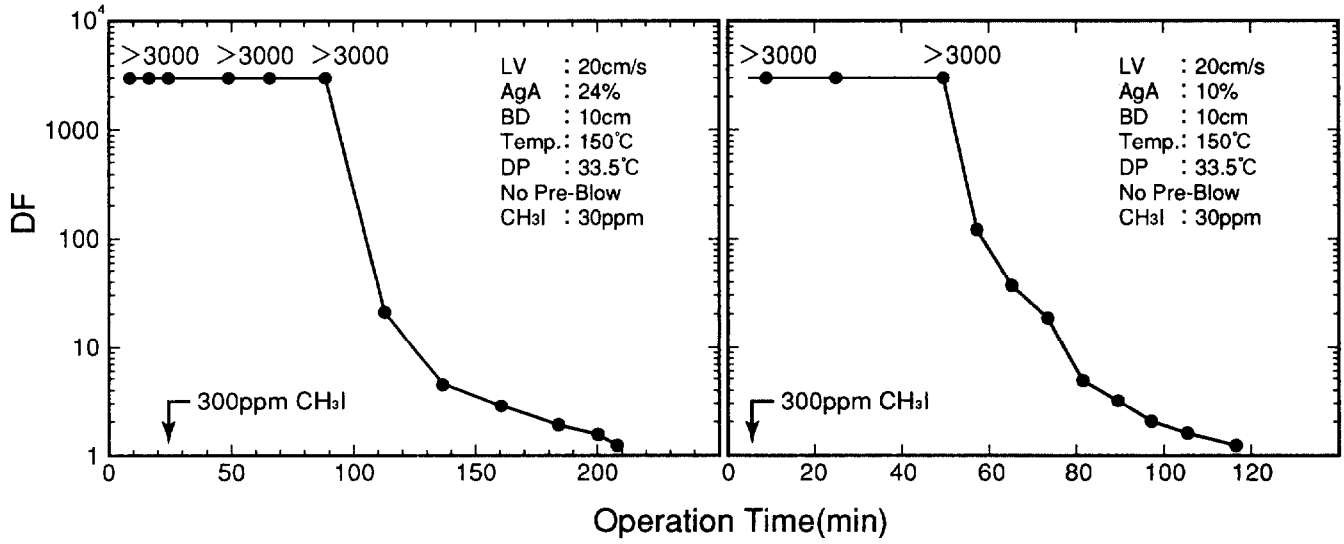

Fig. 9 Iodine Breakthrough Property of AgA

Ⅶ. Long Term Effect of Impurities at Relatively Low Temperatures

In order to check applications to the tank vent and standby gas treatment systems, long term experiments were carried out by blowing simulated off-gas containing various impurities. AgA with 10% silver was exposured for adequate time and iodine was added only at the time of the DF measurement. Impurities were removed from iodine gas to avoid their interference with the DF measurement.

The results are shown in Figs. 10 and 11 for simulated conditions of tank vent and standby systems, respectively. Simulated off-gas of the tank vent system included NOx (5ppb), SO_2 (5ppb), H_2S (<1ppb), HCl (36ppb) and NH_3 (150ppb). Temperature and relative humidity were 30℃ and 70%, respectively. Simulated off-gas of the standby system included NOx (30ppb), SO_2 (<1ppb), H_2S (<1ppb), HCl (<1ppb) and NH_3 (17ppb). Temperature and relative humidity were 66℃ and 70%, respectively. Bed depth of AgA and linear gas velocity were 5cm

and 20cm/s in both cases, respectively. The DF values in Fig. 10 were lower than in Fig. 11 due to the lower temperature for the former. Long term exposures of AgA decreased the DF values in both cases, which would indicate poisoning of AgA by gaseous impurities such as NH_3, NOx and SO_2. The effects of NH_3 and SO_2 were realized by the separate experiments. Nitrogen oxide (NO) reduced $AgNO_3$ to Ag metal and hindered the smooth reaction of CH_3I with silver. The X-ray diffraction pattern showed peaks of Ag metal after exposure to simulated off-gas. But the required DF values were obtained in both cases after long exposure time.

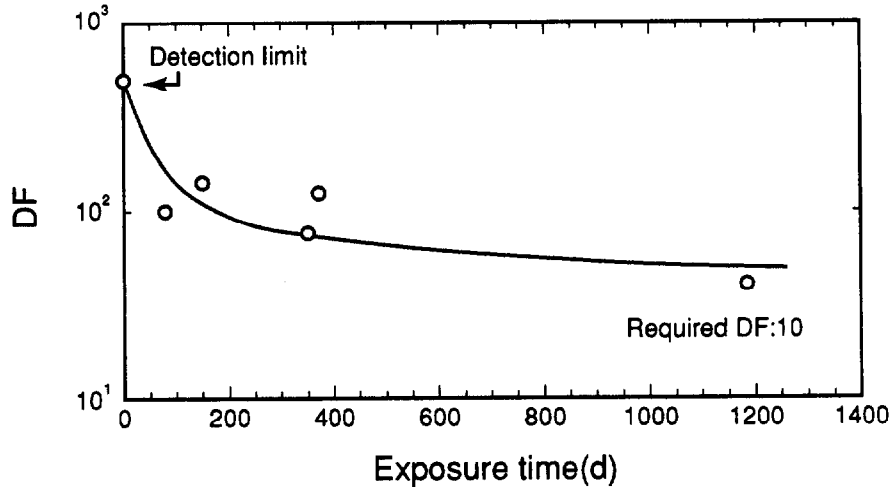

Fig. 10 Long Term DF Change for Simulated Conditions of Tank Vent System

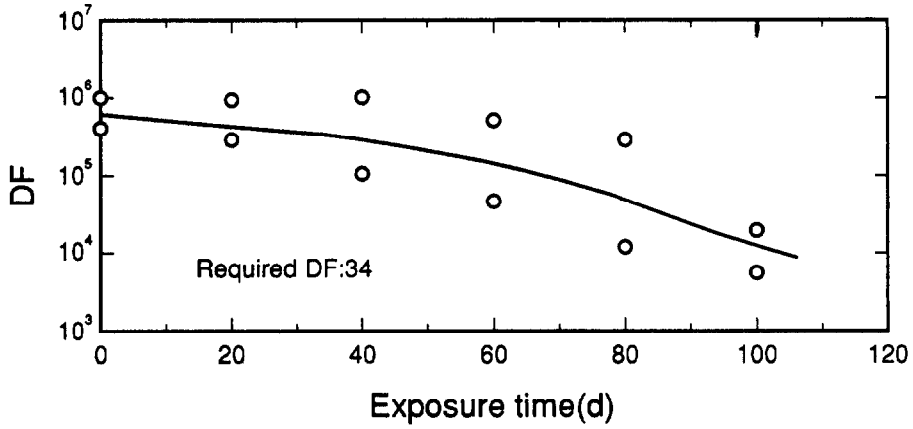

Fig. 11 Long Term DF Change for Simulated Conditions of Standby System

VIII. Conclusions

Silver impregnated alumina adsorbent (AgA), which was developed for iodine removal from off-gas of nuclear power and reprocessing plants, has been tested, placing emphasis on the investigation of influences of gaseous impurities on AgA chemical stability and iodine removal efficiency. Methyl iodide (CH_3I) and molecular iodine (I_2) were chosen as iodine forms for testing. Silver contents

of AgA were 10 and 24 wt%. The main impurities are nitrogen oxides and water vapor in the dissolver off-gas of a reprocessing plant. Their influence on the chemical state of impregnated silver compound ($AgNO_3$) and decontamination factor (DF) value was checked.

At 150℃, air pre-blow with 1.5% nitrogen oxide (NO/NO_2=1/1) reduced silver nitrate to metallic silver, whereas pure air and air with 1.5% NO_2 had no effect on chemical state of silver. Metallic silver showed a lower DF value for methyl iodide in pure air (without impurities) than silver nitrate and the higher DF value in the presence of impurities. These phenomena could be explained by the reactivity difference of methyl iodide with silver in the presence and absence of counter ions (NO_3-, etc.) for methyl ion (CH_3-). Iodine could easily react with silver while methyl ion could react with counter ion. Methyl iodide removal by metallic silver without gaseous impurities could not offer the counter ion for methyl ion and showed a relatively low DF value.

At 40℃, air pre-blow with 1.5% nitrogen dioxide (NO_2) increased the AgA weight by about 20%, which was caused by the adsorption of nitric acid solution on the surface of AgA. AgA with 10wt% silver showed a higher weight increase than that with 24wt% silver which had lower porosity. Adsorption of acid solution lowered the DF value, which would be due to the hindrance of contact between methyl iodide and silver. AgA showed a relatively high DF at high humidity than other iodine adsorbents by keeping high reactivity of dissolved iodine with dissolved silver nitrate, but nitric acid solution would suppress both dissolutions.

The long term influence of other gaseous impurities was also investigated on 10% AgA at 30℃ and 66℃ which simulated the conditions of the tank vent and standby systems, respectively. The impurities of NH_3 and SO_2 decreased the DF value at high humidity. But DF was still over the required value after a long time. AgA indicated superior characteristics at high temperatures.

References

[1]Goossens,W.R.A., Eichhoiz,G.G., Tedder,D.W., eds., "Treatment of Gaseous Effluents at Nuclear Facilities," Radioactive Waste Management Handbook, vol.2, Harwood Academic Publishers, Chur, Switzerland, 1991.

[2]Benedict,M., Pigford,T.H., Levi,H.W., "Nuclear Chemical Engineering, 2nd ed.," McGraw-Hill, Inc., New York (1981).

[3]Long,J.T., "Engineering for Nuclear Fuel Reprocessing," American Nuclear Society, La Grande Park, Illinois (1978).

[4]Kikuchi,M., Kitamura,M., Yusa,H., Horiuchi,S., "Removal of Radioactive Methyl Iodide by Silver Impregnated Alumina and Zeolite," Nucl. Eng. Design, 47,

283(1978).

[5]Kikuchi,M., Funabashi,F., Yusa,H., Takashima,Y., "Adsorption of Radioactive Methyl Iodide by Silver-Impregnated Alumina," Radiochem. Radioanal. Lett., 45, 279(1980).

[6]Kikuchi,M., Funabashi,K., Kawamura,F., Yusa,H., Tsuchiya,H., Takashima,Y., "New Adsorbent, Silver-Alumina for Radioactive Iodine Filter," Proc. 17th DOE Nucl. Air Cleaning Conf., CONF-820833, 2, 626(1983).

[7]Hattori,S., Kobayashi,Y., Ozawa,Y., Kunikata,M., "Removal of Iodine from Off-Gas of Nuclear Fuel Reprocessing Plants with Silver Impregnated Adsorbents," Proc. 18th DOE Nucl. Airborne Waste Management and Air Cleaning Conf., CONF-840806, 2, 1343(1984).

[8]Fujiwara,K., Ohki,K., Siomi,H., Hiraga,Y., Funabashi,K., "The Study for the Confirmation of the Performance of Activated Carbon for Stand By Gas Treatment System," Proc. 1985 Annual Meeting of the Atomic Energy Soc. Jpn., J38(1985).

[9]Mizuno,T., Ito,R., Kobayashi,Y., Ozawa,Y., Funabashi,K., "Stability Study of Iodine Adsorbed on Silver Impregnated Adsorbent for Interim Storage," Eur. Conf. Gaseous Effluent Treatment in Nucl. Installations, Luxembourg, Oct. 14-18(1985).

[10]Kobayashi,Y., Kondo,Y., Hirose,Y., Fukasawa,T., "Removal Characteristics of Some Organic Iodine Forms by Silver Impregnated Adsorbents," Proc. 21st DOE/NRC Nucl. Air Cleaning Conf., CONF-900813, 2, 594(1990).

[11]Sugimoto,Y., Kondo,Y., Hirose,Y., Fukasawa,T., Furrer,J., Herrmann,F.J., Knoch,W., "The Development of Ag-A for Radioactive Iodine Removal from Nuclear Fuel Reprocessing Plants," Proc. 3rd Int. Conf. Nucl. Fuel Reprocessing and Waste Management, RECOD '91, 1, 236(1991).

[12]Kondo,Y., Sugimoto,Y., Hirose,Y., Fukasawa,T., Furrer,J., Herrmann,F.J., Knoch,W., "Removal of Iodine-129 from Dissolver Off-Gas of Reprocessing Plant by Silver Impregnated Adsorbents," Proc. 22nd DOE/NRC Nucl. Air Cleaning and Treatment Conf., CONF-9020823, 1, 118(1992).

[13]Fukasawa,T., Funabashi,K., Kondo,Y., "Separation Technology for Radioactive Iodine from Off-Gas Streams of Nuclear Facilities," J. Nucl. Sci. Technol., 31, 1073(1994).

[14]Funabashi,K., Fukasawa,T., Kikuchi,M., Kawamura,F., Kondo,Y., "Development of Silver Impregnated Alumina for Iodine Separation from Off-Gas Streams," Proc. 23rd DOE/NRC Nucl. Air Cleaning and Treatment Conf., CONF-940738, 352(1994).

DISCUSSION

JUBIN: When you examined the material and determined that you had metallic silver, did you have an opportunity to look at this material through an electron microscope and determine whether the silver was uniformly distributed over the material? Did it, perhaps, conglomerate into nodules of some sort?

FUKASAWA: We did not examine it by microscope in this case, but observed that the silver distribution was under the surface of the other adsorbent. Inside the adsorbent there was still silver nitrate.

HERRMANN: We agree with your experiences that elemental silver has good removal efficiency for iodine. We do not agree with your experience for the removal efficiency of elemental iodine with elemental silver. 85% of I in WAK offgas is organic iodine. With elemental silver on a carrier of silica we found better removal efficiency than with silver nitrate. I agree, we should compare plant and laboratory experiences. Laboratory experiences with I-131 indicate a higher iodine trapping performance than plant experience.

FUKASAWA: I don't know the exact conditions of your offgas, but in these cases the silver nitrate is converted to metallic silver. Without impurities during the iodine separation with metallic silver, this adsorber shows low DF. But with impurities, there should be impurities in the actual offgas, this adsorber showed high DF. So your case is, I think, the same as this case. You get high DF for I_2 with metallic silver with impurities like NO_x or humidity.

HERRMANN: The device for iodine removal is at 140° C. As impurities we have some percent of NO_2. It depends on the dissolution time. We measured it also in the effluent ventilation system where the concentration is much lower. The water content was always approximately 3% absolute, the offgas saturation after the scrubbing columns. This is what we know about the impurities we have.

FUKASAWA: In our case, NO_x concentration is 1.5%. NO is 0.75% and NO_2 is 0.75%. The minimum water content was about 1% in our iodine separation tests. With such an amount of coexisting impurities, you don't have to worry about the DF decrease in this case. In your case you can get high DF I think.

JUBIN: One other question, what is your dew point, is it 35°C?

FUKASAWA: Yes, dew point is 33.5°C at 150°C, humidity is about 1%.

24th DOE/NRC NUCLEAR AIR CLEANING AND TREATMENT CONFERENCE

DIFFUSIONAL ANALYSIS OF THE ADSORPTION OF METHYL IODIDE ON SILVER EXCHANGED MORDENITE

R. T. Jubin
Chemical Technology Division
Oak Ridge National Laboratory
Oak Ridge, Tennessee 37831

and

R. M. Counce
Department of Chemical Engineering
University of Tennessee
Knoxville, Tennessee 37916

Abstract

The removal of organic iodides from off-gas streams is an important step in controlling the release of radioactive iodine to the environment during the treatment of radioactive wastes or the processing of some irradiated materials. Nine-well accepted mass transfer models were evaluated for their ability to adequately explain the observed CH_3I uptake behavior onto the Ag°Z. Linear and multidimensional regression techniques were used to estimate the diffusion constants and other model parameters, which then permitted the selection of an appropriate mass transfer model.

Although a number of studies have been conducted to evaluate the loading of both elemental and methyl iodide on silver-exchanged mordenite, these studies focused primarily on the macro scale (deep bed) while evaluating the material under a broad range of process conditions and contaminants for total bed loading at the time of breakthrough. A few studies evaluated equilibrium or maximum loading. Thus, to date, only bulk loading data exist for the adsorption of CH_3I onto Ag°Z. Hence this is believed to be the first study to quantify the controlling mass transfer mechanisms of this process.

It can be concluded from the analysis of the experimental data obtained by the "single-pellet" -type experiments and for the process conditions used in this study that the overall mass transfer rate associated with the adsorption of CH_3I onto Ag°Z is affected by both micropore and macropore diffusion. The macropore diffusion rate was significantly faster than the micropore diffusion, resulting in a two-step adsorption behavior which was adequately modeled by a bimodal pore distribution model. The micropore diffusivity was determined to be on the order of 2×10^{-14} cm^2/s. The system was also shown to be isothermal under all conditions of this study.

Introduction

One of the promising solid sorbent technologies for the removal and retention of iodine in terms of performance and simplicity is the adsorption on hydrogen-reduced silver mordenite (Ag°Z). This form of the sorbent has been reported by several researchers [Thomas et al. (1977), Jubin (1980, 1982), Scheele et al. (1983), and Sheele and Burger (1987)] to be more effective in trapping I_2 and CH_3I than the ionic silver mordenite (AgZ). Although a number of studies have been conducted to evaluate the loading of both elemental and methyl iodide on silver-exchanged mordenite, they focused primarily on the macro scale (deep bed) while evaluating the material under a broad range of process conditions and

contaminants for total bed loading at the time of breakthrough. Thus for the most part, only bulk loading data appear to exist in the literature for the adsorption of CH_3I onto AgZ or Ag°Z. The specific objective was to provide sufficient insight into the adsorption process to allow the determination of the primary controlling mechanisms and diffusion and/or reaction coefficients associated with the process.

Theory and Assumptions

The process of physical adsorption in porous adsorbent material is generally extremely rapid according to Kärger and Ruthven (1992). As a result, in most cases, mass or heat transfer resistances are the controlling factors for the overall rate of adsorption. Kärger and Ruthven (1992) provided an outstanding discussion on the diffusional resistances in zeolite pellets. What follows is a summary of that discussion as it applies to the problem at hand.

According to the International Union of Pure and Applied Chemistry (IUPAC) classification, pores with a diameter less than 20 Å are considered micropores while pores with a diameter greater than 500 Å are classified as macropores. The region between 20 and 500 Å is classified as mesopores (Kärger and Ruthven, 1992). The mass transport in each of these three size regions is controlled by different diffusion mechanisms. In the macropores, interactions between the pore walls and the diffusing molecule are minor and generally bulk diffusion is observed. Typically, the macropore provides only limited adsorption capacity but may significantly impact the mass transfer rates. As the size of the pore decreases, the interactions with the walls become increasingly important. In the mesopore region, diffusion control is generally associated with Knudsen diffusion; however, both surface diffusion and capillary effects may play significant roles. In the micropore region, surface forces are the most significant, as the diffusing molecule interacts with the wall more frequently than with other diffusing molecules. This form of diffusion is also known as "intracrystalline" diffusion. Micropore diffusion is also quite different from the diffusion processes in either the macropore or mesopore regions in that it is an activated process. This implies that the observed diffusion rate, if this mechanism could be isolated, would vary with temperature in accordance with an Arrhenius form equation:

$$D_c = D_\infty e^{-E_d/RT}. \tag{1}$$

Kärger and Ruthven (1992) further indicate that the analysis of loading data obtained for zeolite crystals that are "sufficiently large" can generally be accomplished through the use of the simple single micropore diffusion resistance model. However, in the case of commercial pelleted adsorbents, there is often a continuous range of pore sizes, which includes micropores, mesopores, and macropores. The analysis of many commercially available zeolite adsorbents is a bit more tractable because these materials are formed from small microporous particles of the actual zeolite crystal to produce a macroporous pellet of a manageable size. In such pellets, the pore size distribution is reported to often exhibit a bimodal-type distribution. In this situation, it is possible that the mass transport is controlled by macropore and/or micropore diffusion resistances.

General Assumptions and Simplifications

In most cases, modeling of the diffusion processes in porous media requires some type of simplifying assumptions. These generally involve the definition of structure of the adsorbent material, the nature or order of the chemical reactions and thermal effects associated with the heat of reaction and adsorption, and finally the behavior of the diffusion coefficient.

Commercially available extruded adsorbents are not of uniform size. While the diameter appears to be nearly the same, the length varies greatly. It is generally accepted to use an equivalent spherical radius, $\bar{r}$, defined as the radius of a sphere having the same external surface-to-volume ratio. In the analysis of Kärger and Ruthven (1992), this is shown to be valid for small changes in conversion. In the case of an infinite cylinder and a material with the equivalent spherical radius determined as stated above, the dimensionless time required to reach 90% conversion is different by about 25%. At 50% conversion, the error is <5%.

The second assumption deals with the structure of the pellet itself, as this will in large part define the nature of the model. The structure of the solid pellet has been conceptualized in numerous ways (Ramachandran and Doraiswamy, 1982; and Kulkarni and Doraiswamy, 1986), ranging from the simplest approach of a spherical, homogenous, nonporous pellet to a porous pellet containing subparticles that may also be porous (Kärger and Ruthven, 1992). The introduction of some type of pore structure also requires an assumption concerning the pore behavior. The pore can either remain constant or change as a function of time.

A third assumption that must be validated is that the process can be considered to occur under isothermal conditions. The models described below assume that the system being studied is isothermal. However, when studying an adsorption/reaction process, the possibility that this assumptions might be invalid as a result of the heat effects from adsorption and/or reaction must be considered. In such a case, the heat effects, which may be significant, must be accounted for in the analysis used to examine the experimental data. The assumption of isothermal conditions is generally only valid when the sorption rates are relatively slow (Kärger and Ruthven, 1992).

Lee and Ruthven (1978) describe the three possible resistances to heat transfer. These are (1) the resistance to heat transfer from the external surface of the pellet to the surrounding fluid; (2) the resistance to heat transfer from the external surface of an individual particle within the pellet or, in other words, the internal heat transfer resistances; or (3) the resistance to heat conduction within the individual particle. It was shown that for all cases the heat transfer from the external surface will be slower than heat transfer between the crystals of the sample. Based on this analysis, the temperature throughout the sample was uniform.

To determine the significance of the potential nonisothermal behavior, an analysis of maximum temperature variation due to the heat of adsorption and chemical reaction was made. The analysis of this system by Jubin (1995), using conservative assumptions for all variables, indicated a maximum delta temperature between the pellet and the bulk fluid as a result of both the heat of adsorption and chemical reaction of 0.37°C. Based on this result, it clearly appeared that the assumption of isothermal adsorption was substantiated.

Finally assumptions about the stability of the process system used in the experimental determinations are generally made. One of the common process assumptions is that of constant bulk gas-phase composition. This is either based on the use of a very large system, a true constant pressure system, or by careful control of a flowing gas stream. If this assumption is not made, then the changing composition of the gas phase must be addressed in the model.

Shrinking or Unreacted Core Model

One of the classic models used to describe noncatalytic reactions of solid particles with a surrounding fluid is the shrinking or unreacted core model. This model, as described by Levenspiel (1972, 1979), was developed by Yagi and Kunii in 1955 and contains five sequential steps for the gaseous reactant and product components.

For the reactant gases:

1. Diffusion through a boundary layer gas film which surrounds the solid particle.
2. Diffusion though the particle to the surface of the unreacted core.
3. Reaction with the solid reactant at the surface of the solid core.

And for the product gases:

4. Diffusion back through the reacted portion of the particle to the outside surface of the particle.
5. Diffusion through the boundary layer gas film surrounding the solid particle.

It was noted by Levenspiel (1972) that there may be significant variations in the relative importance of these five steps, depending on the relative magnitude of the associated resistances to mass transfer. Furthermore, in some situations, some of these steps are not relevant. For example, in the case of an irreversible reaction, steps 4 and 5 do not contribute directly to the observed resistances to the reactions. The same is true of a reaction producing no gaseous products.

The basic conversion equations for the first three steps have been developed. For a gas-solid reaction of the general form

$$A(g) + bB(s) \rightarrow R(g) + S(s) \tag{2}$$

and constant-size spherical particles, the following conversion-time expressions are relevant for the first three resistances and can be used to compare the observed loading rate data with the theoretical uptake curve.

Individual Controlling Resistances

In terms of the flux, the equations describing film diffusion control can be written based on either the moles of the diffusing component, A, or the moles of the solid reactant, B, that is reacted with A according to Eq. (2):

$$-\frac{1}{S_{ex}}\frac{dN_B}{dt} = -\frac{1}{4\pi r_a^2}\frac{dN_B}{dt} = -\frac{b}{4\pi r_a^2}\frac{dN_A}{dt} = bk_g\left(C_{Ag} - C_{As}\right) . \tag{3}$$

For the limiting case when there is only film diffusion control, C_{As} approaches 0. And the fractional conversion, X_B, can be expressed in terms of the unreacted core radius by

$$\frac{t}{\tau_{gasfilm}} = 1 - \left(\frac{r_c}{r_a}\right)^3 = X_B , \tag{4}$$

where the time for total conversion is given by

$$\tau_{gasfilm} = \frac{\rho_B r_a}{3bk_g C_{Ag}} . \tag{5}$$

In a similar manner, expressions can be written for the case of ash diffusion alone. The resulting expression in terms of fractional conversion is

$$\frac{t}{\tau_{ash}} = 1 - 3\left(1 - X_B\right)^{2/3} + 2\left(1 - X_B\right) , \tag{6}$$

where the time to complete conversion is given by

$$\tau_{ash} = \frac{\rho_B r_a^2}{6bD_e C_{Ag}} . \tag{7}$$

For chemical reaction control (rxn), the relationship for the conversion vs time is given by

$$\frac{t}{\tau_{rxn}} = 1 - \frac{r_c}{r_a} = 1 - (1 - X_B)^{1/3} , \tag{8}$$

where k_s is the assumed first-order reaction constant. The time to complete conversion is given by

$$\tau_{rxn} = \frac{\rho_B r_a}{bk_s C_{Ag}} . \tag{9}$$

Full Shrinking Core Model

In many situations, more than one of these resistances is a factor in determining the observed rate of conversion of the particle. The three individual rate expressions can be combined into a single expression (Levenspiel 1972, 1979).

$$-\frac{1}{S_{ex}}\frac{dN_B}{dt} = \left[\frac{b}{\frac{1}{k_g} + \frac{r_a\left(r_a - r_c\right)}{r_c D_e} + \frac{r_a^2}{r_c^2 k_s}}\right] C_{Ag} . \tag{10}$$

This expression can easily be converted into a more usable form for the analysis of the gravimetric loading data by expressing the unreacted core radius, r_c, in terms of conversion, found in Eq. (4), yielding

$$-\frac{1}{S_{ex}}\frac{dN_A}{dt} = \left[\frac{b}{\frac{1}{k_g} + \frac{r_a\left(1 - \left(1 - X_B\right)^{1/3}\right)}{\left(1 - X_B\right)^{1/3} D_e} + \frac{1}{\left(1 - X_B\right)^{2/3} k_s}}\right] C_{Ag} . \tag{11}$$

This is then an expression that can be used to determine the values of the three adjustable parameters through a process of curve fitting to minimize the error between experimentally obtained flux or loading data and the calculated values.

Alternately, it has been shown by Levenspiel (1972, 1979) that the total time to reach a given conversion is the sum of the times for the individual mechanisms to reach the same conversion. In other words,

$$t_{total} = t_{gasfilm} + t_{ash} + t_{rxn}. \tag{12}$$

Likewise, for the complete conversion, the time is given by

$$\tau_{total} = \tau_{gasfilm} + \tau_{ash} + \tau_{rxn}. \tag{13}$$

By replacing the expressions for the individual times to reach a set conversion given by Eqs. (4), (6), and (8) for the individual times into Eq. (12), an expression is obtained that allows the determination of the extent of the conversion for any value of time. It should be noted that the conversion is found as the root of the following equation:

$$t_{total} = X_B \tau_{gasfilm} + \left[1 - 3(1 - X_B)^{2/3} + 2(1 - X_B)\right]\tau_{ash} + \left[1 - (1 - X_B)^{1/3}\right]\tau_{rxn}. \tag{14}$$

Isothermal Models for Porous Media

The previous models do not consider the nature of the media, which in the case of zeolites may be important. Kärger and Ruthven (1992) summarize numerous studies which have focused on the adsorption from the gas phase into a porous zeolite-type structure. In general terms, these studies attempted to incorporate the porous nature of the zeolite pellets by addressing diffusional resistances arising from (1) the micropores, (2) the macropores, or (3) a combination of both macropore and micropore resistance. These models are further summarized as follows.

Micropore Diffusion Controlling

For the case of micropore diffusion alone, the following transient sorption expression is presented by Kärger and Ruthven (1992):

$$X_B = \frac{m_t}{m_\infty} = 1 - \frac{6}{\pi^2}\sum_{n=1}^{\infty}\frac{1}{n^2}\exp\left(-\frac{n^2\pi^2 D_c t}{r_i^2}\right). \tag{15}$$

The two primary assumptions that must be noted are the use of constant diffusivity and that the change in the adsorbed phase concentration is small such that gas phase or surface composition remains constant (Ruthven, 1984).

This model reduces to

$$X_B = \frac{m_t}{m_\infty} = 1 - \frac{6}{\pi^2}\exp\left(-\frac{\pi^2 D_c t}{r_i^2}\right) \tag{16}$$

as the time term becomes large. Kärger and Ruthven (1992) point out that a plot of $\ln[1 - m_t/m_\infty]$ vs t should approach a straight line. This line will have a slope of $-\pi^2 D_c/r_i^2$ and an intercept of $\ln(6/\pi^2)$.

Macropore Diffusion Controlling

For macropore diffusion the solution is the same with the D_c/r_i^2 term replaced by

$$\frac{D_p}{r_a^2}\left(\frac{1}{1+K^*\left(1-\varepsilon_p\right)/\varepsilon_p}\right), \tag{17}$$

where K^* is an equilibrium constant which has an Arrhenius-type temperature dependence.

Combined Micropore and Macropore Diffusion Control

Dual-resistance systems in biporous media have been studied by several researchers. Ruckenstein et al. (1971), discussing the dissertation of Vaidyanathan (1971), pointed out that the macropore diffusivity and micropore diffusivity may, in many cases, be quite different by orders of magnitude. In such a case, the observed diffusion process may be significantly affected by the particular structure of the porous solid. The model developed by Vaidyanathan (1971) appears to be the first to address the analysis of transient sorption with the competing effects of macropore diffusion and micropore diffusion combined. The assumptions made in the development of this model are as follows:

1. The system is isothermal.
2. The particle is spherical and composed of small uniform spherical microporous particles.
3. The sorbent is exposed to an infinite source of sorbate such that the surface concentration is constant.
4. The sorbent is exposed to a step change in sorbate concentration at time zero.
5. Adsorption occurs at the walls of both the macropores and the micropores.
6. Linear isotherms apply.

Ma and Lee (1976) and Lee (1978) extended the original model to address the case of a finite quantity of sorbate. Of these, the model proposed by Lee appeared to be a bit simpler and faster in terms of computer time to apply as it contained only one double summation and the others contained the ratio of two double summations. In the case of constant gas-phase concentrations, the mathematical solution developed by Lee simplifies to

$$X_B=\frac{m_t}{m_\infty}=1-\frac{18}{\beta+3\alpha}\sum_{m=1}^{\infty}\sum_{n=1}^{\infty}\left(\frac{n^2\pi^2}{p_{n,m}^4}\right)\frac{e^{-p_{n,m}^2 D_c t/r_i^2}}{\left\{\alpha+\frac{\beta}{2}\left[1+\frac{\cot\left(p_{n,m}\right)}{p_{n,m}}\left(p_{n,m}\cot\left(p_{n,m}\right)-1\right)\right]\right\}}, \tag{18}$$

where

$$\alpha=\frac{D_c}{r_i^2}\frac{r_a^2}{D_p}, \tag{19}$$

$$\beta=\frac{3\alpha\left(1-\varepsilon_p\right)q_\infty}{\varepsilon_p C_{A,0}}, \text{ and} \tag{20}$$